R75-46

THEORETICAL AND EXPERIMENTAL INVESTIGATION OF EMERGENCY HEAT RELEASES FROM FLOATING NUCLEAR POWER PLANTS

by

Gerhard H. Jirka

Duncan W. Wood

and

Donald R.F.Harleman

Ralph M. Parsons Laboratory

for

Water Resources and Hydrodynamics

Department of Civil Engineering

Massachusetts Institute of Technology

REPORT NO. 206

Prepared under the Support of

Offshore Power Systems

Jacksonville, Florida

November 1975

MIT

DEPARTMENT

OF

CIVIL

ENGINEERING

SCHOOL OF ENGINEERING

MASSACHUSETTS INSTITUTE OF TECHNOLOGY

Cambridge, Massachusetts 02139

DISCLAIMER OF QUALITY

Due to the condition of the original material, there are unavoidable flaws in this reproduction. We have made every effort possible to provide you with the best copy available. If you are dissatisfied with this product and find it unusable, please contact Document Services as soon as possible.

Thank you.

Some pages in the original document contain pictures, graphics, or text that is illegible.

R75-46

OSP 81769
OSP 82763

THEORETICAL AND EXPERIMENTAL INVESTIGATION OF EMERGENCY HEAT RELEASES FROM FLOATING NUCLEAR POWER PLANTS

by

Gerhard H. Jirka
Duncan W. Wood
and
Donald R.F. Harleman

Ralph M. Parsons Laboratory
for
Water Resources and Hydrodynamics
Department of Civil Engineering
Massachusetts Institute of Technology

Report No. 206

Prepared under the Support of
Offshore Power Systems
Jacksonville, Florida

November 1975

ABSTRACT

A combined analytical and experimental study is made of the hydrodynamic and heat transport aspects of transient heat releases during emergency cooling operations at floating nuclear power plants located in protective enclosures. The study has two major objectives, namely (i) the development of a mathematical prediction model for the distribution within the protective enclosure of the released heat and (ii) the specific application of the predictive model to the Atlantic Generating Station (AGS) proposed by the Public Service Electric and Gas Company of New Jersey.

The development of the analytical model proceeded concurrently with the construction and use of an undistorted scale model of the AGS basin. The physical model could not be used to directly predict actual conditions at the AGS due to scaling and operating limitations, but the data gathered were used to aid in understanding the complex mixing and transport phenomena and thus assist in the development of the analytical model.

The analytical model schematized the temperature field within the basin as a two-layered stratified system with a uniform layer depth and temperature rise. The heated upper layer was used as the control volume and all fluxes of heat and mass in or out of the control volume were accounted for at each time step. The four physical processes responsible for the fluxes are: 1) Jet entrainment at the interface due to the near-surface jet discharges, 2) Stratified counterflow through the openings in the breakwater, 3) Selective withdrawal at

the submerged intakes into the cooling system, and 4) Surface heat dissipation to the atmosphere.

The model was used to predict conditions at the AGS for a variety of emergency cooling situations. Sensitivity studies on the design parameters of the AGS and the modeling parameters included in the model were conducted.

The analytical model is verified by comparison with experimental results and presented as a legitimate predictive tool for simulating this complex phenomena.

The report contains a complete listing of the analytical model and appropriate user instructions.

ACKNOWLEDGEMENTS

This study was sponsored by Offshore Power Systems of Jacksonville, Florida, under Office of Sponsored Programs, numbers OSP 81769 and 83297. The cooperation of Mr. Robert Bruce and Mr. Robert Turner of Offshore Power Systems is gratefully acknowledged.

The research work was performed by Mr. Duncan W. Wood and, essentially as given here, but with the exception of Appendix B, was submitted by him to the Department of Civil Engineering in partial fulfillment for the degree of Master of Science. Technical supervision was provided by Prof. Donald R.F. Harleman, Ford Professor of Engineering and Director, R.M. Parsons Laboratory, and by Dr. Gerhard H. Jirka, Research Engineer, M.I.T. Energy Laboratory.

The contributions of the following people are gratefully acknowledged: Mr. Daniel S. Katavola, Research Assistant, was instrumental in the planning and construction of the experimental model. He also conducted an independent investigation on the selective withdrawal of horizontal pipe intakes which was submitted as a Master of Science thesis to the Department of Ocean Engineering at M.I.T. An abbreviated version of Katavola's thesis had been included as Appendix B of this report. Mr. Joseph H. Lee, Research Assistant, was associated with the early stages of the analytical model development. Technical assistance in model construction was provided by Mr. Edward McCaffrey, OSP Staff (Electronics), Mr. Roy Milley, Machinist, and Mr. Harry Garabedian and Mr. Robert Harleman, student helpers.

The manuscript was typed by Ms. Erika Babcock, Ms. Susan Johnson, and Ms. Carole Solomon.

Computational work was carried out at the Civil Engineering-Mechanical Engineering Joint Computer Facility at M.I.T.

TABLE OF CONTENTS

LIST OF TABLES

LIST OF FIGURES

CHAPTER 1

Introduction

1.1 Design Concept and Licensing Aspects

This study is concerned with the hydrodynamic and heat transfer aspects of transient heat releases during emergency cooling operations at floating offshore nuclear power plants.

The design concept of floating nuclear power plants has been proposed as a reasonable solution to many power plant siting problems. The basic plan consists of self-contained nuclear power plants built on large barges that then float within an artificial protective enclosure. The economic advantage of the scheme is that the identical power plant units can be produced on an assembly line at a special manufacturing plant and then towed to their location. This centralized construction of a standard unit can result in considerable reduction in construction costs due to the general advantages of mass production and the ability to use large stationary manufacturing plant equipment rather than smaller mobile equipment. Structural advantages of the design are inherent in the fact that the nuclear plants are floating and therefore largely independent of foundation difficulties. A floating nuclear plant, when properly sited, may also greatly minimize the environmental impacts typically associated with large energy facilities.

The floating nuclear plants have to satisfy specific regulatory standards established by the U.S. Nuclear Regulatory Commission (NRC). A group of standard floating nuclear plants will be licensed under

Appendix "M" to 10CFR50 (Code of Federal Regulations), which permits licensing of the plant independent from the licensing of its future site location. This process requires that an envelope of postulated site parameters is established and sites which fall within this postulated envelope can be licensed without further consideration of the floating nuclear plant. One of the site envelope parameters expresses the requirement that the nuclear plants be operated only when the sea water temperature is 85° or less. Consequently, systematic evaluation of the performance aspects of the plant's emergency and auxiliary cooling systems is required to evaluate the sea water temperature behavior during emergency and cool-down conditions.

1.2 Objectives of this Study

The emergency cooling systems consist of a number of pumping circuits which take in cooling water through submerged intakes, pass it through the heat exchangers and discharge the heated water through pipes located near the water surface into the basin within which the plant floats. Details of design, operation, and heat loading are given in Chapter 2.

There are several physical processes which govern the distribution and build-up of discharged heat within the breakwater basin. These are notably: jet mixing at the discharge, stratified flow within the basin and through the breakwater openings, heat dissipation to the atmosphere and re-entrainment into the intake openings.

The objectives of this study are:

1) The development of a transient mathematical model which allows the prediction of heat distribution within the breakwater basin and in

particular the re-entrainment into the intake openings. The model should be applicable to a variety of geometric, oceanographic and meteorological conditions to allow a generic evaluation of the emergency cooling system for floating nuclear units and provide design guidelines for specific sites and breakwaters.

2) The detailed investigation of the emergency cooling system for the first offshore power plant, namely the Atlantic Generating Station off the coast of New Jersey, as proposed by N.J. Public Service Electric & Gas Company.

3) Additional studies to evaluate the effect on emergency cooling system performance of special installations, such as oil booms and security beams.

1.3 Methods of Analysis

Both mathematical and physical scale model techniques have been employed in the analysis and prediction of the performance of the emergency systems.

The mathematical model consists of a composite, time-dependent numerical description of the various physical processes which occur during an emergency cooling operation. Established techniques for analyzing jet mixing, stratified flow and surface heat exchange were examined, modified as appropriate, and then combined into the model. Recently completed research was used as the basis for predicting the selective withdrawal at the intakes. The combined model is essentially a two-layer stratified model which calculates the transient response of the thickness and temperature of the heated layer as well as the intake temperature under varying operational and oceanographic conditions.

The physical scale model is an undistorted model of the Atlantic Generating Station at a scale of 1:81. The model replicates the salient features of the floating units, the emergency cooling systems, and breakwater enclosure. It also includes the capability of simulating tidal rise and fall.

Modeling limitations constrain the sole use of a physical scale model for prediction of complex flow phenomena as occur during emergency cooling operations. However, the scale model provided valuable insight into the physical aspects of the system by clearly demonstrating the dominating physical processes, such as the stratified nature of the flow, and provided a means of verifying the analytical predictions for the conditions of the laboratory model. This established the analytical model as a credible technique. The actual prototype predictions are concerned with long term behavior and a large number of possible operational situations, all of which are neither accurately nor conveniently simulated by a physical model alone.

1.4 Outline of the Report

The main body of this report is structured as follows. In Chapter 2, the general problems associated with using the confined basin as the ultimate heat sink of a floating nuclear power are discussed. Next, the specific operating characteristics of Offshore Power System's proposed plants are presented, along with the site-specific characteristics of the basin designed for the Atlantic Generating Station.

Chapter 3 provides a complete description of the analytical simulation model that has been developed. Each component of the model struc-

ture is discussed. In particular, the adaptation of the model for use at the Atlantic Generating Station is explained.

Chapter 4 deals with the complete history of the design, construction and operation of the physical model. The various simplifications and assumptions made are outlined and the capabilities and restrictions of the model are discussed.

Chapter 5 reports the results of the experimental program undertaken using the physical model. Operational procedures and problems are described as well as the methods of data reduction. The experimental results are compared to the analytical predictions obtained for the same conditions. The chapter concludes with a discussion of the influence of the oil boom on the physical model.

Chapter 6 presents the actual analytical model predictions for the various operational conditions studied at the Atlantic Generating Station. Results are presented graphically and significant trends in the predictions are interpreted.

Chapter 7 of the report examines the sensitivity of the analytical model to both changes in the assumptions of the mathematics of the model, and changes to the various physical design parameters.

The report includes two appendices. The first contains the complete listing of the computer model deck and user instructions. The second appendix provides a detailed discussion of the separate investigation on selective withdrawal from a two-layer stratified system conducted by Katavola (1975).

CHAPTER 2

Description of Emergency Cooling System for Offshore Power Plants

2.1 General Concept

Nuclear reactors must be provided with reliable and redundant emergency cooling systems that can cool down the reactor core and auxiliary equipment in the event that the primary cooling systems are inactivated. The systems necessary to transfer this heat load to the ultimate heat sink must be reliable and meet stringent standards as established by the NRC.

The performance of an emergency cooling system is determined by the interplay of mechanical components contained within the nuclear plant and of the heat sink mechanism outside the plant proper. In the case of offshore power plants the heat sink mechanism is provided through the water body within the breakwater enclosure with possibilities of heat removal by dissipation to the atmosphere and by exchange of water masses through any breakwater openings.

Normally, the emergency cooling system of a nuclear plant is licensed as a whole. That is the license covers the mechanical components inside and the heat sink mechanism outside the plant as one entity. In the case of floating nuclear power plants, all units will be produced in assembly line fashion and are identical in design. It is therefore the intent of the developer, Offshore Power Systems, to obtain from NRC a common license, for a series of nuclear units to be produced, which applies to the mechanical components inside the plant only, under the assumption that the heat sink mechanism outside the

plant meets certain minimum standards.

The purpose of the present study was to develop predictive tools which can be used to establish guidelines for the design of the outside heat sink mechanism so that the minimum standards can be met. The predictive model once developed was then used to study the Atlantic Generating Station (AGS) which is the first offshore nuclear plant installation, proposed by the New Jersey Public Service Electric and Gas Company.

2.2 Design Description of Emergency Cooling Systems for Floating Nuclear Units

The current design information presented below is the latest information available to M.I.T. at the time of this report. All predictions for the prototype presented in Chapter 6 are based on this information.

The emergency cooling equipment of the proposed floating nuclear power plant consists of two systems. They are the Essential Raw Water system(ERW), and the Auxiliary Raw Water system (ARW). Both systems are designed for once through cooling and each is intended to cool separate portions of the plant complex under differing emergency conditions.

2.2.1 ERW System

The ERW system consists of four independent trains or piping networks. Each of the four trains has its own intakes, strainer, and pump, and an operating capacity of 7500 gpm. Three of the four trains are fed into the common discharge lines also utilized by the three ARW

trains. The fourth ERW train has its own discharge piping. The three trains that join with the ARW system are enclosed mainly in the water tight safe guard compartments that are intended to protect the pumps and control equipment in the event of a sinking accident. The ERW system has two intakes for each train. One intake is located on the vertical side of the plant's hull, with the centerline approximately 28.5 feet below the water surface. The second is located in the bottom of the hull, or approximately 34 feet below the water line. Only the side intakes were modeled in both the physical and analytical models developed. This was done as a conservative worse case situation. Normally, if both intakes are available, the flow rate into the side intake is only approximately one half of the total, and thus the likelihood of recirculating heated water is greater when only the side intake is operated. As a result the ERW intake temperature rise predictions presented are conservatively on the high side. The ERW system is only operated during emergency conditions and the heat load applied is dependent on the operating situation. In all cases, the flow rate is assumed to remain at 7500 gpm per train.

2.2.2 ARW System

The ARW system consists of three identical trains, each including separate intakes, strainers, pumps, and discharge ports. The discharge ports are shared in common with three of the ERW trains. Each of the ARW trains is located mainly within a safe guard compartment, and thus a sinking accident should not effect the ARW system. The flow rate in all situations is assumed to be 15,000 gpm per train and the heat load is assumed to be the same for both a normal cool down cycle and a LOOP

emergency condition. The ARW system is also operated to cool auxiliary equipment at a constant heat load of 66 million BTU/hour during normal plant operations.

2.3 Atlantic Generating Station Breakwater Enclosure

A major thrust of this investigation is aimed at studying the emergency cooling situation for the type of breakwater enclosure designed to protect the Atlantic Generating Station, the first proposed floating nuclear plants. This offshore station will consist of two floating nuclear power plants, each with a 1100 Mw capacity, located inside an artificial breakwater constructed approximately three miles off the New Jersey coast near Atlantic City. Fig. 2-1 illustrates the basic configuration of the plant. The water depth at low mean tide within the breakwater is relatively shallow, with a maximum depth of 47 feet near the center and only 5 feet behind the mooring caissons. At the two sill openings in the breakwater the low mean depth is 20 feet.

The water surface area within the breakwater enclosure at mean water is approximately 660,600 square feet and increases to 663,000 square feet at the highest astronomical tide of +5.3 feet. These values have taken into account the area of the plants and mooring caissons.

The locations of the emergency cooling system intakes and discharge ports are shown in Fig. 2-2. The interconnection between the ERW and ARW systems to use a common discharge is also illustrated.

An additional tentative feature of the AGS configuration that is considered during the investigation is the security/oil boom system located parallel to the stern end of the plants. This structure is

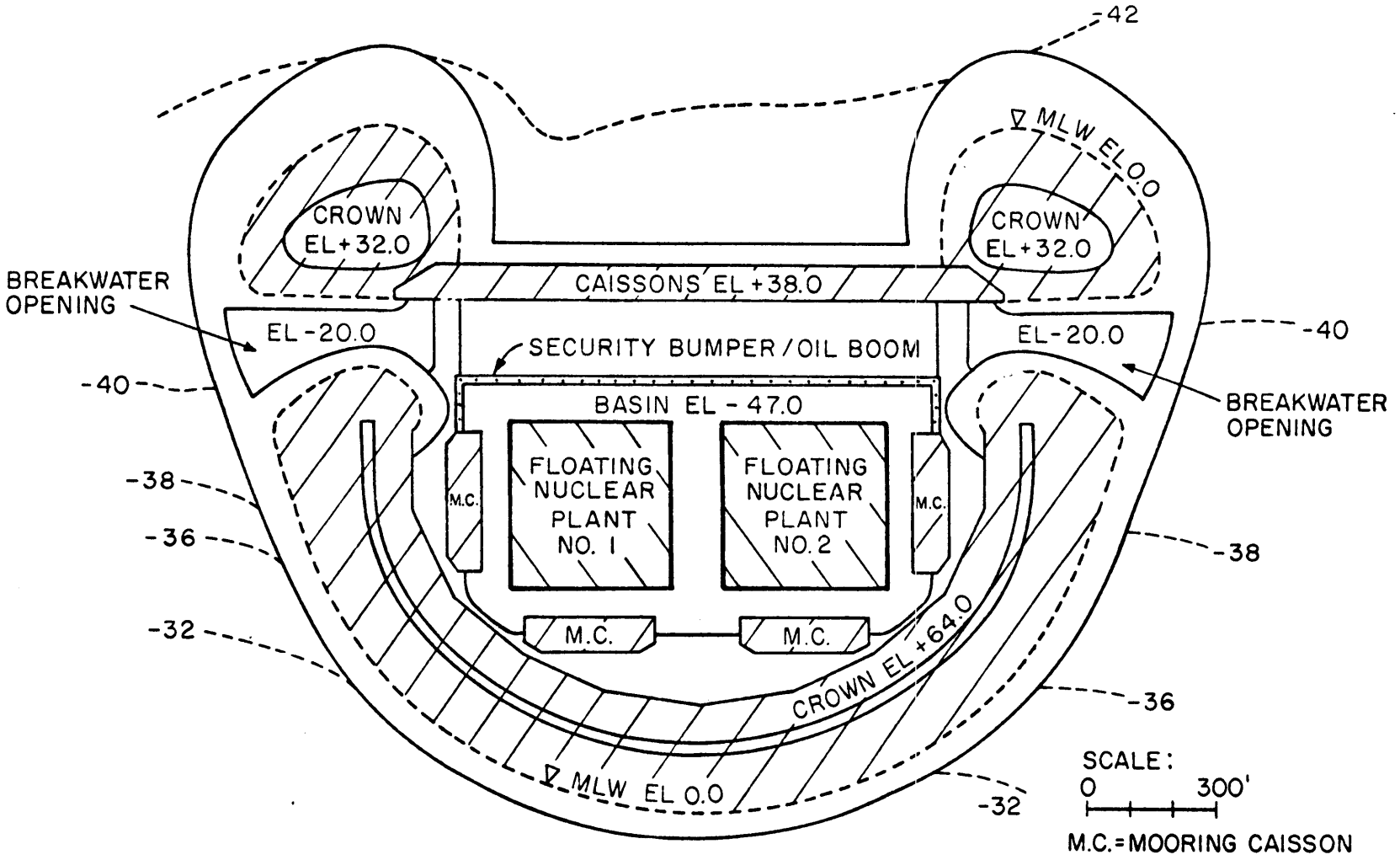

Figure 2-1: Atlantic Generating Station Site Configuration

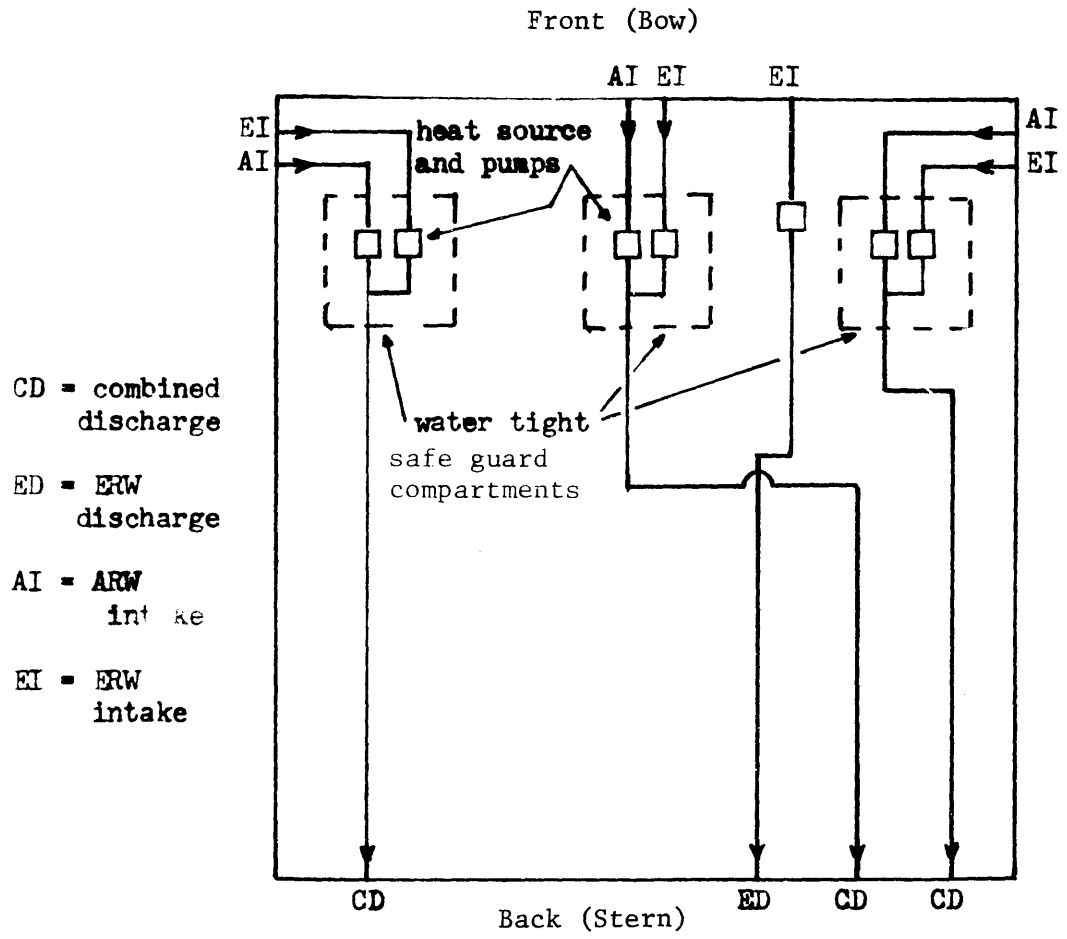

Figure 2-2: Emergency Cooling System Flow Diagram

intended to prevent ship collisions, and act as a skimmer wall to prevent any oil spills from reaching the plants. The location of the boom system can be seen in Fig. 2-1.

2.4 Emergency Situations

Two primary emergency situations are postulated that necessitate the use of the emergency cooling system. These situations are the "loss of coolant accident" (LOCA) and the "loss of offsite power" (LOOP). The case of a LOCA assumes a sudden break in the reactor coolant system piping , and the ERW system acting as the sole heat sink must cool down the reactor and containment. The heat load that must be removed by the ERW system during a LOCA is presented in Fig. 2-3 as a function of time.

A LOOP assumes that the offsite power source which is used to drive the condenser water circulating pumps is lost, and therefore the plant must go through a cool-down cycle using the emergency systems only.

The LOOP situation results in a varying heat load on the ARW system and a simultaneous constant heat load on the ERW system. These heat loadings are given in Fig. 2-3.

A third situation that can occur in combination with either a LOOP or a LOCA is referred to as a "normal shut down". This results in the same ARW varying heat load as applied in the LOOP, but omits the constant ERW loading.

These conditions apply to each plant separately and may occur when all or only a portion of the systems trains are operable. Thus there are many possible combinations of emergency situations when con-

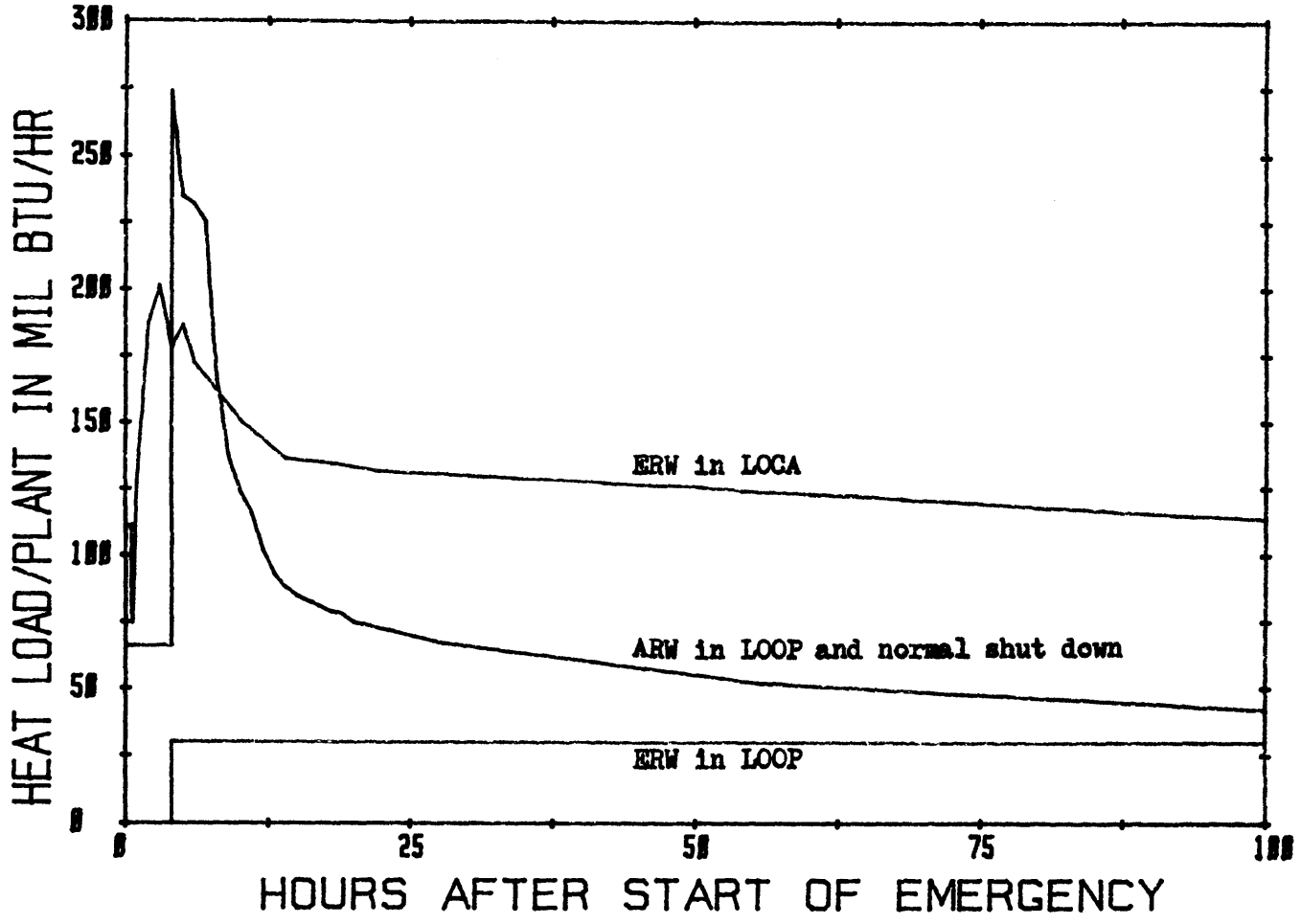

Figure 2-3: AGS Emergency Cooling System Heat Loads

sidering the two plants together. Those situations which have been examined are listed at the beginning of Chapter 6.

CHAPTER 3

Development of the Analytical Model

The analytical model was developed in conjunction with the physical model as a method for prediction of temperature rises within the basin and at the intakes for all possible design alternatives. The model formulation is based on the distinct stratification of the heated layer within the basin. This basic assumption which allows the analysis of the problem as a two layer system was essentially verified by the experimental program described in Chapter 5. The analytical model was formulated in FORTRAN IV and a program listing and user input information are included in Appendix A.

3.1 Basic Governing Equations

The basic structure of the analytical model is given by two first-order differential equations. The first is the Continuity Equation for the water in the heated upper layer and the second is the Conservation of Heat Equation for the upper layer. The schematics of the upper layer control volume with sources and sinks for volume and heat are shown in Fig. 3-1.

3.1.1 Continuity Equation

The continuity equation for a control volume comprised of the upper heated layer within the breakwater enclosure is:

$$\frac{d\forall_1}{dt} = Q_D + Q_E - Q_S - Q_R \qquad (3.1)$$

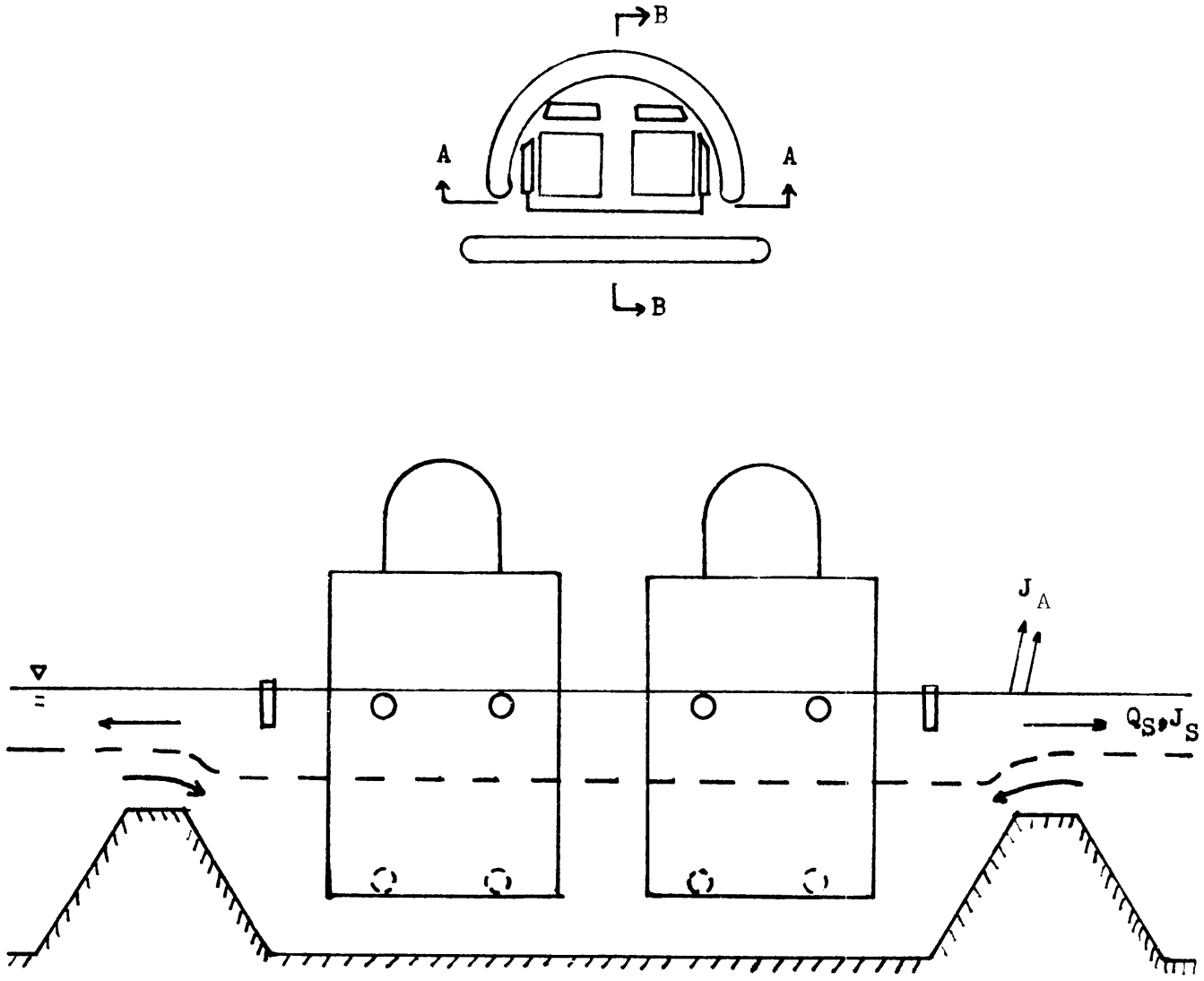

Figure 3-1a: Schematic of Emergency Cooling System Heat and Mass Flux (Section AA)

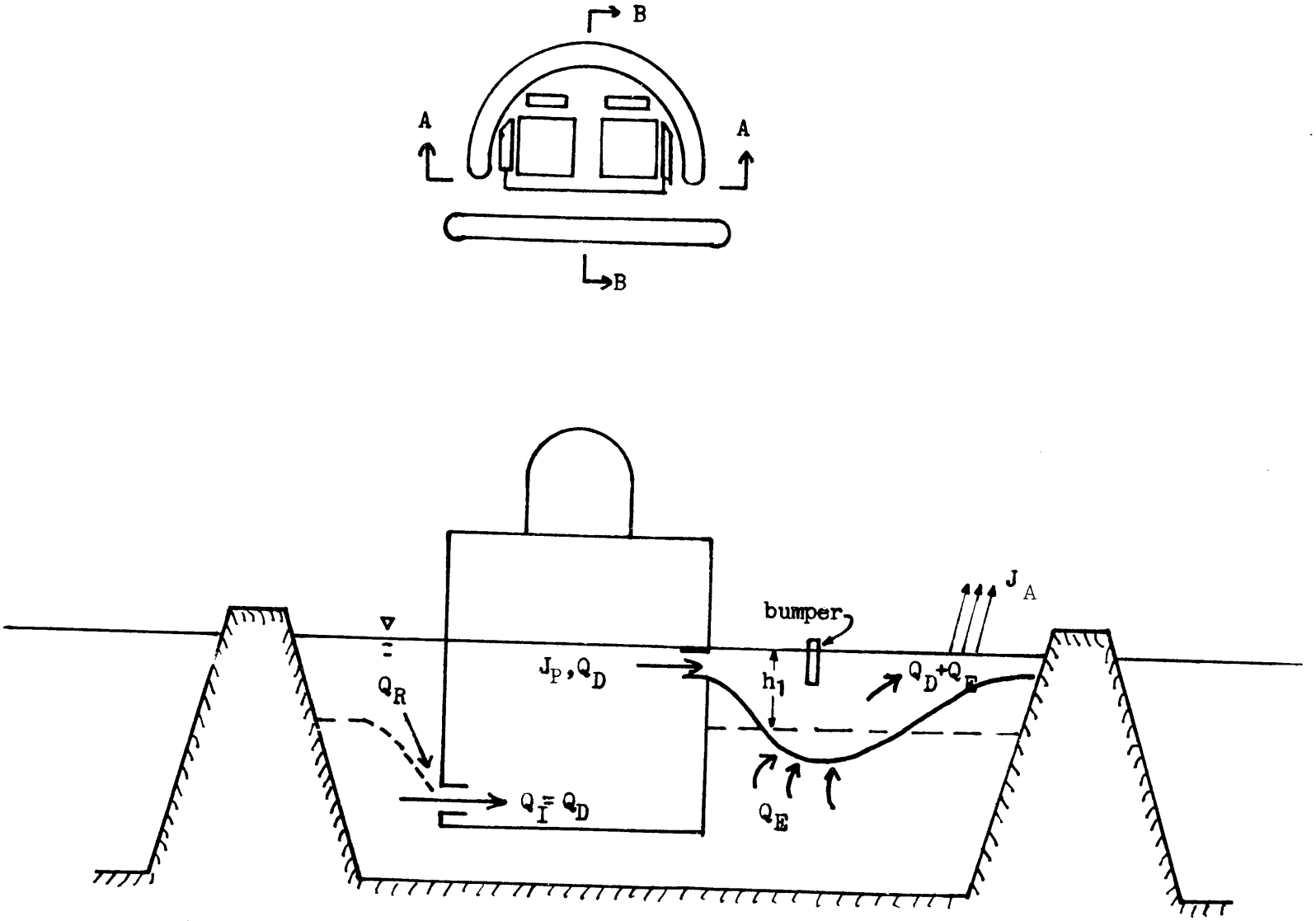

Figure 3-1b: Schematic of Emergency Cooling System Heat and Mass Flux (Section BB)

where $\forall_1$ = volume of upper layer within breakwater basin

Q_D = discharge flow from emergency system

Q_E = flow entrained from lower ambient layer into upper layer due to discharge induced turbulence

Q_S = outflow from upper layer into ocean through breakwater openings

Q_R = recirculation from upper layer into submerged intakes.

Because of tidal changes, the total water depth in the basin H is a function of time and the storage term in the continuity equation can be expressed as:

$$\frac{d\forall_1}{dt} = \frac{d}{dt}\,[\,A_S H] - \frac{d}{dt}\,[\,A_1(H - h_1)] \qquad (3.2)$$

where H = total water depth in basin

h_1 = uniform (average) thickness of the upper layer

A_S = water surface area within the breakwater basin

A_1 = horizontal area at elevation $(H-h_1)$ above bottom

Combining the preceding equations, one obtains:

$$\frac{dh_1}{dt} = \frac{1}{A_1}\left\{Q_D + Q_E - Q_S - Q_R - h_1\frac{dA_1}{dt} - \frac{d}{dt}\,[(A_S - A_1)H]\right\} \qquad (3.3)$$

Eq. (3.3) was further simplified as follows. The horizontal area within the breakwater is typically a function of depth as shown in Fig. 3-2 for the AGS conditions. The variability is due to the

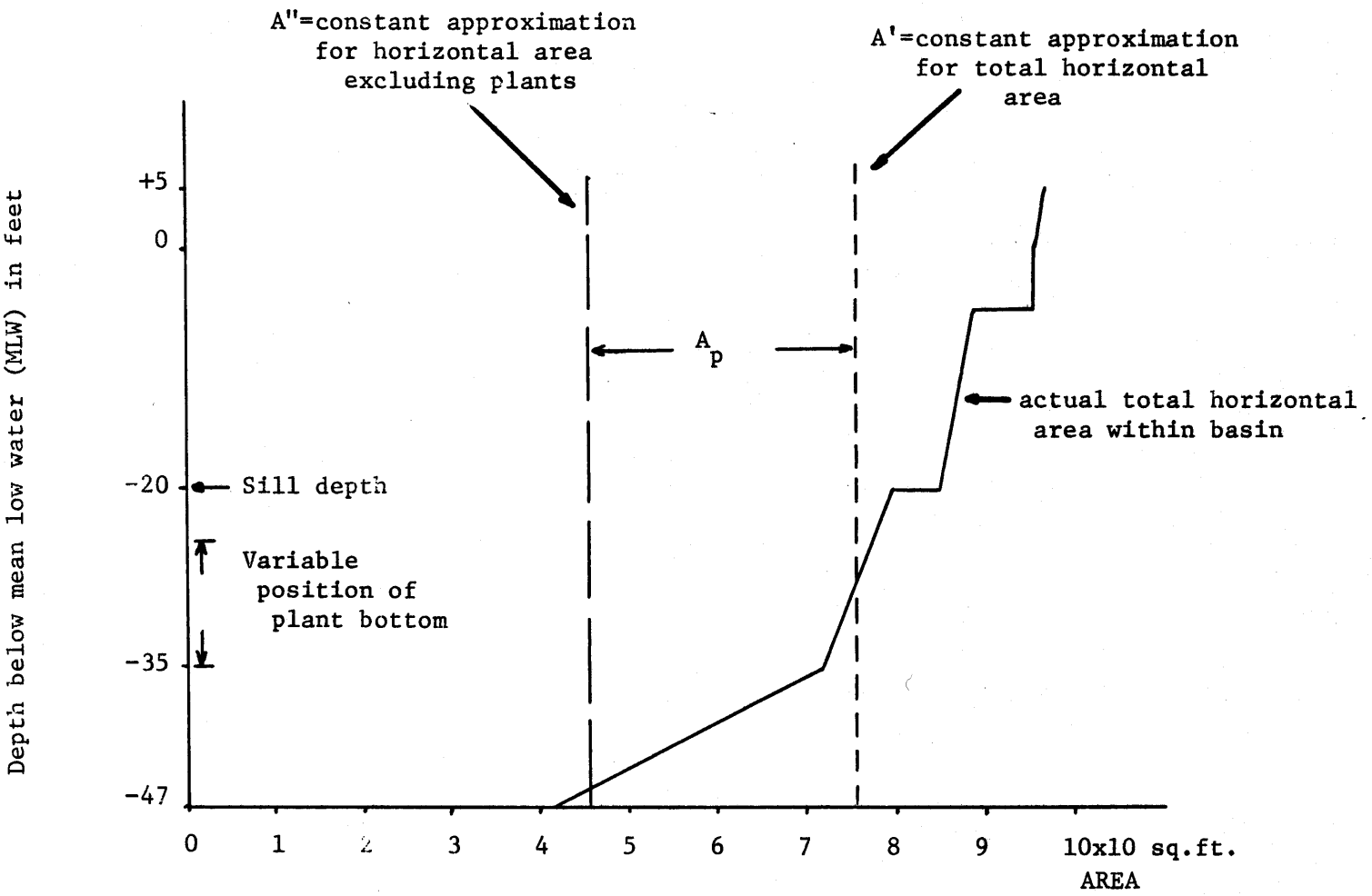

Figure 3-2: Definitions for Horizontal Areas within AGS Basin as a Function of Depth

non-uniformly sloping sides of the breakwater. Within the present study, the actual varying horizontal area, including the plant area, was approximated by a constant value A' as shown on Fig. 3-2. The horizontal area, excluding the plant area, A_p, is then found by subtracting

$$A'' = A' - A_p$$

as shown in Fig. 3-2. Approximating the horizontal area, with a constant value, namely * $A_1 \approx A''$ and $A_S \approx A''$, Eq. (3.3) simplifies to:

$$\frac{dh_1}{dt} = \frac{1}{A_1} [Q_D + Q_E - Q_S - Q_R] \tag{3.4}$$

3.1.2 Conservation of Heat Equation

The conservation of heat equation for the upper layer control volume is:

$$\frac{d}{dt} (\rho c_p \forall_1 \Delta T_1) = J_P - J_S - J_A \tag{3.5}$$

where ρ = density of water

c_p = specific heat of water

ΔT_1 = temperature rise above ambient of upper layer

J_P = heat transfer rate from the heat exchangers of the emergency cooling systems

---

*Except for the case when the layer depth, h_1, exceeds the draft of the plants. Then A_1 is taken equal to A'.

J_S = heat flux by means of convection out of the upper layer as a result of the flow, Q_S over the sills, which $= \rho c_p Q_S \Delta T_1$

J_A = heat flux to the atmosphere from the water surface area within breakwater enclosure.

After expansion of the storage term, use of Eq. (3.2), and substituting for J_S, Eq. (3.5) can be modified to express the change in the average excess temperature of the upper layer:

$$\frac{d\Delta T_1}{dt} = \frac{2}{\rho c_p h_1 (A_S + A_1)} [J_P - J_A - c_p \Delta T_1 (Q_D - Q_R + Q_E)] \qquad (3.6)$$

where $\forall_1 \approx h_1 (A_S + A_1) / 2$

Eq. (3.6) can be simplified if the depth variability of the horizontal area within the breakwater enclosure is neglected, namely $A_1 \approx A''$ and $A_S \approx A''$, as before. The simplified heat conservation equation is then:

$$\frac{d \Delta T_1}{dt} = \frac{J_P - J_S - J_A}{\rho c_p h_1 A_1} - \frac{\Delta T_1}{h_1} \frac{dh_1}{dt} \qquad (3.7)$$

The vertical turbulent diffusion of heat from the upper layer to the lower layer has been neglected in this formulation. It has been shown by several investigators (Kullenberg, 1971, Karelse, 1974) that vertical turbulent diffusion of heat is greatly reduced in the presence of strong density stratification. In comparison with the other

processes which effect the heat conservation Eq.(3.7), the contribution of vertical heat diffusion is assumed negligible over the time scale of interest (i.e. variations in the order of hours of prototype time.)

In the following sections, the auxiliary equations used to determine the various expressions contained in Eqs. (3.4) and (3.7) are presented.

3.2 Auxiliary Equations

All of the volume flux and heat flux terms contained in Eqs. (3.4) and (3.7) need to be expressed as functions of input data, constants, or the two dependent variables, ΔT_1, and h_1. Two terms, the plant flow rate, Q_D, and the heat load J_P, are given as input data, dependent only on the nature of the emergency operating condition being simulated. The remainder of the flux terms require analytical development. They can be divided into four physical processes:

(1) Stratified Counterflow at Sill Openings

(2) Jet Entrainment in Stratified Layer

(3) Selective Withdrawal at Intakes

(4) Heat Dissipation to Atmosphere.

3.2.1 Stratified Counterflow at Sill Openings

The expressions of interest are the total upper layer flow out of the basin, Q_S, and the flux of excess heat out of the basin, J_S, which are related as:

$$J_S = Q_S \rho C_p \Delta T_1 \tag{3.8}$$

The total heated water outflow from the basin, Q_S, is computed using stratified flow theory. Consider Fig. 3-3 which shows the flow condition for stratified flow between two reservoirs connected by a sill opening of length L_s, depth H_s, and width W_s. In the left reservoir, a layer of thickness h_1 and density deficiency $\Delta\rho$ is established. Flow in the upper layer toward the right basin will occur driven by the buoyant spreading forces and opposed by inertial forces (at locations of sudden width and depth changes) and by frictional forces at the interface and bottom. A corresponding inflow occurs in the lower layer observing the continuity relation:

$$q_{net} = q_1 + q_2 \tag{3.9}$$

where q_{net} equals net flow through the opening, such as tidal in- or outflow, q_1 equals upper layer flow, and q_2 equals lower layer flow. All flow quantities are expressed as discharge per unit width of sill and a sign convention has been adopted such that all flows out of the basin are considered positive.

The basic equation which gives the change of interfacial height, a_2, for a channel of uniform width was first given by Schijf and Schönfeld (1953) as:

$$\frac{q_1^2}{ga_1^3}\frac{da_1}{dx} = \frac{\rho_1}{\rho_2}\left(\frac{da_1}{dx} + \frac{da_2}{dx}\right) + \frac{\tau_i}{\rho_2 g a_1} \tag{3.10}$$

$$\frac{q_2^2}{ga_2^3}\frac{da_2}{dx} = \frac{\rho_1}{\rho_2}\frac{da_1}{dx} + \frac{da_2}{dx} - \frac{(\tau_i - \tau_b)}{\rho_2 g a_2} \tag{3.11}$$

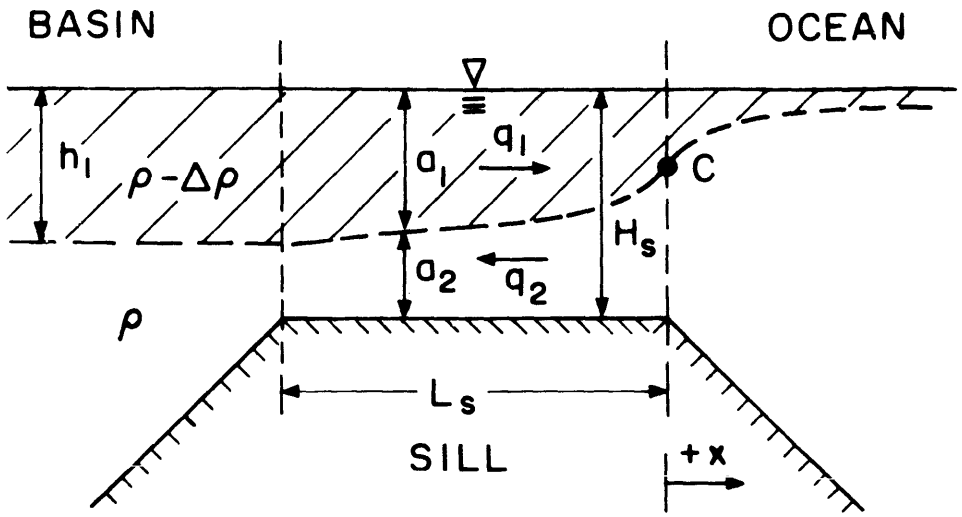

a) SINGLE CONTROL CONDITION

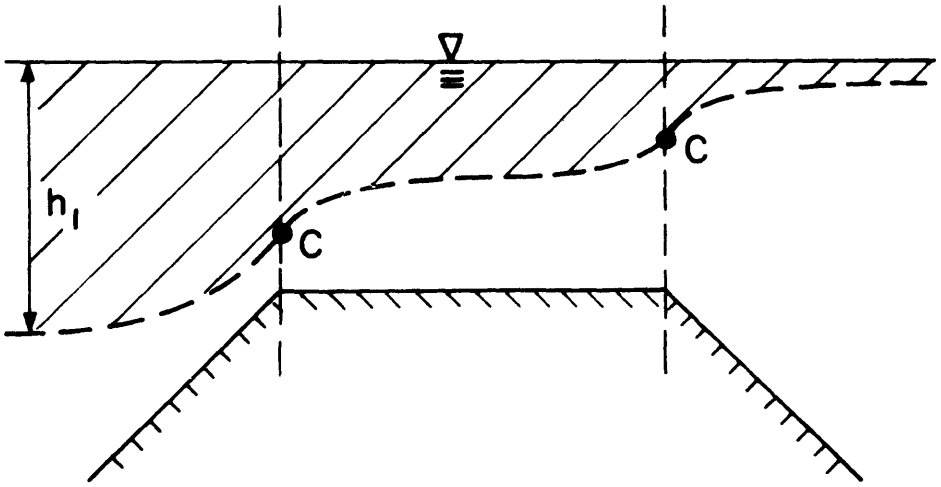

b) DOUBLE CONTROL CONDITION

Fig. 3-3: Stratified Counterflow Over a Sill

For the limiting case of small density differences, the total depth $H_s = a_1 + a_2$ can be assumed constant and the equation for the upper layer further simplifies to:

$$\frac{da_1}{dx} = \frac{\frac{1}{\Delta\rho/\rho_2}\left[\frac{\tau_b}{\rho_2 g[H_s - a_1]} - \frac{\tau_i}{\rho_2 g}\left(\frac{1}{a_1} + \frac{1}{H_s - a_1}\right)\right]}{1 - F_1^2 - F_2^2} \tag{3.12}$$

where $\Delta\rho = \rho_2 - \rho_1$

$$\tau_b = \rho_2 \frac{f_o}{8} \frac{q_2}{a_2} \left|\frac{q_2}{a_2}\right| \qquad \text{bottom stress}$$

$$\tau_i = \rho_2 \frac{f_i}{8} \left(\frac{q_1}{a_1} - \frac{q_2}{a_2}\right) \left|\frac{q_1}{a_1} - \frac{q_2}{a_2}\right| \qquad \text{interfacial stress}$$

$$F_1^2 = \frac{q_1^2}{\frac{\Delta\rho}{\rho_2} g a_1^3} \tag{3.13}$$

$$F_2^2 = \frac{q_2^2}{\frac{\Delta\rho}{\rho_2} g a_2^3} \tag{3.14}$$

Densimetric Froude numbers

In its general form it can be seen that as $(F_1^2 + F_2^2)$ approaches 1, the slope of the interface $\frac{da_1}{dx}$ will tend to infinity. This situation results in a critical control section, as shown on the right hand side of Fig. 3-3a. The concept of this critical section is analogous to control sections in open channel flow.

Solutions of this equation are readily established by inverting the above equation. For the special cases of arrested wedges

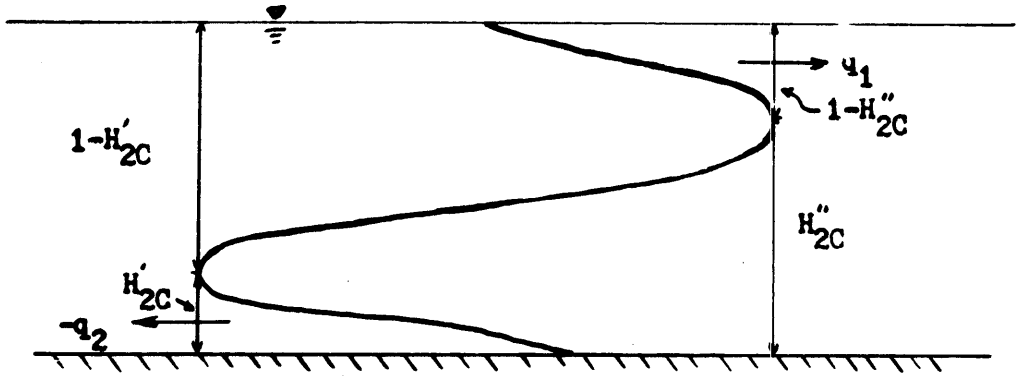

Figure 3-4: General Form of Solution to Equation (3.14)

(either $q_1 = 0$, or $q_2 = 0$) and for the equal counterflow ($q_1 = -q_2$) analytical solutions are possible (see for example, Jirka and Harleman, 1973). For more general cases, numerical integration procedures have to be used (see Rifter, 1970, and Jirka and Harleman, 1973). For this purpose, the integral expression obtained after inverting is written in non-dimensional form:

$$X_2 - X_1 = \int_{H_1(X_1)}^{H_1(X_2)} \frac{8[F_{1H}^2 (1-H_1)^3 + (F_{net}-F_{1H})^2 H_1^3 - H_1^3 (1-H_1)^3]}{f_o (F_{net}-F_{1H})^2 H_1^3 + f_i [F_{1H}(1-H_1) - (F_{net}-F_{1H}) H_1]^2} \, \mathrm{sign}(q_1) \, dH_1 \tag{3.15}$$

where the following non-dimensional lengths apply

$$X = x/H_s, \quad H_1 = a_1/H_s, \quad H_2 = a_2/H_s$$

and constant densimetric Froude numbers based on total depth are defined as

$$F_{1H} = \frac{q_1}{\sqrt{\frac{\Delta\rho}{\rho} g H_s^3}} = F_1 H_1^{3/2} \tag{3.16}$$

$$F_{2H} = \frac{q_2}{\sqrt{\frac{\Delta\rho}{\rho} g H_s^3}} = F_2 H_2^{3/2} \tag{3.17}$$

$$F_{net} = \frac{q_{net}}{\sqrt{\frac{\Delta\rho}{\rho} g H_s^3}} = F_{1H} + F_{2H} \tag{3.18}$$

The general form of the solution to Eq. (3.15) is indicated in Fig. 3-4 for a counterflow condition and consists of three branches which are divided by critical sections, where the slope of the interface goes

to infinity. The critical relation can be found by setting the numerator in Eq. (3.15) equal to zero

$$F_{1H}^{2}(1- H_1)^3+ (F_{net}- F_{1H})^{2} H_1^{3} - H_1^{3}(1- H_1)^{3} = 0 \qquad (3.19)$$

For the particular sign convention of Fig. 3-3, the following definitions hold:

$$X_1 = -L_s/H_s$$

$$X_2 = 0$$

$$\text{sign } (q_1) = +1$$

so that Eq. (3.15) can be modified to

$$\Phi = f_o \frac{L_s}{H_s} = -\int_{H_1(0)}^{H_1(\frac{-L_s}{H_s})} \frac{8[F1_H^2 (1-H_1)^3+(F_{net}-F_{1H})^2 H_1^3 -H_1^3(1-H_1)^3]}{(F_{net}-F_{1H})^2 H_1^3+\alpha[F_{1H}(1-H_1)-(F_{net}-F_{1H})H_1]^2} dH_1 \qquad (3.20)$$

where $\alpha = f_i/f_o$ is the ratio between interfacial and bottom shear factors. A constant value $\alpha = \frac{f_i}{f_o} \approx 0.5$ has been demonstrated to be adequate over a wide range of counterflow conditions (see Jirka and Harleman, 1973). The left hand side of Eq. (3.20) includes the product of the bottom friction factor times the non-dimensionalized channel length. This combination defined as Φ is considered a governing parameter of the stratified flow condition.

Eq. (3.23) can not be used directly to obtain the volume flux

through the breakwater opening, Q_S, required by Eqs. (3.4) and (3.7). Instead, an iterative procedure was used to develop a series of solution graphs, which in turn can be used to obtain Q_S during the simulation runs. The development of the solution graphs proceeded as follows:

(i) Values of F_{1H}, Φ, and F_{net} are specified.

(ii) The critical equation, Eq. (3.19) is solved to obtain the two critical values. The smaller value is $H_1(X_2 = 0)$, which is the starting condition, at the outer (ocean) end of the channel.

(iii) (a) Single Critical Regime:

The depth at the inner end of the channel, $H_1(X_1 = -L_s/H_s)$, is obtained by numerical integration of the interface equation, Eq. (3.23), i.e. making a stepwise change in H_1, until the specified value of Φ is encountered.

(b) Double Critical Regime:

Under certain conditions the equation indicates that the second critical condition is reached prior to encountering Φ. In physical terms, this would mean that a control section would be established within the channel proper which is an impossible condition. Solutions for the double critical regime are given through those parameter combinations of F_{1H}, Φ, and F_{net}, for which the upper integration limit, $H_1(X_1 = -L_s/H_s)$, in Eq. (3.20) is exactly equal to the second solution of the critical relation, Eq. (3.19). This means in physical terms that a control

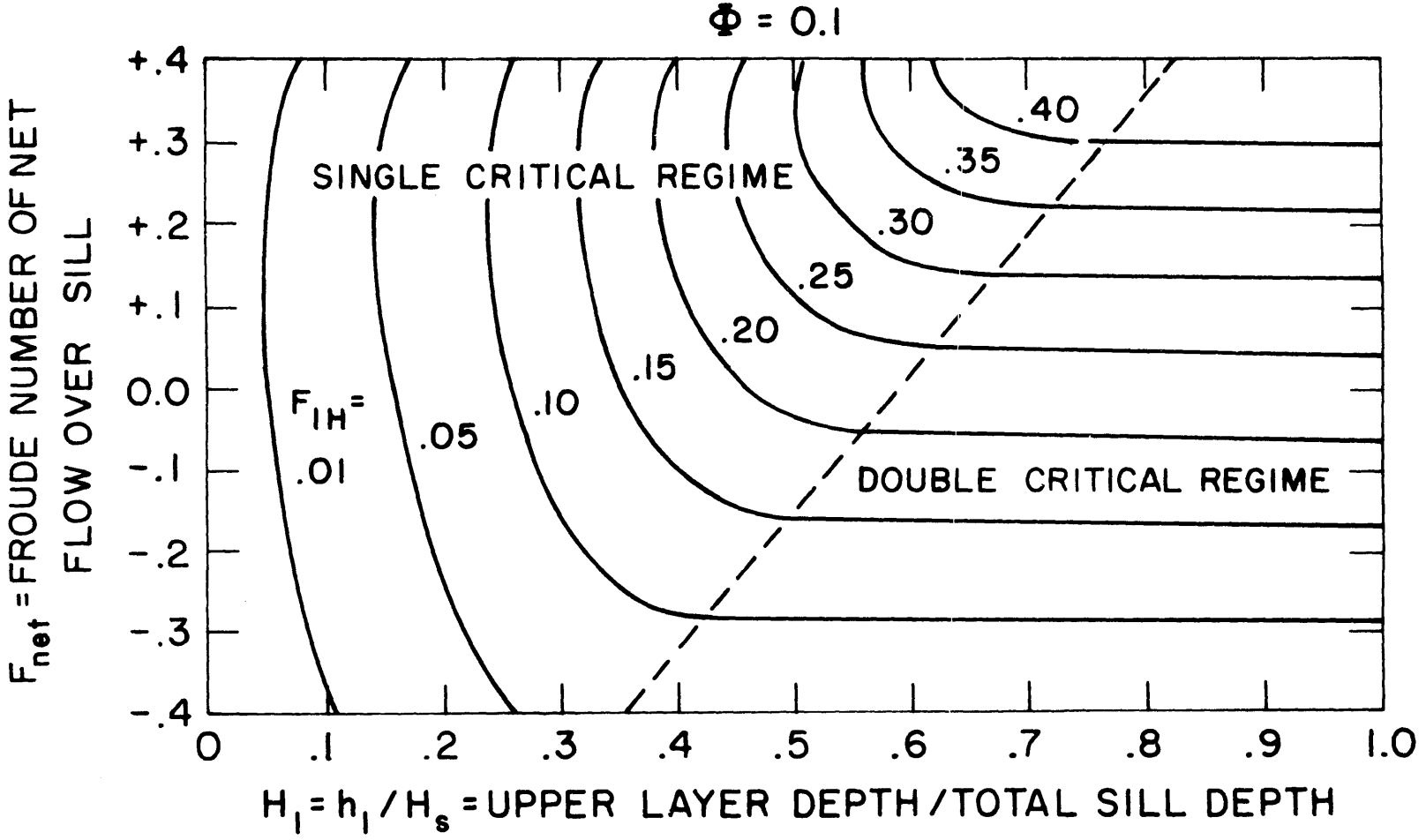

Figure 3-5: Stratified Counterflow Solution Graph for $\Phi = 0.1$

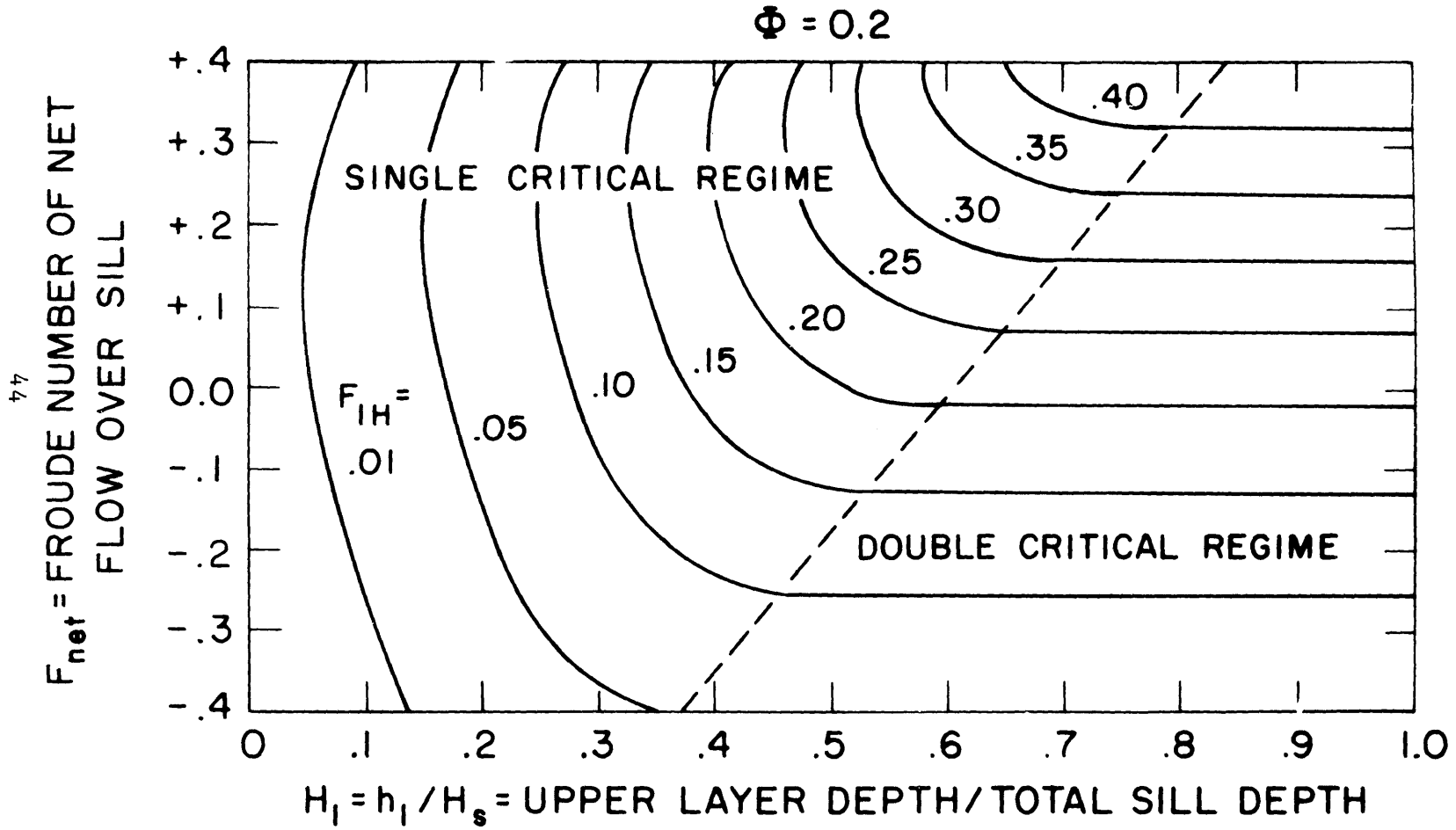

Figure 3-6: Stratified Counterflow Solution Graph for $\Phi = 0.2$

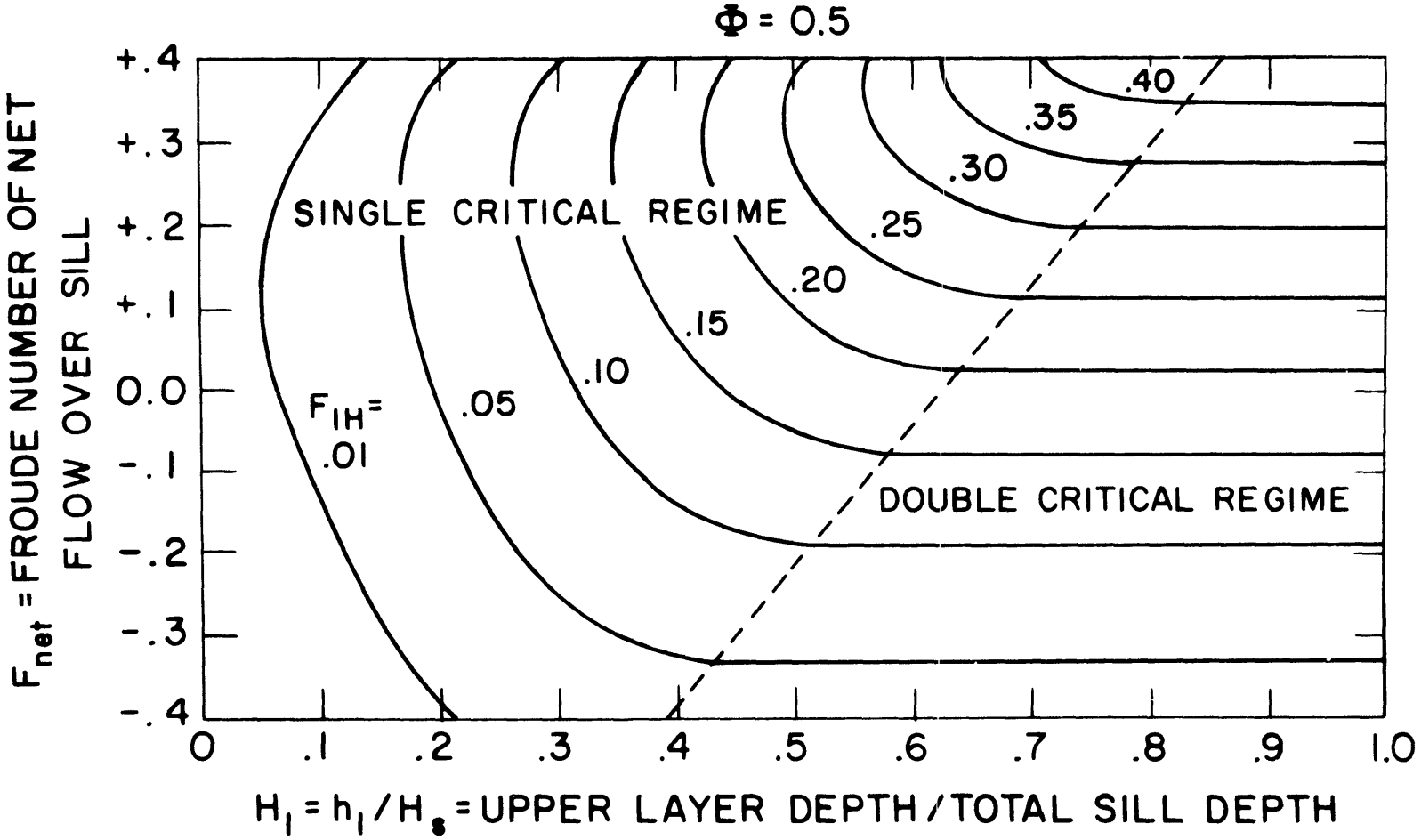

Figure 3-7: Stratified Counterflow Solution Graph for Φ = 0.5

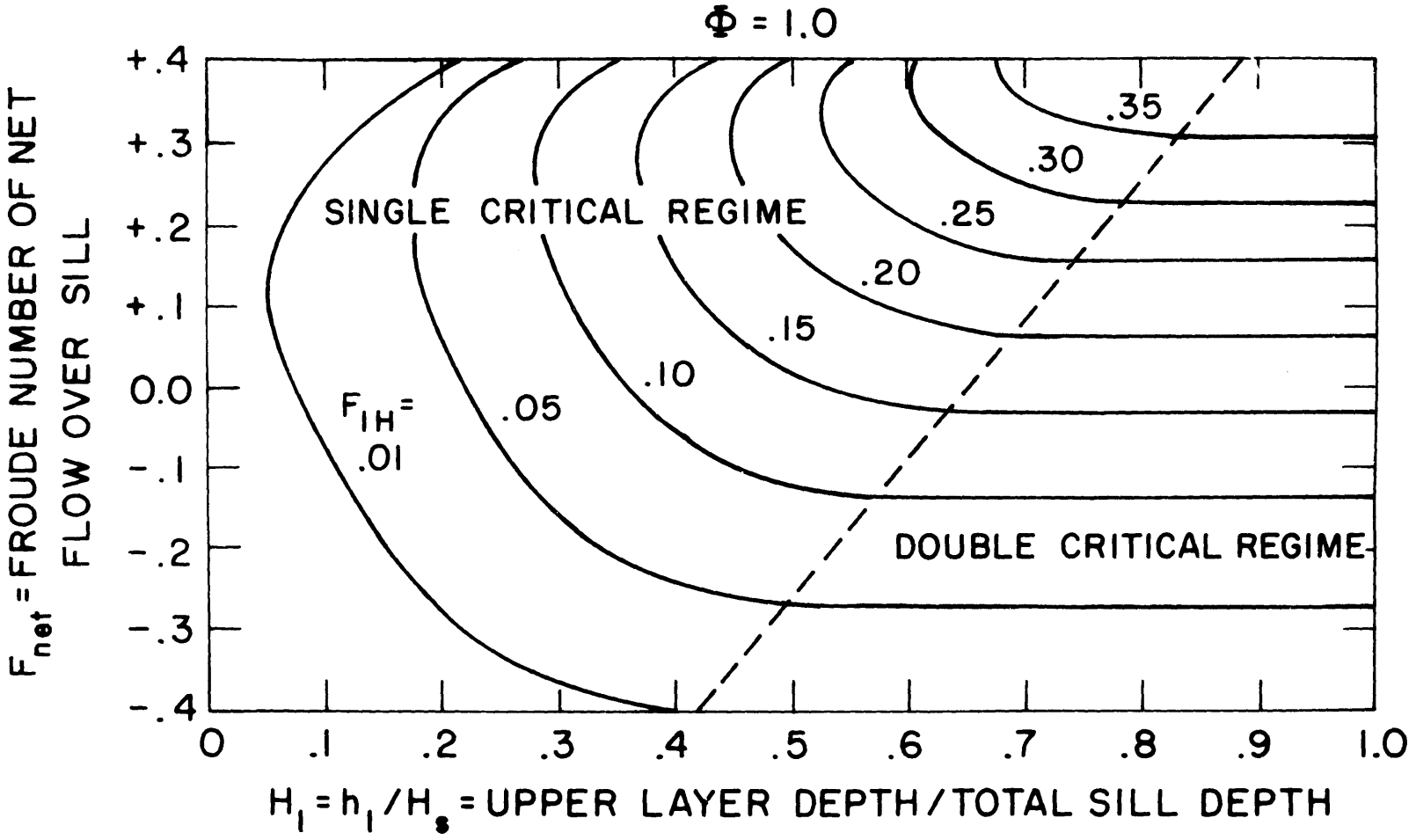

Figure 3-8: Stratified Counterflow Solution Graph for Φ = 1.0

section is also established at the inner end of the channel, see Fig. 3-3b.

(iv) This solution provides the appropriate value of H_1, which can then be used to plot a point in a solution graph such as Fig. 3-5.

(v) Repeating this procedure for various parameter combinations yields lines of constant F_{1H} as shown in Figs. 3-5 to 3-8, for given values of F_{net} and Φ. The solution graphs are divided into the single and double critical regimes. Only in the single critical regime is the resulting heated layer outflow (represented by F_{1H}) dependent on the depth H_1 at the inner channel end, as a control section exists at the outer end only. In the double critical regime, a control section exists also at the inner end. The heated layer outflow will therefore be independent of the layer depth H_1 inside the basin.

The solution graphs, Figs. 3-5 to 3-8, address the ideal case of steady flow through an interconnecting channel of rectangular cross-section. The actual conditions exhibit non-steady tidal flow and may have a rather irregular channel shape (see the AGS configuration in Fig. 2-1). The following assumptions have been made:

1) Quasi-steady approximation: it is reasonable to assume steady flow conditions during the computational time interval (0.2 hours) which is short compared to the tidal period (12.4 hours).

2) Channel schematization: the factor which controls the flow is $\Phi = \frac{f_o L_s}{H_s}$. The bottom friction factor is similar to a Darcy Weisbach friction factor in pipe flow. Typical values range from 0.01 to 0.1 depending on bottom roughness and Reynolds number. As an example, for the AGS prototype predictions, a value of 0.02 was chosen as reasonable. For the physical model prediction, a larger value of 0.05 was used. The value of L_s and H_s are taken from the assumption that a rectangular channel can approximate the more complex breakwater openings of the AGS. A rectangular cross section of 130 feet wide by 20 feet deep closely matches the cross sectional area of the actual opening at mean low water. The length, L_s, was selected as representative of the constricted distance on the sill at a depth of 20 feet and set equal to 200 feet. The value of H_s actually varies with the tide but it was assumed that a constant value of H_s = 20 feet could be used when determining Φ since normal tides are less than 5 feet at the AGS site. The result is that Φ was set equal to 0.2 for the prototype predictions and equal to 0.5 for the physical model predictions, the ratio in the Φ values being equal to the ratios in the f_o values.

From general considerations of depth, length, and friction that could be encountered during a counterflow situation, these values are reasonable. In general, the practical range of the parameter Φ should be from about 0.1, to 1.0. Figs. 3-5 to 3-8 represent calculations for

Φ equal to 0.1, 0.2, 0.5, and 1.0.

The sensitivity of the model to Φ is considered in Chapter 7 where a tidal case is considered for both Φ = 0.2, and 0.5.

In summary, solution graphs, such as Figs. 3-5 to 3-8, are used in the following manner during actual calculations. The graphs are stored in the computer in matrix form. For each simulation run, the value of Φ is specified and the appropriate matrix is selected. During each time step the following is computed:

$$q_{net} = \frac{A_t}{m\, W_s} \frac{dH_s}{dt} \tag{3.21}$$

where A_t = total horizontal surface area within the breakwater including plant areas, m = the number of breakwater openings of identical width W_s. From q_{net}, F_{net} is calculated, as in Eq. (3.20).

Referring to Fig. 3-3, the boundary condition, $H_1(-L_s/H_s)$, at the inner end of the channel is assumed to be given by the normalized average heated layer depth in the basin, h_1/H_s. This is approximately correct, since small changes in the interfacial depth will occur even during subcritical flow conditions.

Given the values of F_{net} and H_1 for each time step, the corresponding value of F_{1H} is found by interpolation between the given points in the matrix grid. Q_S is then found as follows:

$$q_1 = \sqrt{F_{1H}^2 \left[\frac{\Delta\rho}{\rho_2} g H_s^3\right]} \tag{3.22}$$

$$Q_S = m q_1 W_s \tag{3.23}$$

3.2.2 Jet Entrainment in Stratified Layer

Unstratified Receiving Water: When heated water is discharged horizontally at the surface of a receiving water body, a jet is formed that increases in size depending on the distance from the discharge point. All along the jet boundary, surrounding water is entrained into the jet as a result of the shearing action of the discharge. Fig. 3-9 illustrates the basic characteristics of a heated surface jet. At the discharge point, the discharge flow, Q_d, the average velocity, U_d, and the temperature T_d, are known. The ambient temperature of the receiving body is T_2. Several mathematical models have been proposed and verified experimentally to predict the temperature reduction and velocities in the jet as a function of distance from the discharge point.

These models have been reviewed by Jirka et al (1975). Buoyancy effects the behavior of heated surface jets in two ways: a) it tends to suppress turbulence in the vertical direction and hence entrainment into the jet at the bottom boundary, and b) in a more global fashion, it causes strong lateral spreading of the jet boundary, similar to a density front. As a consequence of this influence of buoyancy, the jet attains a maximum vertical dimension, h_{max} (since further thickening is counteracted by the lateral spreading) and the overall dilution is limited to a stable value S_S (as further dilution is inhibited because of the suppression of vertical entrainment). The behavior of a buoyant surface jet is generally measured through a densimetric discharge Froude number and a geometric discharge parameter (aspect ratio). However, if the overall condition outside the zone of flow establishment are of primary concern, it has been shown by Stolzenbach et al (1972) that a single modified Froude

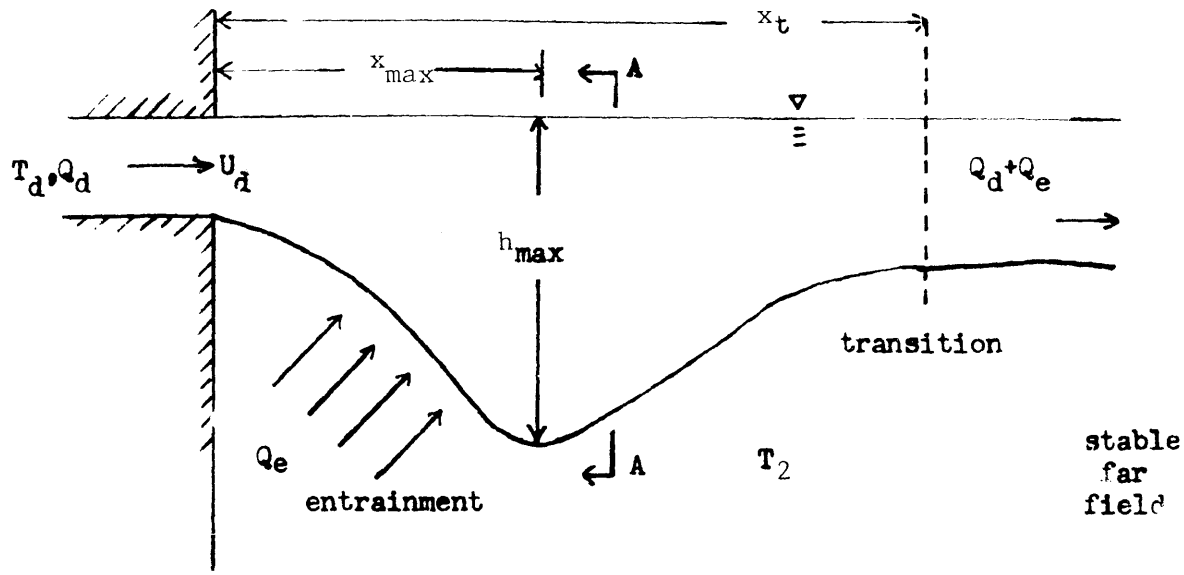

Figure 3-9a: Generalized Characteristics of a Surface Jet (Elevation View)

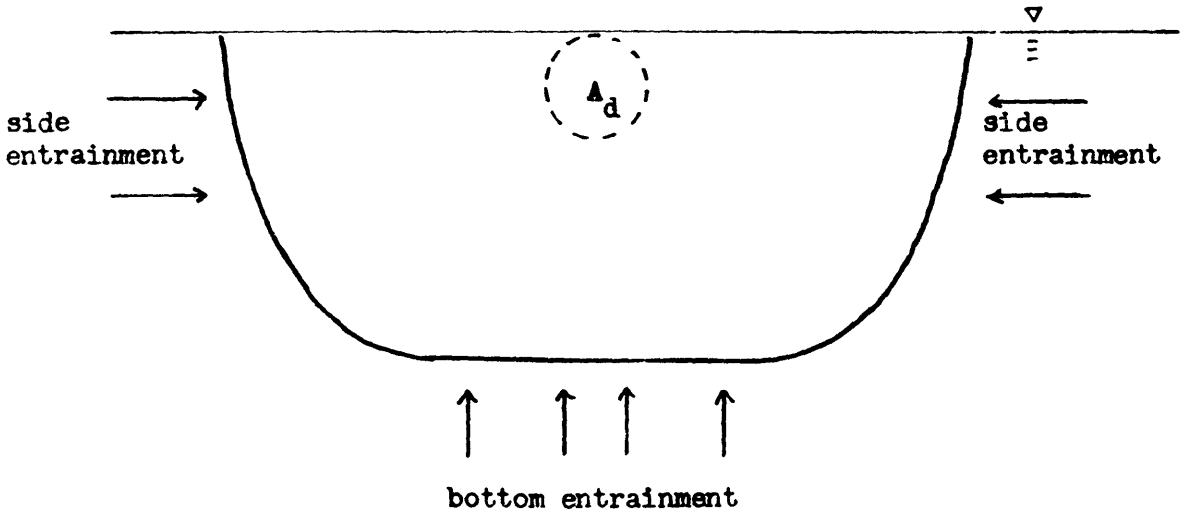

Figure 3-9b: Generalized Characteristics of a Surface Jet (Section AA)

number suffices to characterize the phenomenon

$$F_o' = \frac{U_d}{\sqrt{\frac{\Delta\rho_d}{\rho} g\, d}} \tag{3.24}$$

where U_d = discharge velocity

$\Delta\rho_d/\rho$ = relative density difference of the discharge point with respect to ambient

$d = \sqrt{\frac{A_d}{2}}$ = characteristic dimension of the discharge

A_d = total cross-sectional area of the discharge.

Using the buoyant jet model by Harleman and Stolzenbach (1971) as one of the available predictive models, Jirka et al (1975) have summarized major overall jet characteristics:

Stable (Overall) Dilution:

$$S_S = 1.4\, F_o' \tag{3.25}$$

Maximum Jet Thickness:

$$n_{max} = 0.42\, F_o'\, d \tag{3.26}$$

Inspection of the model predictions also allowed to separate the total entrained flow combined in Eq. (3.25) into two parts, namely lateral and vertical entrainment. The contribution of vertical entrainment was found to be

$$\frac{Q_{ev}}{Q_d} = E_V = 1.2\, [F_o' - 1] \tag{3.27}$$

where Q_{ev} = vertically entrained flow

Q_d = discharge flow

Stratified Receiving Water: All available predictive models for buoyant surface jets, including the above utilized model by Stolzenbach and Harleman, have been developed and are limited to unstratified

(homogeneous) receiving water.

One primary aspect of this study was to modify the existing buoyant jet formulae to take into account the distinct stratification that develops in the basin over time and the varying temperature of the stratified layer. A second problem was that since the heat load applied was a transient varying phenomena, the discharge temperature varied and could, for advanced times, become cooler than the upper layer of the receiving body.

Furthermore, in cases when the layer thickness approaches the total depth of the basin, it is likely that the entrainment flow from the lower layer into the upper layer becomes limited through the control of the stratified counterflow at the sill openings. Six possible discharge combinations in terms of buoyancy, heated layer depth and sill control are illustrated in Fig. 3-10 (cases A through F). For each of these cases, formulations for the entrainment flow from the ambient lower layer into the heated upper layer have been provided. These formulations present largely modifications of the basic buoyant jet formulae into unstratified surroundings as discussed above.

i) Buoyant Jet into Unstratified Receiving Water (Initial Phase)

Prior to the start of an emergency cooling operation, the water within the basin is assumed to be fully mixed and of uniform temperature without existing stratification. (Case A, Fig. 3-10) . Thus, for a short initial period, ambient water is being entrained into the jet zone and a heated layer starts to be established. The rate of

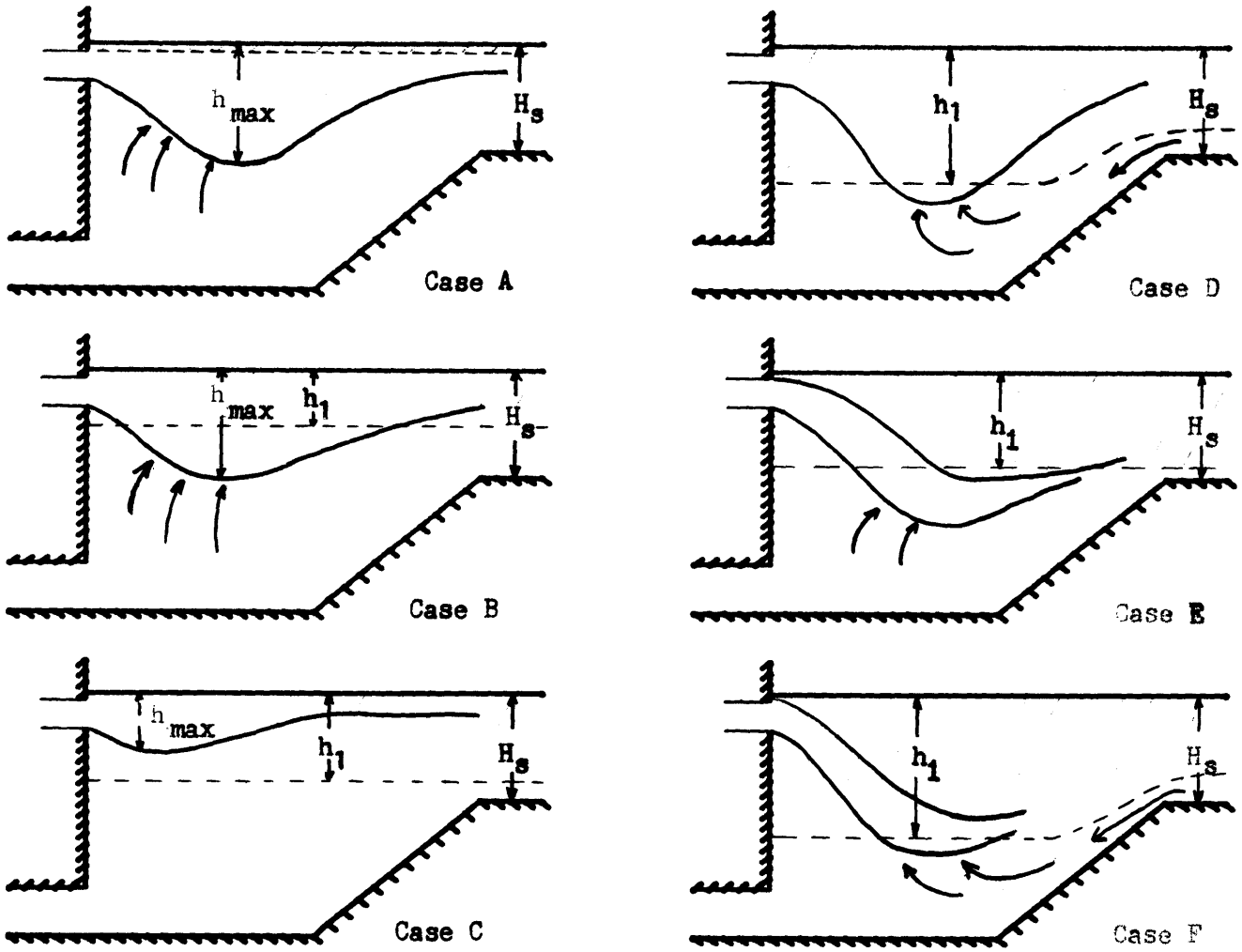

Figure 3-10: Six Possible Jet Discharge Situations into a Stratified Layer

this entrainment for each discharge jet is calculated from Eq. (3.25) as

$$Q_e^A = (S_S - 1)\, Q_d = (1.4\, F_o' - 1)\, Q_d \qquad (3.28)$$

For the condition of the AGS geometry, the duration of the initial period has been assumed as 0.2 hours (prototype based on considerations of the advance speed of a density front and using information from the physical model studies. At the end of this initial phase, a layer of uniform thickness is assumed to be present in the basin which provides the starting conditions for the subsequent entrainment calculations with stratified receiving water.

ii) Buoyant Jet in Stratified Receiving Water

The primary assumption in case of stratified receiving water is that only vertical entrainment of lower layer water affects the volume and excess heat content of the upper layer. Lateral jet entrainment is assumed to only represent recirculation of upper layer water which does not effectively change the volume and excess heat content. Secondly, it was hypothesized that the vertical entrainment of lower layer water is reduced as a function of the ratio of actual layer depth to the maximum predicted jet thickness h_{max} (Eq.3.26). Two cases are possible:

Case C (Fig. 3-10):

When the maximum predicted jet thickness h_{max} is less than a certain fraction of the layer depth h_1:

*In Eq.3.28 and all of the following formulae for Q_e, the entrainment flow that is solved for is the entrainment flow at one single discharge port based on the discharge flow through one port, Q_d. For use in the continuity equation, all of the Q_e's are summed to give Q_E or $Q_E = \Sigma Q_e$ and $Q_D = \Sigma Q_d$.

$$\frac{h_{max}}{h_1} \leq \beta \qquad (3.29)$$

then no vertical entrainment from the lower layer is assumed, $Q_e^C = 0$. This means, the entire jet dynamics including the flow outside the jet proper are confined to the upper layer without affecting the lower layer. A value of

$$\beta = 0.33$$

has been found through extensive comparison with the physical model results.*

Case B (Fig. 3-10):

Whenever the predicted jet thickness exceeds the value specified in Eq. (3.29) vertical entrainment from the lower layer will take place. The actual entrainment should therefore lie between the limits $Q_e^C = 0$ and $Q_e = Q_{ev}$ given in Eq. (3.28). A reasonable transition between these two limits is given by

$$Q_e^B = Q_d \; [1.2 \; (F_o'-1)] \; [1-0.33 \frac{h_1}{h_{max}}] \qquad (3.30)$$

In this equation, the densimetric Froude number F_o' contains, as usual, the relative density difference between discharge and ambient (lower layer). However, the value of h_{max} is predicted using a discharge Froude

*It is interesting to compare this value with the behavior of shallow water jets. Jirka et al (1975) report that the behavior of a buoyant surface jet is uninfluenced by the presence of a solid bottom as long as $h_{max}/H < 0.75 = \beta$ where H = total water depth.

number with relative density difference between discharge and upper layer water as a measure to characterize the ability of the jet to effectively penetrate into the lower layer.

Case D: (Fig. 3-10):

The third buoyant case that must be considered is the situation when the layer depth is greater than the depth of the sill openings. In this situation, the flow of water into the lower layer from the ocean is restricted by critical conditions at the breakwater openings. Under certain discharge conditions, the layer will continue to grow deeper but eventually the amount of water entrained will be limited by the flow entering the lower layer at the sills.

In the intermediate stage when the layer depth lies between the depth at the sill, H_s (20 ft below MLW for AGS) and the total depth, H_t, (47 ft below MLW for AGS), the following linear transition for the entrainment flow was assumed

$$Q_e = Q_e^B + (Q_S^* - Q_e^B) \frac{h_1 - H_s}{H_t - H_s} \qquad (3.31)$$

where Q_e^B = entrainment flow from Eq. (3.30)

Q_S^* = flow entering basin controlled by sill opening Q_S (Sect. 3.2.1) weighted by ratio of individual discharge flow Q_d to total plant(s) discharge flow Q_D

iii) Sinking (Negatively Buoyant) Jets into Stratified Receiving Water:

The third grouping of entrainment conditions deals with the situation of a sinking jet. This is possible during operation of the tran-

sient heat load when the heat load drops more rapidly than the heated layer temperature decreases. The result is a discharge density that is greater than the upper layer density but always less than the ambient density. Thus the jet will be negatively buoyant with respect to the upper layer, but positively buoyant with respect to the lower layer and will therefore wedge in between the layers. Turbulent entrainment from both upper and lower layers will occur, where the upper layer entrainment is merely considered as recirculation with no net effect.

Case E (Fig. 3-10):

The assumption is made that the sinking jet retains its full entrainment capacity when it encounters the lower layer so that

$$Q_e^E = Q_d \, [1.2 \, F_o' - 1] \qquad (3.32)$$

Case F (Fig. 3-10):

Depending on layer depth, transition similar to Eq. (3.31) is assumed between the limits of Eq. (3.32) and complete sill control when the layer depth equals the basin depth.

3.2.3 Selective Withdrawal at Intakes

The overall objective of this study was the prediction of the temperature rise at the intakes of the emergency cooling system for varying operating conditions. For this purpose, an accurate analytical expression was required to relate the percentage of upper layer heated water contained in the total intake flow into the plant.

The selective withdrawal characteristics are important not

only as regards the intake temperature rise, but also to define one flow component, Q_R, in the continuity Eq. (3.4).

A review of the literature showed that the problem of selective withdrawal into single pipe intakes with horizontal axis had only received modest attention in research. Craya (1949) treated theoretically the idealized problem of a point sink and discrete density stratification. A value for the critical Froude number of incipient withdrawal was obtained and subsequently confirmed according to Gariel's (1949) experimental investigation.

No studies had been directed at selective withdrawal into a finite size intake from a fluid system which is generally well stratified but has a diffuse interface, as shown in Fig. 3-11. A separate experimental study of this situation was undertaken and has been reported by Katavola (1975). Pertinent results of this investigation have been summarized as Appendix B. Given the geometry of the situation, three governing densimetric Froude numbers have been defined by Katavola

$$F_H = \frac{Q_i}{\sqrt{\frac{\Delta\rho}{\rho} g H_i^5}} \tag{3.33}$$

$$F_D = \frac{Q_i}{\frac{\pi}{4}\sqrt{\frac{\Delta\rho}{\rho} g D^5}} \tag{3.34}$$

$$F_\ell = \frac{Q_i}{\sqrt{\frac{\Delta\rho}{\rho} g \ell^5}} \tag{3.35}$$

where

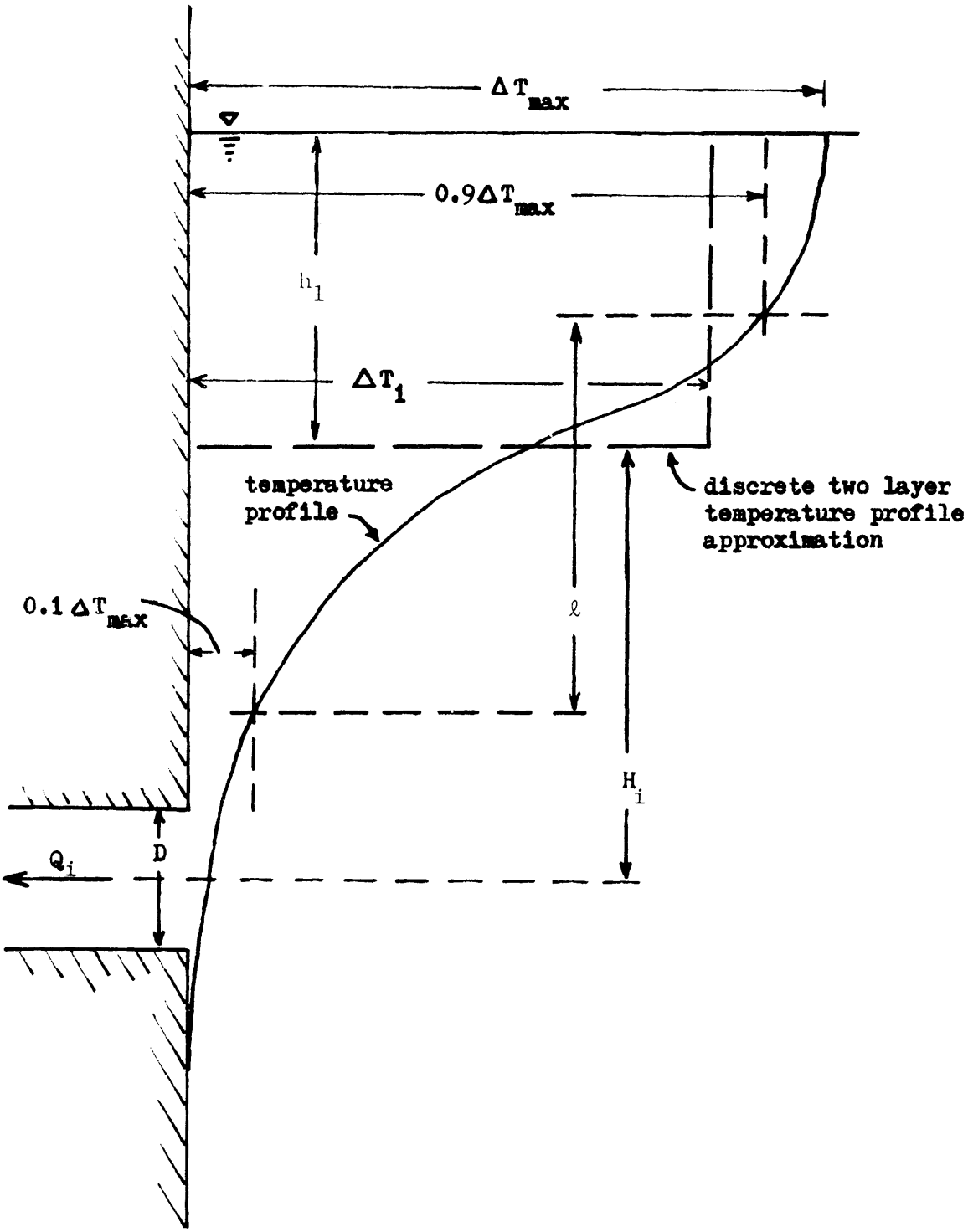

Figure 3-11: Selective Withdrawal from a Stratified Fluid

Q_i = intake flow into a given intake

H_i = distance between layer interface and centerline of intake

D = diameter of circular intake

ℓ = the thickness of the interface transition zone defined as the vertical distance between a 10% and a 90% rise in the temperature above ambient

$\Delta\rho$ = density difference between upper and lower layers.

The major parameter which defines the general response of the system in terms of selective withdrawal is F_H. The additional parameters F_D and F_ℓ are of secondary nature and signify geometric effects superimposed on the major response. Typical withdrawal curves which relate the withdrawal rate λ

$$\lambda = \frac{Q_r}{Q_i} = \frac{T_i - T_2}{T_1 - T_2} \tag{3.36}$$

where Q_r = intake flow from upper layer

Q_i = total intake flow for an individual opening

T_i = intake temperature

to the parameters F_H, F_D and F_ℓ are shown in Appendix B. Katavola concluded that the values of F_D and F_ℓ do not affect the shape of the withdrawal curve but only its location. In particular, a critical Froude number F_{H_C} for incipient withdrawal * (λ=0) can be defined which is a function of F_D and F_ℓ only

*This neglects small withdrawal effects (in the order of $< 3\%$) which are always indicated even at lower values of F_H.

$$F_{H_C} = 0.026 \ell n F_D + 0.64 F_\ell \quad (3.37)$$

Using this definition, the withdrawal Froude number F_H can be normalized and experimental results can be plotted on a single graph (Appendix B). The best-fit analytical expression derived from such graph is

$$\text{For } \frac{F_H}{F_{H_C}} \leq 300 \quad \lambda = 6.2 \ell n \left[\frac{F_H}{F_{H_C}} \right] \% \quad (3.38a)$$

$$\text{For } \frac{F_H}{F_{H_C}} > 300 \quad \lambda = 50 \left[1.0 - \left(\frac{F_H}{F_{H_C}} \right)^{-.22} \right] \% \quad (3.38b)$$

When entering these expressions into the analytical model, consideration had to be given to the situation where the layer depth exceeds the intake depth. The formulation of Equation 3.38b reaches a maximum of 50% when H goes to zero, or the interface is located at the centerline level of the intake. For the condition when the interfaee drops below the centerline level, lower layer water is being selectively drawn up into the intake in a fashion symmetric to the original case. Thus H is taken as the absolute value of the difference between layer depth and intake center line, and the values of λ as indicated by the above equations in fact refer to the withdrawal of the lower layer water.

For use in the continuity equation Q_r is defined as:*

$$Q_r = \lambda Q_i \quad (3.39)$$

---

*Q_r is the recirculation flow at one single intake. For use in the continuity equation, all the intakes are summed, or $Q_R = \Sigma Q_r$

The intake temperature rise is defined as:

$$\Delta T_i = \lambda[\, T_1 - T_2 \,] = \Delta T_r \qquad (3.40)$$

3.2.4 Heat Dissipation to the Atmosphere

The term J_A in the heat conservation Eq. (3.7), represents the net flux of heat from the heated water surface within the basin. Ryan and Harleman (1973) presented a comprehensive study of heat dissipation from heated water surfaces.

A complete expression for the net heat flux across the air-water interface has been given by Ryan and Harleman as:

$$\phi_n = \phi_r - \left[4\times10^{-8}(T_s+460) + [22.4(\Delta\theta_v)^{1/3} + 14W_2][(e_s - e_a) + 0.255(T_s - T_a)]\right] \qquad (3.41)$$

where ϕ_n = net heat flux (BTU/day - sq.ft)

ϕ_r = net radiation

$\Delta\theta_v$ = virtual temperature difference = $T_{sv} - T_{av}$ (°R)

where $T_{sv} = (T_s + 460)/(1 - 0.378\, e_s/p)$ (°R)

$T_{av} = (T_a + 460)/(1 - 0.378\, e_a/p)$ (°R)

T_s = surface temperature (°F)

T_a = air temperature (°F)

e_s = saturated vapor pressure at T_s (mm Hg)

e_a = water vapor pressure 2 meters above surface (mm Hg)

p = atmospheric pressure (mm Hg)

W_2 = wind speed at 2 meters above surface (mph)

Prototpye Conditions. - The proper use of this formulation requires extensive meteorological data. Due to the lack of a standard set of meteorological conditions for the purpose of emergency cooling computations it was decided that the prototpye predictions utilize the linear approximation for Φ_n given by:

$$\Phi_n = K_e [T_s - T_E] \tag{3.42}$$

where K_e = heat exchange coefficient (BTU/hr - °F - sq.ft.)

T_s = surface temperature (°F)

T_E = equilibrium temperature of the water body (°F), defined by the condition of zero net heat flux across the surface

Further simplifying assumptions were made as follows: (i) The equilibrium temperature T_E was assumed to be equal to the ambient water temperature and high values were chosen for the latter, corresponding to summer conditions. (ii) Conservatively low values for the surface heat exchange coefficient, K_e, were assumed. Using these assumptions, the total heat flux from the basin surface area is

$$J_A = K_e \Delta T_1 A_S \tag{3.43}$$

The sensitivity of the results due to the above assumptions was evaluated (see Chapter 7).

Laboratory Simulations: - The actual laboratory "meteorological" data was available for the mathematical simulation of the

experimental runs. The air temperature and relative humidity were measured, and this permitted the use of a modified version of the complete heat dissipation equation, Eq. (3.41). The following modification to the radiation component in Eq. (3.41) was recommended by Ryan and Harleman (1973).

$$\Phi = 0.97\ [4 \times 10^{-8} (T_a + 460)^4] \qquad (3.44)$$

This formulation considers the interior of the laboratory to be radiating as a grey body. Forced convection was neglected as the windspeed w_2 was taken as zero.

3.3 Solution Technique

The basic differential Equations, Eqs. (3.4) and (3.7) are solved simultaneously using the RKGS subroutine (Runge-Kutta solution algorithm), available on the SSP package with FORTRAN IV. In this Runge-Kutta subroutine, the user specifies the right hand side of each differential equation, initial conditions, and the time step to be used during the simultaneous solution. At each time step, the program solves the right hand side of each equation using the dependent variables determined at the previous time step. A time step of 0.2 hours (prototype)was found to provide good results, and was used in all simulation runs discussed in the remainder of the report.

CHAPTER 4

Development of the Physical Scale Model

The physical scale model was constructed and operated in order to provide a) basic insight into the fluid dynamics to aid in the development of the predictive theoretical model, b) a verification base for the theoretical model, and c) initial physical data on system performance. The physical model simulated the Atlantic Generating Station and incorporated all the major physical features. The experimental program and results are reported in Chapter 5. This chapter reports the design, construction, and operating procedures relating to the model.

4.1 Scaling Considerations

In order to obtain accurate quantitative data from a physical model study, it is necessary that the characteristic dynamic and geometric non-dimensional parameters of the model equal those of the prototype. Strict fulfillment of this requirement is generally impossible to achieve for all parameters, and thus a choice relating the relative importance of the parameters must be made.

The key parameter in any thermal discharge problem is the densimetric Froude number. This can be generally defined as:

$$F = V/\left[\frac{\Delta\rho}{\rho} gZ\right]^{1/2}$$

where

V = characteristic velocity

Z = characteristic vertical length

$\Delta\rho$ = characteristic density difference due to temperature differences

ρ = ambient density

In the following development the subscript p indicates the prototype, the subscript m is the model, and the subscript r is the ratio of prototype quantity to model quantity. The velocity ratio that will insure equality of the densimetric Froude numbers can then be obtained as follows:

$$\frac{V_p}{\left[\left(\frac{\Delta\rho}{\rho}\right)_p g Z_p\right]^{1/2}} = F_p = F_m = \frac{V_m}{\left[\left(\frac{\Delta\rho}{\rho}\right)_m g Z_m\right]^{1/2}}$$

$$V_r = \frac{V_p}{V_m} = \frac{\left[\left(\frac{\Delta\rho}{\rho}\right)_p g Z_p\right]^{1/2}}{\left[\left(\frac{\Delta\rho}{\rho}\right)_m g Z_m\right]^{1/2}} = \left[\left(\frac{\Delta\rho}{\rho}\right)_r Z_r\right]^{1/2}$$

Since density differences in the model are conveniently taken equal to the prototype, $\left(\frac{\Delta\rho}{\rho}\right)_r = 1$, it follows that:

$$V_r = Z_r^{1/2} \tag{4.1}$$

The time ratio is then

$$t_r = Z_r/V_r = Z_r^{1/2} \tag{4.2}$$

Equation 4.1 is the single most important scaling requirement for modeling a heated discharge. It describes the convective responses (current field) due to the basic driving forces (elevation changes and

buoyancy). Due to the importance of convection for heat transport, the condition of Equation 4.1 can never be relaxed.

The distortion of a physical scale model is defined by

$$D = \frac{Z_r}{L_r} \tag{4.3}$$

A model which observes the Froude criterion can be either undistorted (D=1) or distorted ($D \neq 1$). The choice of the distortion ratio is dependent on the similitude requirements for the additional physical phenomena of importance. These are from the discussion in Chapter 3:

i) Jet mixing

ii) Stratified flow

iii) Heat dissipation

(i) In the case of turbulent jet mixing, the parameter of interest is the Reynolds number. The requirement for Reynolds similarity can not be satisfied in a Froude model. The Reynolds number in the model is always smaller than in the prototype. However, it has been found that if the Reynolds number is larger than a critical value, the jet mixing characteristics are essentially independent of the Reynolds number. In his experiments, Ungate (1974) found that jet dilution was independent of Reynolds numbers as long as a critical Reynolds number

$$Re_c = \frac{V_o D}{\nu} = 1500$$

was exceeded, where V_o = jet exit velocity, D = jet diameter, and ν = kinematic viscosity. This criterion provides a limit

on the minimum scale ratio which can be used in the model. A model involving jet mixing processes also should be undistorted (D=1), since turbulent jet geometries (such as spreading angles, penetration depths, etc.) cannot be changed according to distortion ratios. A complete discussion on this requirement for an undistorted model has been given by Jirka et al. (1975).

(ii) When considering stratified flow or any other flow that is controlled by friction, correct modeling of the frictional resistance is important. For the case of stratified flow, the necessary condition (derived from stratified flow equations) is that

$$f_i \left(\frac{L}{Z}\right)_r = 1 \qquad (4.5)$$

where f_i is the interfacial friction factor.

Since $(f_i)_r$ is not normally = 1 because of low Reynolds number effects in scale models, the above condition requires a distorted model (typical distortions are of the order of 4 to 10).

(iii) In order to provide complete similitude when modeling surface heat loss, the condition (derived from a linearized heat loss equation)

$$\left(\frac{K_r L_r}{Z_r^{3/2}} \right) = 1 \qquad (4.6)$$

where K = surface heat loss coefficient, should be satisfied. The required distortion ratio

$$D = \frac{K_r}{Z_r^{1/2}} \qquad (4.7)$$

is therefore dependent both on the vertical scale of the model and the laboratory heat loss conditions. Typical required values are on the order of 3 to 5.

Thus the need to have an undistorted model to properly represent jet mixing is in direct conflict with the distortion ratios required for exact modeling of stratified flow and heat dissipation: As jet mixing is expected to be a critical factor in prototype behavior, an undistorted model was chosen. Thus this model by necessity does not provide an exact replication of the prototype, but serves as a reliable data base for verification of the analytical model.

4.2 Breakwater-Basin Construction

The physical model was constructed in the 37 ft x 18 ft x 1.5 ft test basin on the first floor of the Parsons Laboratory. The topography of the AGS breakwater enclosure was extracted from prototype drawings prepared by F.R. Harris Inc., Consulting Engineers, for the New Jersey Public Service Electric and Gas Company. All dimensions were reduced by a factor of 1/81 and then rounded to the nearest 1/8 inch. This represented an accuracy of ±0.42 feet in the prototype. Figure 4-1 illustrates the scaled dimensions of the model relative to the basin in which it was located. Only the interior details were modeled as the exterior of the breakwater arrangement was not of concern to the study.

The bottom topography within the basin, including the sills, was modeled by means of wooden templates. The templates were cut to properly model a given cross section of the prototype. They were then placed in the model tank at the correct position and the void space between

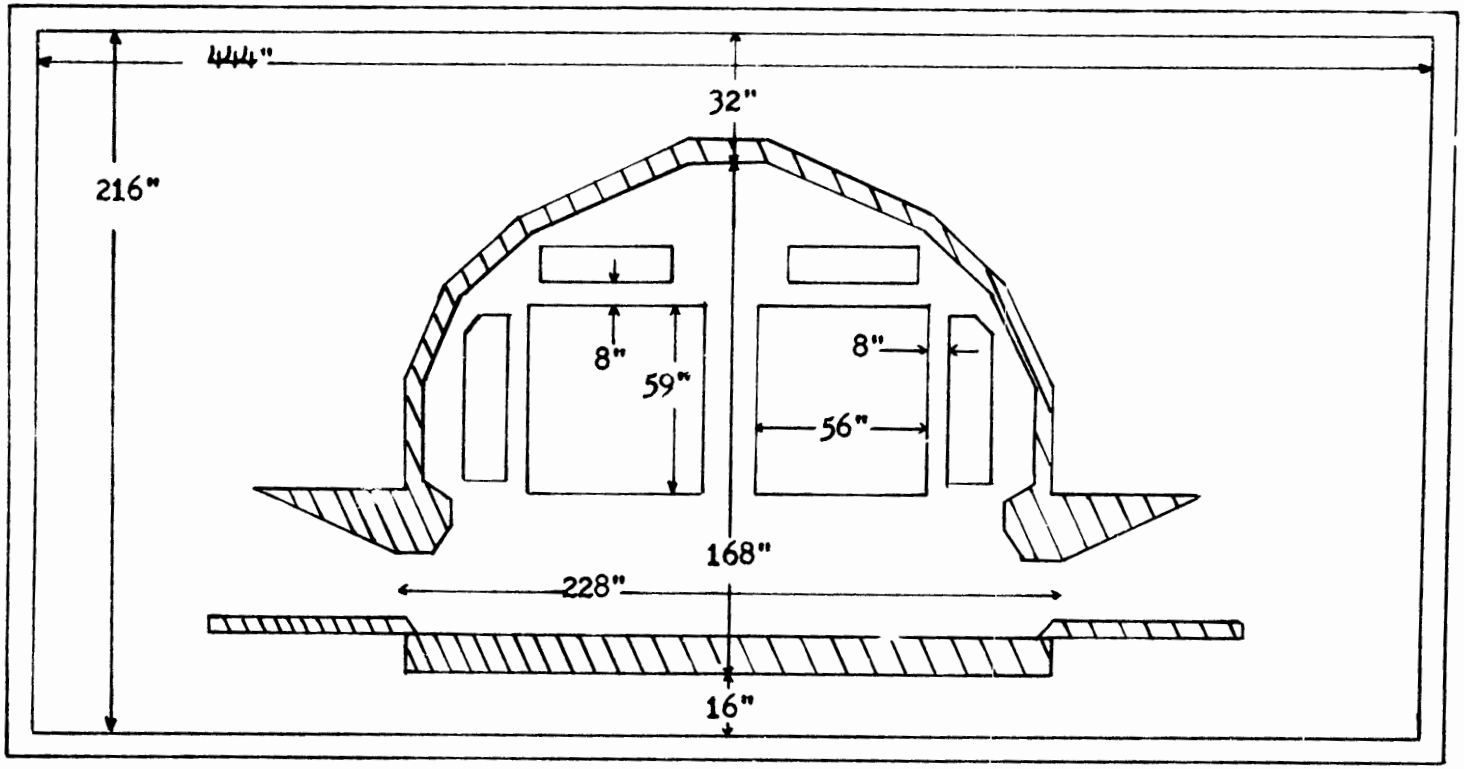

Figure 4-1: Dimensions of Physical Scale Model

adjacent templates was filled with concrete poured at a continuous slope between the pair of templates. The elevation of each template was referenced to a common datum with the aid of a surveyor's level. Figures 4.2 and 4.3 illustrate the model construction stages before and after the fill was poured between the templates.

The mooring caissons were constructed with concrete blocks. Attached to each caisson were two rods to which the stabilizing struts of the floating plants were attached.

The breakwater was also constructed of concrete block along the straight section at the front of the plants. The interior side of the curved section of the breakwater was built using plywood templates and concrete fill. The exterior side was formed through concrete blocks. Most of the construction features of the basin can be seen in Figures 4-4 and 4-5.

4.3 Floating Plant Construction

The floating nuclear power plants were modeled as plywood boxes. They were attached to the caissons using struts to provide lateral stability, but waterproofed and designed to float so that they would rise and fall with the tide. The draft of each plant was established using concrete bricks as ballast and then water to provide the final trim. The water line was clearly marked on all sides of the plant to assist in maintaining the correct elevation.

4.4 Operating Systems

The operating systems of the model included the ARW and ERW

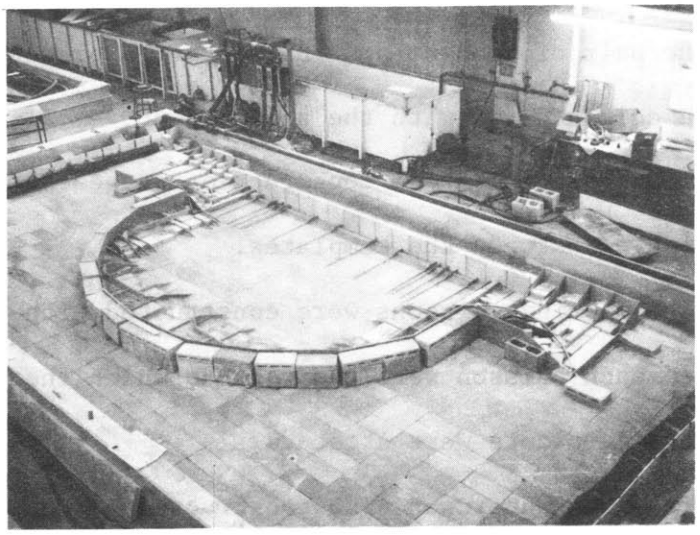

Figure 4-2: Physical Model during Construction Showing Bottom Templates

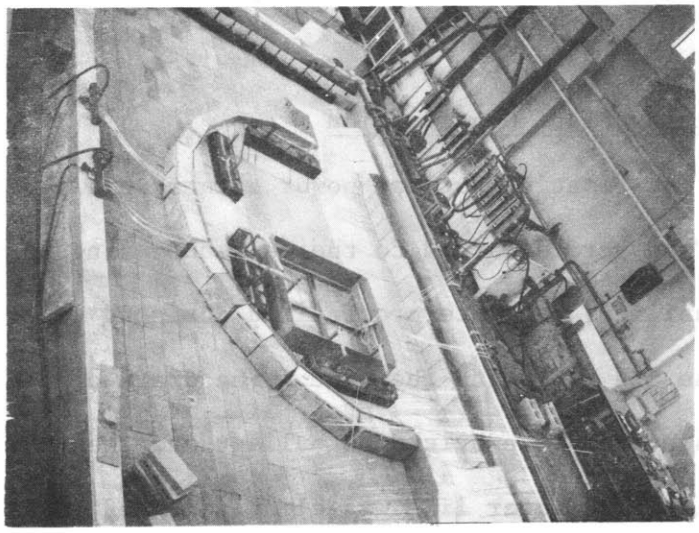

Figure 4-3: Physical Model during Construction after Templates were filled with Concrete

Figure 4-4: Close Up of Physical Model Breakwater Opening

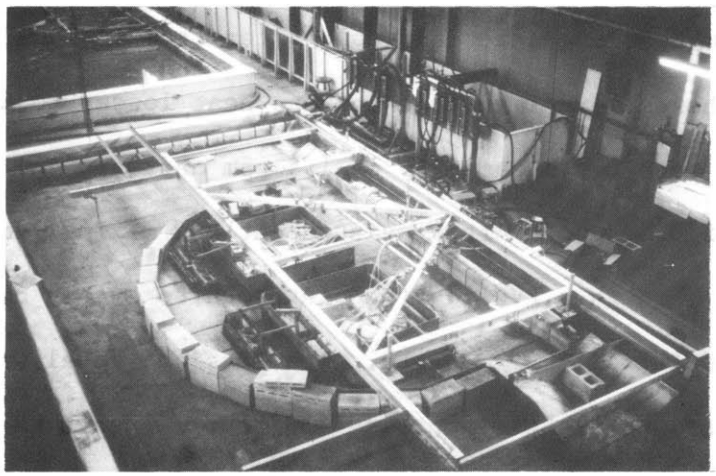

Figure 4-5: Complete Physical Model Showing Moveable Probe Support Frame

intakes and discharge piping, the temperature instrumentation network, and the tidal pumping system.

4.4.1 Intake and Discharge Systems

The central purpose of this investigation was to study heat dissipation by the emergency cooling systems of floating power plants. Thus it was necessary to model the emergency cooling systems in such a way as to permit variation of flow rates and heat loads. Figure 4-6 illustrates the system in its final development. The basic plan was to mix hot and cold water at the appropriate ratio to provide the same ΔT at the discharge as in the prototype. The intake system then removed the same volume of water but discharged it into a drain. Thus the model does not operate in a closed loop mode where the intake water is heated by the plant and then discharged as is the case with the prototype.

The source of hot water was a mixing valve taking hot water from a steam heat exchanger and cold water from the building system. The hot water hoses were insulated to keep heat losses to a minimum. The flow meters each had a capacity of 1.5 gpm and were calibrated with an accuracy of 0.02 gpm. After measurement and mixing, the discharge water passed through a PVC manifold intended to evenly distribute the flow to each of the discharge ports. The physical model was constructed with three separate ARW discharges and four separate ERW discharges since that was the design at the time of model construction. Thus the system varies from the current design that utilizes three combined discharge ports. The discharge ports were made of copper tubing with inside dia-

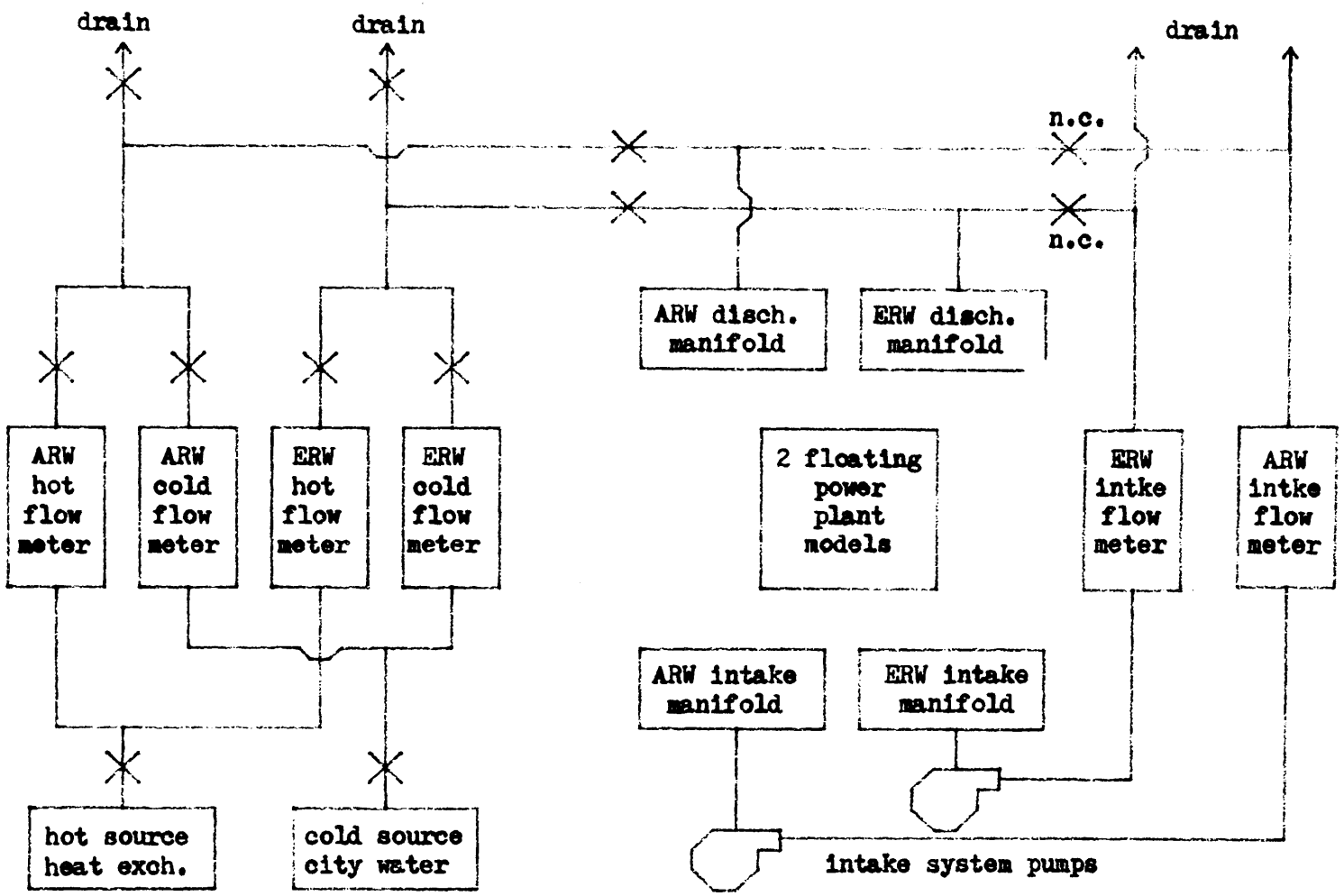

Fig. 4-6: **Flow Diagram of Physical Model's ARW and ERW Systems**

meters selected to match as closely as possible the initially designed diameters of the discharges. For the ARW discharge, $\frac{13}{16}$ " tubing was used, that equates to a 5.48 ft. diameter. For the ERW discharge, $\frac{9}{16}$" tubing was used that equates to a 3.8 ft diameter. Tygon tubing was used to connect the manifolds with the discharge ports. Care was taken to use the same length of tubing for each discharge to attempt to provide uniform head loss and thus equal flow to each discharge port.

On the intake side, a 1/2 hp centrifugal pump was used to provide suction to each intake manifold. Tygon tubing was used to connect the manifolds with the individual intakes. The intakes were placed at the initial design depth of twenty feet (prototype) below the water surface. The intake ports again used standard copper tubing. The ARW intake used 1" tubing which equals a 6.96 ft. diameter and the ERW intake was $\frac{13}{16}$ " tubing or the equivalent of 5.48 feet in diameter.

During normal operation, the intake and discharge systems were completely separated but prior to the start of an experiment they were cross connected using those valves marked n.c., for normally closed, on Figure 4-6. This permitted introduction of ambient water from the basin into all sections of intake and discharge lines prior to the start of the experiment.

4.4.2 Temperature Instrumentation

The primary data collected during the course of an experimental run were the temperatures at a large number of locations in the basin and associated water circulation systems. The temperatures were measured using two types of thermistor probes. The majority of basin readings were

taken using a wafer type thermistor probe No. 15203x of Yellow Springs Instrument Company.

The second type of probe was mostly used to measure temperature within the hoses and manifolds of the piping networks. These were Yellow Springs Series 400 interchangeable probes with flexible tips.

All of the probes were connected to a 100 channel digital thermal scanner supplied by Data Entry Systems. The scanner automatically scanned the full set of probes and then recorded the temperature on both a printed tape and on teletype punch tape. The scanner was intended to operate at one channel per second, but experience showed that accuracy was seriously impaired at the higher speed and thus the experiments were run at about 2 seconds per probe. The entire system accuracy of the temperature measurements is 0.1°F which includes individual calibration of each probe.

The majority of probes were attached to an aluminum frame equipped with motor driven screw jacks that permitted the automatic, vertical movement of the frame, and thus the probes, to any desired depth. The frame is evident in Figure 4-5.

During the course of the investigation, three probe location arrangements were utilized. Figure 4-7 illustrates the arrangement for experiments 1 to 9. Figure 4-8 illustrates the improved version used for experiments 10 to 14, and 19 to 20. Fig. 4-9 illustrates the slight modification used when an oil boom was in place. The primary difference between the first and second arrangements is the use of vertical clusters of four probes rather than individual probes. A typical cluster is shown in Figure 4-10. The need for this became apparent after the first series of experiments were completed. The problem was in the total length

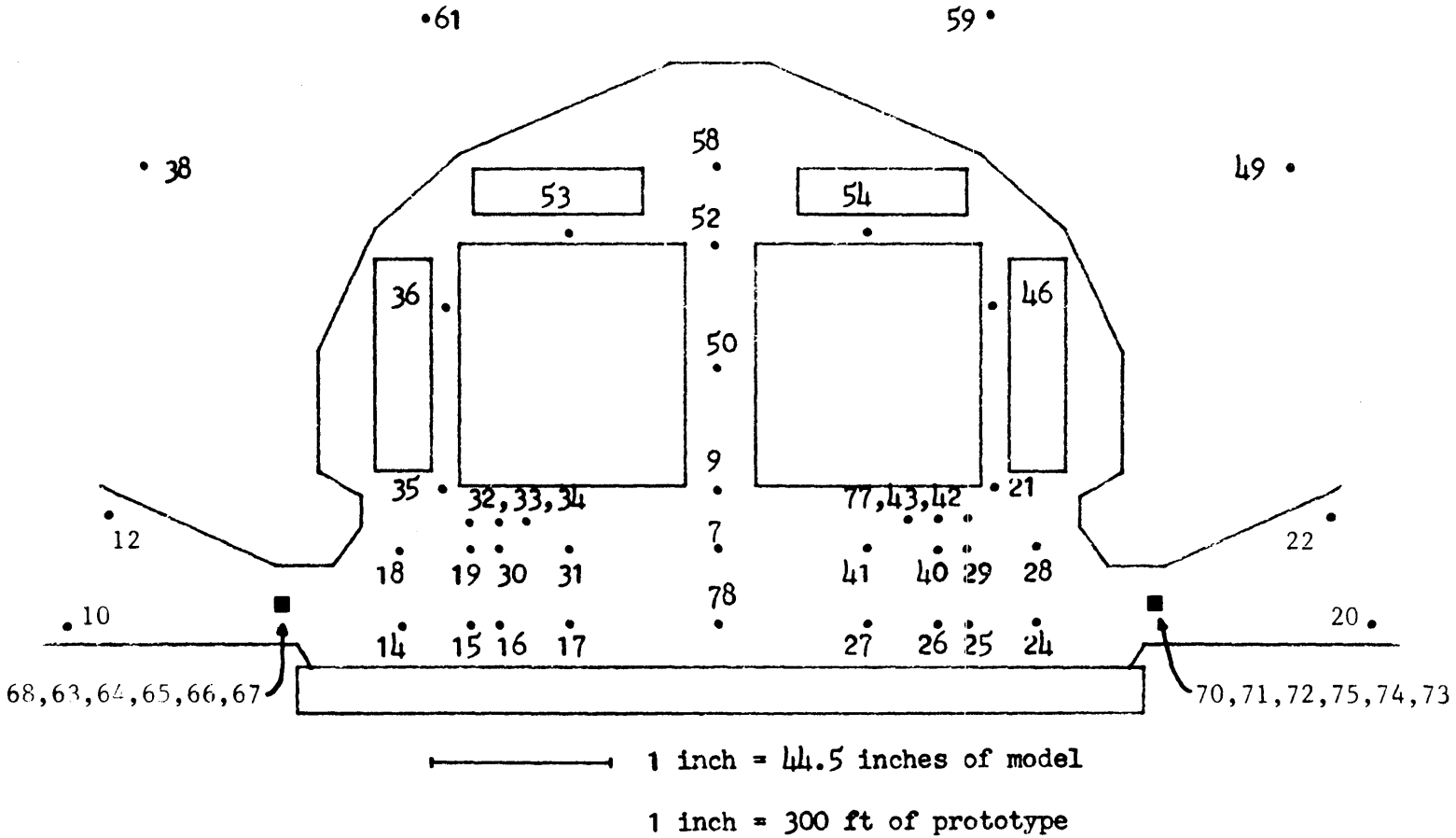

Figure 4-7: Probe Locations for Experiments 1-9

Location #	1	2	3	4	5	6	7	8	9	10	11	12	13	14	15	16
top	2	38	34	42	30	20	6	24	15	46	10	50	63	71	75	74
	3	39	35	43	31	21	7	26	16	47	12	51	64	73	76	
Probes	4	40	36	44	32	22	8	27	17	48	13	52	65			
bottom	5	41	37	77	33	23	9	29	18	49	14	53	66			
												54	67			
												55	68			

16

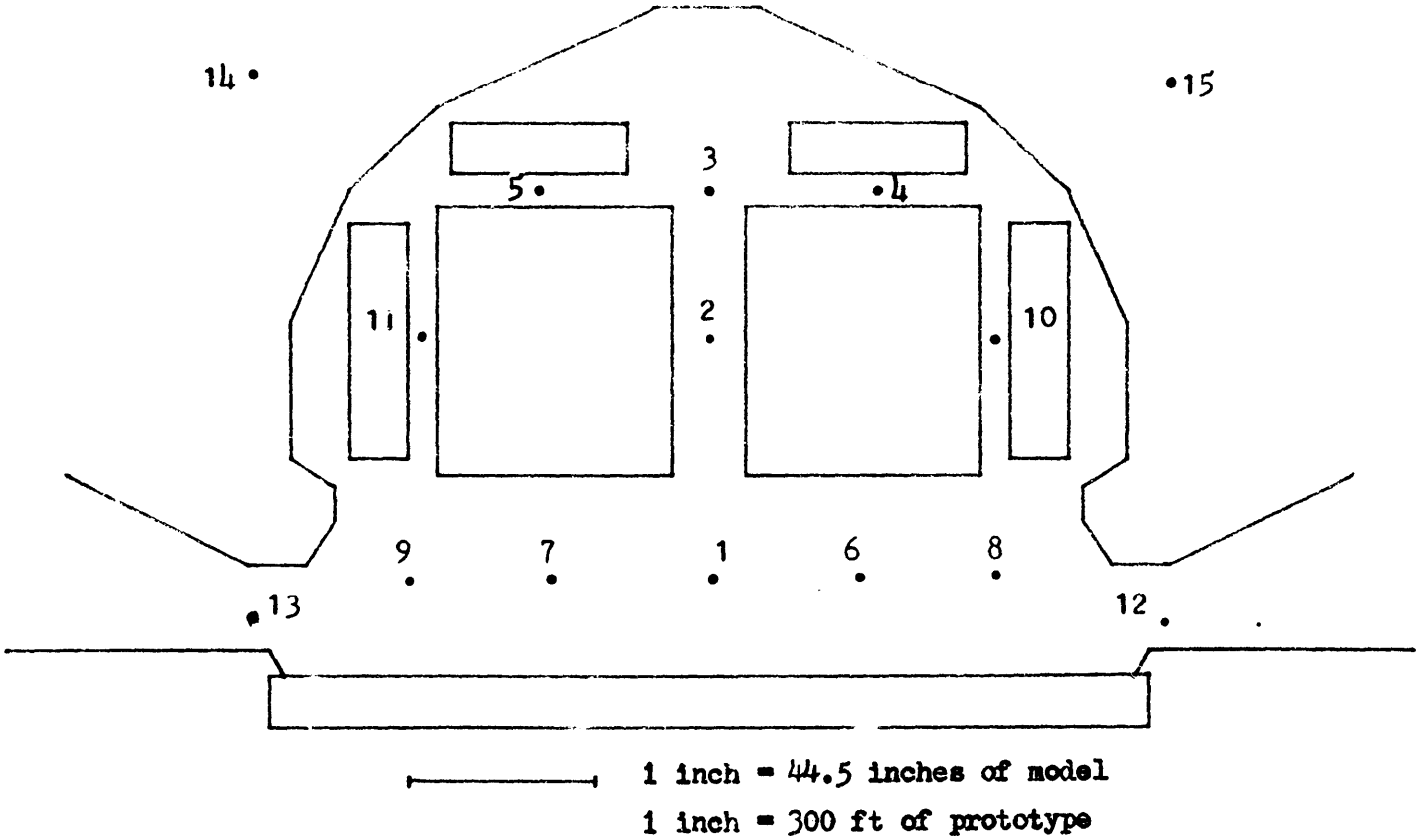

Figure 4-8: Probe Locations for Experiments 10-14, 19, 20

Location #	1	2	3	4	5	6	7	8	9	10	11	12	13	14	15	16
top	2	38	34	42	30	20	6	24	15	46	10	50	63	71	75	74
	3	39	35	43	31	21	7	26	16	47	12	51	64	73	76	
Probes	4	40	36	44	32	22	8	27	17	48	13	52	65			
bottom	5	41	37	77	33	23	9	29	18	49	14	53	66			
												54	67			
												55	68			

16

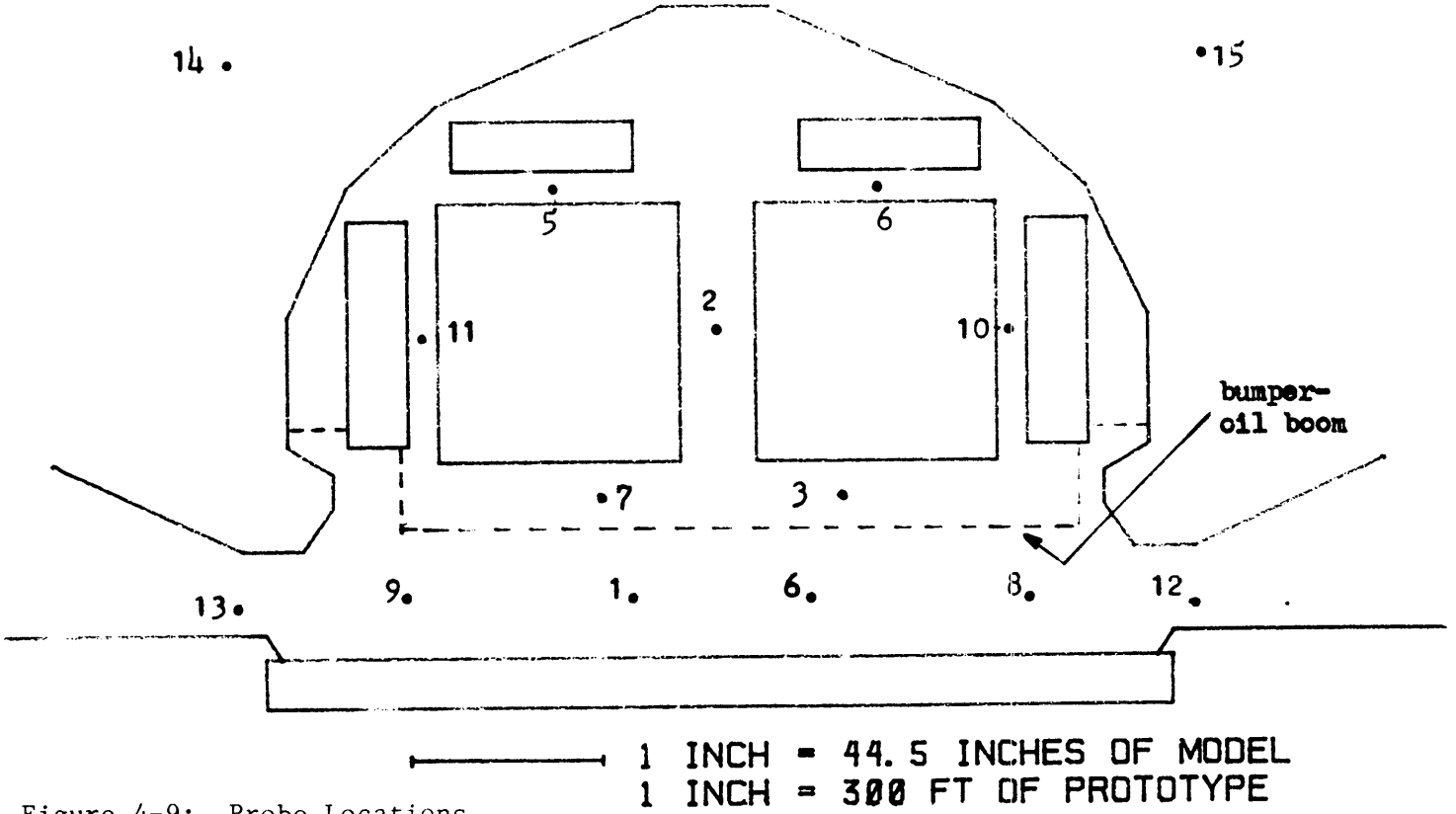

Figure 4-9: Probe Locations
for Experiments 15-18 (with Oil Boom)

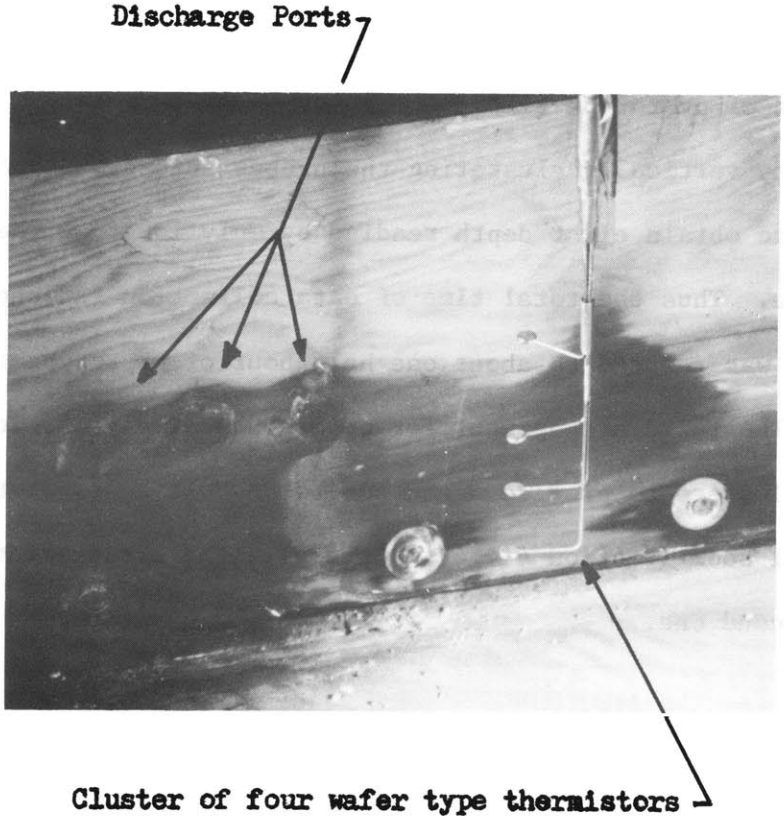

Figure 4-10: Close Up of a Four Probe Cluster in front of Discharge Ports

of time it took to collect all the information that was to be reduced as representative of a single point in time. In the original system the moveable frame to which the majority of probes were attached had to be lowered six times in order to read the scan at seven different depths. The entire procedure for one set of measurements was equivalent to $2\frac{1}{2}$ to 3 hours of prototype time.

By vertically clustering the probes into groups of four it was possible to obtain eight depth reading by only lowering the supporting frame once. Thus the total time of data collection for one set of measurements was reduced to about one half hour of prototype time.

The third arrangement for probes was simply a relocation of several clusters to provide measurements on both sides of the modeled bumper/oil boom (Section 4.4.4). Otherwise the arrangement was identical to the second one.

4.4.3 Tidal System

In order to simulate tidal motion in the basin containing the physical model, a simple tidal generator was constructed. An arrangement of pump, flow-meter, four-way valve, and a storage reservoir in the basement of the laboratory were connected in such a manner as to permit filling or emptying of the model basin. Using the area of the basin, the flow rates were determined as the product of the derivative of the tidal elevation curve and the model basin area. A point gauge was used to check the elevation at five minute intervals to insure that the varying flow was adequately simulating the tide.

4.5 The Oil Boom

During the course of the investigation, concern arose over the effect on the heat distribution of the proposed oil skimmer-security boom that has been tentatively designed, to be placed parallel to the FNP's approximately one hundred feet away from the discharge ports. A plywood and plexiglass model was constructed and installed as shown in Figure 2-1 and 4-9. The boom did not float and thus could not be used with a tidal test but it was possible to vary the depth of the boom to study the varying effects that might result from a different design. Four experiments were conducted with this configuration.

4.6 Experimental Procedure

An actual experimental simulation was complicated to perform due to the intricate nature of the flow control system, the small flow quantities involved and the highly transient nature of the heat release. It was practically impossible to simulate the actual prototype heat release curves with better than about 10 to 20% accuracy. However, as the physical model was not intended as the basic predictive tool but only served as a verification base for the mathematical model, these difficulties did not affect the predictive task. The actual experimental conditions, which were carefully monitored during each experiment, formed the input into the mathematical model the prediction of which could then be compared to the experimental results.

Prior to the start of an experiment, the basin was well mixed to eliminate any ambient stratification. Usually, the basin was filled at least one day in advance to insure that the ambient temperature had

approached equilibrium, so that heating or cooling effects, other than related to the excess heat dissipation, were minimized during the experimental run (2 hours typically). The initial uniformity of the temperature distribution was checked though several temperature scans. The intake manifolds were also primed before the start of an experiment to insure that they contained initially water of ambient temperature.

The start of an experiment consisted of the switching on of the discharge flow. The discharge flow which was generated by mixing of a hot water source and a cold water source was continuously monitored and adjusted according to a pre-determined schedule to simulate the specified discharge heat load as close as possible. Variations in both flow rates (due to pressure fluctuations in the building water supply) and temperatures of either hot and cold source limited the accuracy of this simulation to about 10 - 20% despite continuous checks and re-adjustments.

During the early experiments problems also developed in the discharge distribution system as the air, which went out of solution in the heated discharge water, would accumulate in the individual feeder lines (Tygon tubing). This problem was subsequently eliminated due to installations of bleeder valves in the distribution manifolds.

CHAPTER 5

Experimental Program, Results and Verification of the Analytical Model

This chapter presents experimental observations and results obtained from a run program of fourteen experiments. The experimental results demonstrate the major assumption of the analytical model, namely the well stratified nature of the fluid system within the basin enclosure. The remainder of the chapter is devoted to the verification of the analytical model (using input from the actual run conditions) with the experimental results.

5.1 Experimental Program

A total of twenty documented experiments were conducted using the physical model described in Chapter 4. Of these six are not included in the final comparison due to initial shakedown problems. The remaining fourteen experiments are described in Table 5-1.

The experiments can be sub-divided into five groups as follows:

a) Constant Heat Load - The majority of experiments were run using an intended constant heat load. This is a simpler situation than the varying heat loads of the prototype and it permitted more careful study of various interactions without concern for the effect of a changing heat load.

b) Variable Heat Load - These experiments were an attempt to simulate conditions similar to the LOOP-LOOP emergency in the prototype although it should be emphasized that these were not

TABLE 5-1[1]: List of Experiments Conducted and Evaluated.

Experiment No.	Discharge Temp. Rise[2]	Flow Rate per plant (gpm)	Tidal Conditions[3] (Total ft)	Comments
4	ARW=11°F	ARW=45000		
	ERW=15°F	ERW=22500	0	
5	ARW=11°F	ARW=45000		
	ERW= 0	ERW= 0	0	
7	Simulated	ARW=45000		
	Double Loop	ERW=22500	10 foot	
8	Simulated	ARW=45000		
	Double Loop	ERW=22500	0	
11	ARW=4°F	ARW=45000		
	ERW=4°F	ERW=22500	0	
12	ARW=11°F	ARW=45000		
	ERW=11°F	ERW=22500	0	
13	Simulated	ARW=45000		
	Double Loop	ERW=22500	0	
14	ARW=7°F	ARW=45000		
	ERW=7°F	ERW=22500	10 foot	
15	ARW=6°F	ARW=45000		
	ERW=6°F	ERW=22500	0	Oil Boom set at 4 ft.
16	ARW=11°F	ARW=45000		
	ERW=11°F	ERW=22500	0	Oil Boom set at 4 ft.
17	ARW=11°F	ARW=45000		
	ERW=11°F	ERW-22500	0	Oil Boom set at 10 feet
18	Simulated	ARW=45000		
	Double Loop	ERW=22500	0	Oil Boom set at 6 ft.
19	ARW=6°F	ARW=45000		
	ERW=6°F	ERW=22500	10 foot	
20	ARW=11°F	ARW=45000		One Breakwater
	ERW=11°F	ERW=22500	0	Opening blocked

Notes: 1) All dimensions are given as prototype values

2) The constant discharge temperatures given are the average about which the actual discharge fluctuated. Actual readings were used in experiment prediction work. Simulated Double Loop means attempt was made to match prototype conditions to within (0-20%).

3) Three experiments with a tide each had a 10 foot rise above MLW. The accident occurred at low tide and a cycle of sinusoidal shape was assumed.

exact simulations of the prototype.

c) Variable Tidal Elevation - The majority of experiments were run with a constant depth of water in the basin. Three experiments included a simulated tide that rose to a maximum of 10 feet above MLW.

d) Oil Boom - Four experiments were run with the simulated oil boom-security bumper in place, in order to study the effect of the boom on the flow pattern within the basin.

e) Variable Sill Conditions - One experiment was run with one of the sills blocked to study the effect of reducing the cross sectional area available for sill counter-flow.

5.2 Experimental Observations

A series of general observations were made during all of the experiments. The first is that the heated water spreads across the interior of the basin very quickly after the start of the emergency. This was seen both from dye tests and from the temperature rises recorded throughout the basin soon after the start of an experiment. The dye reached the most remote portions of the basin within 10 minutes of experimental time or 90 minutes of prototype time. The general pattern of flow that was observed is illustrated by Figure 5-1. The jets impinged on the inner wall of the straight breakwater and split in half. The half that headed for the sill was partially reflected by the control condition that exist at the sill, thus causing the circular eddy inside the sill opening. The portion of the flow that is directed toward the center of the basin meets its counterpart from the other plant and then

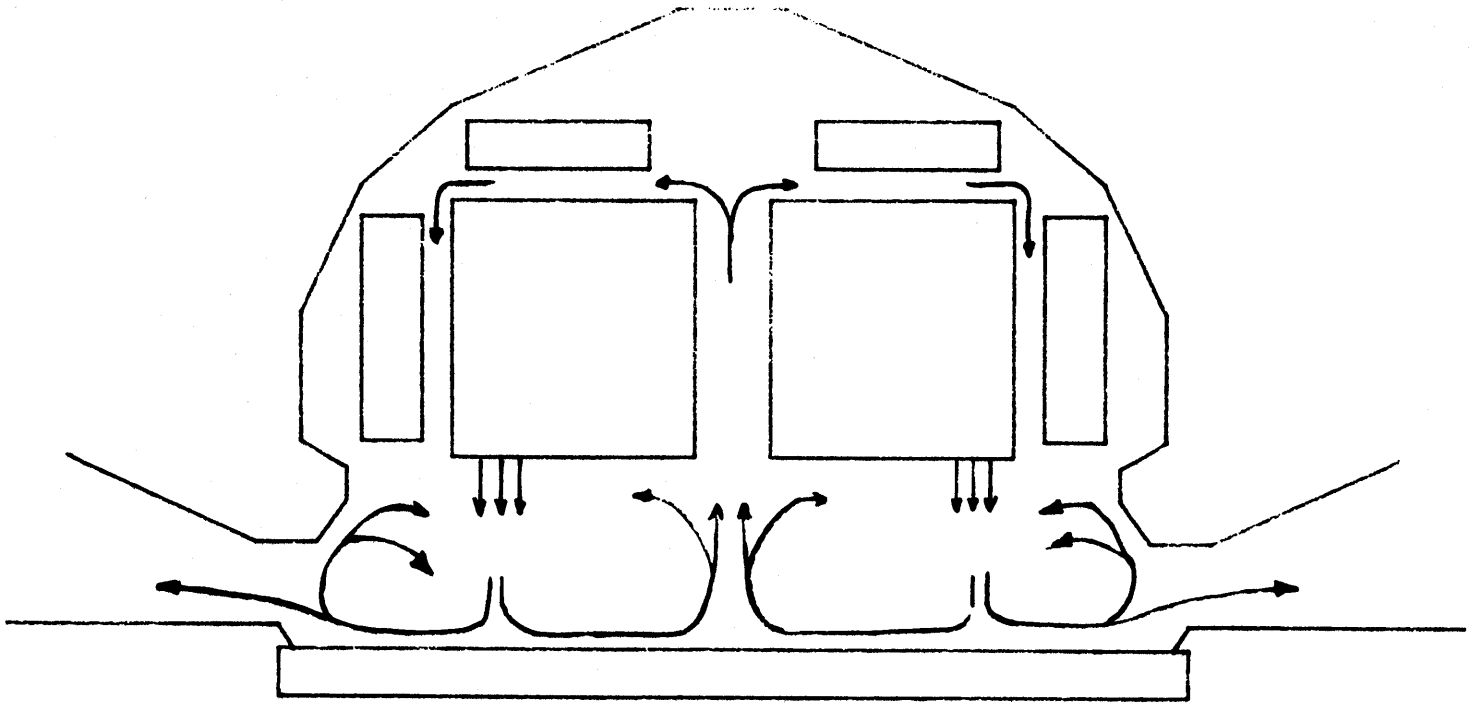

Figure 5-1: General Pattern of Observed Heat Flow

diverts back through the channel between the plants. At the back of the plant it splits again and follows around the back and side of each plant. Figure 5-2 is a photograph of a dye test illustrating part of the same phenomenon.

Once the initial spreading period was over, the upper layer was nearly uniform throughout the basin. Figure 5-3 illustrates this for experiment No. 12. The probe locations plotted represent probes at the back and front of the plants (see Figure 4-8 for exact locations), but the general shape of the profiles is quite similar for all three locations. Based on this similarity it seems legitimate to determine a single basin average profile which then could be used to compute the schematized two layer system values for comparison with the theoretical model. Figure 5-4 illustrates the averaged values used for experiment No. 12.

The degree of stratification and the depth of layer, which developed for prolonged times, were closely related to the discharge temperatures. An experiment such as No. 12 with a "hot" discharge produced a warmer shallower layer than a comparative experiment with a "cooler" discharge. Experiment No. 11 had an average ΔT of 4° rather than the 11° of No. 12. A comparison of Figures 5-4 and 5-5 illustrate this point.

The counter flow situation was clearly evident at the sills as indicated by dye tests. Figure 5-6 is a photograph of dye at a sill and shows the change in direction of flow from the upper to lower layer.

The presence of the oil boom in the basin did not significantly modify these flow patterns or temperature distributions. This is further

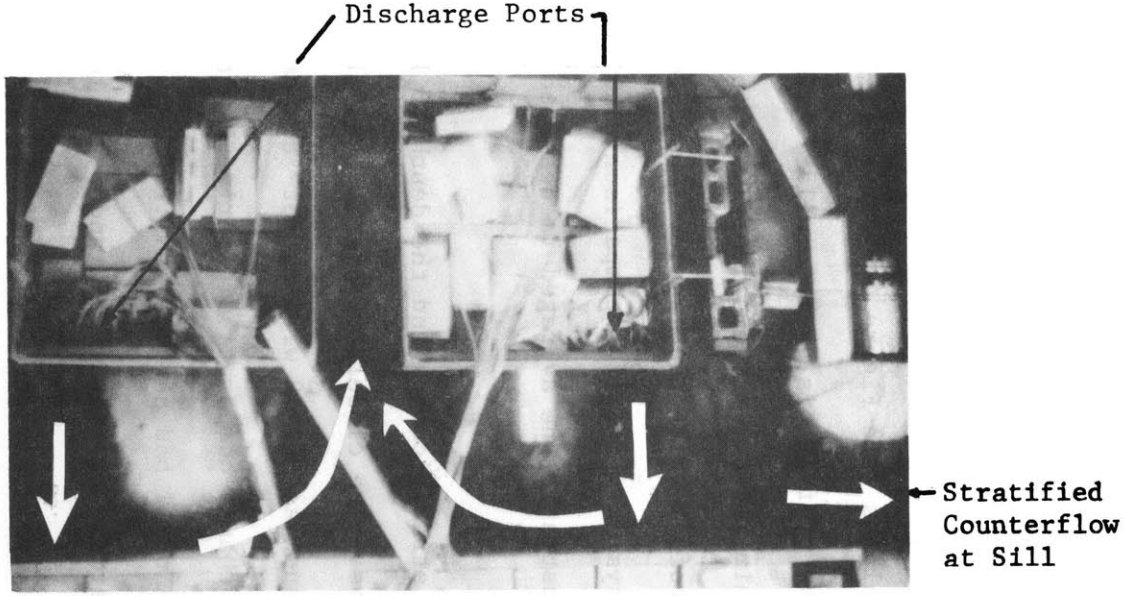

Figure 5-2: Overhead Photograph of Physical Model Showing Flow Pattern of Dye Released in Discharges (See Also Figure 5-1)

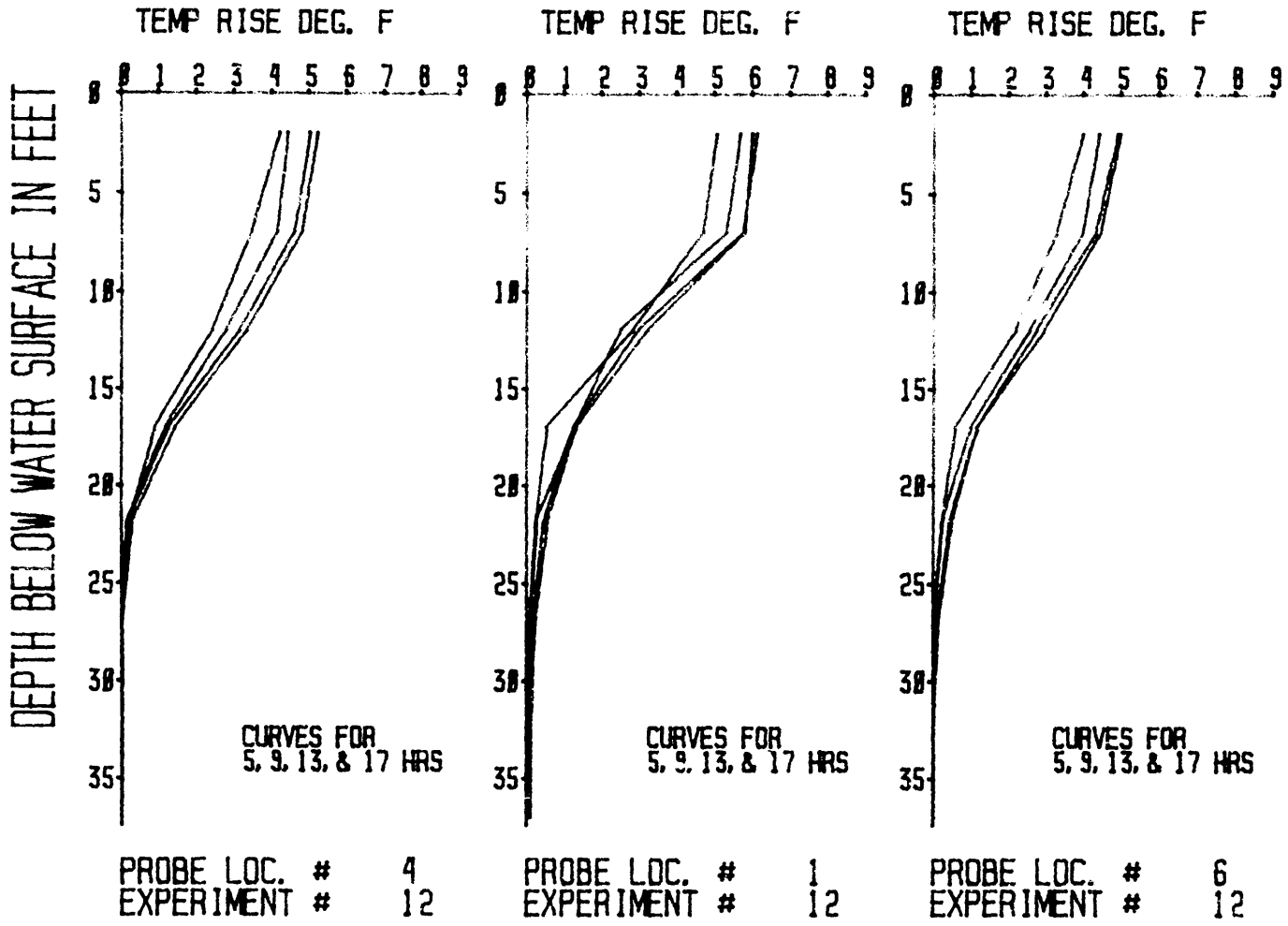

Figure 5-3: Temperature Profiles at Three Locations for Experiment No. 12

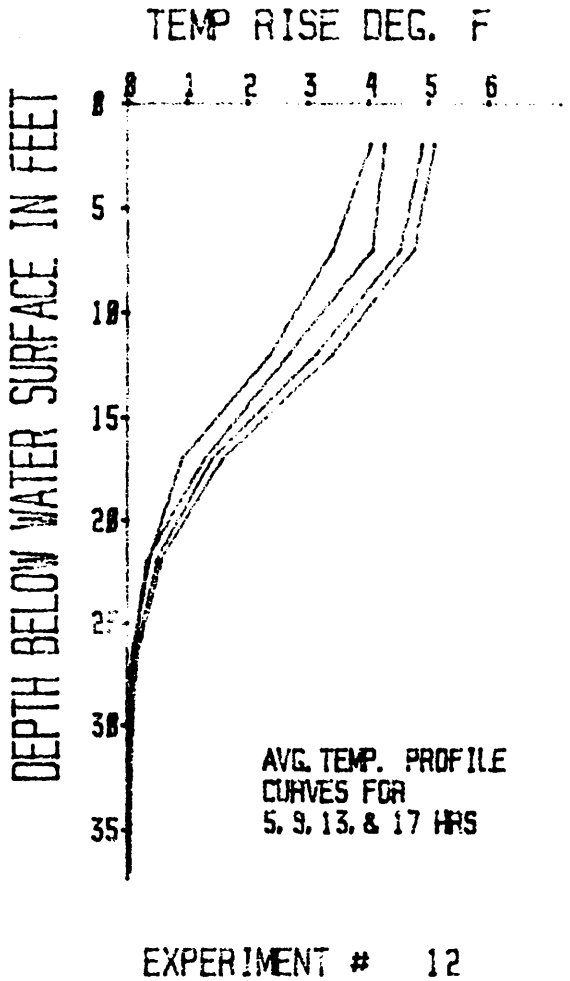

Figure 5-4: Average Temperature Profiles for Experiment No. 12 with $\Delta T = 11^{\circ}F$

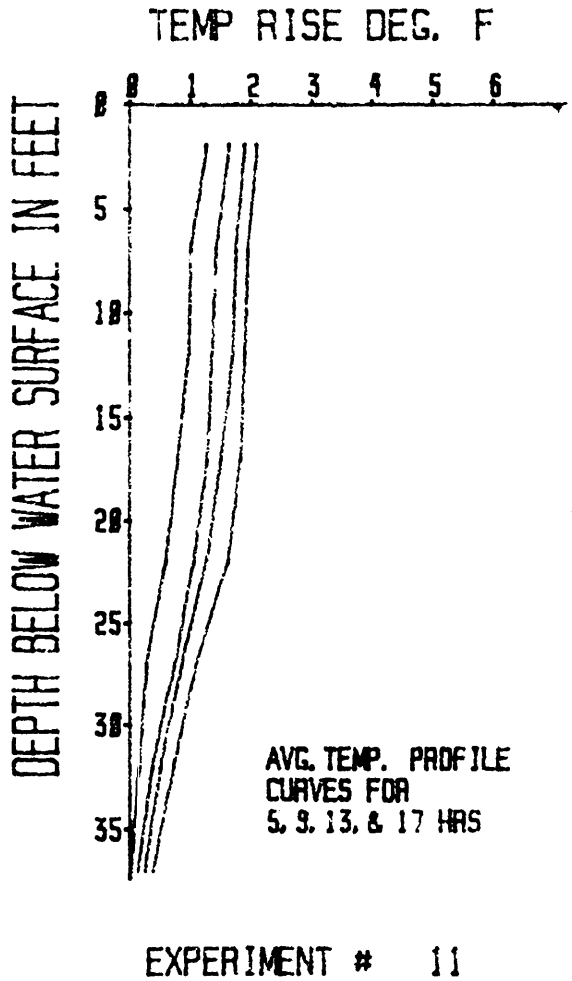

Figure 5-5: Average Temperature Profiles for Experiment No. 11 with $\Delta T = 4^{\circ}F$

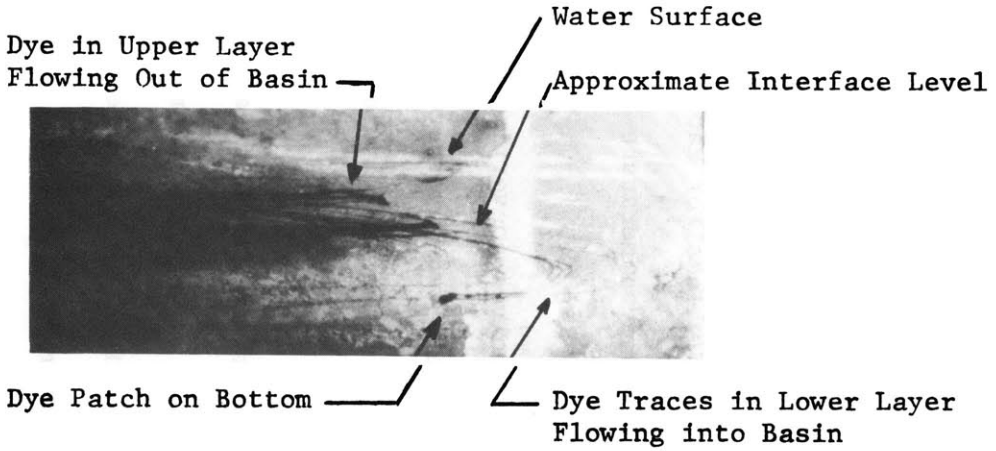

Figure 5-6: Oblique Photograph of Descending Dye Particles at Sill Illustrating Stratified Counterflow

discussed in Section 5.5.

5.3 Schematization of Experimental Results into Two Layer System

The raw data obtained during the course of an experiment consisted of temperature readings at various positions and depths, spaced in time throughout the experiment. The analytical model is based on a simplified two-layer system, and thus in order to compare the physical results with a corresponding prediction it was necessary to convert the distributed information into two values for each time of data collection, namely the average layer depth and temperature rise in an equivalent two layer system.

The basic procedure involved converting an actual temperature profile into a simplified discrete two layer profile as illustrated in Figure 5-7 for an actual set of temperature readings. This involved the following steps:

(i) At the start of an experiment an ambient scan measured the initial temperature reading for each probe. For all later scans, the ambient values were subtracted from the probe readings to give a temperature rise for a given position at that time. The values of temperature rise above ambient can then be displayed at the appropriate depths as in Figure 5-7.

(ii) Determination of Layer Depth h_1: A large number of recorded profiles were examined and in general the point of inflection in the profiles appeared to be at approximately one half the maximum (i.e. surface) temperature rise. Thus, a consistent definition of layer depth is the point where the temperature equals one half the maximum (surface)

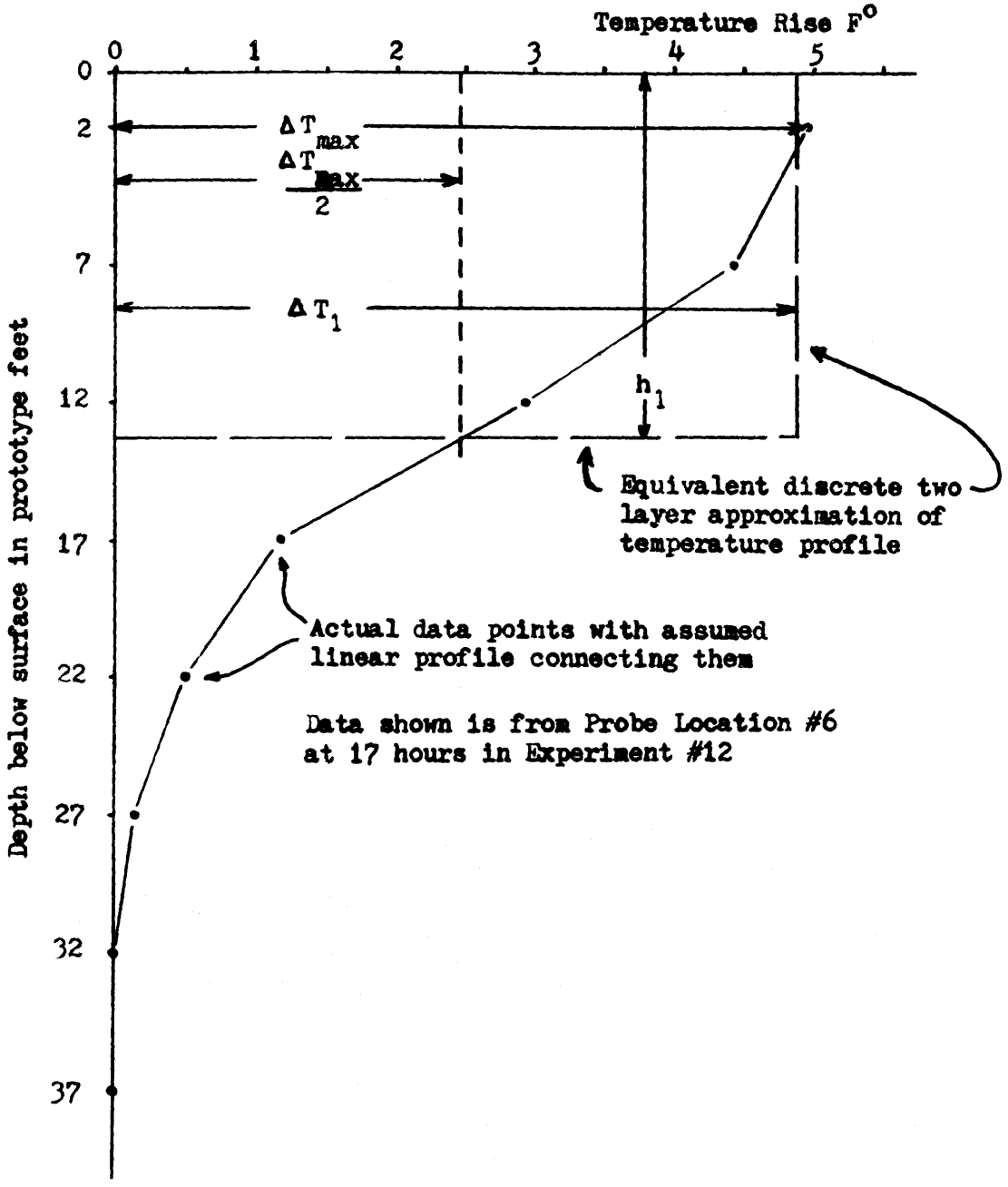

Fig. 5-7: Two Layer Schematization Procedure

temperature rise was used in the data reduction (see Fig.5-7).

(iii) Determination of upper layer temperature rise ΔT_1: Since the analytical model assumes that all the excess heat is contained in the defined upper layer, a consistent schematization of upper layer temperature rise was used. This involved the depth integration of the excess temperature profile and averaging over the upper layer depth, h_1.

The above values were obtained for each probe position at each time. Single values for the basin were then obtained by averaging the various probes including weighting factors that indicated the portion of the basin the probe position represented. There were distinct differences between the various locations in the basin. To illustrate the variation, the maximum and minimum values for both the layer depth and temperature rise were plotted as well as the average value on the graphs that follow.

The intake temperature rise was obtained directly from a probe inserted in the intake manifold.

5.4 Comparison of Experimental Results and Analytical Model Predictions (Verification Phase)

The analytical model has been formulated on well established physical principles to the degree possible, as discussed in Chapter 3. Major hypotheses which influence the overall results and need to be verified against the experimental data are:

1) The structure of the entrainment assumptions, Eq. 3.28 to Eq. 3.32 in particular the value of β.

2) The parameter $\Phi = f_o \frac{L}{H}$ which controls the stratified counter flow at the sills.

Subsequent comparison has shown that the basic assumptions in the model structure are reasonable and the model is a reliable tool both with respect to trends and relative accuracy in predicting the response of the modeled system. A value of $\beta = 0.33$ has been shown to provide the most satisfactory agreement for the entire experimental program. This in fact is the only matching constant in the analytical model. All other parameters can be estimated reasonably well, including the sill parameter Φ (Section 3.2.1) A value of $\Phi = 0.5$ has been chosen based on the analysis of the geometry and friction factor (laminar regime in the model) of the sill.

The heat dissipation has been calculated in the model using actual measured laboratory "meteorological" conditions.

Thus all subsequent calculations have been performed using the above parameter specifications. Sensitivity studies on model assumptions are shown in Chapter 7.

The results of one example of each of the five groups of experiments listed in Section 5.1 is included in this report. They are:

Group		Example	Figures
Constant Heat Load	-	Experiment No. 12	5- 8
Variable Heat Load	-	Experiment No. 13	5- 9
Tidal	-	Experiment No. 14	5-10
One Sill Blocked	-	Experiment No. 20	5-11
Oil Boom	-	Experiment No. 16	5-12

For each case the four major parameters of interest are plotted

with both the experimental results and the predicted values. For the layer depth and layer temperature rise the maximum, average, and minimum experimental values are given. This variation represents the difference in layer thickness and temperature at different points in the basin for a given time. Only single values of the intake temperature rises are recorded.

5.4.1 Constant Heat Load Experiments

The results shown in Figures 5-8a to 5-8d are typical of all the constant heat load experiments. All four parameters rise comparatively rapidly during the first ten hours and then level off in a "steady state" condition. For those experiments with lower heat loads the layer depth was deeper and the average temperature rise less. In general, the intake temperature rise was higher due to the strong dependence on layer depth.

5.4.2 Variable Heat Load Experiments

Figures 5-9a to 5-9d illustrate the results of Experiment No. 13. This attempt to simulate a double LOOP is very similar to the other double LOOP experiments. The experimental and predicted temperature rise peaks soon after the peak heat load which is at 4 hours. Then as the temperature rise drops off, the layer depth continues to increase. The intake temperature rises follow the pattern of the increasing layer depth.

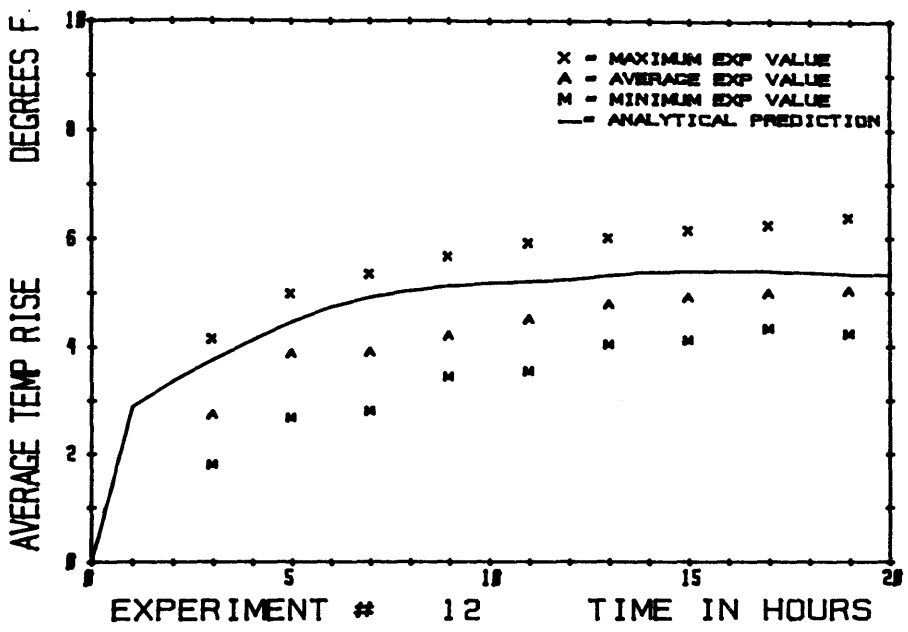

a) Average Upper Layer Temperature Rise

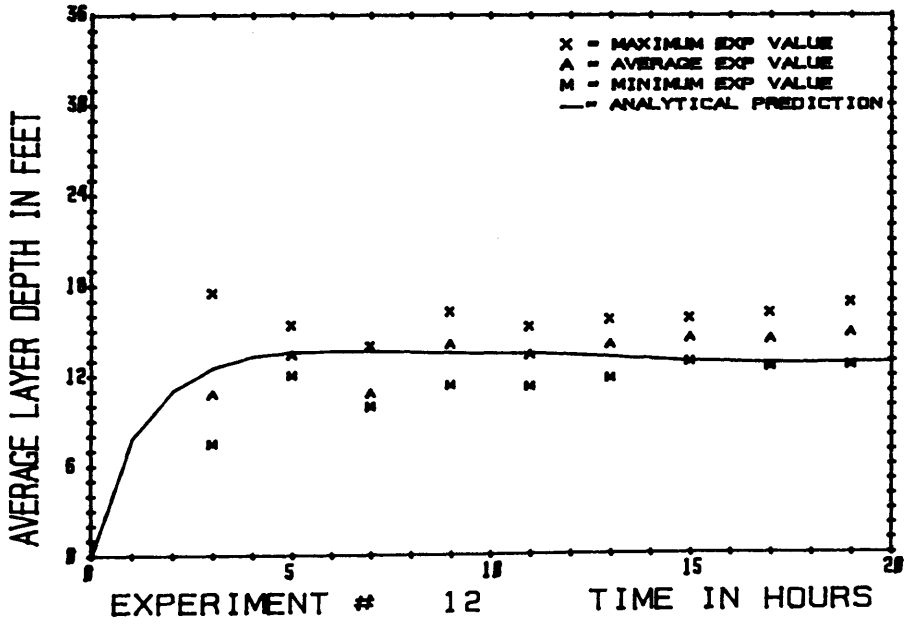

b) Average Upper Layer Depth

Figure 5-8: Comparison of Analytical and Experimental Results for Constant Heat Load Experiment

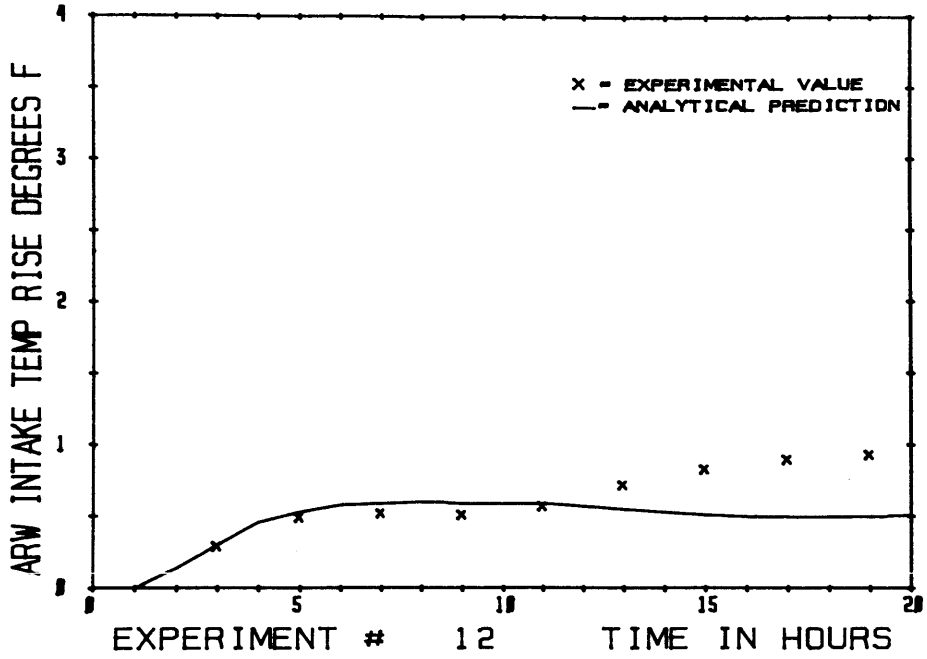

c) ARW System Intake Temperature Rise

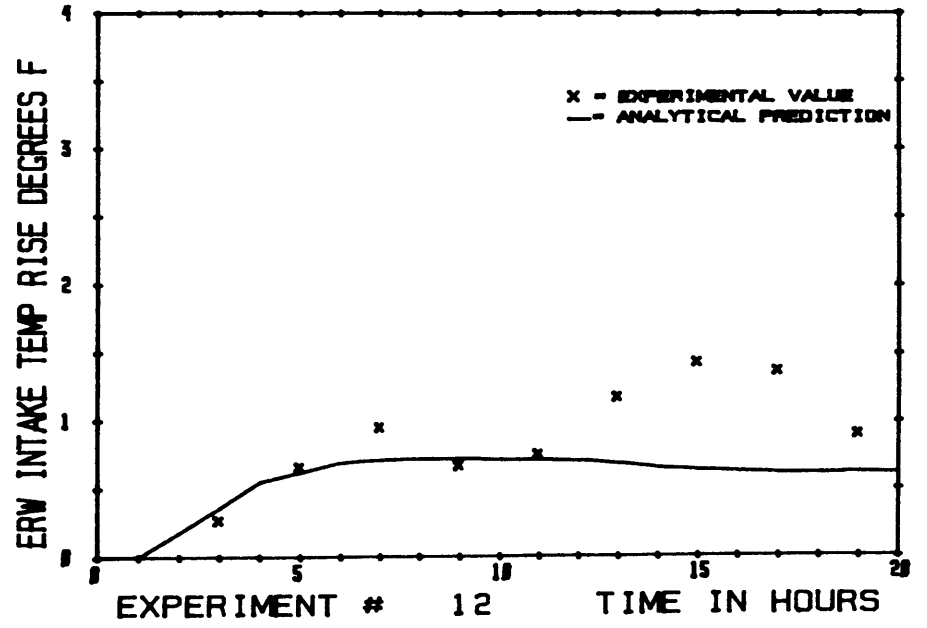

d) ERW System Intake Temperature Rise

Figure 5-8: Comparison of Analytical and Experimental Results for Constant Heat Load Experiment

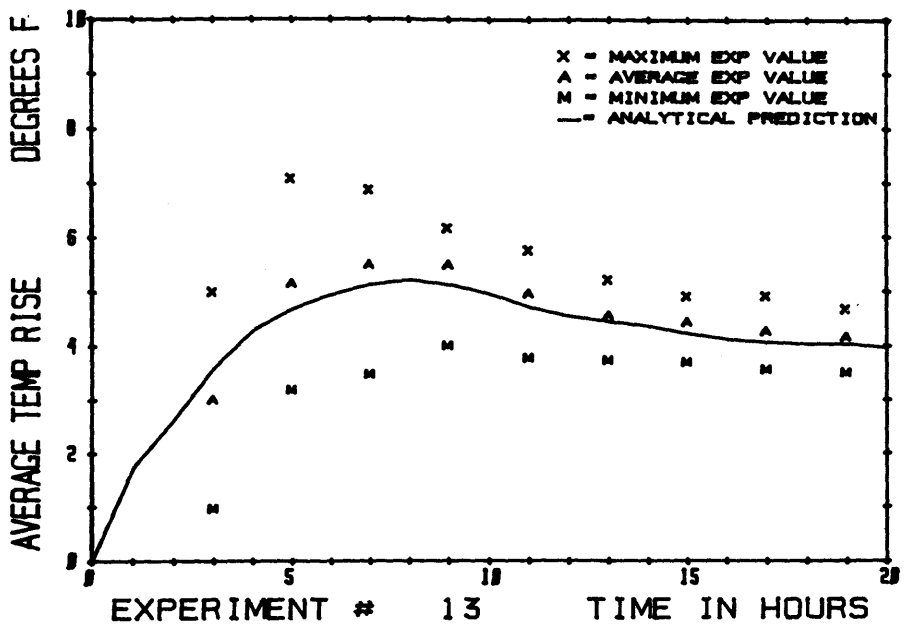

a) Average Upper Layer Temperature Rise

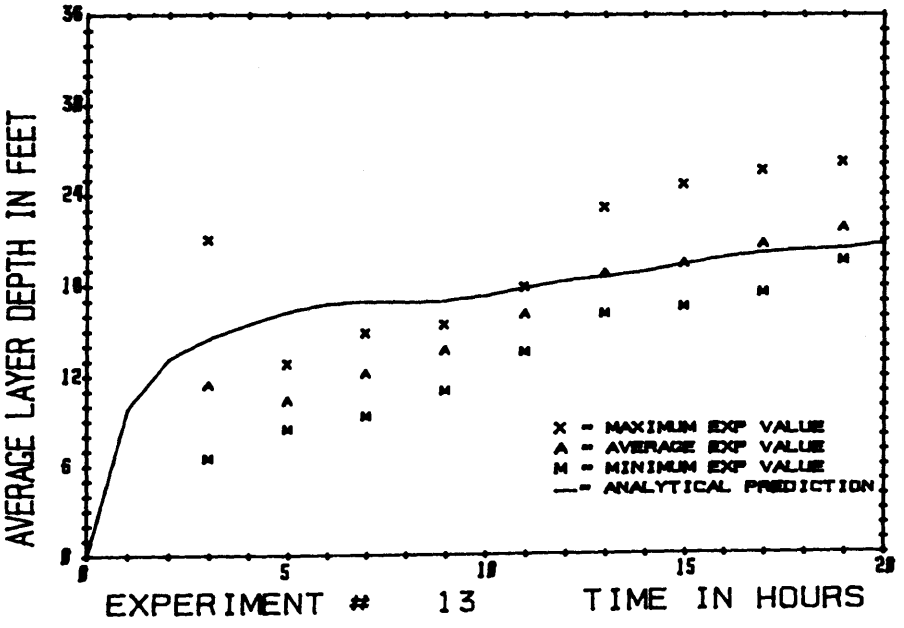

b) Average Upper Layer Depth

Figure 5-9: Comparison of Analytical and Experimental Results for Simulated Double LOOP Experiment

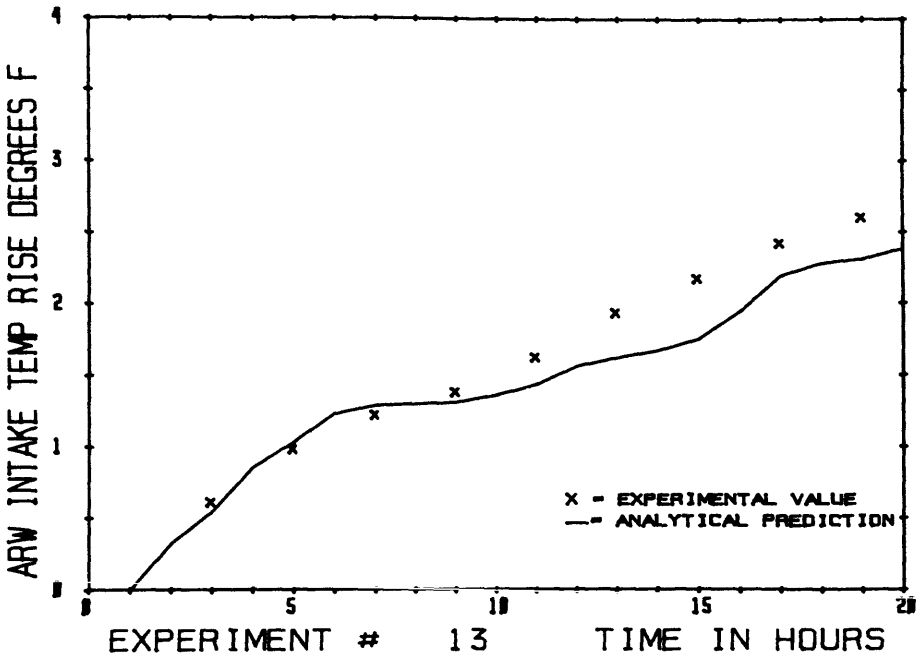

c) ARW System Intake Temperature Rise

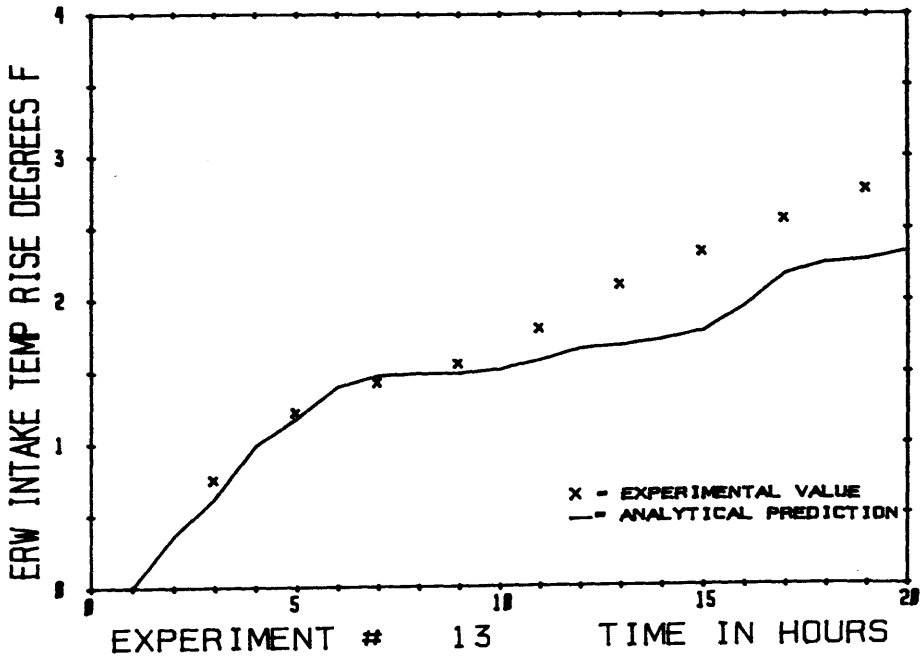

d) ERW System Intake Temperature Rise

Figure 5-9: Comparison of Analytical and Experimental Results for Simulated Double LOOP Experiment

5.4.3 Variable Tide Experiments

The tidal case presented is experiment No. 14 which is illustrated in Figures 5-10a to 5-10d. The results are very similar to those obtained in Experiments No. 7 and No. 19. In each case, the accident occurs at low water and thus high tides are reached at 6 and 18 hours, with low tides at 0 and 12 hours. Both the experimental and analytical results show that the layer is trapped in the basin as the tide is rising and then flushes out during the falling tide. The analytical predictions for intake temperature rise appear to overpredict the peaks somewhat, but do successfully follow the rise and fall sequence.

5.4.4 Constricted Breakwater Opening -- One Sill Blocked

Experiment No. 20, illustrated in Figures 5-11a to 5-11d, was conducted to examine the effect of reducing the cross-sectional area of the breakwater openings. One sill opening was blocked and sealed to prevent any flow between the basin and ocean on that side. Comparison of Figures 5-8 and 5-11, experiments 12 and 20 illustrate the general effects. The heat loads of the two experiments were not identical but both were approximately in the range that produce a discharge temperature rise of $\approx 11°F$. Both the experimental results and the predictions for the temperature rise and layer depth are distinctly higher in Experiment No. 20. This is the intuitively expected result since the volume of flow out of the upper layer is more severely restricted. The experiment confirms the general ability of the analytical model to properly reflect changes in design parameters.

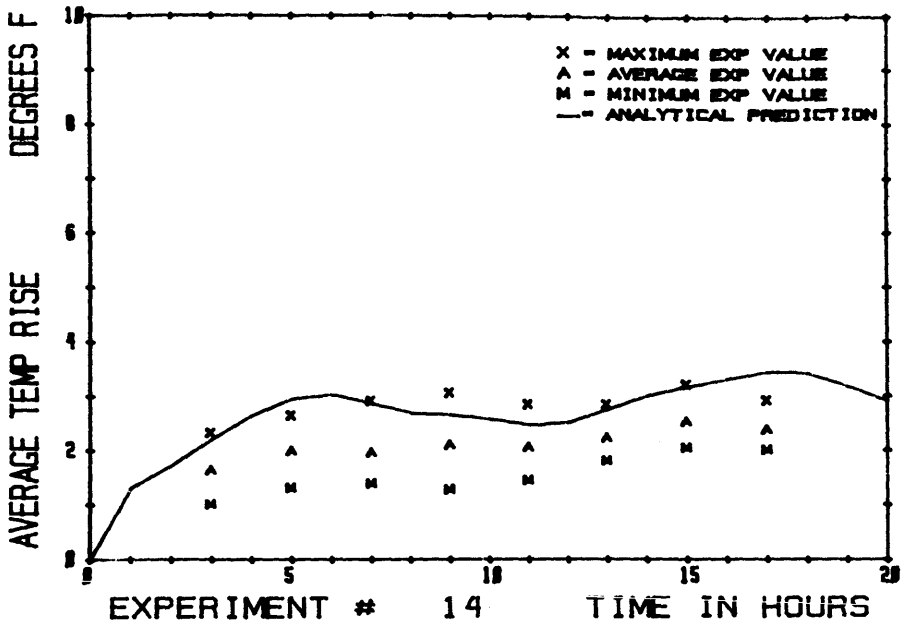

a) Average Upper Layer Temperature Rise

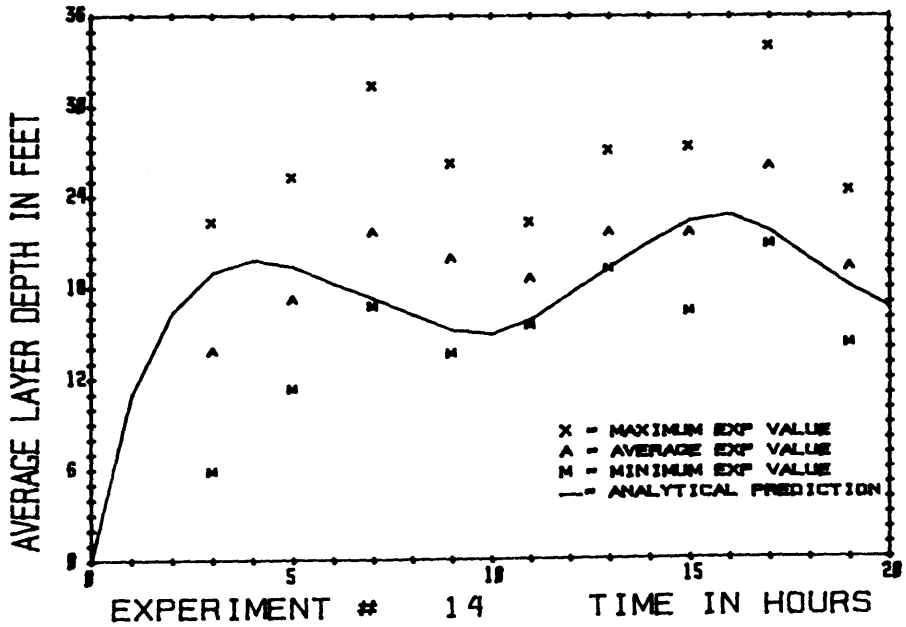

b) Average Upper Layer Depth

Figure 5-10: Comparison of Analytical and Experimental Results for Tidal Experiment

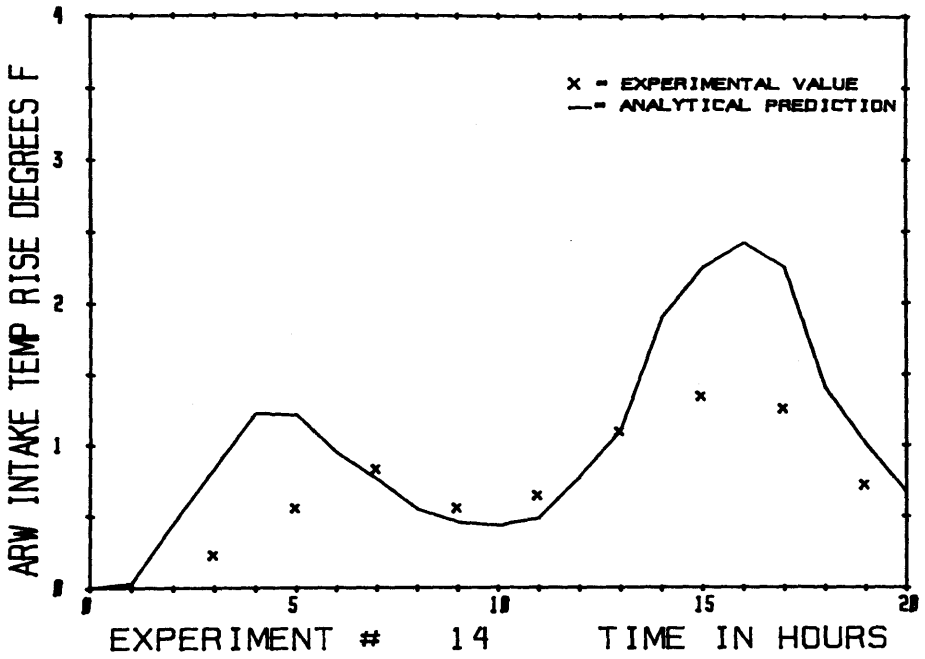

c) ARW System Intake Temperature Rise

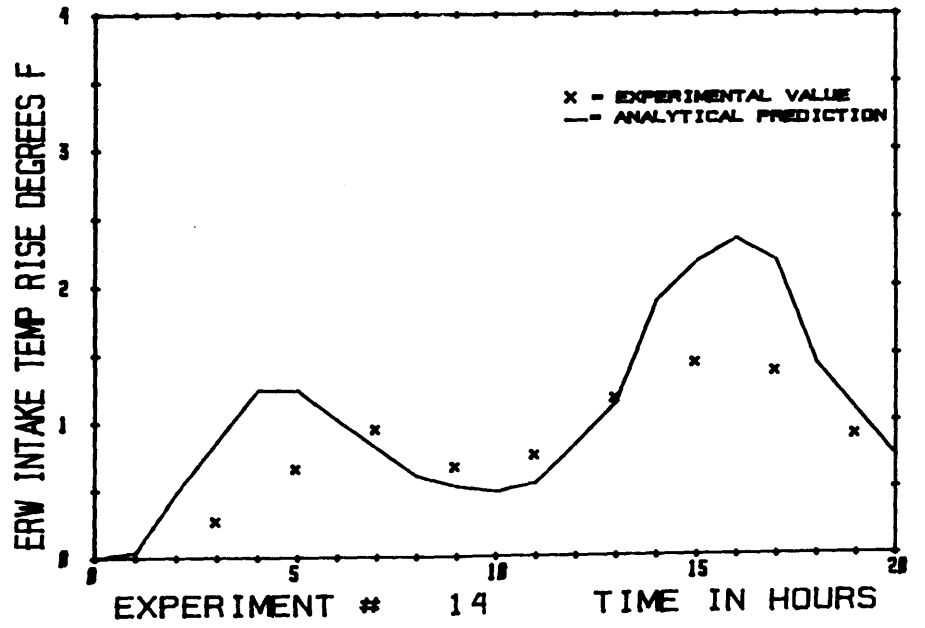

d) ERW System Intake Temperature Rise

Figure 5-10: Comparison of Analytical and Experimental Results for Tidal Experiment

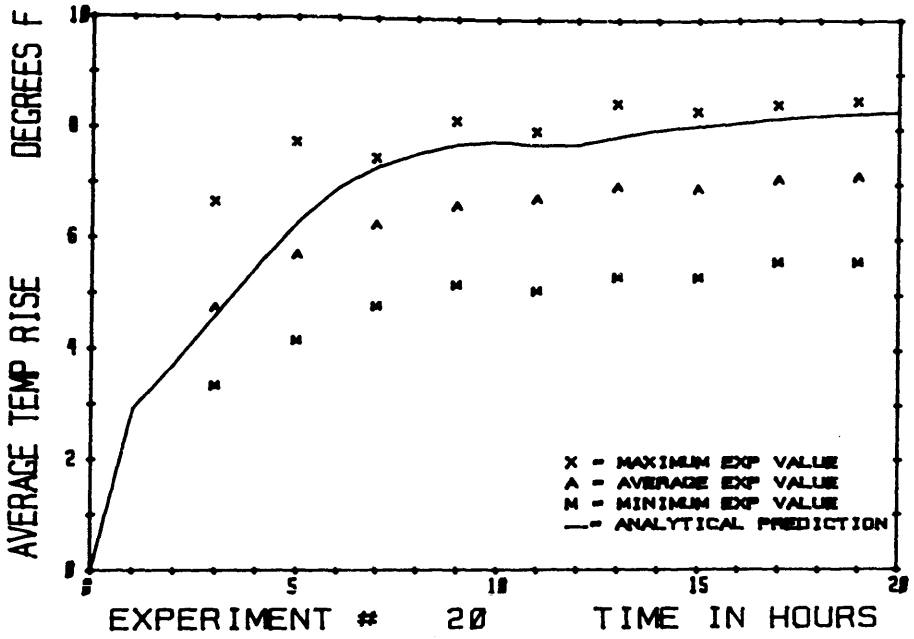

a) Average Upper Layer Temperature Rise

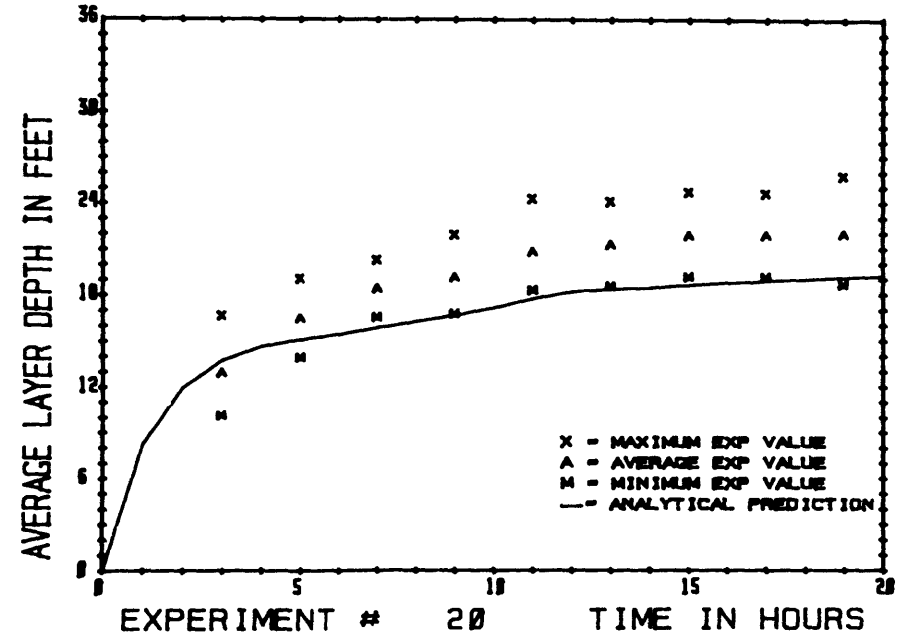

b) Average Upper Layer Depth

Figure 5-11: Comparison of Analytical and Experimental Results for Experiment with Blocked Breakwater Opening

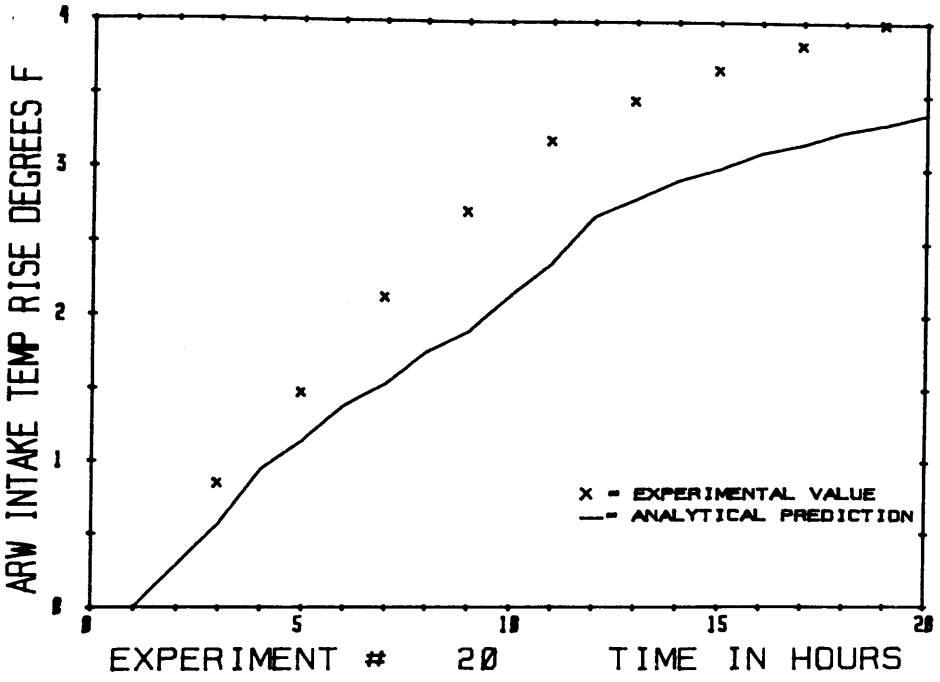

c) ARW System Intake Temperature Rise

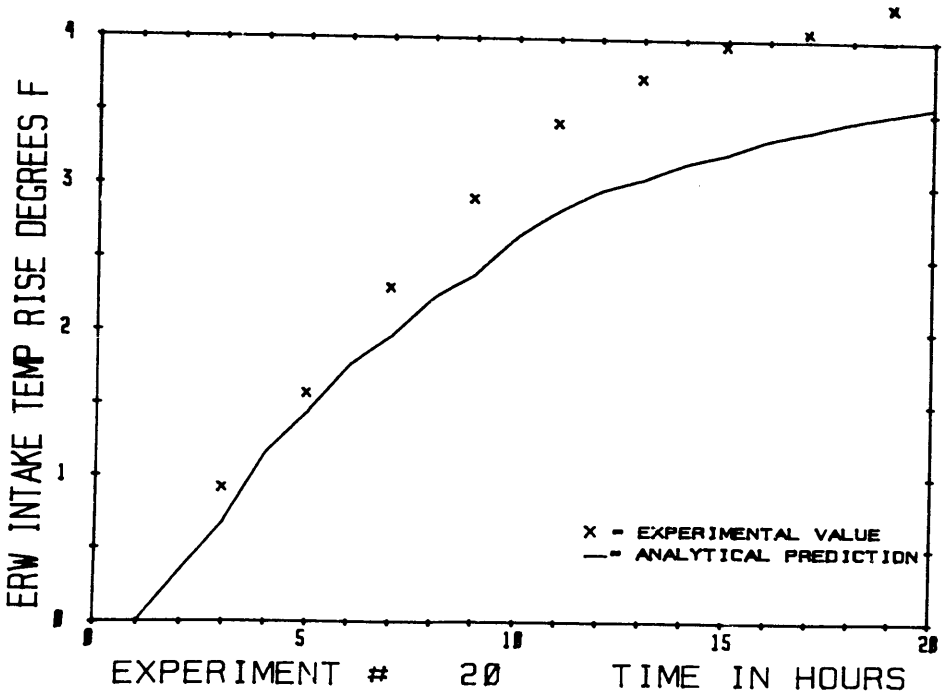

d) ERW System Intake Temperature Rise

Figure 5-11. Comparison of Analytical and Experimental Results for Experiment with Blocked Breakwater Opening

5.5 Experimental Results and Observations for the Oil Boom Installations

The current design for AGS includes a security bumper-oil boom intended to protect the plants from the hazard of ship collision and prevent an oil spill from reaching the plants. The boom will be located 100 feet in front of the discharges perpendicular to the discharge ports. The depth of the boom is not yet finalized but will probably be between four to six feet deep for the majority of its length, and approximately ten feet deep at two removable gates.

A model of the oil boom was constructed and tests 15 to 18 run with it in place. The results of Experiment No. 16 are shown in Figures 5-12a to 5-12b. The conclusion of the investigation is that when the boom was only four feet deep, its effect could not be clearly detected on the performance of the physical model. When the boom was set at 10 feet, an effect could be detected, but it was still not strong enough to cause concern. Figures 5-4, 5-13, and 5-14 help to illustrate the situation. Figure 5-4 shows the profiles of three probes for experiment No. 12. Probe location No. 4 is at the bow of one plant, and probe locations No. 1 and No. 6 are at the stern of the plants. There is some variation in the shape of the profile, based on the position, as was generally the case. Figure 5-13 is for experiment No. 16 which had roughly the same heat load as Experiment No. 12, but the oil boom was in place at a depth of four feet. In this case, probe location No. 4 is as before at the bow of the plant, but probe location No. 3 is at the stern of the plant between the plant and the oil boom, while probe location No. 6 is between the oil boom and the breakwater. Again there is no major difference between the three profiles. The profile at the

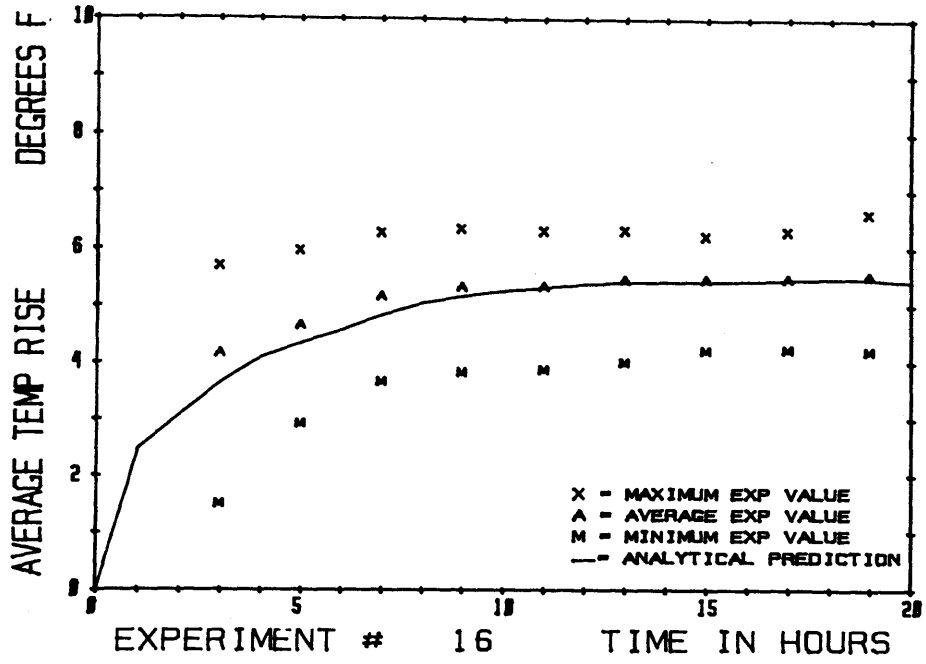

a) Average Upper Layer Temperature Rise

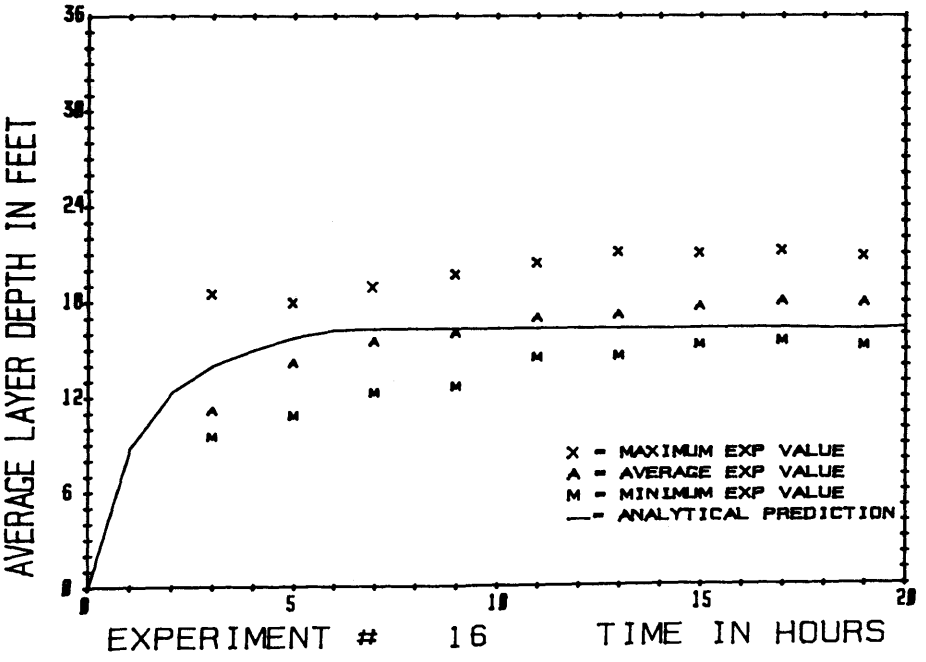

b) Average Upper Layer Depth

Figure 5-12: Comparison of Analytical and Experimental Results for Oil Boom Experiment

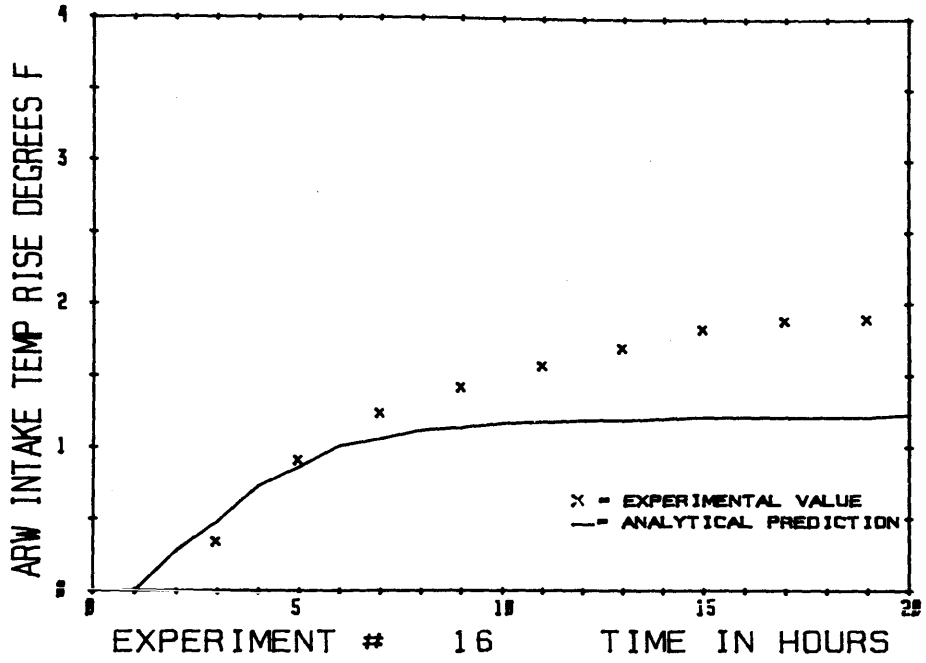

c) ARW System Intake Temperature Rise

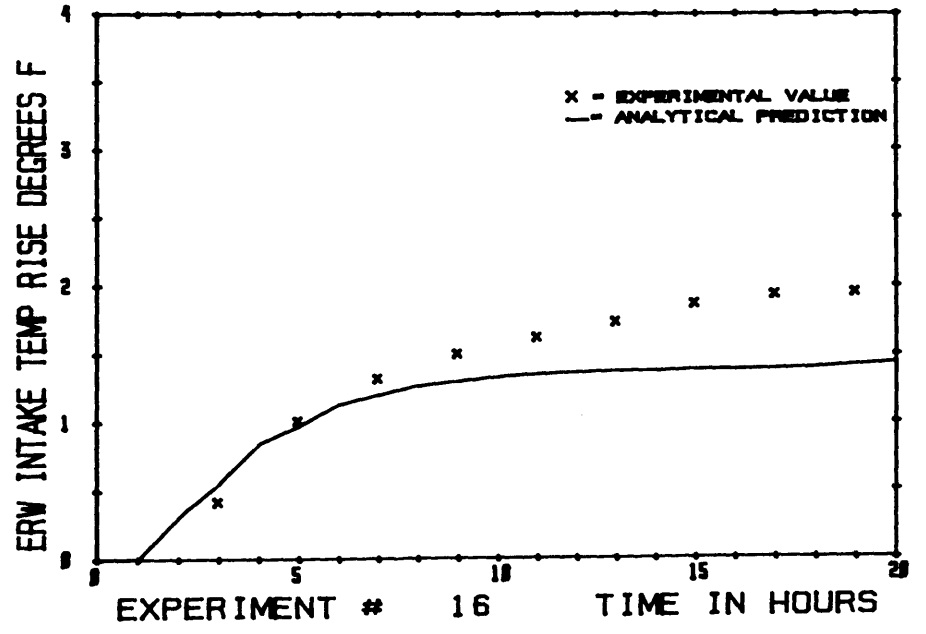

d) ERW System Intake Temperature Rise

Figure 5-12: Comparison of Analytical and Experimental Results for Oil Boom Experiment

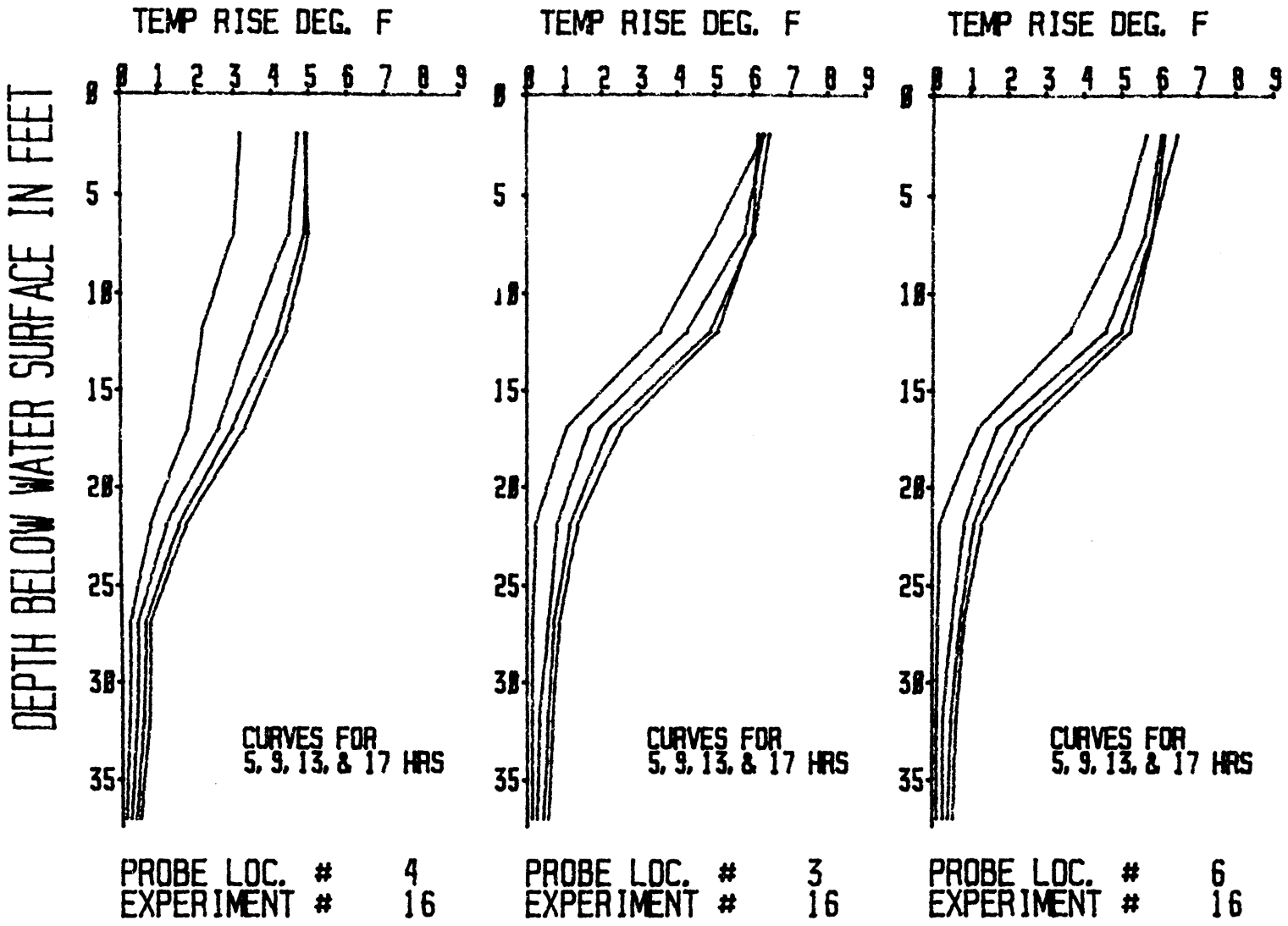

Figure 5-13: Temperature Profiles at Three Locations for Experiment No. 16

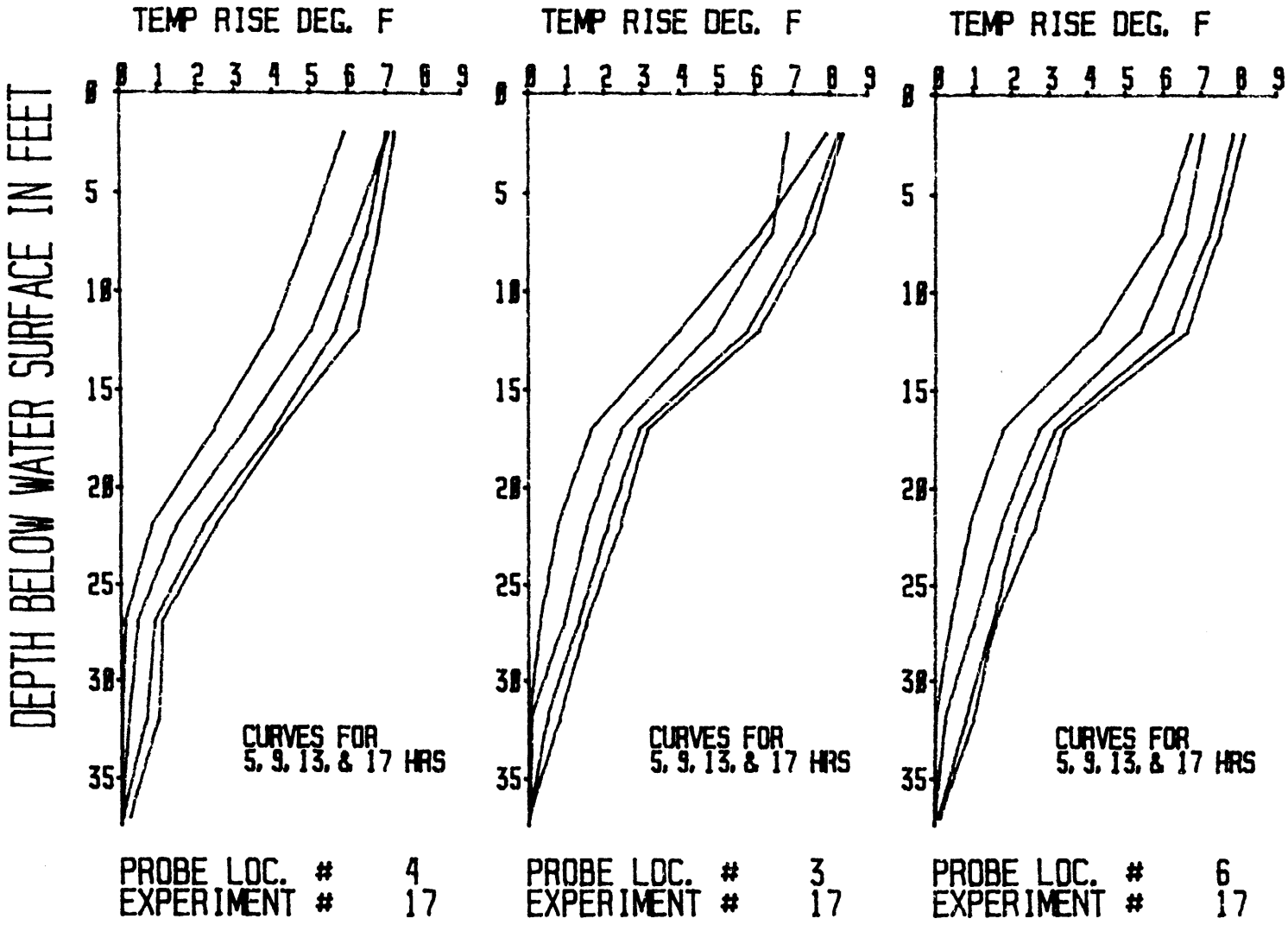

Figure 5-14: Temperature Profiles at Three Locations for Experiment No. 17

bow of the plant is less clearly stratified which is reasonable since it was located not far from the intakes and thus probably shows some of the drawdown effect. But the major point of interest is that there is no real difference between probe locations No. 3 and No. 6.

Figure 5-14 shows the same information for Experiment No. 17. In this experiment, the heat load was again about the same, but the oil boom was at a ten foot depth. The conclusions are the same as for Experiment No. 16, except that the maximum temperature rise appears to be somewhat greater and the rise at lower levels greater.

The comparison of analytical and experimental data was presented in the previous section for Experiments No. 12 and No. 16. For Experiment No. 17, the predictions were on the low side for both layer depth and temperature rise. This tends to indicate that the heat in the upper layer was being at least partially confined to the area enclosed within the oil boom structure.

The question then arises as to whether the discharge jets are being trapped behind the oil boom. This was not evident from the dye tests conducted during the experiments. Most of the dye injected into the hot water passed beneath the boom and impinged on the breakwater. It then passed back beneath the boom and down the center channel as before.

Given the fact that the average temperature and depth seen in the experiments increased from No. 12 to No. 16 (4 ft boom) to No. 17 (10 ft boom), it may be concluded that the oil boom does affect the basin response to some, however limited, extent. This limited effect of the oil boom should be understood in the light of the small vertical dimension

of the oil boom (4 ft in Experiment 16, 10 ft. in Experiment No. 20) which is considerably less than typical average layer depths (excluding a short initial period) and jet penetration depth (determined from Eq. 3.11).

A further point of importance is that the actual discharge temperature of the AGS is considerably less than 11° for most of the time during emergency cooling. Thus the actual less buoyant discharge conditions should be even less affected by the oil boom than the experimental simulations.

In general, a modification of the analytical model to incorporate the stratified flow conditions under the oil boom would have been possible. However, based on the experimental results and analytical comparisons, it was found, that oil boom installations with less than 10 ft submergence depth have limited effects on the emergency cooling dynamics. Thus, no further adaptations of the analytical model were undertaken and the model appears flexible for predictions of the oil boom conditions if the above condition is met.

5.6 Summary

The experimental model was intended to replicate the major features of the AGS site and the varying heat load experiments attempted to simulate a double LOOP emergency. The experimental program, however, did not provide accurate predictions for the prototype behavior. This limitation is due to a few significant differences between the model and prototype, namely:

1) Separate Intake and Discharge Systems - The model did not replicate the continuous intake discharge circuit of the

prototype. Thus the discharge temperature in the model was equal to the temperature increase provided by the heat load added to the ambient temperature, but not to the intake temperature as in the prototype.

2) Heat Dissipation - The undistorted model which was required to simulate the jet entrainment did not model correctly the heat dissipation to the atmosphere.

3) Sill Control - The undistorted model did not correctly model the controlling effects of counter flow at the breakwater openings.

4) Heat Load Simulation - Due to experimental limitations it was impossible to exactly simulate the design heat load curves of the AGS.

However, despite these limitations, the experimental program provided an excellent data base for the verification of the concurrently developed mathematical model. The experimental conditions sufficiently approximated the prototype conditions to establish the analytical model as a reliable tool for the actual prototype predictions presented in Chapter 6.

CHAPTER 6

Prototype Predictions

The previous chapter established the validity of the analytical model by comparison with the physical model experiments. This chapter presents the application of the analytical model to the various possible operating conditions of the Atlantic Generating Station.

6.1 Prototype Geometry, Hydrography, and Meteorology

6.1.1 Basin Geometry

The basic geometry of the AGS basin has been shown earlier (see Figure 2-1). In summary, the plants are located behind an artificial breakwater that resembles a horseshoe with a straight bar across the open end. The maximum water depth at MLW will be 47 feet in the central portion of the basin beneath the plants. At the breakwater opening, the maximum depth at MLW will be 20 feet.

A security bumper - oil boom system is planned in front of the plants and divides the large open water surface into two regions. But as previously discussed, the experiments indicate that the boom will have a negligible dynamic effect.

6.1.2 Plant Geometry

The plants are constructed as large barges, about square in plan view, and with a draft of 35 feet. The location of the emergency cooling system intakes and discharge ports was illustrated on Figure 2-2. The intake centerline will be at a depth of 28.5 feet below the water

line and the top of each discharge pipe will be located at the water line.

The intake diameters were determined based on a design objective of limiting the maximum intake velocity to 1 ft/sec. The minimum diameters that meet the velocity restriction for the design flow rates are: ERW diameter = 5.0 feet and ARW diameter = 6.5.

In the case of the discharge ports, the limiting factor is the degree of entrainment that results from a given discharge diameter. This effect is characterized by the densimetric Froude number F_o' which should be kept low to minimize jet entrainment. F_o' depends also on the relative density difference and thus varies continually as the heat load changes. In the case of the combined discharge ports it is highly sensitive to the mode of operation. After studying the densimetric Froude number conditions that resulted from the AGS heat loads and various diameters it was determined to use values of 5.5 feet for the combined discharge and 4.0 feet for the single ERW discharge. These values were selected based on the criteria of providing a Froude number in the range 2.0 - 2.5 for each discharge at the time when the cooling water temperature rise is a maximum. These dimensions also represent reasonable compromises with pipe installation requirements within the plant which dictate limits on pipe sizes.

Unlike the predictions for the experimental cases in the prototype predictions, the discharge temperatures that are simulated reflect the actual conditions, namely that the discharge temperature is the

result of applying the heat load to the intake temperature (continuous intake discharge circuit).

6.1.3 Hydrographic Conditions

For the prototype predictions, the tidal range was considered to be either zero or 10 feet. In the latter case, the tidal elevation was added to the MLW depth. The time of the start of the accident was also varied relative to the tidal stage. Cases where the accident occurred at low tide, high tide, and at mean water on a falling tide were considered. The tide was simulated as a cosine curve with a tidal period of 12.4 hours.

It is recognized that the lateral currents along the shore may result in a net throughflow through the breakwater enclosure. This was neglected in the prediction as the conservative case, since if a throughflow exists it should aid in the flushing of the basin and thus reduce the heated layer buildup.

Prior to the start of an emergency cool down sequence it is assumed that the basin is completely mixed. The main condenser system will be shut down at the start of the emergency but its operation prior to the emergency should insure no stratification within the basin due to the large flowrates involved.

6.1.4 Meteorology

No specific values for the meteorologic conditions at the AGS site at the time of an accident have been assumed. Hence, the sur-

face heat dissipation has been simulated utilizing the linearized heat dissipation equation (3.42) with a conservatively low value for the heat exchange coefficient K = 5 BTU/sq.ft-hr-°F.

6.2 Standard Conditions for Prototype

The prototype prediction runs were all run using a standard set of conditions and parameters and then varying the parameters of interest in each case. In the runs reported in this chapter, the operating conditions, namely heat load and tide, were varied. In Chapter 7, the design and formulation parameters are varied as a study of the sensitivity of the model. The standard set of conditions are summarized in Table 6-1.

6.3 Prototype Emergency Heat Release Conditions

There were eight basic heat release conditions that required investigation. These were each simulated under the condition of no tide. Four of these eight were further simulated under tidal conditions.

Prior to listing the cases studied as consolidation of terms previously presented in Chapter 2 and an explanation of additional terms is required.

A LOOP is a "loss of offsite power" emergency. During a LOOP the ARW system receives a varying heat load that peaks at four hours after the start of the emergency. The ERW system receives a constant heat load of 30 million BTU/hour starting at four hours. The heat load curves were presented in Figure 2-3.

Table 6-1

Standard Prototype Parameters

Flow Rates:	15,000 gpm per train for ARW	
	7,500 gpm per train for ERW	
Discharge Diameters:	Combined =	5.5 feet
	Single ERW =	4.0 feet
Intake Diameters:	ARW =	6.5 feet
	ERW =	5.0 feet
Sill Depth at MLW	=	20 ft
Sill Width	=	130 feet
Sill Friction Factor Φ	=	0.2
Intake Depth	=	28.5 feet
Surface Heat Dissipation Coeff.	=	5 BTU/sq.ft.-hour-°F
Area of Layer	=	455,000 square feet
Limiting Ratio of Jet Depth to Layer Depth, β ,	=	0.333
Tide	=	0.0 feet
Ambient Temperature	=	85°F

A LOOP2 is an emergency condition similar to a LOOP except that the single ERW train is assumed to have been unavailable throughout the emergency.

A LOCA is a "loss of coolant accident" where the primary cooling system is assumed to become inoperative. In this case, the ERW receives a varying high heat load, while the ARW system does not operate.

A NORM is a "normal shut down" situation in one plant that is assumed to accompany a LOOP or LOCA in the other plant. A NORM experiences the same varying ARW heat load as a LOOP, but the ERW does not operate.

The expression "ALL SYSTEM" means that all available trains are operating. The expression "SINGLE FAIL" means that one of the three combined ARW-ERW trains in a safe guard compartment is inoperative and thus the total flow through the plant is reduced.

Table 6-2 summarizes the fourteen operating situations that have been simulated to predict the system response to the applied transient heat loads. The "types" of discharges are coded in the column heading as follows:

Type 1 = Combined discharge with both ARW and ERW flow

Type 2 = Combined discharge but only with ARW flow

Type 3 = Combined discharge but only with ERW flow

Type 4 = Single ERW discharge

All prototype simulations indicated on Table 6-2 are based on the same "standard" design condition as listed in Table 6-1.

Prototype Case #	Plant # 1					Plant # 2					Maximum Tide ft	Accident begins at
	Operating Condition	# of disch. by type				Operating Condition	# of disch. by type					
		1	2	3	4		1	2	3	4		
1A	LOOP - ALL SYST	3	0	0	1	NORM - ALL SYST	0	3	0	0	0	-
1B	LOOP - SING FAIL	2	0	0	1	NORM - ALL SYST	0	3	0	0	0	-
2A	LOOP2- LOOP2	3	0	0	0	NORM - ALL SYST	0	3	0	0	0	-
2B	LOOP2- LOOP2	2	0	0	0	NORM - ALL SYST	0	3	0	0	0	-
3A	LOCA - ALL SYST	0	0	3	1	NORM - ALL SYST	0	3	0	0	0	-
3B	LOCA - SING FAIL	0	0	2	1	NORM - ALL SYST	0	3	0	0	0	-
4A	LOOP - ALL SYST	3	0	0	1	LOOP - ALL SYST	3	0	0	1	0	-
4B	LOOP - SING FAIL	2	0	0	1	LOOP - ALL SYST	3	0	0	1	0	-
5A	LOCA - ALL SYST	0	0	3	1	NORM - ALL SYST	0	3	0	0	10	low tide
5B	LOCA - SING FAIL	0	0	2	1	NORM - ALL SYST	0	3	0	0	10	low tide
6A	LOOP - ALL SYST	3	0	0	1	LOOP - ALL SYST	3	0	0	1	10	low tide
6B	LOOP - SING FAIL	2	0	0	1	LOOP - ALL SYST	3	0	0	1	10	low tide
6D	LOOP - ALL SYST	3	0	0	1	LOOP - ALL SYST	3	0	0	1	10	mean water falling
6E	LOOP - ALL SYST	3	0	0	1	LOOP - ALL SYST	3	0	0	1	10	high tide

Table 6-2: Simulated Prototype Operating Conditions

6.4 Prototype Heat Release Predictions

6.4.1 Simulation Time Period

It was necessary to select the length of time over which to carry out the simulation of the full set of prototype predictions. Based upon the time frame of the significant changes in the heat load curves and their peaks it was decided to use a simulation period of 72 hours for the first set of runs and then examine individual cases for longer times if needed. The results from the 72 hour predictions showed that in some cases the intake temperature was still rising slowly at 72 hours due to a gradual increase in layer depth. But in every case, the average layer temperature was decreasing which provided a decreasing upper bound on the maximum possible intake temperature rises. Generally, the simulation period of 72 hours was found reasonable as it presented the period of the most significant changes and extremes in prototype behavior.

6.4.2 Non Tidal Cases.

Figure 6-1 illustrates the comparison of the four output parameters for cases 1A, 2A, 3A and 4A. These cases are the four basic types of emergencies occurring with all pump trains operating and no tide. The results for Cases 1A and 2A are very similar but the later case has less ERW flow through the plant and thus a higher ERW discharge temperature. The result is less entrainment due to the more buoyant jet and a slightly thinner and warmer layer. Since the intake temperature is strongly dependent on the layer depth, the intake tem-

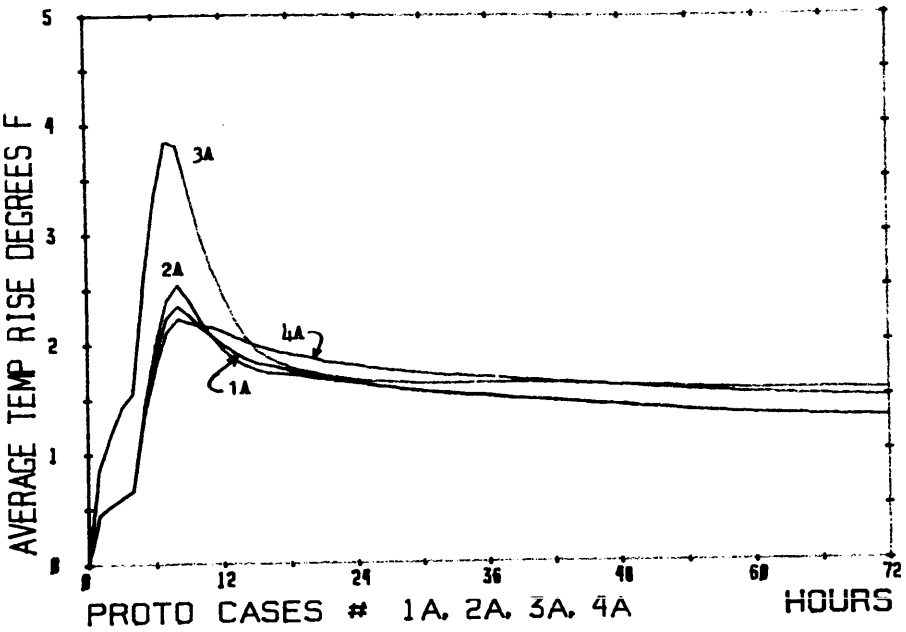

a) Average Upper Layer Temperature Rise

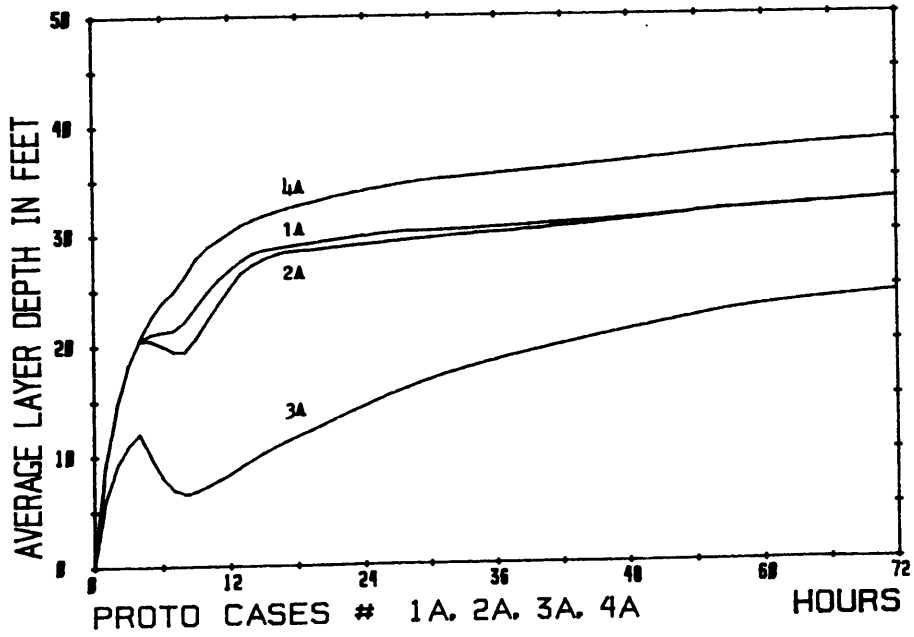

b) Average Upper Layer Depth

Figure 6-1: Comparison of Four Basic Prototype Operating Conditions (See Table 6-1)

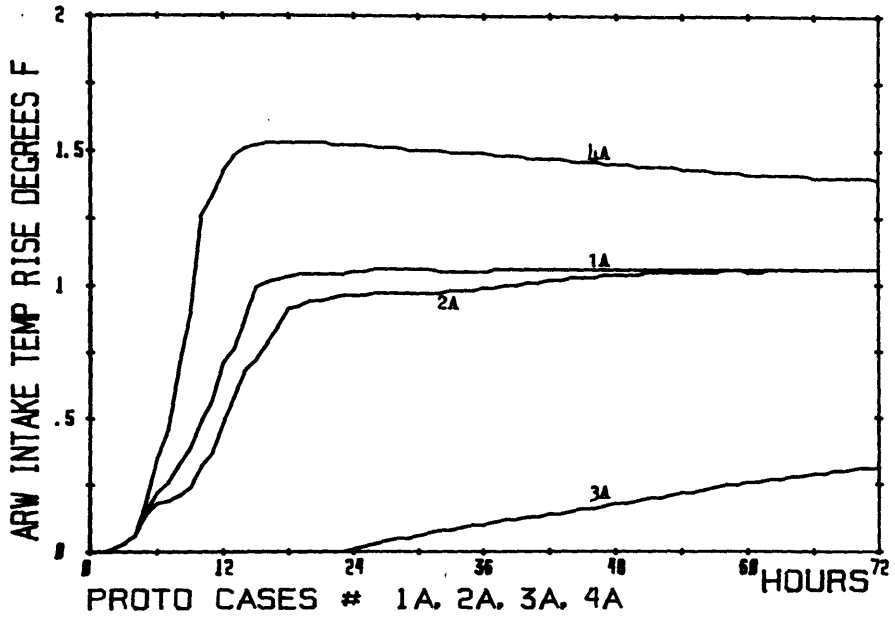

c) ARW System Intake Temperature Rise

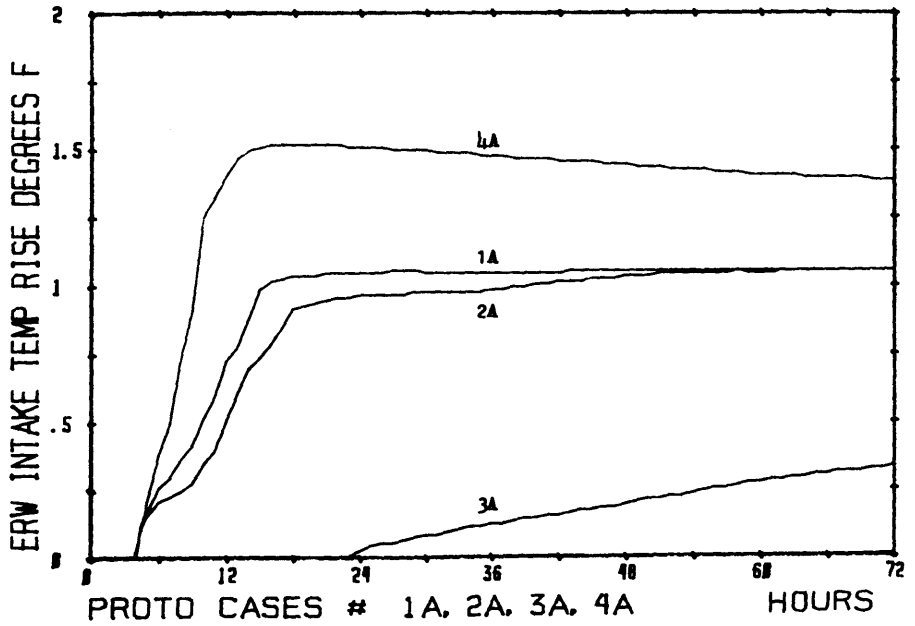

d) ERW System Intake Temperature Rise

Figure 6-1: Comparison of Four Basic Prototype Operating Conditions (See Table 6-1)

perature rises for 1A are higher than for 2A during the time period of differences in layer thickness.

The LOOP-LOOP case (4A) shows the highest intake temperature rises. It has the greatest total flow rates and the lowest average discharge temperatures. As a result, the entrainment is greatest and the resulting deep layer causes intake temperature rises of up to 1.5°F. Case 3A has the highest discharge temperatures which in turn results in reduced discharge mixing, shallow layer depth and the lowest intake temperature rise.

Figs. 6-1 considered emergency conditions in which all the cooling water trains were operative. If a single failure of any train is assumed, then the remaining trains will have to carry the same heat load, but with a reduced discharge flow and hence at increased temperature rises. The ERW intake temperature rise predictions for the equivalent "SING FAIL" conditions are shown in Figs. 6-2, plotted against the "ALL SYST" operating cases. The increased buoyancy of the discharge uniformly decreases entrainment from the lower layer, resulting in decreased layer thicknesses, increased average layer temperature rises and decreased intake temperatures.

6.4.3 Tidal Cases

When the 10 foot tide is introduced, a distinct transient variation in each parameter develops in accordance with the tidal cycle. As the tide rises, a net inflow into the basin occurs and the outflow of heated upper layer water from the basin over the sills is reduced.

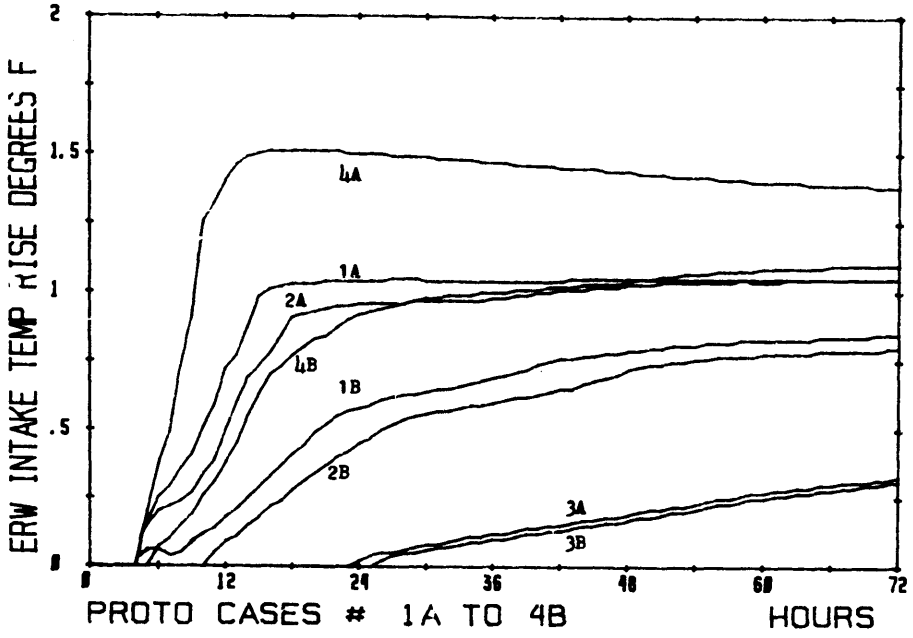

Figure 6-2: Comparison of ERW System Intake Temperature Rise for the Four Basic Operating Conditions and a Single Failure of each (see Table 6-1)

Thus the volume of heated water inside the breakwater increases during the tidal rise relative to the non-tidal case. This causes an increase in layer depth. As the tide falls, the upper layer volume is flushed, as the outflow of upper layer water exceeds the outflow under non-tidal conditions. Thus the layer thickness decreases to a minimum near low tide. The intake temperature rise closely follows the layer depth pattern. The average layer temperature rises also demonstrates the oscillatory response but exhibits some phase lag with respect to the response of layer depth or intake temperature rise.

Figures 6-3a to 6-3d illustrate the response for the LOOP-LOOP situation and Figures 6-4a to 6-4d illustrate the LOCA-NORM condition. It is interesting to note that on Figure 6-3b the layer depth of the tidal case oscillates around the one of the non-tidal case, as opposed to Figures 6-4b where the layer depth of the tidal case oscillates generally below the non-tidal case. This is due to the magnitude of the layer depth, and the nature of the heat curve. The deeper layer is more sensitive to the flow rate over the sills. Secondly, the heat load in the LOOP situation drops off more rapidly after the peak at four hours and is down to about 40% of the peak by 12 hours. This contrasts to the LOCA heat curve that decreases comparatively slowly and is still at 75% of its peak at 12 hours. The result is that the decrease in layer depth gained by the first tidal flushing effect is maintained in the LOCA case as compared to the LOOP case where the lower discharge temperatures and thus increased entrainment counteract the initial reduction in layer depth and the subsequent values oscillate

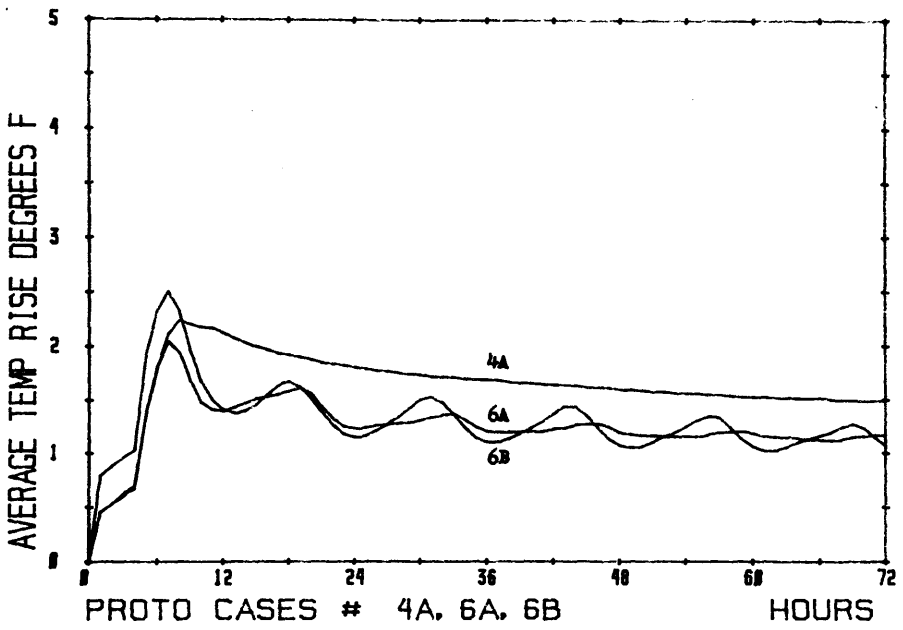

a) Average Upper Layer Temperature Rise

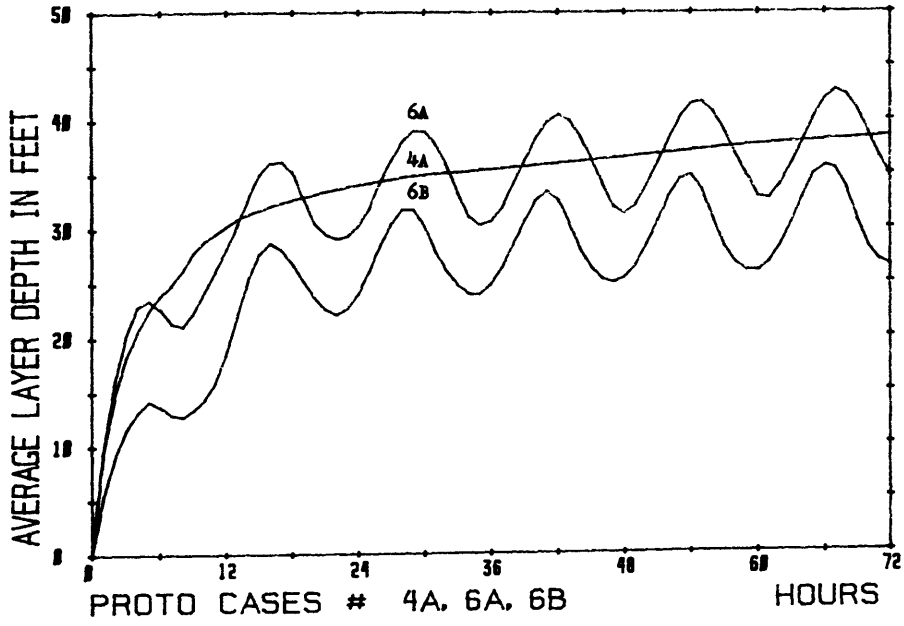

b) Average Upper Layer Depth

Figure 6-3: Comparison of a Tidal and Non-Tidal LOOP-LOOP (See Table 6-1)

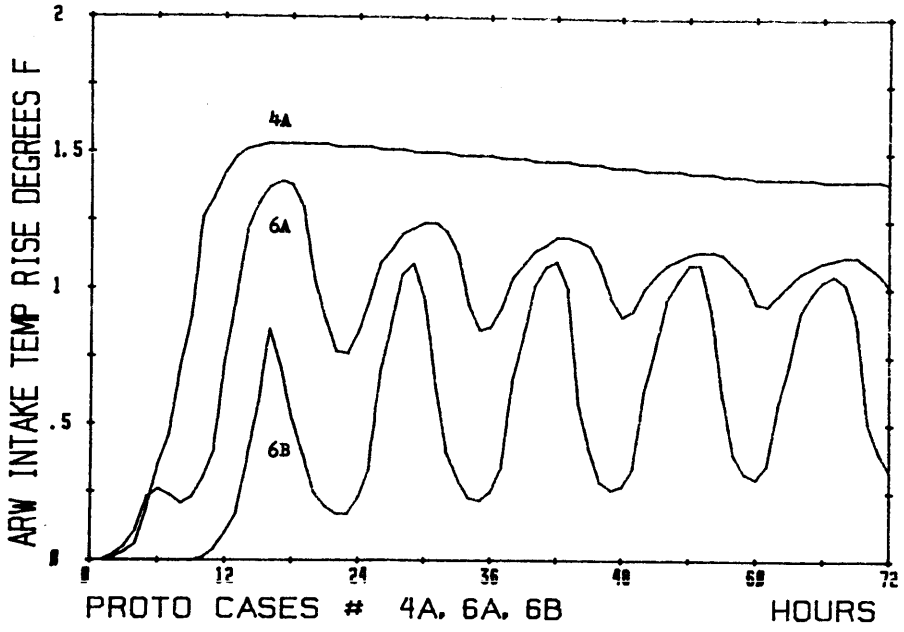

c) ARW System Intake Temperature Rise

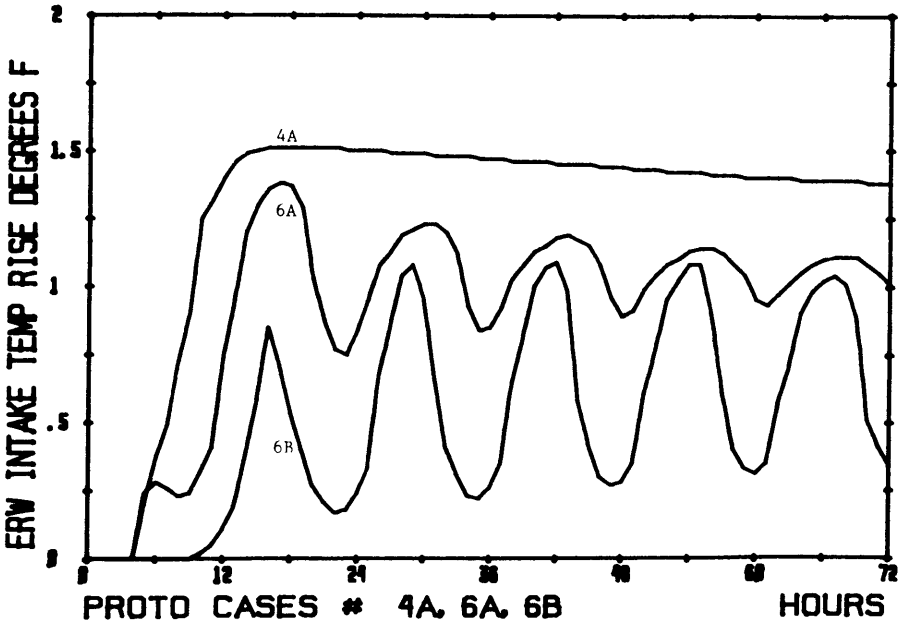

d) ERW System Intake Temperature Rise

Figure 6-3: Comparison of a Tidal and Non-Tidal LOOP-LOOP (See Table 6-1)

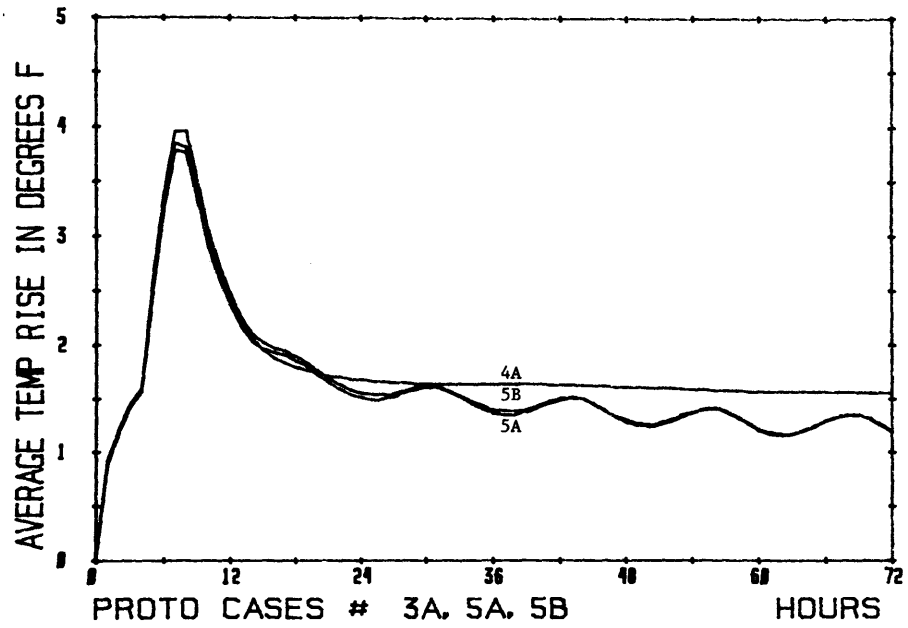

a) Average Upper Layer Temperature Rise

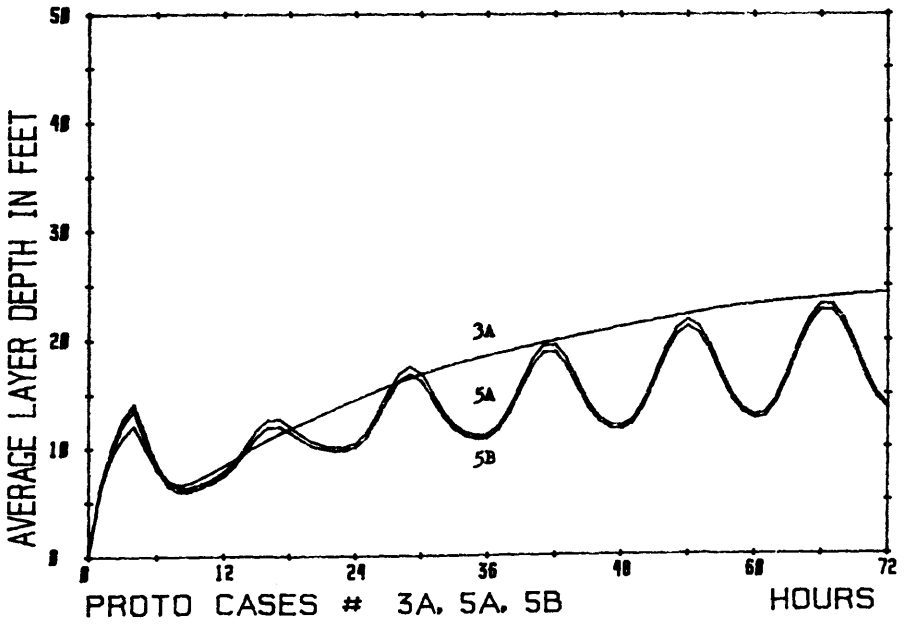

b) Average Upper Layer Depth

Figure 6-4: Comparison of a Tidal and Non-Tidal LOCA-NORM (See Table 6-1)

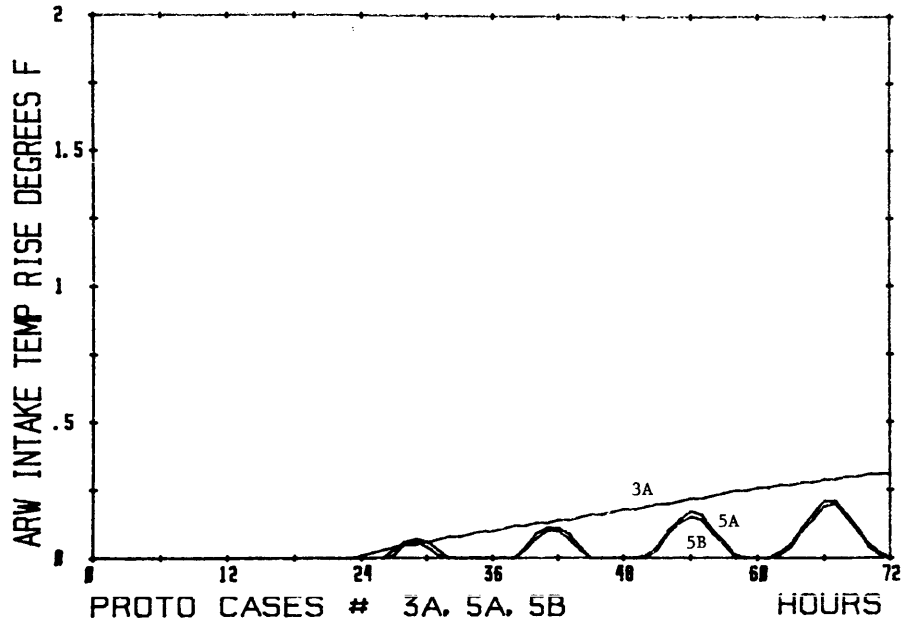

c) ARW System Intake Temperature Rise

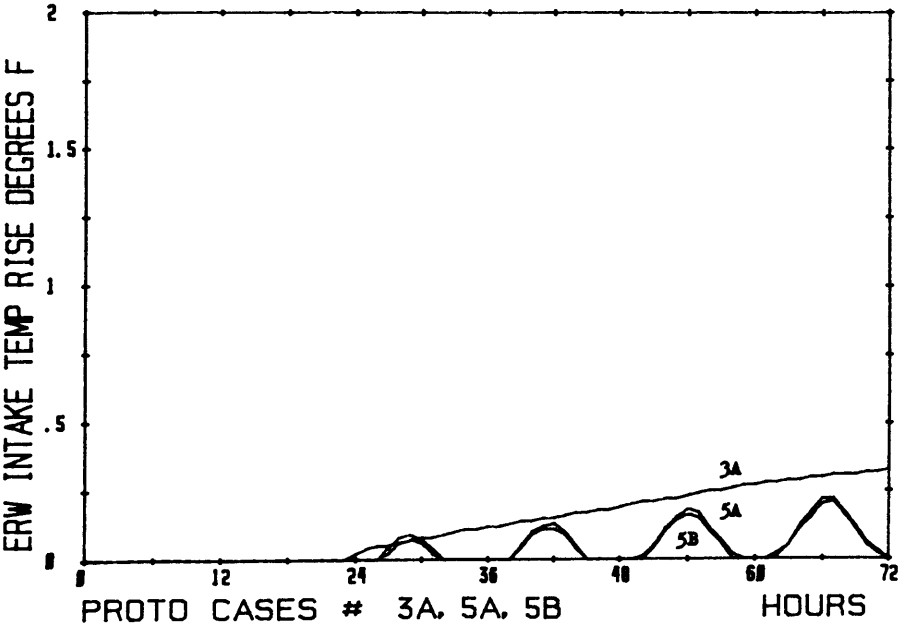

d) ERW System Intake Temperature Rise

Figure 6-4: Comparison of a Tidal and Non-Tidal LOCA-NORM (See Table 6-1)

around the non-tidal condition.

Although the layer depth exceeds the non-tidal prediction for the LOOP-LOOP, this is not reflected in the intake temperature since the average layer temperature is sufficiently reduced to compensate for the depth increase.

In the preceding tidal cases, the emergency heat release is assumed to begin at low tide. Figures 6-5a to 6-5d illustrate the shift due to simulating emergency conditions that initiate at mean water on a falling tide, case 6D, and at high tide, case 6E. The phase shifts are clearly illustrated but there is no significant change in the magnitude of any of the parameters.

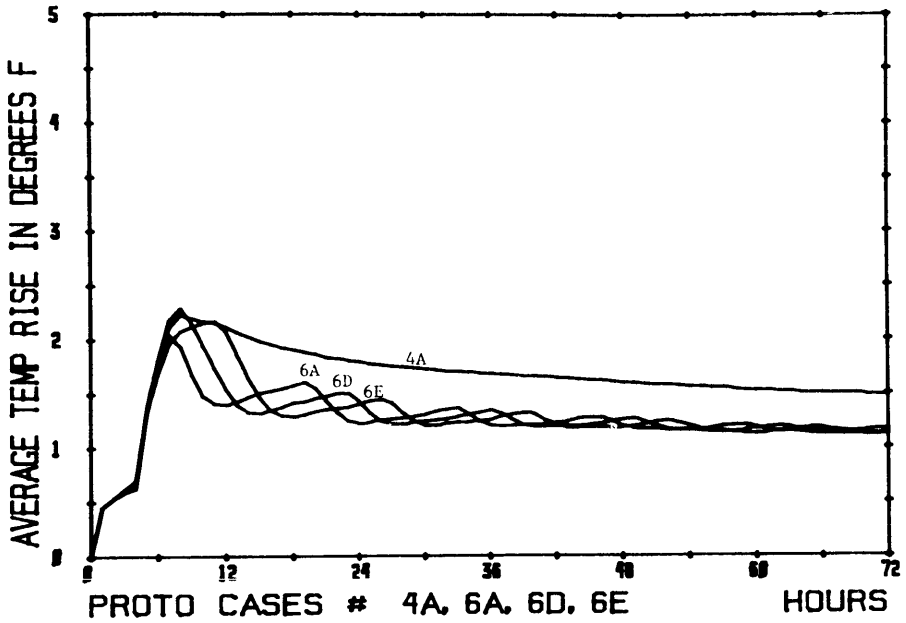

a) Average Upper Layer Temperature Rise

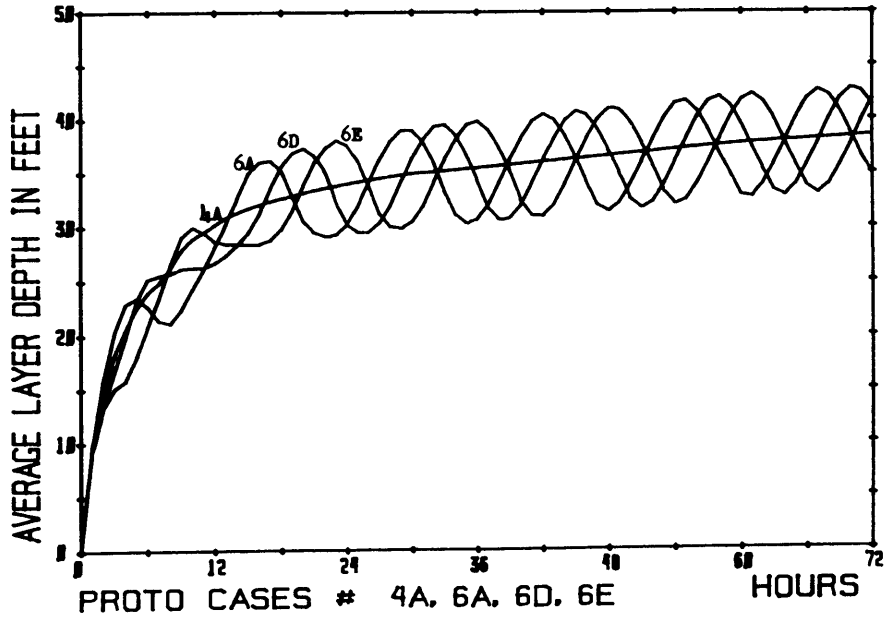

b) Average Upper Layer Depth

Figure 6-5: Comparison of Various Tidal Stages at Start of Tidal LOOP-LOOP (See Table 6-1)

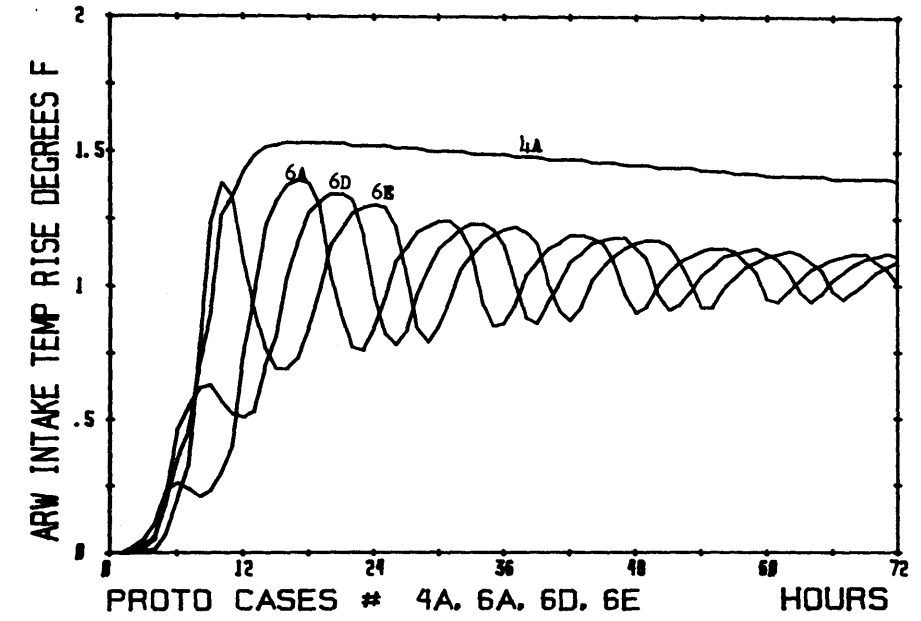

c) ARW System Intake Temperature Rise

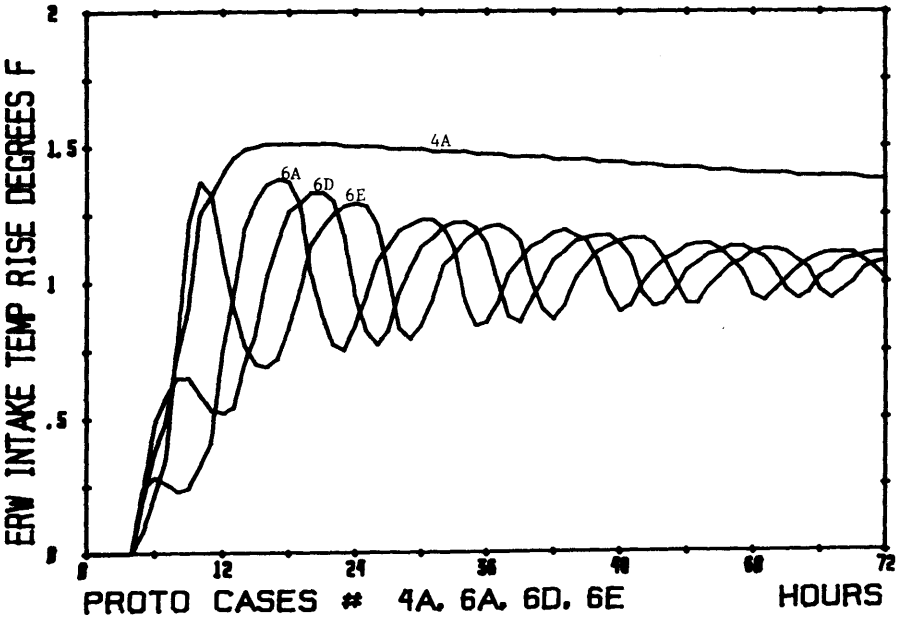

d) ERW System Intake Temperature Rise

Figure 6-5: Comparison of Various Tidal Stages at Start of Tidal LOOP-LOOP (See Table 6-1)

CHAPTER 7

Analytical Model Sensitivity Studies

The analytical model was run for a series of sensitivity studies to determine the response of predicted values to changes in individual parameters. Cases 4A (non-tidal conditions) and 6A (tidal conditions) were used as the standards for comparison. Both cases simulate a LOOP-ALL SYSTEM condition occurring at the two plants simultaneously, and thus represent the most significant intake temperature rises. The sensitivity tests can be divided into two groups: (1) design sensitivity to the physical parameters of the AGS design, and (2) formulation sensitivity to non-dimensional parameters in the formulation of the analytical model. Table 7-1 summarizes the fifteen sensitivity tests that were made. Cases 7 through 12B are related to design sensitivity. Cases 6C, 9 and 13 study formulation sensitivity.

7.1 Design Sensitivity

7.1.1 Intake and Discharge Design

a) Intake submergence: The standard design specifies intake submergence (depth to centerline) of 28.5 feet. As a comparison a submergence of 20.0 feet was simulated in Case 7. The results are plotted in Figures 7-1a to 7-1d as well as the results from Case 4A (28.5 feet). The shallower intake allows for a greater degree of recirculation of upper layer water and because of the closed loop opera-

Operating Condition: All cases listed below were LOOP - LOOP - ALL SYST

Proto Case #	Variation from standard conditions
6C	Φ = 0.5, Tide = 10 ft., Phase = π
7	Intakes at 20.0 feet below waterline
8A	Diameter of combined discharge = 7.0 feet Diameter of single ERW discharge = 5.5 feet
8B	Diameter of combined discharge = 4.0 feet Diameter of single ERW discharge = 2.5 feet
8C	Diameter of ARW intakes = 8.0 feet Diameter of ERW intakes = 6.5 feet
9	Area of layer, A_1, increased by 25%
10A	Sill width = 195 feet
10B	Sill width = 65 feet (equivalent to blockage of one sill)
10C	Sill depth at mean low water = 30 feet
10D	Sill depth at mean low water = 10 feet
11A	All heat loads are increased by 20%
11B	All heat loads are decreased by 20%
12A	Surface heat dissipation coef. increased by 20%
12B	Surface heat dissipation coef. decreased by 20%
13	Limiting ratio of jet depth to layer depth, β = 0.5

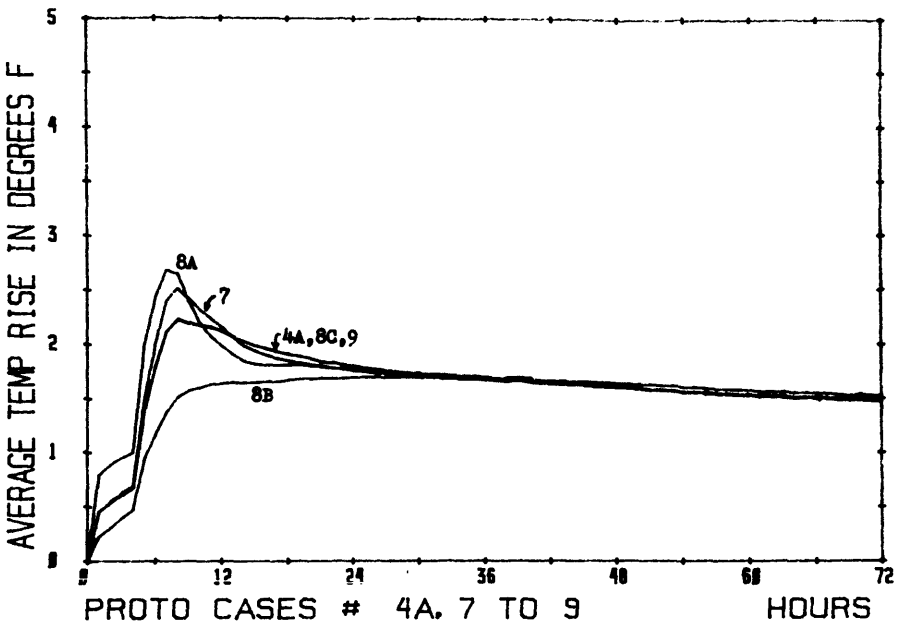

a) Average Upper Layer Temperature Rise

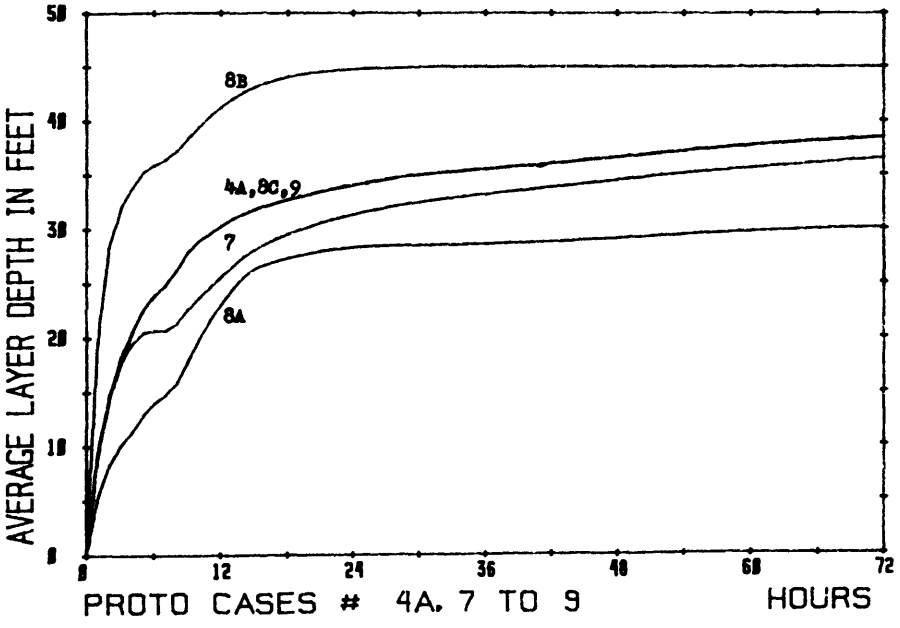

b) Average Upper Layer Depth

Figure 7-1: Comparison of Prototype Predictions with Variations of Intake Depth, Surface Area, and Discharge and Intake Diameters (see Table 7-1).

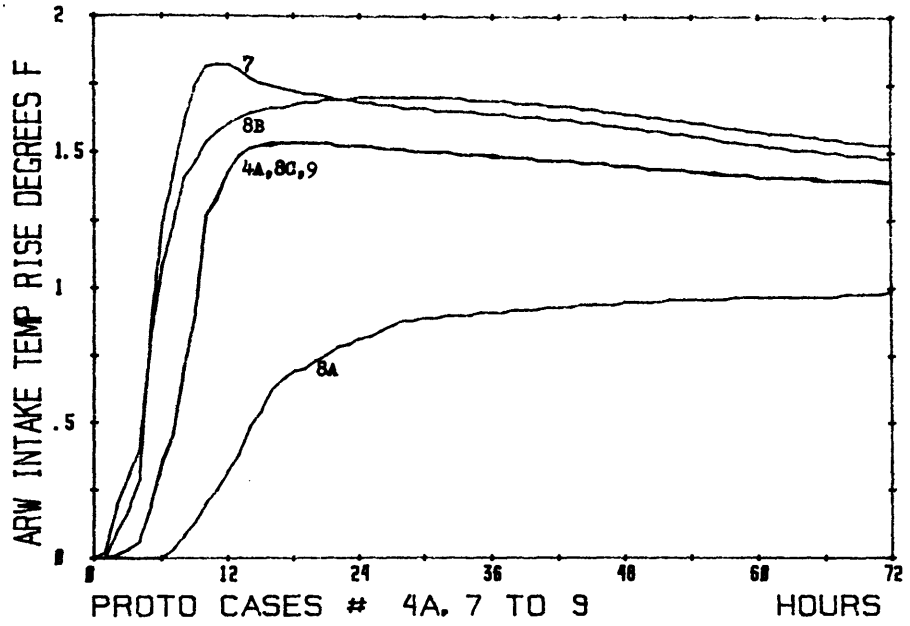

c) ARW System Intake Temperature Rise

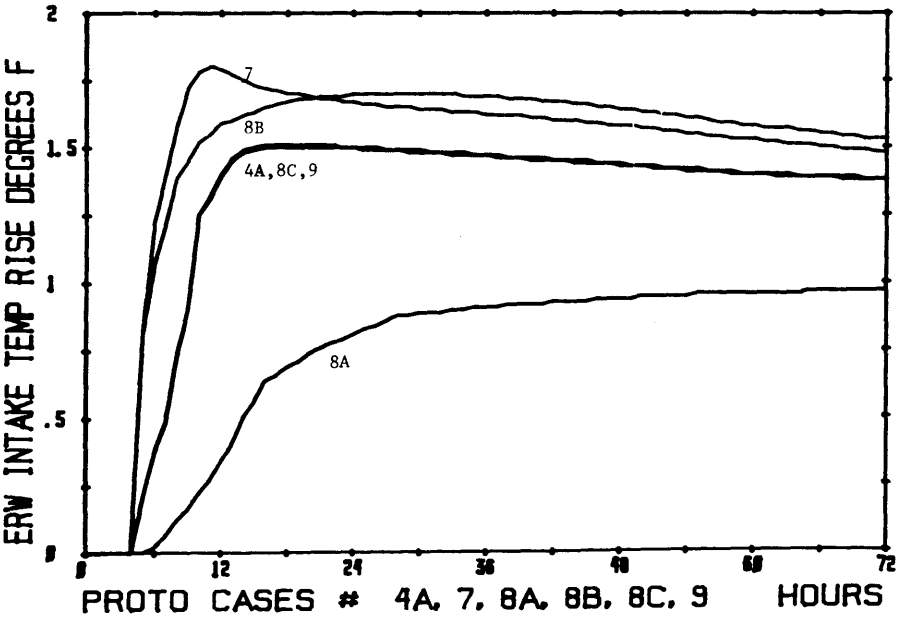

d) ERW System Intake Temperature Rise

Figure 7-1: Comparison of Prototype Predictions with Variations of Intake Depth, Surface Area, and Discharge and Intake Diameters (see Table 7-1).

tion, both the intake and discharge temperature rises above ambient will be increased. The higher discharge temperature rise results in less entrainment and thus a shallower layer. Furthermore, the greater recirculation coefficient also reduces the thickness of the layer by virtue of continuity. The differences in temperature rise are most evident in the earlier stage of peak heat loadings.

b) Intake diameter: Case 8C involved a 1.5 foot increase to the intake diameters from the original values of 6.5 feet (ARW) and 5.0 feet (ERW) to 8.0 feet and 6.5 feet, respectively. The combined model predictions are only weakly sensitive to changes in these intake diameters and the resulting simulation shows only very minor differences which are within the plotting accuracy with respect to the standard Case 4A. Changes in intake diameter affect the secondary parameter F_D (Eq. 3.34) only and are indeed expected to have minor impact as can be seen from the percent withdrawal equation, Eq. (3.38).

c) Discharge diameters: Changes in the discharge diameter affect the average discharge velocity and in turn the densimetric Froude number F_o' of the discharge. Considering Eq. (3.24), the larger the diameter, i.e., smaller F_o', the less entrainment. In Case 8A the standard diameters, namely 5.5 feet (combined) and 5.0 feet (ERW), are increased by 1.5 feet each and in Case 8B they are decreased by 1.5 feet each. Results are included in Figs. 7-1a to 7-1d. The larger diameters result in less entrainment and a consistently

thinner layer. The average layer temperature rise goes to a higher peak but then declines more rapidly than in the standard case 4A and ultimately levels off to the same level. The net result is a strong reduction in the intake temperature rises (from a maximum of about $1.5^{o}F$ for Case 4A to about $1.0^{0}F$ for Case 8A).

The effect of the smaller diameters in Case 8B is the opposite. A cooler but thicker layer results in more recirculation and thus higher intake temperature rises.

7.1.2 Area Within Breakwater Enclosure

Also illustrated on Figures 7-1 is Case 9, where the area of the breakwater enclosure A_1 (see Section 3.1), which is important for layer development, was increased by 25%. A priori, the increased area would be expected to yield a thinner layer since the same volume of hot water is spread over a larger area. However, this storage effect is only of significance during the initial highly transient period and has negligible effects on an overall basis. This is due to the fact that the jet discharge, sill control and selective withdrawal, all of which determine the overall response, are not dependent on the horizontal basin area. The comparison of Cases 9 and 4A in Figures 7-1 shows practically identical behavior.

7.1.3 Design of Breakwater Openings (Sills)

The breakwater openings control the heat from the upper layer. Variations in their design may be expected to have significant effects on the overall response. As has been reported in Section

3.2.1, the actual trapezoidal, curved, non-uniform sill opening has been schematized as a rectangular, straight, uniform canal of a certain depth, width and length. The sensitivity studies reported herein, therefore, do not only address the changes in design dimensions but also the problem of schematization. In the standard Case 4A, the sill width was schematized as 130 feet, and the depth at low water was 20 feet. In both Cases 10A and 10C the total sill cross sectional area was increased by 50%. In the first case the increase resulted from a width of 195 feet and in the second case a depth of 30 feet. In Cases 10B and 10D the cross sectional area was similarly reduced by 50%, in Case 10B by a width decrease to 65 feet, in Case 10D by a depth decrease to 10 feet. The results are plotted on Figures 7-2a to 7-2d. The larger sill opening, Cases 10A or 10C, permits greater outflow over the sill and thus produces both a lower temperature and a shallower layer, while the opposite trend occurs for the smaller sill openings. It is interesting to note that for the same change in cross sectional area, the results were more affected when the sill depth was changed rather than the sill width. This is reasonable since changes in the sill width only affect the cross sectional areas available for outflow, while changes in the sill depth affect both the cross sectional area and the buoyant driving force.

Based on the above comparisons the effect of schematization of the trapezoidal channel into a rectangular section can be assumed to be negligible as both the total cross sectional area and sill depth H_s were conserved. The additional schematization variable,

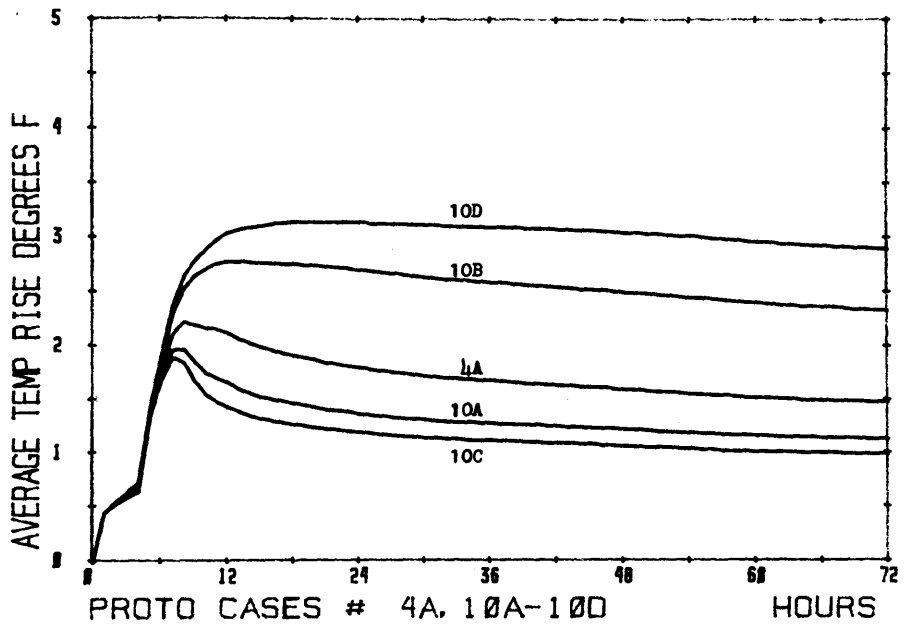

a) Average Upper Layer Temperature Rise

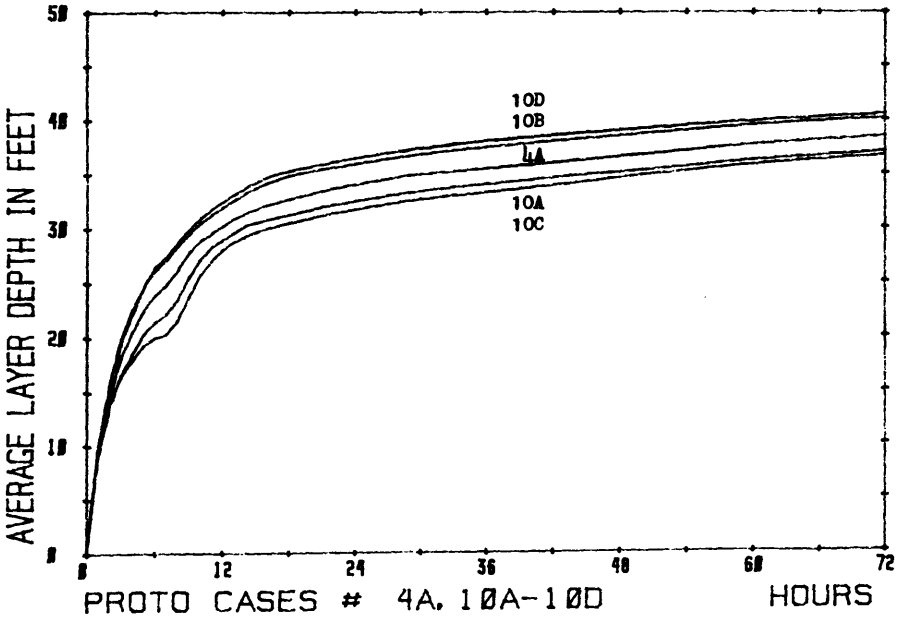

b) Average Upper Layer Depth

Figure 7-2: Comparison of Prototype Predictions with Variations of Dimensions of Breakwater Openings (see Table 7-1).

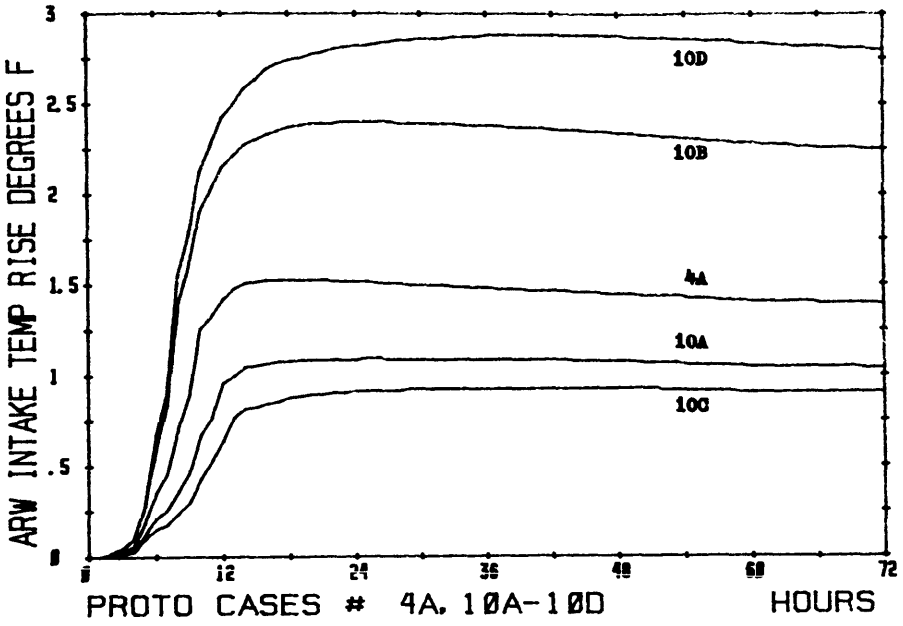

c) ARW System Intake Temperature Rise

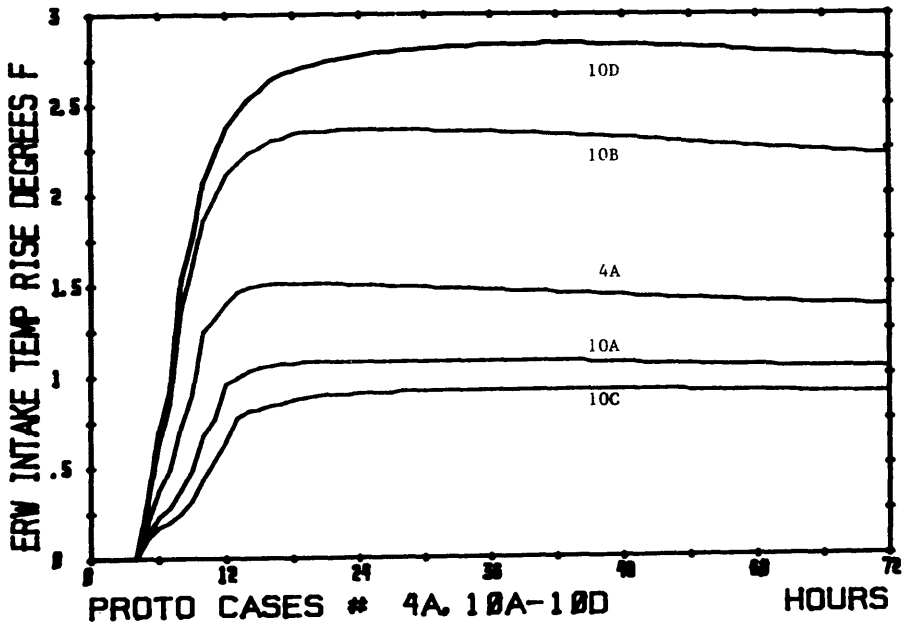

d) ERW System Intake Temperature Rise

Figure 7-2: Comparison of Prototype Predictions with Variations of Dimensions of Breakwater Openings (see Table 7-1).

namely the sill length L_s, is included in the parameter $\Phi = f_o L_s / H_s$, the sensitivity of which is discussed in paragraph 7.2.1.

7.1.4 Heat Loading

The transient heat load data used in the standard Case 4A was that provided by Offshore Power Systems. The intent was to examine how sensitive the model was to a change in the actual heat load, if the current specifications were modified. Case 11A represents an increase of 20% and Case 11B is a decrease of 20% in the applied heat loadings, that is, at each time step the actual specified values of Case 4A are changed by these percentage figures. Figures 7-3a to 7-3d illustrate the results. The increased heat load in Case 11A creates a warmer and thinner layer due to entrainment changes. However, the effect of the increased temperature rise is large enough to overcome the stabilizing effect of the shallower layer, so that the intake temperature rises after twelve hours are increased with respect to the Case 4A. Of all the simulation cases, this is the only situation where the relative ranking of the intake temperature use does not agree with the ranking of the layer depth.

7.1.5 Heat Dissipation

In the prototype computations of Chapter 6 a linearization function for the surface dissipation of the excess heat to the atmosphere was assumed. A conservatively low value of the heat dissipation coefficient K_e = 5 BTU/sq. ft.-hour - ^oF was taken. The sensitivity of the selection of this coefficient is shown in Figs. 7-4a

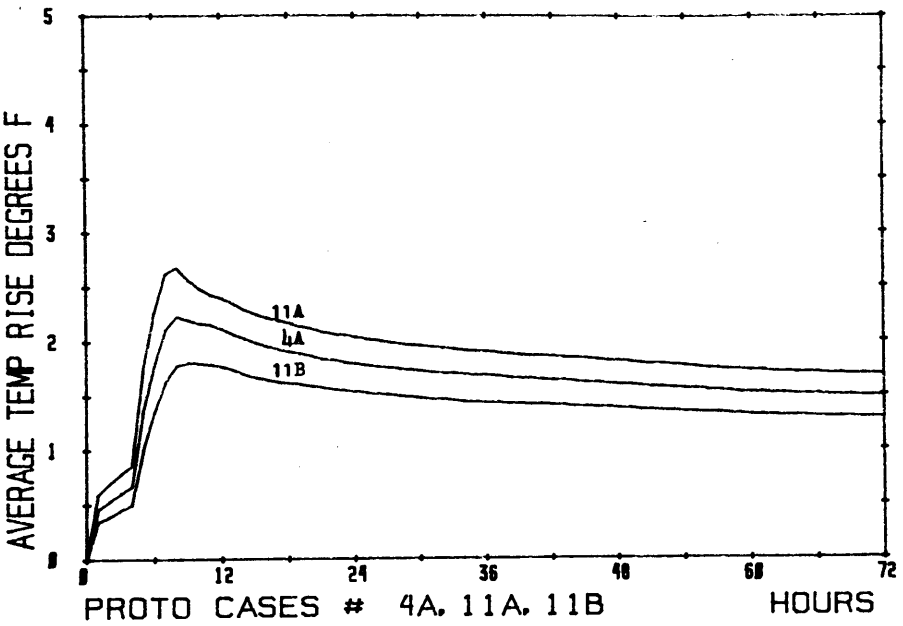

a) Average Upper Layer Temperature Rise

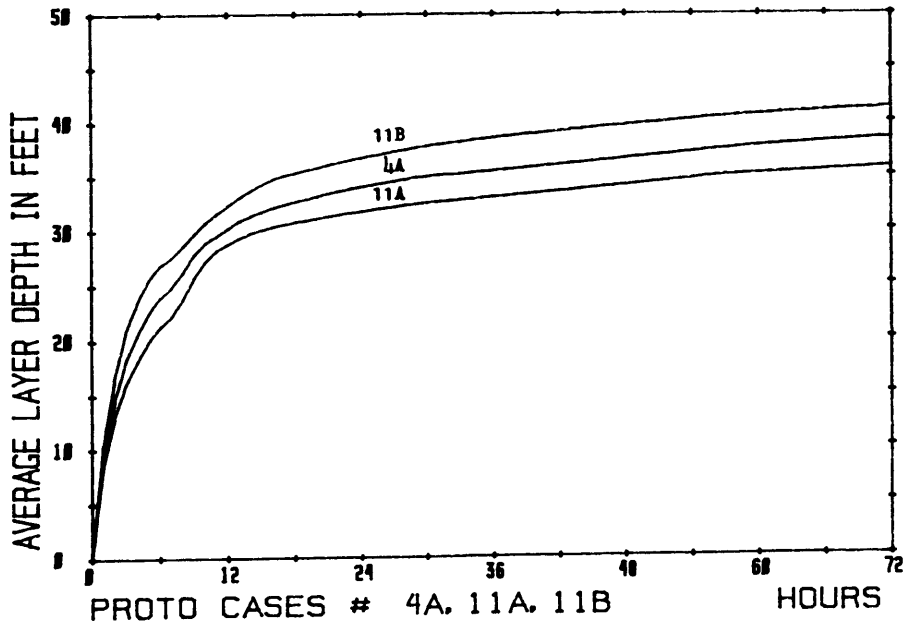

b) Average Upper Layer Depth

Figure 7-3: Comparison of Prototype Predictions with Variations of Applied Heat Loads (see Table 7-1).

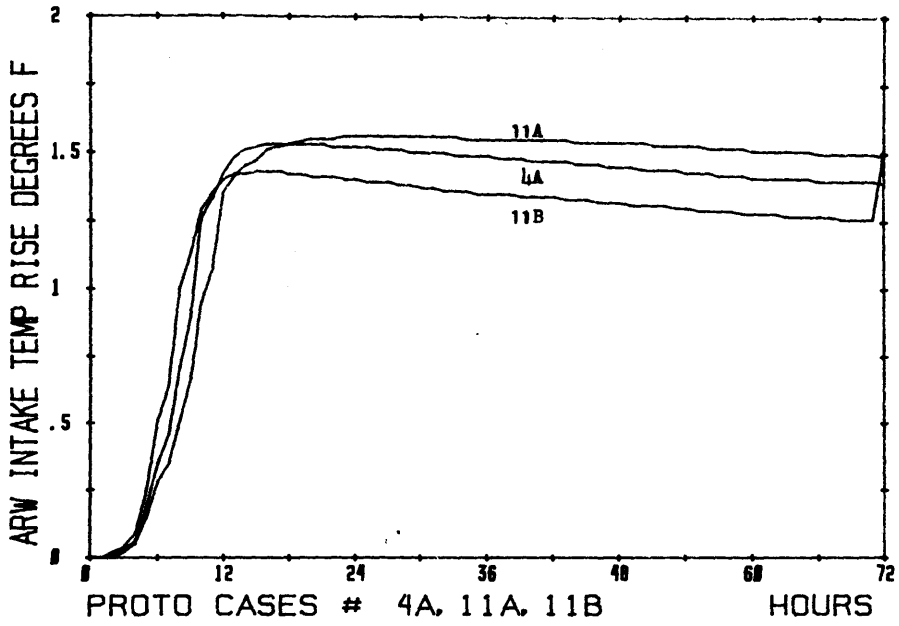

c) ARW System Intake Temperature Rise

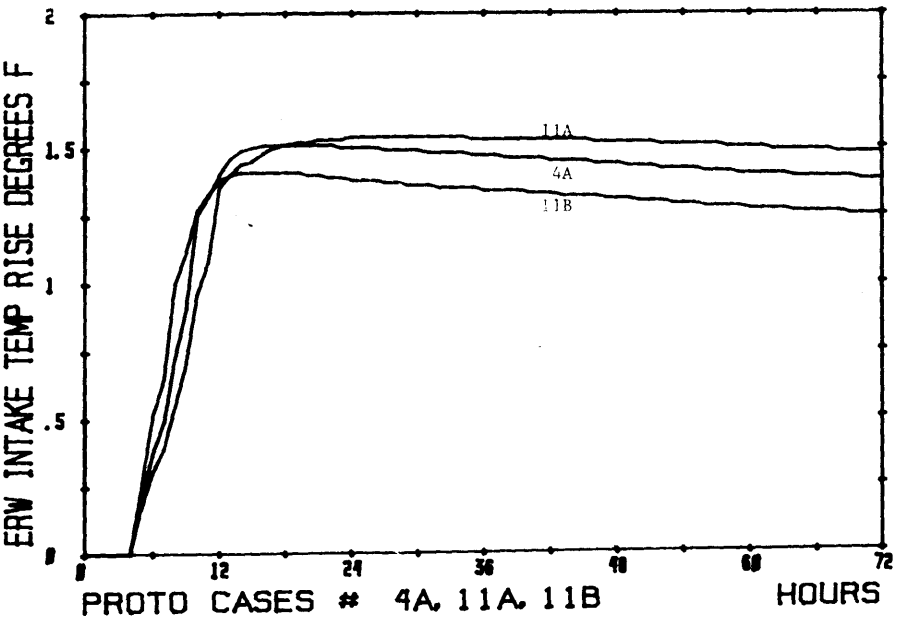

d) ERW System Intake Temperature Rise

Figure 7-3: Comparison of Prototype Predictions with Variations of Applied Heat Loads (see Table 7-1).

to 7.4d. In Case 12A the value was increased by 20%, and in Case 12B decreased by 20%. The response curves vary insignificantly from those for Case 4A. Thus the effect of the surface heat dissipation term on the total heat balance is small and a difference of as much as 40% in the coefficient yields only very minor differences in the results.

7.1.6 Summary

The two processes which are important for the ultimate removal of waste heat out of the breakwater enclosed basin are the heat transport by means of stratified flow through the sill openings and surface heat dissipation. Of these, the stratified flow heat transport is by far the most important. For the standard Case 4A (see also Appendix A) this advective mechanism represents at every instant of time between 95 and 98% (values depend on time) of the total heat flux out of the basin, while surface heat loss is responsible for the remaining few percent.

Furthermore, the total system response, primarily in terms of intake temperature rises, is strongly dependent on the geometry of the sill openings. Thus, if one of the two sills becomes completely blocked (Case 10B) during an emergency condition, then significant changes in the intake temperatures occur.

The second most sensitive design variable is the diameter of the discharge openings. Larger diameters (smaller discharge densimetric Froude numbers) generally decrease the computed intake temperature rises.

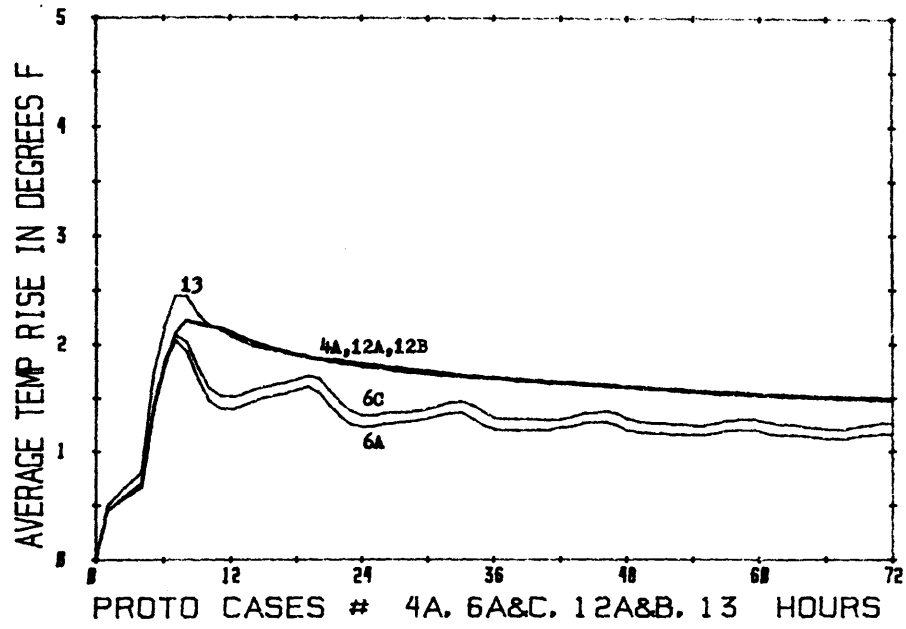

a) Average Upper Layer Temperature Rise

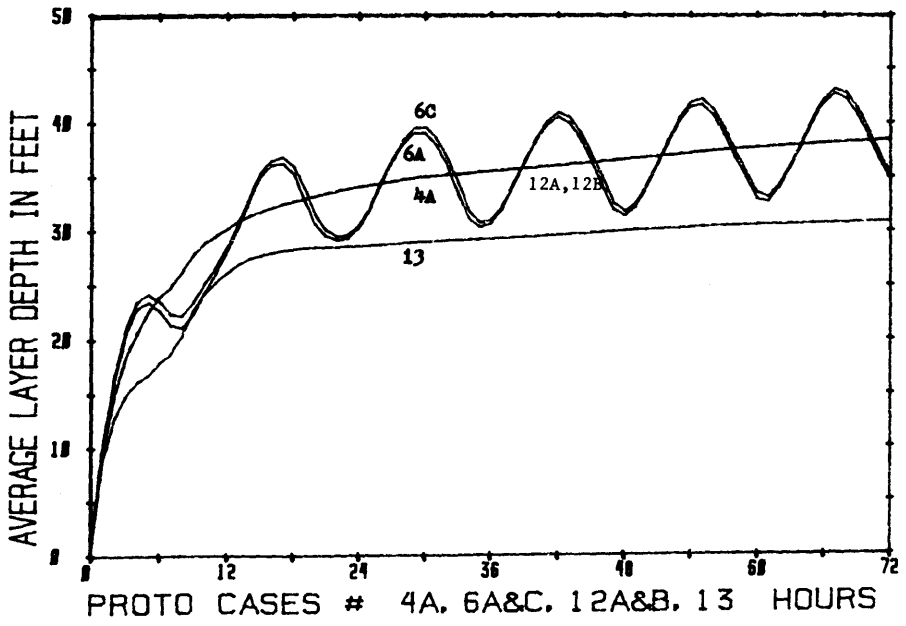

b) Average Upper Layer Depth

Figure 7-4: Comparison of Prototype Predictions with Variations of Heat Dissipation Coefficient, Sill Factor, and Entrainment Depth Ratio β (see Table 7-1).

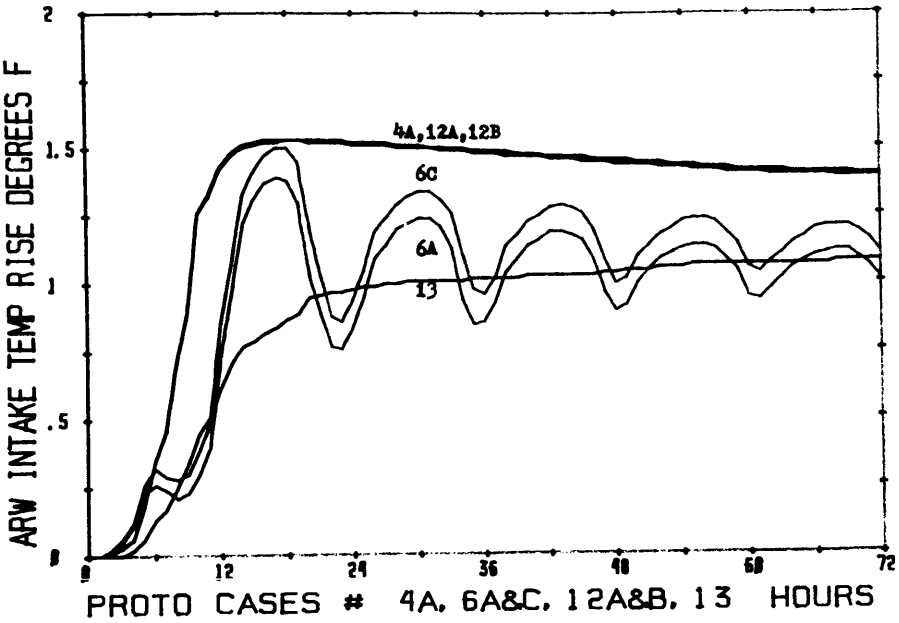

c) ARW System Intake Temperature Rise

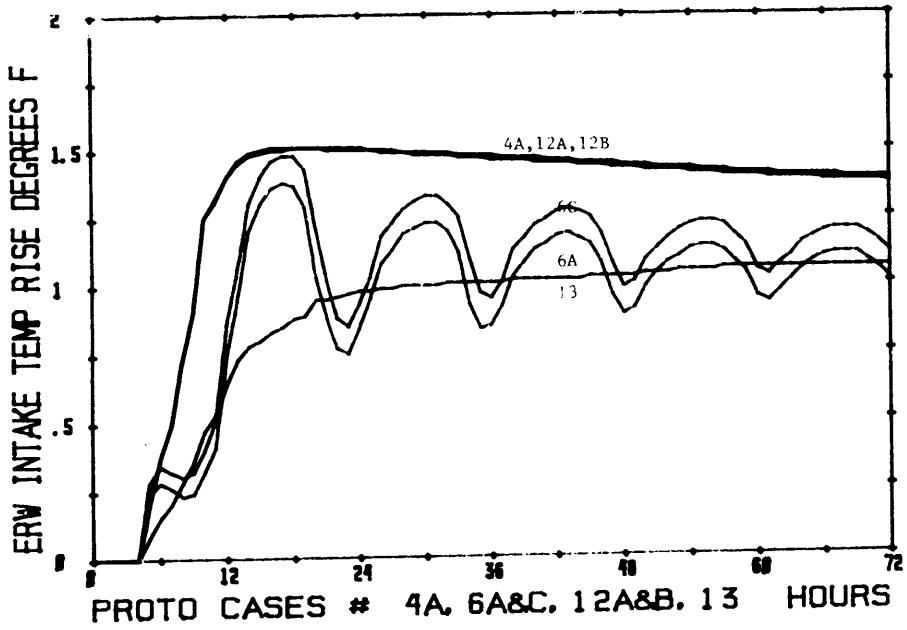

d) ERW System Intake Temperature Rise

Figure 7-4: Comparison of Prototype Predictions with Variations of Heat Dissipation Coefficient, Sill Factor, and Entrainment Depth Ratio β (see Table 7-1).

7.2 Formulation Sensitivity

7.2.1 Schematization of Sill Control

The rounded breakwater entrance has been schematized as a straight channel with control sections at the outer (ocean) end and occasionally at the inner end. The effects of this schematization and the bottom friction of the channel are contained in the value of the factor, $\Phi = f_o L_s / H_s$. A standard value of $\Phi = 0.2$ was used in all computations which represented a scaling of the best-fit value ($\Phi = 0.5$) of the hydraulic scale model verification, the scaling factor being the ratio of friction factors in prototype and model. Case 6C used a value of $\Phi = 0.5$ for the prototype calculations. The comparison with Case 6A is shown in Fig. 7-4. The increased value of Φ, i.e., the increased friction at the sill, results in reduced heated water outflow and thus both a deeper and a warmer layer. This then results in greater intake temperature rise. The effects, however, are limited and can be conceived as scale effects since the model was undistorted, thus not observing the scaling condition for stratified flow or shallow water flow (Eq. 4.5).

7.2.2 Entrainment of Buoyant Jets in Stratified Receiving Water

The modification of the jet mixing relationships for buoyant discharges into unstratified receiving water were discussed in Section 3.2.2. One of the major parameters introduced was the value β (Eq. 3.29) which specified the ratio of predicted jet penetration depth and depth of the heated layer below which no entrainment of

water from the lower (ambient) into the upper layer occurs. This parameter is thus a measure of the mixing effectiveness of the buoyant jet discharge. Based on the verification phase with the experimental data on optimal value of $\beta = 0.33$ was determined, which indicates that some interfacial entrainment will occur even if the jet penetration is only one third of the upper layer thickness. Case 13 (see Fig. 7-4) considers a value of $\beta = 0.5$ for comparison purpose, i.e., the interfacial stratification is assumed to cause a more pronounced dampening of entrainment. The reduced entrainment yields a shallower layer and subsequently reduced intake temperature rises. Thus while choice of $\beta = 0.33$--although supported by the experimental results--seems intuitively low; it can be considered as a conservative estimate, since any increase in the parameter could yield lower intake temperature rises. Indeed, the problem of jet entrainment in a stratified fluid system was identified in this study as the most pressing research area for future investigations.

7.2.3 Schematization of Horizontal Area

The horizontal area within the breakwater enclosure, which is important for the storage terms in the basin continuity and heat conservation Eqs. (3-4) and (3-7) , is variable with the depth below the water surface. The variability for the AGS design was shown in Fig. 3-2. The variable area has been schematized by an average value as shown in the same figure. The effect of this schematization can be considered as negligible based on the design

sensitivity studies discussed in paragraph 7.1.2 which considered a percentage change in the total design area.

CHAPTER 8

Conclusions

This study was concerned with the hydrodynamic and heat transport aspects of transient heat releases during emergency cooling operations at nuclear power plants located in offshore breakwater enclosures. The study had two major objectives, namely (i) the development of a mathematical prediction model for the distribution within the breakwater enclosure of the released heat and (ii) the specific application of the predictive model to the Atlantic Generating Station proposed by the New Jersey Public Service Electric and Gas Company. The study consisted of concurrent theoretical and experimental phases.

8.1 Mathematical Predictive Model

The mathematical model consists of the simultaneous, time-dependent numerical description of the various physical processes which occur during an emergency cooling operation. Insight into the occurrence of these processes was obtained through the concurrent experimental study. The mathematical model schematizes the temperature field within the breakwater enclosure as a two-layered stratified system with uniform layer depth and average temperature rise; the validity of this assumption being verified in the experiments. Mass and heat fluxes in and out of the upper layers control volume are given through these four processes: 1) Jet entrainment at the interface, governed by the characteristics of the near-surface jet

discharges, 2) Stratified flow control of the breakwater openings which controls the exchange flow rates between the enclosed basin and the surrounding ocean, 3) Selective withdrawal at the submerged intakes into the cooling system, and 4) Surface heat dissipation to the atmosphere. Formulations for these processes, based on established analytical techniques or basic experimental data, were included in the mathematical model which consisted of two time-dependent conservation equations for the volume and heat of the upper layer control volume, respectively.

8.2 Experimental Study and Verification of the Mathematical Model

A physical scale model of the Atlantic Generating Station was constructed at an undistorted scale of 1:81. The model replicated the salient features of the floating units, the emergency cooling systems and the breakwater enclosure, and included the capability of simulating tidal effects.

The physical scale model was not used to provide actual prediction for the prototype. This was because of several limitations in the experimental setup and scaling inconsistencies, all of which constrain the accuracy and flexibility of physical scale models for predictions of complex mixing and heat transport phenomena.

The physical scale model, however, provided a valuable data base for the verification of the mathematical model, which could be applied using the test conditions as input. The mathematical model and experimental data were compared for a variety of conditions, simulating constant heat loads, variable heat loads and/or tidal

effects. The model-data comparison established the mathematical model as a reliable tool for actual prototype predictions.

8.3 Predictions for the Atlantic Generating Station

The analytical model was applied to predict the temperature distribution within the breakwater and intake temperature rises for the Atlantic Generating Station. The model was run for standard design conditions (listed in Table 6-1) and for conservative assumptions of hydrographic and meteorological conditions during the hypothetical emergency events. Several combinations of emergency heat releases were simulated. For the standard design, maximum intake temperature were always below a value of $1.5^{o}F$ which occurred during the initial 12-hour period for a condition of loss of offsite power (LOOP) at both plants simultaneously.

For the geometry of the Atlantic Generating Station, the mathematical model established the importance of the stratified flow at the breakwater openings. The stratified flow acts as the major mechanism which removes the excess heat from the breakwater enclosed basin. In comparison, surface heat loss which is the second mechanism for ultimate heat removal is of lesser importance. Tidal changes significantly influence the cooling performance within a tidal period, but have little overall effect.

Studies on the sensitivity of the design parameters for the Atlantic Generating Station were also performed. The most significant design variables are in the order of their importance:

geometry of breakwater openings, size of discharge ports and submergence of intakes. Table 8-1 gives a qualitative summary of design sensitivity studies that were conducted.

The security beam - oil boom structure which is proposed to be constructed within the breakwater enclosure was found to have a limited effect on the heat release conditions, as long as the immersion of the oil boom is less than about 10 feet.

8.4 Recommendation for Future Research

The initial jet mixing has a significant effect on the transient development of the heated layer within the basin. As time proceeds, the buoyant jets discharge into a stratified fluid system. Modifications of jet discharge formulations into unstratified receiving water were used in the present model to account for the influence of stratification and were verified in the experimental comparison. It is recommended that further research be directed at this phenomenon which is also of importance in general cooling pond applications.

Table 8-1: Qualitative Summary of Prototype Design Sensitivity

Parameter Change*	Effect relative to standard condition**			Comments	Detailed Description (Chapter 7)
	Layer Thickness	Layer Temp.	Intake Temp.		
Increase heat load while maintaining flow rates	thinner	higher	higher	Higher discharge temp. yields more buoyant layer. Intake temperature reflects layer temperature increase	pg. 146
Tide (emergency begins at low water)	oscillates about non-tidal	lower	lower	Flushing action of tide reduces layer heat content	pg. 128
Tide (emergency begins at high water)	Same as above but oscillations shifted to follow tide			Variation in starting time yields a phase lag	pg. 133
Decrease submergence of intakes	thinner	higher at start	higher	Greater recirculation results in warmer, more buoyant layer	pg. 136
Increase discharge diameters	thinner	higher at start	lower	Larger diameters result in lower exit velocities, thus less entrainment and a thinner layer	pg. 140
Increase intake diameters	negligible	negligible	negligible	Selective withdrawal relatively insensitive to diameter changes in intake	pg. 140
Increase horizontal area of breakwater basin	negligible	negligible	negligible	Added storage has little dynamic effect	pg. 141
Increase cross-sectional area of breakwater opening	thinner	lower	lower	Larger opening permits greater outflow of heated layer over sills	pg. 141
Increase surface heat dissipation	negligible	negligible	negligible	Major ultimate heat sink is given by stratified flow through breakwater openings	pg. 146

* Parameter changes within about 25% of standard conditions are considered

** Standard condition: Double loop heat release, MLW, no tidal change, (see Table 6-1).

LIST OF SYMBOLS

a_1 = depth of upper layer at sill

a_2 = depth of lower layer at sill

A_1 = horizontal basin area at elevation $(H-h_1)$ above bottom

A_d = cross-sectional area of a discharge port

A_p = horizontal area of floating plants

A_S = total water surface area within basin excluding plants

A_t = $A_S + A_p$ = horizontal area within basin at surface elevation

A' = constant approximation for total horizontal area

A'' = $A' - A_p$ = constant approximation for horizontal area excluding plants

c_p = specific heat of water

d = characteristic "diameter" of discharge port = $A_d/2$

D = diameter of intake port

D = distortion ratio of model (Section 4.1)

E_V = vertical entrainment ratio

F = generalized densimetric Froude number

F_o' = characteristic densimetric Froude number of a surface discharge

F_r = ratio of prototype Froude number to model Froude number

F_1 = Froude number of upper layer at sill

F_2 = Froude number of lower layer at sill

F_{1H} = modified Froude number of upper layer at sill

F_{2H} = modified Froude number of lower layer at sill

F_{net} = Froude number of net flow at sill

F_H = Froude number of intake based on distance to layer interface

F_D = Froude number of intake based on intake diameter

F_ℓ = Froude number of intake based on interface thickness

F_{H_c} = critical limiting value of intake Froude number

f_i = interfacial friction factor

f_o = friction factor of schematized breakwater openings

g = gravitational constant

H = total water depth in basin

H_i = distance from intake centerline to interface

H_1 = non-dimensionalized depth of upper layer at sill

H_2 = non-dimensionalized depth of lower layer at sill

H_s = total depth at sill

h_{max} = maximum effective depth of surface jet

h_1 = schematized average upper layer depth

J_A = heat dissipation to atmosphere

J_P = heat load of plant discharge

J_S = flux of heat out of basin through breakwater openings

K_e = surface heat dissipation coefficient

L_s = schematized length of breakwater opening

ℓ = thickness of layer interfacial zone

n = number of breakwater openings

Q = ratio of outflow/inflow at sills

Q_d = discharge flow from a single discharge port

Q_D = total discharge flow from plants

Q_e = total entrainment flow from a single jet

Q_{ev} = vertical entrainment flow from a single jet

Q_E = total entrainment flow from all jets

Q_i = intake flow into a single intake port

Q_I = total intake flow into all intakes

Q_r = recirculation flow into a single intake

Q_R = total recirculation flow into all intakes

Q_r = also used as ratio of prototype to model flows

Q_S = total flow out of upper layer through breakwater openings

Q_S^* = limiting entrainment flow based on restruction at sill openings

q_{net} = net flow over sills per unit width

q_1 = upper layer flow per unit width at sills

q_2 = lower layer flow per unit width at sills

S_S = dilution ratio of surface jet discharge

t = time in hours

t_r = ratio of prototype time to model time

T_1 = schematized average upper layer temperature

T_2 = ambient, lower layer water temperature

T_d = discharge temperature

T_i = intake temperature

T_E = equilibrium temperature

T_s = surface temperature

ΔT_1 = temperature rise of upper layer above ambient

ΔT_i = intake temperature rise

U_d = average discharge velocity of jet

$\forall_1$ = volume of the heated upper layer

V_m = characteristic velocity of model

V_p = characteristic velocity of prototype

V_r = ratio of prototype of model velocities

W_s = schematized width of breakwater openings

X_{max} = non-dimensional distance from discharge point where maximum jet depth is predicted

Z_m = characteristic vertical length of model

Z_p = characteristic vertical length of prototype

Z_r = ratio of prototype length to model length

α = ratio of interfacial friction to bottom friction, f_i/f_o

β = limiting depth ratio of jet entrainment

λ = recirculation ratio

Φ_n = net heat flux to or from atmosphere

Φ = non-dimensional sill control factor

ρ = density of water

$\Delta\rho$ = density difference due to temperature change

ρ_1 = density of upper layer

ρ_2 = density of lower layer

τ_b = bottom shear factor

τ_i = interfacial shear factor

REFERENCES

1. Craya, A., "Recherches Théoriques sur L'Écoulement de Couches Superposées de Fluides de Densités Differentes," La Houille Blanche, Jan.-Feb., 1949, pp. 44-55.

2. Gariel, P., "Recherches Experimentales sur L'Écoulement de Couches Superposées de Fluides de Densités Differentes," La Houille Blanche, Jan.-Feb., 1949, pp. 56-64.

3. Jirka, G.H., Abraham, G., and Harleman, D.R.F., "An Assessment of Techniques for Hydrothermal Prediction," Technical Report No. 203, Ralph M. Parsons Laboratory for Water Resources and Hydrodynamics, Department of Civil Engineering, MIT, July 1975.

4. Jirka, G.H. and Harleman, D.R.F., "The Mechanics of Submerged Multiport Diffusers for Buoyant Discharges in Shallow Water," R. M. Parsons Laboratory for Water Resources and Hydrodynamics, Department of Civil Engineering, MIT, Technical Report No. 169 (1973).

5. Karelse, M., "Vertical Exchange Coefficients in Stratified Flows, Chapter 2 of "Momentum and Mass Transfer in Stratified Flows," (H.N.C. Breusers, Editor), Delft Hydraulic Laboratory, Report R. 880, Delft, The Netherlands (1974).

6. Katavola, Daniel S., "An Experimental Study of Three-Dimensional Selective Withdrawal from Thermally Stratified Fluid System," Masters Thesis for the Department of Ocean Engineering, MIT, September 1975.

7. Kullenberg, G., "Vertical Diffusion in Shallow Water," Tellus 23, 2 (1971).

8. Pearce, A.F., "Critical Reynolds Number for Fully-Developed Turbulence in Circular Submerged Water Jets," Council for Scientific and Industrial Research, Report ME6475, Pretoria, South Africa, August 1966.

9. Rigter, B.P., "Density Induced Return Currents in Outlet Channels," Proc. ASCE, J. of Hydraulics Div., HY2 (1970).

10. Ryan, P.J. and Harleman, D.R.F., "Analytical and Experimental Study of Transient Cooling Pond Behavior," Technical Report No. 161, Ralph M. Parsons Laboratory for Hydrodynamics and Water Resources, MIT, February, 1973.

11. Schijf, J.B. and Schonfeld, J.C., "Theoretical Considerations on the Motion of Salt and Fresh Water," Proc. Minnesota Int. Hydraulics Convention, IAHR and Hydr. Div., ASCE (1953).

12. Stolzenbach, K.D., Adams, E.E., Harleman, D.R.F., "A User's Manual for Three-Dimensional Heated Surface Discharge Computations," Technical Report No. 156, Ralph M. Parsons Laboratory for Water Resources and Hydrodynamics, Department of Civil Engineering, MIT, September 1972.

13. Stolzenbach, K.D. and Harleman, D.R.F., "An Analytical and Experimental Investigation of Surface Discharges of Heated Water," Technical Report No. 135, R. M. Parsons Laboratory for Water Resources and Hydrodynamics, Department of Civil Engineering, MIT, February 1971.

14. Ungate, C., Harleman, D.R.F., and Jirka, G.H., "Mixing of Submerged Turbulent Jets at Low Reynolds Numbers," Technical Report No. 197, Ralph M. Parsons Laboratory for Hydrodynamics and Water Resources, MIT, February 1975.

Appendix A

Program Listing and User Instructions

The simulation program is written in FORTRAN IV. A complete program listing is presented in Table A-1, a sample set of input data cards in Table A-2, and a sample output in Table A-3.

The program utilizes one library subroutine from the SSP package supplied by IBM. This subroutine "RKGS" is a Runge-Kutta solution algorithm for solving simultaneous first order differential equations. The program listing contains a large number of COMMENT cards on which variables are described and key operational steps in the program identified.

A.1 Input Data

The program was written to permit easy adaptation to differing computer systems. The variables, IWRIT, and IREAD entered by the user at lines 7 and 8 specify the unit identification code for the printer and card reader on the system being used. These codes must be checked when attempting to utilize the program on a new system.

The following list describes the input data requirements:

Card No.	Variable	Format
1	NRUN	I2
	NRUN: the number of simulations to be included in the computer run	
2	G	F5.1
	C1	F10.6

Card No.	Variable	Format
	C2	F6.1
	C3	F8.1

G: gravitational constant ft/sec^2

C1: ft^3/sec per gallons/min

C2: density times specific heat of water $BTU/ft^3, °F$

C3: seconds/hour

3	L	I1
	PRMT(1)	F5.1
	PRMT(2)	F5.1
	PRMT(3)	F5.1
	PRMT(4)	F7.3
	DERY(1)	F5.1
	DERY(2)	F5.1

L: number of simultaneous differential equations to be solved, usually 2

PRMT(1): lower limit of solution range, starting time

PRMT(2): upper limit of solution range, ending time

PRMT(3): normal size of time increment

PRMT(4): upper limit on RKGS errors

DERY(1); weight on errors in Equation #1

DERY(2): weight on errors in Equation #2

Note: these variables are all required by RKGS.

Card	Variables	Format
4	KQHA	I4
	KQHE	I4
	QHEC	F6.1

KQHA: number of points on ARW heat curve to be read in

KQHE: number of points on ERW heat curve to be read in

QHEC: constant heat load of ERW system during a LOOP in million BTU/hour

Card Group	Variable	Format
5	TMA(I), QHLA(I) for I=1 to KQHA	12 F6.2

QHLA(I): the ARW heat load for a LOOP at time TMA(I) in million BTU/hour.

6	TME(I), QHLE(I) for I=1 to KQHE	12F6.2

QHLE(I): the ERW heat load for a LOCA at time TME(I) in million BTU/hour

Card group 7 to card group 6+NRUN consist of 5 cards each and contain data specific to each simulation condition:

Card No.	Variable	Format
7.1	TITLE	20A4

TITLE: any 80 character title that will be used to label output for specific simulation condition

7.2	HMRT	F5.2
	JP	I3
	CDIS	F5.1

Card No.	Variable	Format

HMRT: re-entrainment ratio β, see Chapter 3

JP: code indicating value of Φ. For

$\Phi = 0.1$, use JP = 1; $\Phi = 0.2$, JP = 2;

$\Phi = 0.5$, JP = 3; and $\Phi = 1.0$, JP = 4.

CDIS: surface heat dissipation coefficient

BTU/hour, °F, ft^2.

7.3	A1	F10.1
	AT	F10.1
	AP	F10.1
	DRAFT	F6.1
	DCD	F5.1
	DED	F5.1
	DAI	F5.1
	DEI	F5.1
	HI	F6.1
	HSLW	F6.1
	WS	F7.1

A1: average horizontal area of heated layer, ft^2.

AT: entire area within the sills effected by the tide, ft^2.

AP: horizontal area of the plants below the water line, ft^2.

DRAFT: draft of the plants, ft

DCD: diameter of the combined discharge ports, ft

Card No.	Variable	Format

DED: diameter of the single ERW discharge ports, ft.

DAI: diameter of the ARW intake ports, ft.

DEI: diameter of the ERW intake ports, ft.

HI: depth of the intake port center line, ft.

HSLW: depth of water at the sills at mean low tide, ft.

WS: schematized width of the breakwater opening, ft.

7.4	T2	F6.1
	TIDE	F5.1
	PHASE	F8.4

T2: ambient water temperature, °F

TIDE: amplitude of tide from mean water to extreme, ft

PHASE: Phase lag of tidal cycle in radians

phase lag of π means that heat release starts at low tide; phase lag of zero at high tide.

7.5	QAG	F6.0
	QEG	F6.0
	PLT(1)	F3.0
	PLT(2)	F3.0
	N(1,1)	F3.0
	N(1,2)	F3.0

Card No.	Variable	Format
	N(1,3)	F3.0
	N(1,4)	F3.0
	N(2,1)	F3.0
	N(2,2)	F3.0
	N(2,3)	F3.0
	N(2,4)	F3.0

QAG: ARW flow rate per train, gpm

QEG: ERW flow rate per train, gpm

PLT(I): code indicating operating mode of plant I

PLT(I)= 1.0 for normal shut down

PLT(I)= 2.0 for LOOP

PLT(I)= 3.0 for LOCA

N(I,J): number of discharges of type J operating in plant I. The code for J is:

J = 1, large discharge, both ARW and ERW flow

J = 2, large discharge, ARW flow only

J = 3, large discharge, ERW flow only

J = 4, small discharge, ERW flow only

Note: the correct input of N(I,J) permits the indication of a system failure.

A.2 Program Operation

The MAIN program serves two purposes. First, it reads in all the required data and stores it for use in the other subroutines, and second it establishes the initial conditions for the solution of the simultaneous differential equations. The initial conditions were taken at the end of a 0.2 hour period after the start of a transient heat release. Once the MAIN program has determined the layer depth and upper layer temperature at 0.2 hours, it calls the library subroutine RKGS.

RKGS solves first order simultaneous differential equations using a Runge-Kutta procedure. The subroutine requires two external subroutines, namely FCT and OUTP. In FCT, the right hand side of each differential equation is determined for each time step, using the various physical formulations as presented in Chapter 3. The subroutine OUTP prints out the solution of the differential equations for time intervals of one hour.

RHO is a function subroutine to determine the density of water as a function of temperature.

A.3 Output Data

Table A.3 is a sample output for the Proto Case 4A, a double LOOP with all systems operating. This section of the appendix is intended to explain each column of the output print out.

Column	Variable	Description
1	T	Simulation time in hours
2	IHLF	Number of bisections used for RKGS convergence
3	HS	Depth of water at sill, ft

Column	Variable	Description
4	QHA	ARW heat load, million BTU/hr
5	QHE	ERW heat load, million BTU/hr
6	DTV(1)	Avg. discharge temperature rise above ambient for plant #1, °F
7	DTV(2)	Avg. discharge temperature rise above ambient for plant # 2, °F
8	X(1)	Average layer depth, ft.
9	DT1	Average layer temperature rise above ambient,°F
10	DTAI	ARW intake temperature rise above ambient, °F
11	DTEI	ERW intake temperature rise above ambient, °F
12	PDISS	% of heat removed from basin due to atmospheric dissipation
13	POPEN	% of heat removed from basin due to stratified counterflow
14	SC(1)	Dilution ratio at large discharges of plant #1
15	SE(1)	Dilution ratio at small discharge of plant #1
16	SC(2)	Dilution ratio at large discharges of plant #2
17	SE(2)	Dilution ratio at small discharge of plant #2
18	JC(1),JE(1)	Four digit code indicating entrainment
	JC(2), JE(2)	situation at each type of discharge for each plant. First digit is the large discharges of plant #1, second digit is small port plant #1, third digit is large ports plant #2, and fourth digit is small port of plant #2. The code is as follows: (refer to Figure 3-10 of text) 0 = discharge port(s) not operating 1 = no entrainment since layer is too deep, Case C 2 = normal jet entrainment, Case B 3 = jet entrainment limited by sill flow, case D

		4 = negative buoyant jet, Case E 5 = negative buoyant jet limited by sill, Case F 8 = sill flow greater than induced entrainment due to tidal action
19	QNET	Net flow per unit width over the sill, positive sign indicates outflow, negative sign inflow cfs/ft
20	HEAT	Total excess heat content of upper layer. Represents volume of upper layer times temperature rise and specific heat of water, billion BTU.

A.4 Input Example

The sample set of input data presented as Table A-2 illustrates the data requirements for four of the prototype cases discussed in the text: Cases 1B, 4A, 5A, and 8A. The first seventeen cards are the data required for the entire computer run. Starting with card 18, four data groups of five cards each are supplied.

For Case 1B it is necessary to indicate a LOOP-normal condition with a single system failure in the plant with the LOOP. The key variables to obtain this condition are:

PLT(1) = 2.0 for the LOOP

PLT(2) = 1.0 for the normal shutdown

N(1,1) = 2.0 indicating failure of a combined train in the LOOP plant

For Case 4A, the simulation required a double LOOP with all systems operating. Key variables are:

PLT(1) = PLT(2) = 2.0 for LOOP

N(1,1) = N(2,1) = 3.0
N(1,4) = N(2,4) = 1.0 } all trains operating for a LOOP

For Case 5A, the simulation required a LOCA-normal shutdown, and a ten foot tide beginning at low tide. Key variables are:

PLT(1) = 3.0 for LOCA

PLT(2) = 1.0 for normal shutdown

N(1,3) = 3.0 } for LOCA all systems
N(1,4) = 1.0 }

TIDE = 5.0 for a total tidal difference of 10 ft

PHASE = 3.1416 for accident at low tide

For Case 8A, the only difference is in the diameters of the discharge ports. Thus, all variables are the same as Case 4A, except that

DCD = 7.0 ft

DED = 5.5 ft.

REFERENCE:

International Business Machines Corporation, "System/360 Scientific Subroutine Package, Version III, Programmer's Manual", IBM Application Program, Publication # GH 20-0205-4, 1970

```
C
C     SIMULATION PROGRAM FOR PREDICTION OF TRANSIENT HEAT LOAD
C     CONDITIONS OF THE ATLANTIC GENERATING STATION BASIN.
C     MODEL DEVELOPED AT MIT, RALPH PARSONS LABORATORY, FOR
C     OFFSHORE POWER SYSTEMS,INC. BETWEEN OCT.74 AND SEPT 75.
C     PRINCIPAL CONTRIBUTORS WERE DR.D.R.F.HARLEMAN, DR. G. JIRKA,
C     AND MR. C.W. WOOD.
C
C     GENERAL VARIABLE DESCRIPTION:
C     MOST VARIABLES FOLLOW A CODING SYSTEM TO TELL THE USER WHAT
C     THE VARIABLE REPRESENTS. THE FIRST LETTER OR TWO LETTERS GIVE
C     THE NAME OF THE VARIABLE. THE SUFFIX LETTERS OR NUMBERS THAT
C     FOLLOW GIVE THE LOCATION.  THOSE VARIABLES THAT DO NOT FIT
C     THE CODING SYSTEM ARE DESCRIBED SEPARATELY BELOW, BUT
C     GENERALLY HAVE EITHER LITERAL INTERPRETATIONS OR ARE REQUIRED
C     BY THE LIBRARY SUBROUTINE THAT IS USED.
C
C     NAME CODES:
C     A = AREA  SQ FT
C     B = DUMMY INTERMEDIATE STEP IN A CALCULATION
C     C = CONSTANT OR CONVERSION COEFICIENT
C     D = DIAMETER   FT
C     DT = DELTA T, TEMPERATURE DIFFERENCE  DEGREES F
C     DR = DELTA RHO/RHO   RELATIVE DENSITY DIFFERENCE
C     F = FROUDE NUMBER
C     G = GRAVITIONAL CONSTANT   FT/SEC**2
C     H = DEPTHS  FT
C     HT = HEAT LOAD COMBIATION FOR CALC. OF HEAT CONSERV. EQUATION
C     J = "FLAG" TO INDICATE METHOD OF DILUTION CALCULATION
C     N = NUMBER OF DISCHARGES IN A GIVEN MODE
C     Q = FLOW RATES    CFS
C     QH = HEAT LOAD RATES  MIL BTU/HR
C     R = RECIRCULATION COEFFICIENT
C     S = DILUTION RATIO RESULTING FROM JET ENTRAINMENT
C     T = BY ITSELF IS TIME   HOURS
C     T = WITH SUFFIX IS TEMPERATURE     DEGREES F
```

```
C      U = VELOCITY      FT/SEC
C      W = WIDTH      FT
C      X = MAIN VARIABLE OF RKGS SUBROUTINE USED TO SOLVE THE TWO
C          MAIN DIFFERENTIAL EQUATIONS.
C      SUFFIXES:
C      1 = UPPER LAYER
C      2 = LOWER LAYER
C      A = ARW SYSTEM
C      E = ERW SYSTEM
C      S = AT SILL
C      D = AT DISCHARGE
C      I = AT INTAKE
C      0 = INTIAL TIME STEP AT TIME EQUAL 0 HOURS
C
       EXTERNAL OUTP,FCT
       REAL N,NA,NE
       DIMENSION S(4),QD(4),QT(2),QHT(2),TITLE(20)
       DIMENSION QAT(2),QET(2),QATG(2),QETG(2),TD(4),DTV(2)
       DIMENSION X(2),PRMT(5),DERY(2),AUX(8,2),RHS(2)
       DIMENSION FRS1(11,9),FRS2(11,9),FRS3(11,9),FRS4(11,9)
       COMMON/IOPUT/ IWRIT,IREAD
       COMMON/INOPS/ JP,HMRT,TMA(31),QHLA(31),TME(55),QHLE(55),
      2 SC(2),SE(2),KRUN,CH,G,C1,C2,C3,CDIS,QHEC,KQHA,KQHE
       COMMON/OPS/ QAG,QEG,PHASE,TIDE,T2,A1,AT,AP,DRAFT,PLT(2),
      1 FR2H(11,9,4),QA,QE,AC(4),N(2,4)
       COMMON/INPHY/ WS,HI,HSLW,DAI,DEI,DCD,DED,AAI,AEI
C
C      VARIABLES READ IN THAT APPLY TO ALL OF THE SIMULATIONS
C      INCLUDED IN THE COMPUTER RUN OF THE MODEL.  INCLUDED ARE:
C
C      NRUN= TOTAL NUMBER OF SIMULATION RUNS TO BE PERFORMED DURING
C      THE COMPUTER RUN.
C      G = GRAVITATIONAL CONSTANT  FT/SEC**2
C      C1 = (CU FT/SEC) PER (GAL/MIN)
C      C2 = DENSITY OF WATER TIMES SPECIFIC HEAT OF WATER,
C           BTU/CU FT-DEG F
```

```
C      C3 = SECONDS PER HOUR
C      L = SPECIFIES NUMBER OF DIFF. EQUA. TO BE SOLVED BY RKGS
C      PRMT(1) = LOWER LIMIT TO RANGE FOR SOLUTION OF DIFF. EQUA.
C      PRMT(2) = UPPER LIMIT TO RANGE FOR SOLUTION OF DIFF. EQUA.
C      PRMT(3) = NORMAL SIZE OF INCREMENTAL TIME STEP
C      PRMT(4) = UPPER LIMIT TO ABSOLUTE ERROR IN CALCULATIONS
C      DERY(1) = WEIGHT FACTOR FOR ERROR IN EQUATION #1
C      DERY(2) = WEIGHT FACTOR FOR ERROR IN EQUATION #2
C      KQHA = NUMBER OF ARW VARIABLE HEAT LOAD DATA POINTS TO BE READ
C      KQHE = NUMBER OF ERW VARIABLE HEAT LOAD DATA POINTS TO BE READ
C      QHEC = CONSTANT ERW HEAT LOAD FOR USE IN LOOP, MILLION BTU/HR
C      QHLA(I) = ARW HEAT LOAD PER PLANT AT TMA(I)      MIL BTU/HR
C      QHLE(J) = ERW HEAT LOAD PER PLANT AT TME(J)      MIL BTU/HR
C
    7  IWRIT=5
    8  IREAD=8
       READ(IREAD,9) NRUN
    9  FORMAT(I2)
       READ(IREAD,10) G,C1,C2,C3
   10  FORMAT(F5.1,F10.6,F6.1,F8.1)
       READ(IREAD,11) L,(PRMT(K),K=1,4),(DERY(K),K=1,2)
   11  FORMAT(I1,3F5.1,F7.3,2F5.1)
       READ(IREAD,12) KQHA,KQHE,QHEC
   12  FORMAT(2I4,F6.1)
       READ(IREAD,13) (TMA(I),QHLA(I),I=1,KQHA)
       READ(IREAD,13) (TME(I),QHLE(I),I=1,KQHE)
   13  FORMAT(12F6.2)
C
       DO 89   KRUN=1,NRUN
C
C      KRUN = NUMBER OF THE SIMULATION BEING PERFORMED AT ANY POINT
C
C      VARIABLES THAT ARE READ IN AS A DATA SET FOR EACH SIMULATION
C      RUN TO BE PERFORMED.  VARIATIONS BETWEEN SIMULATIONS ARE
C      ENTERED AS DIFFERENCES BETWEEN THE DATA SETS.      BEGIN BY
C      READING A TITLE CARD THAT DESCRIBES THE INDIVIDUAL SIMULATION.
```

```
C
C      SCHEMATIZATION VARIABLES OF THE MODEL:
C      HMRT = LIMITING RATIO OF JET DEPTH TO LAYER DEPTH, THAT
C             DETERMINES WHEN ENTRAINMENT GOES TO ZERO.
C      JP =  AN INTEGER CODE INDICATING THE VALUE OF PHI ,THE NON-
C      DIMENSIONAL FRICTION FACTOR FOR THE BREAKWATER OPENINGS.
C      IF PHI = 0.1     SET JP=1
C      IF PHI = 0.2     SET JP=2
C      IF PHI = 0.5     SET JP=3
C      IF PHI = 1.0     SET JP=4
C      CDIS = SURFACE HEAT DISSIPATION COEFICIENT,  BTU/SQ FT-DEG F
C      PHYSICAL DIMENSIONS OF THE PLANTS:
C      A1 = HORIZONTAL AREA OF HEATED LAYER, SQ FT
C      AT = ENTIRE AREA WITHIN SILLS EFFECTED BY TIDAL FLOW, SQ FT
C      AP = TOTAL HORIZONTAL AREA OF PLANTS BELOW WATER LINE, SQ FT
C      DRAFT = DRAFT OF PLANTS IN FEET
C      DCD = DIAMETER OF COMBINED DISCHARGE PORT IN FEET
C      DED = DIAMETER OF SINGLE ERW DISCHARGE  PORT IN FEET
C      DAI  = DIAMETER ARW INTAKE IN FEET
C      DEI  = DIAMETER ERW INTAKE IN FEET
C      HI = DEPTH OF INTAKE CENTERLINE, FEET
C      HSLW= DEPTH OF WATER AT SILL AT LOW MEAN TIDE, FEET
C      WS= WIDTH OF SILL OPENING, FT
C      TEMPERATURE AND TIDAL CONDITIONS
C      T2 = AMBIENT TEMPERATURE OF THE WATER,DEGREES F
C      TIDE = AMPLITUDE OF TIDE FROM MEAN TO EXTREME IN FEET
C      PHASE = PHASE LAG OF TIDE IN RADIANS.  ZERO LAG MEANS THAT
C              THE ACCIDENT OCCURS AT HIGH TIDE. A LAG OF PI RADIANS
C              MEANS THAT THE ACCIDENT OCCURES AT LOW TIDE.
C      OPERATING CONDITIONS:
C      QAG = ARW FLOW RATE PER TRAIN IN GPM
C      QEG = ERW FLOW RATE PER TRAIN IN GPM
C      PLT(I) = A CODED VARIABLE INDICATING THE MODE OF OPERATION
C               FOR PLANT I.  THE CODE IS AS FOLLOWS:
C                   1.0 = NORMAL SHUT DOWN
C                   2.0 = LOOP
```

```
C                    3.0 = LOCA
C      N(I,J) = NUMBER OF DISCHARGES OF TYPE J OPERATING IN PLANT I
C      J = 1 IS THE LARGER PIPE WITH COMBINED ARW AND ERW FLOW, LOOP
C      J = 2 IS THE LARGER PIPE WITH ARW FLOW ONLY, NORMAL SHUTDOWN
C      J = 3 IS THE LARGER PIPE WITH ERW FLOW ONLY, IN A LOCA
C      J = 4 IS THE SMALLER PIPE WITH ERW FLOW ONLY IN LOOP OR LOCA
C
       READ(IREAD,14)(TITLE(K),K=1,20)
    14 FORMAT(20A4)
       READ(IREAD,15) HMRT,JP,CDIS
    15 FORMAT(F5.2,I3,F5.1)
       READ(IREAD,16) A1,AT,AP,DRAFT,DCD,DEC,DAI,DEI,HI,HSLW,WS
    16 FORMAT(3F10.1,F6.1,4F5.1,2F6.1,F7.1)
       READ(IREAD,17) T2,TIDE,PHASE
    17 FORMAT(F6.1,F5.1,F8.4)
       READ(IREAD,18) QAG,QEG,PLT(1),PLT(2),((N(I,J),J=1,4),I=1,2)
    18 FORMAT(2F6.0,10F3.0)
C
C
C      THE FOLLOWING VARIABLES ARE ASSOCIATED WITH EACH
C      PLANT. THE SUBSCRIPT I REPRESENTS THE PLANT NUMBER.
C
C      DTV(I) = AVERAGE DELTA T FOR ALL DISCHARGES OF EACH PLANT
C      JC(I) = CODE FOR ENTRAINMENT SITUATION AT COMBINED DISCHARGE
C      JE(I) = CODE FOR ENTRAINMENT SITUATION AT SINGLE ERW DISCH.
C      QAT(I) = TOTAL ARW DISCHARGE FLOW IN CFS
C      QET(I) = TOTAL ERW DISCHARGE FLOW IN CFS
C      QATG(I) = TOTAL ARW FLOW IN A PLANT IN GAL PER MINUTE
C      QETG(I) = TOTAL ERW FLOW IN A PLANT IN GAL PER MINUTE
C      QHT(I) = TOTAL HEAT LOAD APPLIED BY PLANT (I)
C      QT (I) = TOTAL FLOW INTO UPPER LAYER AS RESULT OF PLANT I
C      SC(I) = DILUTION RATIO FOR  COMBINED  DISCH FOR GIVEN PLANT
C      SE(I) = DILUTION RATIO FOR SINGLE ERW DISCH FOR GIVEN PLANT
C
C      THE FOLLOWING VARIABLES ARE ASSOCIATED WITH DISCHARGE TYPE J.
C      AD (J) = AREA OF ONE DISCHARGE PORT OF TYPE J
```

```
C      QD(J) = FLOW RATE THROUGH DISCHARGE PORT OF TYPE J
C      S(J) = DILUTION RATIO FOR GIVEN DISCHARGE COMBINATION
C      TD(J) = DISCHARGE TEMPERATURE AT PORT OF TYPE J
C
C      THE FOLLOWING VARIABLES ARE USED IN INTERMEDIATE CALCULATIONS
C      MOST CHANGE FOR EACH TIME STEP AND COMBINATION OF I AND J
C
C      AAI = AREA OF AN ARW INTAKE
C      AEI = AREA OF AN ERW INTAKE
C      CH= CHECKING DUMMY TO MAKE PROGRAM PRINT ON INTERGER T ONLY
C      DRD1 = NORMALIZED DENSITY DIFF BETWEEN UPPER LAYER AND DISCH
C      DRD2 = NORMALIZED DENSITY DIFF BETWEEN LOWER LAYER AND DISCH
C      FRD1 = DISCH DENSIMETRIC FROUDE NUMBER BASED ON UPPER LAYER
C      FRD2 = DISCH DENSIMETRIC FROUDE NUMBER BASED ON LOWER LAYER
C      FQAI = ARW INTAKE DENSI. FROUDE BASED ON DIST. TO INTERFACE
C      FQEI = ERW INTAKE DENSI. FROUDE BASED ON DIST. TO INTERFACE
C      FCAI = ARW INTAKE DENSI. FROUDE BASED ON INTERFACE THICKNESS
C      FCEI = ERW INTAKE DENSI. FROUDE BASED ON INTERFACE THICKNESS
C      FDAI = ARW INTAKE DENSI. FROUDE BASED ON DIAMETER OF INTAKE
C      FDEI = ERW INTAKE DENSI. FROUDE BASED ON DIAMETER OF INTAKE
C      FQCAI = ARW CRITICAL INTAKE DENSIMETRIC FROUDE NUMBER DERIVED
C      AS A FUNCTION OF FCAI AND FDAI.
C      FQCEI = ERW CRITICAL INTAKE DENSIMETRIC FROUDE NUMBER DERIVED
C      AS A FUNCTION OF FCEI AND FDEI
C      FRNET = FROUDE NUMBER OF NET FLOW OVER THE SILLS
C      F2H = DENSIMETRIC FROUDE NUMBER OF LOWER LAYER AT SILL
C      H1 = DEPTH OF HEATED LAYER
C      HS = DEPTH OF WATER OVER SILLS
C      HIN = INTERFACE THICKNESS
C      HDFM = MAX DEPTH OF WATER BELOW SILL ELEVATION
C      HM = MAXIMUM DEPTH OF IDEALIZED JET
C      HTIDE = MAGNITUDE OF TIDE ABOVE LOW MEAN WATER
C      H2SH = NON-DIMENSIONALIZED LOWER LAYER DEPTH AT SILL
C      HTLAY = HEAT CONTENT CHANGE IN LAYER DUE TO THICKNESS CHANGE
C      HTDIS = TOTAL HEAT DISSIPATED TO ATMOSPHERE
C      HTSIL = TOTAL HEAT FLOW OUT OVER SILLS
```

```
C      HTSOR = TOTAL HEAT SOURCE
C      HEAT = PRODUCT OF TEMPERATURE RISE,LAYER DEPTH, AND SURFACE
C             AREA, OR TOTAL EXCESS HEAT IN UPPER LAYER AT TIME T
C      PDISS = % OF HEAT DISSIPATED TO ATMOSPHERE
C      POPEN = % OF HEAT LOST OUT BREAKWATER OPENINGS
C      Q = TOTAL FLOW ENTERING UPPER LAYER INCLUDING ENTRAINMENT
C      QH = TOTAL HEAT LOAD ENTERING BASIN FROM PLANTS
C      QA = FLOW RATE THROUGH ONE ARW TRAIN IN CFS
C      QE = FLOW RATE THROUGH ONE ERW TRAIN IN CFS
C      QAR = FLOW OUT OF UPPER LAYER INTO ARW INTAKE
C      QER = FLOW OUT OF UPPER LAYER INTO ERW INTAKE
C      QHAO= INITIAL ARW HEAT LOAD PER PLANT, MILLION BTU/HR
C      QHEO= INITIAL ERW HEAT LOAD PER PLANT, MILLION BTU/HR
C      QNET = NET FLOW THROUGH SILLS DUE TO TIDAL ACTION
C      CFS PER UNIT WIDTH PER SILL.
C      Q1S = FLOW OVER SILL AT UPPER LAYER
C      Q2S = FLOW OVER SILL IN LOWER LAYER
C      QSIL = TOTAL FLOW OUT OF UPPER LAYER OVER SILLS
C      QTDIS = TOTAL DISCHARGE FROM BOTH PLANTS
C      QAN = CONTROL INDICATING IF ARW HEAT CURVE APPLIES
C      QEN = CONTROL INDICATING IF ERW HEAT CURVE APPLIES
C      RA = RECIRCULATION RATIO AT ARW INTAKE
C      RE = RECIRCULATION RATIO AT ERW INTAKE
C      RHS(1) = RIGHT HAND SIDE OF CONTINUITY EQUATION
C      RHS(2) = RIGHT HAND SIDE OF CONSERVATION OF HEAT EQUATION
C      SB = BASIC BOTTOM ENTRAINMENT RATIO
C      SBE = MODIFIED BOTTOM ENTRAINMENT RATIO
C      SBR = DILUTION FLOW RATIO
C      SS = MAX. ENTRAINMENT FLOW WHEN ENTRAINMENT LIMITED BY SILL
C      UD = VELOCITY OF DISCHARGE
C
C      CONVERSION OF LOWER LAYER FROUDE NUMBERS ENTERED  AS BLOCK
C      DATA INTO A SINGLE THREE DIMENSIONAL ARRAY.
C      FR2H= A MATRIX OF LOWER LAYER FROUDE NUMBERS FOR VARIOUS NET
C      FLOWS OVER THE SILLS.  USED TO DETERMINE PROPER COUNTERFLOW.
C
```

```
      IF(KRUN.NE.1) GO TO 40
      DATA FRS1/6*-.47,-.46,-.45,-.43,-.41,-.39,
     1 -.395,-.395,-.395,-.395,-.395,-.395,-.390,-.375,-.345,-.310,
     1 -.285,-.330,-.330,-.330,-.330,-.330,-.330,-.320,-.290,-.252,
     1 -.220,-.195,-.275,-.275,-.275,-.275,-.275,-.270,-.250,-.210,
     1 -.160,-.125,-.100,-.225,-.225,-.225,-.225,-.225,-.215,-.175,
     1 -.125,-.070,-.030,+.000,-.177,-.177,-.177,-.177,-.170,-.148,
     1 -.096,-.030,+.025,+.070,+.100,-.135,-.135,-.135,-.135,-.120,
     1 -.075,-.010,+.060,+.120,+.170,+.210,-.098,-.098,-.098,-.095,
     1 -.060,+.002,+.080,+.160,+.225,+.275,+.320,-.070,-.070,-.068,
     1 -.050,+.015,+.105,+.200,+.275,+.335,+.380,+.425/
      DATA FRS2/-.450,-.450,
     1 -.450,-.450,-.450,-.450,-.450,-.440,-.420,-.405,-.370,-.380,
     1 -.380,-.380,-.380,-.380,-.380,-.375,-.360,-.335,-.310,-.280,
     1 -.320,-.320,-.320,-.320,-.320,-.318,-.310,-.280,-.245,-.215,
     1 -.195,-.265,-.265,-.265,-.265,-.265,-.260,-.235,-.195,-.155,
     1 -.125,-.100,-.212,-.212,-.212,-.212,-.210,-.195,-.160,-.115,
     1 -.060,-.025,-.000,-.165,-.165,-.165,-.165,-.160,-.130,-.080,
     1 -.025,+.030,+.070,+.100,-.125,-.125,-.125,-.122,-.105,-.060,
     1 +.005,+.070,+.125,+.170,+.210,-.088,-.088,-.088,-.078,-.045,
     1 +.025,+.095,+.175,+.230,+.275,+.330,-.055,-.055,-.052,-.030,
     1 +.030,+.125,+.210,+.280,+.340,+.390,+.420/
      DATA FRS3/-.425,-.425,-.425,
     1 -.425,-.425,-.425,-.425,-.420,-.410,-.395,-.360,-.360,-.360,
     1 -.360,-.360,-.360,-.360,-.355,-.340,-.320,-.300,-.280,-.295,
     1 -.295,-.295,-.295,-.295,-.295,-.280,-.260,-.230,-.205,-.190,
     1 -.240,-.240,-.240,-.240,-.235,-.230,-.210,-.175,-.140,-.120,
     1 -.100,-.190,-.190,-.190,-.190,-.185,-.165,-.130,-.095,-.050,
     1 -.025,-.000,-.140,-.140,-.140,-.140,-.130,-.100,-.055,-.010,
     1 +.040,+.075,+.100,-.100,-.100,-.100,-.095,-.070,-.030,+.025,
     1 +.080,+.135,+.175,+.220,-.065,-.065,-.065,-.050,-.010,+.050,
     1 +.120,+.180,+.240,+.280,+.330,-.030,-.030,-.025,+.005,+.075,
     1 +.150,+.235,+.300,+.355,+.410,+.450/
      DATA FRS4/-.410,-.410,-.410,-.410,
     1 -.410,-.410,-.405,-.402,-.400,-.398,-.395,-.340,-.340,-.340,
     1 -.340,-.340,-.340,-.330,-.320,-.310,-.290,-.280,-.275,-.275,
```

```
     1 -.275,-.275,-.275,-.270,-.260,-.240,-.220,-.200,-.190,-.220,
     1 -.220,-.220,-.220,-.220,-.210,-.190,-.160,-.135,-.115,-.095,
     1 -.165,-.165,-.165,-.165,-.160,-.145,-.115,-.080,-.045,-.020,
     1 -.000,-.120,-.120,-.120,-.120,-.105,-.075,-.040,+.002,+.048,
     1 +.080,+.110,-.080,-.080,-.080,-.070,-.050,-.010,+.040,+.095,
     1 +.140,+.180,+.210,-.047,-.047,-.042,-.025,+.020,+.075,+.135,
     1 +.195,+.245,+.300,+.350,-.020,-.020,-.005,+.040,+.100,+.200,
     1 +.275,+.330,+.400,+.430,+.460/
      DO 1 JH=1,11
      DO 1 JF=1,9
      FR2H(JH,JF,1)=FRS1(JH,JF)
      FR2H(JH,JF,2)=FRS2(JH,JF)
      FR2H(JH,JF,3)=FRS3(JH,JF)
      FR2H(JH,JF,4)=FRS4(JH,JF)
    1 CONTINUE
   40 AEI=3.1416*((DEI/2.0)**2)
      AAI=3.1416*((DAI/2.0)**2)
      AD(1)=3.1416*((DCD/2.0)**2)
      AD(2)=AD(1)
      AD(3)=AD(1)
      AD(4)=3.1416*((DED/2.0)**2)
      QT(1)=0.0
      QT(2)=0.0
      QHAO=0.0
      QHEO=0.0
C
C     CALCULATION OF INITIAL STATIFICATION DURING FIRST 0.2 HOURS.
C     END RESULT IS INITIAL VALUES OF X(1) AND X(2) FOR USE IN
C     THE RKGS SUBROUTINE.
C
      DO 54 I=1,2
      IF(PLT(I).EQ.3.0) QHEO=QHLE(1)
      IF(PLT(I).EQ.1.0.OR.PLT(I).EQ.2.0) QHAO=QHLA(1)
      QA=QAG*C1
      QE=QEG*C1
      IF(PLT(I).NE.3.0) QE=0.0
```

```
      QD(1)=QA+QE
      QD(2)=QA
      QD(3)=QE
      QD(4)=QE
      NA=N(I,1)+N(I,2)
      NE=N(I,1)+N(I,3)+N(I,4)
      QAT(I)=QA*NA
      QET(I)=QE*NE
      IF(QAT(I).EQ.0.0) DTA=0.0
      IF(QAT(I).EQ.0.0) GO TO 50
      DTA=(QHAO*1.0E+6)/(QAT(I)*C2*C3)
      IF(QET(I).EQ.0.0) DTE=0.0
      IF(QET(I).EQ.0.0) GO TO 51
   50 DTE=(QHEO*1.0E+6)/(QET(I)*C2*C3)
   51 TED=T2+DTE
      TAD=T2+DTA
      TD(1)=((TAD*QA)+(TED*QE))/(QA+QE)
      TD(2)=TAD
      TD(3)=TED
      TD(4)=TED
      V=TD(1)*N(I,1)*QD(1)+TD(2)*N(I,2)*QD(2)+TD(3)*N(I,3)*QD(3)
      DTV(I)=((V+TD(4)*N(I,4)*QD(4))/(QAT(I)+QET(I)))-T2
      DO 53 J=1,4
      IF(N(I,J).EQ.0.0) GO TO 52
      IF(PLT(I).EQ.2.0.AND.J.EQ.4) GO TO 52
      DRD2=(RHO(T2)-RHO(TD(J)))/RHO(T2)
      UD=QD(J)/AD(J)
      FRD2=UD/SQRT(G*DRD2*((AD(J)/2.0)**0.5))
      IF(FRD2.LT.1.0)  FRD2=1.0
      S(J)=1.4*FRD2
      IF(PLT(I).EQ.2.0.AND.J.EQ.3) S(J)=0.0
      IF(PLT(I).EQ.2.0.AND.J.EQ.4) S(J)=0.0
      GO TO 53
   52 S(J)=0.0
   53 CONTINUE
      SC(I)=S(1)+S(2)+S(3)
```

```
      SE(I)=S(4)
      QT(I)=(N(I,1)*(QA+QE)*S(1))+(N(I,2)*QA*S(2))+(N(I,3)*QE*S(3))
      QT(I)=QT(I)+(N(I,4)*CE*S(4))
      QEN=0.0
      QAN=0.0
      IF(N(I,1).GT.0.0.OR.N(I,3).GT.0.0.OR.N(I,4).GT.0.0)  QEN=1.0
      IF(N(I,1).GT.0.0.OR.N(I,2).GT.0.0)  QAN=1.0
      QHT(I)=(QHAO*QAN)+(QHEO*QEN)
      QA=QAG*C1
      QE=QEG*C1
      QAT(I)=QA*NA
      QET(I)=QE*NE
      QATG(I)=QAT(I)/C1
      QETG(I)=QET(I)/C1
   54 CONTINUE
      C=QT(1)+QT(2)
      QH=QHT(1)+QHT(2)
      DT10=(QH*1.0E+6)/(Q*C2*C3)
      T=0.2
      X(2)=T2+DT10
      X(1)= T*C*C3/A1
C
C     PRINT OUT OF APPROPRIATE HEADINGS:
C
      WRITE(IWRIT,59)(TITLE(K),K=1,20)
   59 FORMAT(1H1,20A4)
      WRITE(IWRIT,60) QATG(1),QETG(1)
   60 FORMAT(1HC,'ARW FLOW PLT #1= ',F7.1,' GPM',6X,'ERW FLOW PLT',
     3 ' #1= ',F7.1,' GPM')
      WRITE(IWRIT,61) QATG(2),QETG(2)
   61 FORMAT(1HO,'ARW FLOW PLT #2= ',F7.1,' GPM',6X,'ERW FLOW PLT',
     1 ' #2= ',F7.1,' GPM')
      WRITE(IWRIT,62) TIDE,PHASE
   62 FORMAT(1HO,'TIDAL AMPLITUDE= ',F3.1,' FT',
     2 9X,'TIDAL PHASE= ',F4.2,' RADIANS')
      WRITE(IWRIT,63) T2,WS,HI
```

```
   63 FORMAT(1H0,'AMBIENT WATER TEMP= ',F4.1,' F          SILL',
     3 ' WIDTH= ',F5.1,' FT          INTAKE DEPTH= ',F4.1,' FT')
      WRITE(IWRIT,64)
   64 FORMAT(1H0,1X,'TIME  DEPTH   ARW    ERW   AVG    AVG     ',
     4 'AVG    AVG   ARW    ERW    %      %      DILUTION RATIOS  ',
     4 '  DILU   NET   LAYER')
      WRITE(IWRIT,65)
   65 FORMAT(9X,'AT     MIL    MIL   DISC   DISC   LAYER   TEMP  ',
     5 'INTK   INTK  HEAT  HEAT  PLT  #1   PLT  #2   CONT   SILL',
     5 '  HEAT')
      WRITE(IWRIT,66)
   66 FORMAT(8X,'SILL    BTU/   BTU/  DELT   DELT   DEPTH   RISE',
     6 '  DELT   DELT  DIS   CLT-   C    E    C    E   CODE   ',
     6 'FLOW  E9 BTU')
      WRITE(IWRIT,67)
   67 FORMAT(9X,'FT      HR     HR   # 1    # 2     FT      F',
     7 5X,'F      F',11X,'FLOW')
      WRITE(IWRIT,80) T,QHAO,CHEO,DTV(1),DTV(2),X(1),DT10,SC(1),
     3 SE(1),SC(2),SE(2)
   80 FORMAT(F6.1,F14.1,F7.1,F6.1,F7.1,F8.2,F7.2,F30.1,3F5.1)
      CH=1.0
C
C     AT THIS POINT THE PROGRAM ENTERS SUBROUTINE RKGS WHICH THEN
C     CALLS FOR FCT, AND CLTP.  WHEN RKGS IS COMPLETED EACH TIME
C     CONTROL RETURNS TO THE MAIN PROGRAM AT LINE 89 WHERE THE DO
C     LOOP REPEATS THE PROCESS FOR SUBSEQUENT SIMULATION CONDITIONS
C
   81 CALL RKGS(PRMT,X,DERY,L,IHLF,FCT,CLTP,AUX)
   89 CONTINUE
      STOP
      END
```

```
C
C     THE PURPOSE OF THIS SUBROUTINE IS TO SOLVE THE RIGHT HAND SIDE
C     OF EACH OF THE FIRST ORDER DIFFERENTIAL EQUATIONS BEING SOLVED
C     SIMULTANEOUSLY BY RKGS.  EACH TIME THE PROGRAM GOES TO FCT THE
C     RECENT VALUES OF X(1) AND X(2) ARE UTILIZED  TO FIND THE RIGHT
C     HAND SIDES FOR USE IN THE NEXT TIME STEP.
C
      SUBROUTINE FCT(T,X,RHS)
      REAL N,NA,NE
      DIMENSION S(4),QD(4),QT(2),QHT(2),TITLE(20)
      DIMENSION QAT(2),QET(2),QATG(2),QETG(2),TD(4)
      DIMENSION JD(4)
      DIMENSION X(2),PRMT(5),DERY(2),AUX(8,2),RHS(2)
      COMMON/IOPUT/ IWRIT,IREAD
      COMMON/INOPS/ JP,HMRT,TMA(31),QHLA(31),TME(55),QHLE(55),
     2 SC(2),SE(2),KRUN,CH,G,C1,C2,C3,CDIS,QHEC,KQHA,KQHE
      COMMON/OPS/ QAG,QEG,PHASE,TIDE,T2,A1,AT,AP,DRAFT,PLT(2),
     1 FR2H(11,9,4),QA,QE,AD(4),N(2,4)
      COMMON/INPHY/ WS,HI,HSLW,DAI,DEI,DCD,DED,AAI,AEI
      COMMON/OUT/ PDISS,POPEN,JE(2),JC(2),HS,QHA,QHE,DTV(2),DTAI,
     3 DTEI,CNET
      H1=X(1)
      HDIF=HI-H1
      HIN=H1
      IF(HIN.GT.15.0)  HIN=15.0
      T1=X(2)
      INDEX=3
C
C     CALCULATE DEPTH OF WATER AT SILL USING COSINE APPROX FOR
C     TIDAL CYCLE
C
      HSM=HSLW+TIDE
      HS=HSM+TIDE*COS((3.1416*T/6.2)+PHASE)
      HTIDE=HS-HSLW
      A1C=A1
      IF(X(1).GT.DRAFT) A1C=A1+AP
```

```
      IF(X(1).GT.(HTIDE+45.0)) A1C=AT
C
C     A "FLAG" TO INDICATE A SERIOUS PROBLEM IN PROGRAM.  WILL
C     ACTIVATE WHEN LAYER DEPTH EXCEEDS DEPTH OF BASIN OR EXIT
C     VELOCITY IS LESS THAN ZERO.
C
      IF(X(1)-55.0) 94,94,92
   92 WRITE(IWRIT,93) T,H1,T1
   93 FORMAT(2X,3(2X,F8.3))
      INDEX=1
      GO TO 700
   94 DR21=(RHO(T2)-RHO(T1))/RHO(T2)
      H2SH=(HS-H1)/HS
      IF(H2SH.LE.0.0)  H2SH=0.0
C
C     DETERMINE OUTGOING FLOW RATE FROM UPPER LAYER OVER THE SILL AS
C     FUNCTION OF THE DENSITY DIFFERENCE, HEATED LAYER DEPTH, AND
C     TOTAL NET FLOW OVER THE SILL DUE TO TIDAL ACTION.
C
      QNET=(AT/2.0)*TIDE*(3.1416/6.2)*(+SIN(((3.1416*T)/6.2)+PHASE))
      QNET=QNET/(C3*WS)
      FRNET=QNET/SQRT(G*DR21*(HS**3))
      DO 95  JH=1,11
      HG=(FLOAT(JH-1))/10.0
      IF(HG.GT.H2SH)  JH2=JH
      IF(HG.GT.H2SH)  JH1=JH-1
      IF(HG.GT.H2SH)  GO TO 96
   95 CONTINUE
   96 DO 97  JF=1,9
      FRNTG=(FLOAT(JF-5))/10.0
      IF(FRNTG.GT.FRNET)  JF2=JF
      IF(FRNTG.GT.FRNET)  JF1=JF-1
      IF(FRNTG.GT.FRNET)  GO TO 98
   97 CONTINUE
   98 B14=(H2SH*10.0)-FLOAT(JH1-1)
      B15= (FR2H(JH2,JF1,JP)-FR2H(JH1,JF1,JP))*B14
```

```
      B16= (FR2H(JH2,JF2,JP)-FR2H(JH1,JF2,JP))*B14
      FRH1=FR2H(JH1,JF1,JP)+B15
      FRH2=FR2H(JH1,JF2,JP)+B16
      F2H =FRH1+((FRH2-FRH1)*((FRNET*10.0)-FLOAT(JF1-5)))
      Q2S= F2H*SQRT(G*DR21*(HS**3))
      Q1S=(QNET-Q2S)*WS
C
C     DETERMINE RECIRCULATION RATIO AND ARW INTAKE TEMPERATURE
C
      HID=ABS(HI-H1)
      FQAI=QA /SQRT(DR21*G*(HID**5.0))
      FDAI=QA /((3.1416/4.0)*SQRT(DR21*G*(DAI**5.0)))
      FLAI=QA /SQRT(DR21*G*(HIN**5.0))
      FQCAI=(0.C26*ALOG(FDAI))+(0.64*FLAI)
      Z=FQAI/FQCAI
      IF(Z.LE.1.0) RA=0.0
      IF(Z.LE.1.0.AND.HDIF.LT.0.0)  GO TC 106
190   IF(Z.LE.1.0) GO TO 107
      IF(Z.LE.300.0) GO TC 104
      RA=0.5*(1.0-(Z**(-.22)))
      GC TO 105
  104 RA=0.0622*ALOG(Z)
  105 IF(HDIF.LT.0.0) GO TO 106
      GC TC 107
  106 RA=1.0-RA
  107 CTAI=(T1-T2)*RA
      TAI=T2+CTAI
C
C     DETERMINE RECIRCULATION RATIO AND ERW INTAKE TEMPERATURE
C
      IF(PLT(1).NE.3.0.AND.PLT(2).NE.3.0.AND.T.LT.4.0)  QE=0.0
      IF(QE.EQ.0.0) RE=0.0
      IF(QE.EQ.C.0) GO TC 111
      FQEI=QE /SQRT(DR21*G*(HID**5.0))
      FLEI=QE /SQRT(DR21*G*(HIN**5.0))
      FDEI=QE /((3.1416/4.0)*SQRT(DR21*G*(DEI**5.0)))
```

```
      FQCEI=(0.026*ALOG(FDEI))+(0.64*FLEI)
      Z=FCEI/FQCEI
      IF(Z.LE.1.0) RE=0.0
      IF(Z.LE.1.0.AND.HDIF.LT.0.0)  GO TO 110
      IF(Z.LE.1.0) GO TO 111
      IF(Z.LE.300.0) GO TO 108
      RE=0.5*(1.0-(Z**(-.22)))
      GO TO 109
  108 RE=0.0622*ALOG(Z)
  109 IF(HDIF.LT.0.0) GO TO 110
      GO TO 111
  110 RE=1.0-RE
  111 DTEI=(T1-T2)*RE
      TEI=T2+DTEI
C
C     DETERMINE HEAT LOAD AS FUNCTION OF TIME
C
      DO 112 I=1,KQHA
      IF(TMA(I).GT.T)  GO TO 113
  112 CONTINUE
  113 NDUM=I
      TDEL=TMA(NDUM)-TMA(NDUM-1)
      QHA=QHLA(NDUM-1)+(T-TMA(NDUM-1))*(QHLA(NDUM)-QHLA(NDUM-1))/TDEL
      IF(PLT(1).EQ.2.0.OR.PLT(2).EQ.2.0) GO TO 203
      DO 201 J=1,KQHE
      IF(TME(J).GT.T) GO TO 202
  201 CONTINUE
  202 NDUM=J
      TDEL=TME(NDUM)-TME(NDUM-1)
      QHE=QHLE(NDUM-1)+(T-TME(NDUM-1))*(QHLE(NDUM)-QHLE(NDUM-1))/TDEL
      GO TO 204
  203 QHE=QHEC
  204 DO 220 I=1,2
      NA=N(I,1)+N(I,2)
      NE=N(I,1)+N(I,3)+N(I,4)
      QA=QAG*C1
```

```
      QE=QEG*C1
      IF(PLT(I).EQ.2.0.AND.T.LT.4.0) QE=0.0
      QD(1)=QA+QE
      QD(2)=QA
      QD(3)=QE
      QD(4)=QE
      QAT(I)=QA*NA
      QET(I)=QE*NE
  220 CONTINUE
C
C     DETERMINE MAX ENTRAINMENT POSSIBLE WHEN LIMITED BY SILL FLOW
C
      QTDIS=QAT(1)+QAT(2)+QET(1)+QET(2)
      SS=(-2.0*Q2S*WS)/QTDIS
C
C     THE DO 400 LOOP ALLOWS CONSIDERATION OF EACH PLANT SEPARATELY
C     BUT CONSECUTIVELY.
C
      DO 400 I=1,2
      NA=N(I,1)+N(I,2)
      NE=N(I,1)+N(I,3)+N(I,4)
      QA=QAG*C1
      QE=QEG*C1
      IF(PLT(I).EQ.2.0.AND.T.LT.4.0) QE=0.0
      IF(PLT(I).EQ.2.0.AND.T.LT.4.0) QHE=0.0
      QD(1)=QA+QE
      QD(2)=QA
      QD(3)=QE
      QD(4)=QE
      QAT(I)=QA*NA
      QET(I)=QE*NE
      IF(QAT(I).EQ.0.0) DTA=0.0
      IF(QAT(I).EQ.0.0) GO TO 250
      DTA=(QHA *1.0E+6)/(QAT(I)*C2*C3)
      IF(PLT(I).EQ.2.0.AND.T.LT.4.0) DTE=0.0
      IF(PLT(I).EQ.2.0.AND.T.LT.4.0) GO TO 260
```

```
      IF(QET(I).EQ.0.0) DTE=0.0
      IF(QET(I).EQ.0.0) GO TO 260
  250 DTE=(QHE *1.0E+6)/(QET(I)*C2*C3)
  260 TEC=TEI+CTE
      TAC=TAI+DTA
      TD(1)=((TAD*QA)+(TED*QE))/(QA+QE)
      TC(2)=TAC
      TC(3)=TED
      TD(4)=TED
      V=TD(1)*N(I,1)*QD(1)+TC(2)*N(I,2)*QD(2)+TD(3)*N(I,3)*QD(3)
      DTV(I)=((V+TD(4)*N(I,4)*CD(4))/(QAT(I)+QET(I)))-T2
C
C     THE DO 300 LOOP EXAMINES EACH POSSIBLE TYPE OF DISCHARGE
C     COMBINATION FOR EACH PLANT.
C
      DO 300 J=1,4
C
C     DETERMINE ENTRAINMENT FLOW RATIO FOR EACH TYPE OF DISCHARGE
C
      IF(N(I,J).EQ.0.0)  GO TO 270
      IF(PLT(I).EQ.2.0.AND.T.LT.4.0.AND.J.EQ.4) GO TO 270
      DRD2=(RHO(T2)-RHO(TD(J)))/RHO(T2)
      UC=QD(J)/AD(J)
      FRD2=UD/SQRT(G*DRD2*((AC(J)/2.0)**0.5))
      IF(FRD2.LT.1.0)  FRD2=1.0
      SB=1.2*(FRD2-1.0)
      DRD1=(RHO(T1)-RHO(TD(J)))/RHO(T1)
      IF(DRD1.LE.0.0) GO TO 265
      FRD1=UD/SQRT(G*DRD1*((AC(J)/2.0)**0.5))
      HM=0.42*FRD1*SQRT(AD(J)/2.0)
      IF((HM/H1).LT.HMRT)  JD(J)=1
      IF((HM/H1).LT.HMRT)  S(J)=1.0
      IF((HM/H1).LT.HMRT)  GO TO 300
      SBE=SB*(1.0-HMRT*(H1/HM))
      SBR=1.0+SBE
      JD(J)=2
```

```
      GO TO 266
  265 SBR=1.0+SB
      SBE=SB
      JC(J)=4
  266 HDF=H1-HS
      SDIF=SS-SBE
      HDFM=45.0-HSLW
      IF(HDF.LE.0.0) HDF=0.0
      IF(HDF.GT.HDFM) HDF=HDFM
      IF(HDF.GT.0.0.AND.JD(J).EQ.2)  JD(J)=3
      IF(HDF.GT.0.0.AND.JD(J).EQ.4)  JD(J)=5
      IF(HDF.GT.0.0.AND.SDIF.GT.0.0) JD(J)=8
      S(J)=SBR+SDIF*(HDF/HDFM)
      GO TO 300
  270 S(J)=0.0
      JD(J)=0
  300 CONTINUE
      JC(I)=JC(1)+JC(2)+JC(3)
      JE(I)=JC(4)
      DO 320 J=1,4
      IF(S(J).EQ.0.0) GO TO 320
      IF(S(J).LT.1.0) S(J)=1.0
  320 CONTINUE
      SC(I)=S(1)+S(2)+S(3)
      SE(I)=S(4)
      QT(I)=(N(I,1)*(QA+QE)*S(1))+(N(I,2)*QA*S(2))+(N(I,3)*QE*S(3))
      QT(I)=QT(I)+(N(I,4)*QE*S(4))
      QEN=0.0
      QAN=0.0
      IF(N(I,1).GT.0.0.OR.N(I,3).GT.0.0.OR.N(I,4).GT.0.0)  QEN=1.0
      IF(N(I,1).GT.0.0.OR.N(I,2).GT.0.0)  QAN=1.0
      QHT(I)=((QHA*QAN)+(QHE*QEN))*1.0E+6
  400 CONTINUE
      Q=QT(1)+QT(2)
      QH=QHT(1)+QHT(2)
      QAR=(QAT(1)+QAT(2))*RA
```

```
      QER=(QET(1)+QET(2))*RE
      QSIL=2.0*C1S
      IF(QSIL.LE.0.0) GO TO 52
C
C     SUMMATION OF TERMS IN EACH DIFFERENTIAL EQUATION
C
      RHS(1)=((Q/A1C)-((QSIL+QER+QAR)/A1C))*C3
      HTSOR=QH/(A1C*C2*H1)
      HTDIS=(CDIS*(T1-T2))/(C2*H1)
      HTSIL=(C3*QSIL*(T1-T2))/(H1*A1C)
      HTLAY=(RHS(1)*(T1-T2))/H1
      RHS(2)=HTSOR-HTSIL-HTDIS-HTLAY
      PDISS=(HTDIS*100.0)/(HTDIS+HTSIL)
      POPEN=(HTSIL*100.0)/(HTDIS+HTSIL)
  700 RETURN
      END
```

```
C
C     THIS SUBROUTINE IS USED TO COLLECT, SELECT, AND ORGANIZE ALL
C     DATA PRODUCED FOR EACH TIME STEP IN EITHER RKGS OR FCT.  THE
C     DATA IS THEN PRINTED OUT FOR THE INTEGER HOUR VALUES.
C
      SUBROUTINE OUTP(T,X,RHS,IHLF,M,PRMT)
      REAL N,NA,NE
      DIMENSION X(2),PRMT(5),DERY(2),AUX(8,2),RHS(2)
      COMMON/IOPUT/ IWRIT,IREAD
      COMMON/INOPS/ JP,HMRT,TMA(31),QHLA(31),TME(55),QHLE(55),
     2 SC(2),SE(2),KRUN,CH,G,C1,C2,C3,CDIS,QHEC,KQHA,KQHE
      COMMON/OPS/ QAG,QEG,PHASE,TIDE,T2,A1,AT,AP,DRAFT,PLT(2),
     1 FR2H(11,9,4),QA,QE,AC(4),N(2,4)
      COMMON/OUT/ PDISS,POPEN,JE(2),JC(2),HS,QHA,QHE,DTV(2),DTAI,
     3 CTEI,QNET
      DT1=X(2)-T2
      IF(INDEX.EQ.1)   PRMT(5)=1.0
C
C     CONTROL THAT SELECTS HOURLY INTERVAL FOR PRINT OUT OF DATA
C
      IF(ABS(CH-T).LE.0.1) GO TO 799
      GO TO 900
  799 HEAT=X(1)*DT1*A1*C2/10.0E8
      HEATP=(X(1)-DRAFT)*DT1*AP*C2/10.0E8
      IF(X(1).GT.DRAFT) HEAT=HEAT+HEATP
      WRITE(IWRIT,800) T,IHLF,HS,QHA,QHE,DTV(1),DTV(2),X(1),DT1,
     8  DTAI,CTEI,PDISS,POPEN,SC(1),SE(1),SC(2),SE(2),JC(1),JE(1),
     E  JC(2),JE(2),QNET,HEAT
  800 FORMAT(F6.1,I2,F5.1,2F7.1,F6.1,F7.1,F8.2,F7.2,F6.2,F7.2,2F6.1,
     9 4F5.1,2X,4I1,F7.2,F8.2)
  899 CH=CH+1.0
  900 RETURN
      END
```

```
C
C       THIS FUNCTION CALCULATES THE DENSITY OF WATER FOR ANY TEMP F
C
        FUNCTION RHO(TF)
        TC=(TF-32.0)/1.8
        RHO=1.0-(1.97E-6*(TC+288.9)*(TC-3.98)**2)/(TC+68.13)
        RETURN
        END
```

Table A-2

Input Data Sample

```
 4
 32.2  0.002228  64.0  3600.0
2  0.2 72.0  0.2  0.001  0.5  0.5
  24  51  30.0
 00000 06600 00399 06600 00400 27400 00500 23500 00600 23200 00700 22500
 00800 16600 00900 13800 01000 12400 01100 11600 01200 10200 01300 09300
 01400 08800 01500 08500 01600 08300 01700 08100 01800 07900 01900 07800
 02000 07500 02780 06700 05560 05200 11110 03800 16670 03300 27778 02600
 00000 11100 00046 11100 00052 08278 00063 07468 00100 12734 00200 18723
 00300 20149 00400 17767 00500 18652 00600 17262 01000 15087 01400 13661
 01800 13483 02200 13198 02600 13091 03000 13007 03400 12913 03800 12871
 04200 12734 04600 12627 05200 12592 05600 12413 06000 12295 06400 12299
 06800 12128 07200 12021 07600 11950 08000 11807 08400 11736 08800 11629
 09200 11522 09600 11451 10000 11344 10400 11273 10800 11166 11200 11059
 11600 10887 12000 10880 12400 10809 12800 10702 13200 10595 13600 10524
 14400 10346 15200 10132 16000 09954 16800 09775 17600 09597 18400 09419
 19200 09205 20000 09027 31200 06689
  PROTO 1B   LOOP-NORMAL   SINGLE SYSTEM FAILURE
 0.33  2  5.7
  455000.0  960000.0  300000.0  35.0  5.5  4.0  6.5  5.0  28.5  20.0  130.0
  85.0  0.0  0.0000
15000. 7500. 2. 1. 2. 0. 0. 1. 0. 3. 0. 0.
  PROTO 4A   LOOP-LOOP      ALL SYSTEMS OPERATING
 0.33  2  5.7
  455000.0  960000.0  300000.0  35.0  5.5  4.0  6.5  5.0  28.5  20.0  130.0
  85.0  0.0  0.0000
15000. 7500. 2. 2. 3. 0. 0. 1. 3. 0. 0. 1.
  PROTO 5A   LOCA-NORMAL   ALL SYSTEMS, 10 FT TIDE, PHASE = PI
 0.33  2  5.7
  455000.0  960000.0  300000.0  35.0  5.5  4.0  6.5  5.0  28.5  20.0  130.0
  85.0  5.0  3.1416
15000. 7500. 3. 1. 0. 0. 3. 1. 0. 3. 0. 0.
  PROTO 8A   LOOP-LOOP  ALL SYSTEMS  DCD=7.0 FEET  DED= 5.5 FEET
 0.33  2  5.7
  455000.0  960000.0  300000.0  35.0  7.0  5.5  6.5  5.0  28.5  20.0  130.0
  85.0  0.0  0.0000
15000. 7500. 2. 2. 3. 0. 0. 1. 3. 0. 0. 1.
```

PROTO 4A LOOP=LOOP ALL SYSTEMS OPERATING

ARM FLOW PLT #1= 45000.0 GPM ERM FLOW PLT #1= 30000.0 GPM

ARM FLOW PLT #2= 45000.0 GPM ERM FLOW PLT #2= 30000.0 GPM

TIDAL AMPLITUDE= 0.0 FT TIDAL PHASE= 0.00 RADIANS

AMBIENT WATER TEMP= 85.0 F SILL WIDTH= 130.0 FT INTAKE DEPTH= 28.5 FT

TIME	DEPTH AT SILL FT	ARM MIL BTU/ HR	ERM MIL BTU/ HR	AVG DISC DELT # 1	AVG DISC DELT # 2	AVG LAYER DEPTH FT	AVG TEMP RISE F	ARM INTK DELT F	ERM INTK DELT F	% HEAT DIS	% HEAT OUT= FLOW	DILUTION RATIOS PLT C	#1 E	PLT C	#2 E	DILL CONT CODE	NET SILL FLOW	LAYER HEAT E9 BTU
0.2		66.0	0.0	2.9	2.9	2.65	0.34					8.5	0.0	8.5	0.0			
1.0	V 20.0	66.0	0.0	2.9	2.9	9.20	0.45	0.00	0.00	5.2	94.8	5.1	0.0	5.1	0.0	2020	0.00	0.12
2.0	V 20.0	66.0	0.0	2.9	2.9	14.50	0.53	0.02	0.00	4.0	96.0	3.9	0.0	3.9	0.0	2020	0.00	0.22
3.0	V 20.0	66.0	0.0	2.9	2.9	18.25	0.61	0.05	0.00	3.9	96.1	3.3	0.0	3.3	0.0	2020	0.00	0.32
4.0	1 20.0	273.6	0.0	11.9	11.9	20.48	0.65	0.08	0.00	3.6	96.4	1.0	0.0	1.0	0.0	1010	0.00	0.41
5.0	0 20.0	235.0	30.0	7.1	7.1	22.34	1.36	0.22	0.21	2.6	97.4	1.8	4.4	1.8	4.4	8383	0.00	0.89
6.0	0 20.0	230.6	30.0	7.1	7.1	23.75	1.86	0.38	0.37	2.2	97.8	1.8	4.9	1.8	4.9	8383	0.00	1.24
7.0	0 20.0	225.0	30.0	7.1	7.1	24.71	2.12	0.49	0.48	2.1	97.9	1.8	5.1	1.8	5.1	8383	0.00	1.52
8.0	V 20.0	166.4	30.0	5.7	5.7	26.10	2.23	0.73	0.72	2.0	98.0	2.4	4.1	2.4	4.1	8383	0.00	1.70
9.0	V 20.0	138.0	30.0	5.3	5.3	27.77	2.20	0.90	0.90	2.0	98.0	2.6	3.3	2.6	3.3	8383	0.00	1.78
10.0	0 20.0	122.4	30.0	5.2	5.2	28.85	2.17	1.24	1.25	2.1	97.9	2.5	2.3	2.5	2.3	8888	0.00	1.82
11.0	0 20.0	116.0	30.0	5.1	5.1	29.55	2.15	1.31	1.32	2.1	97.9	2.5	2.1	2.5	2.1	8888	0.00	1.85
12.0	V 20.0	100.2	30.0	4.8	4.8	30.26	2.11	1.39	1.40	2.1	97.9	2.6	1.8	2.6	1.8	3838	0.00	1.86
13.0	V 20.0	93.0	30.0	4.6	4.6	30.96	2.06	1.44	1.46	2.1	97.9	2.6	1.0	2.6	1.0	3131	0.00	1.86
14.0	V 20.0	87.4	30.0	4.5	4.5	31.44	2.02	1.47	1.49	2.1	97.9	2.6	1.0	2.6	1.0	3131	0.00	1.85
15.0	0 20.0	85.0	30.0	4.5	4.5	31.87	1.98	1.49	1.50	2.2	97.8	2.6	1.0	2.6	1.0	3131	0.00	1.84
16.0	0 20.0	82.6	30.0	4.4	4.4	32.24	1.95	1.49	1.51	2.2	97.8	2.6	1.0	2.6	1.0	3131	0.00	1.83
17.0	0 20.0	81.0	30.0	4.4	4.4	32.55	1.93	1.50	1.51	2.2	97.8	2.6	1.0	2.6	1.0	3131	0.00	1.83
18.0	0 20.0	78.8	30.0	4.3	4.3	32.84	1.90	1.50	1.51	2.2	97.8	2.5	1.0	2.5	1.0	3131	0.00	1.82
19.0	0 20.0	78.0	30.0	4.3	4.3	33.10	1.88	1.50	1.51	2.2	97.8	2.5	1.0	2.5	1.0	3131	0.00	1.81
20.0	0 20.0	74.8	30.0	4.2	4.2	33.36	1.86	1.50	1.51	2.2	97.8	2.6	1.0	2.6	1.0	3131	0.00	1.81
21.0	0 20.0	74.0	30.0	4.2	4.2	33.62	1.84	1.50	1.51	2.2	97.8	2.5	1.0	2.5	1.0	3131	0.00	1.80
22.0	V 20.0	72.7	30.0	4.2	4.2	33.84	1.82	1.50	1.51	2.2	97.8	2.5	1.0	2.5	1.0	3131	0.00	1.80
23.0	0 20.0	71.5	30.0	4.1	4.1	34.05	1.81	1.49	1.51	2.3	97.7	2.5	1.0	2.5	1.0	3131	0.00	1.79
24.0	V 20.0	70.7	30.0	4.1	4.1	34.24	1.79	1.49	1.50	2.3	97.7	2.5	1.0	2.5	1.0	3131	0.00	1.79
25.0	0 20.0	69.5	30.0	4.1	4.1	34.42	1.78	1.49	1.50	2.3	97.7	2.5	1.0	2.5	1.0	3131	0.00	1.79
26.0	0 20.0	68.6	30.0	4.1	4.1	34.59	1.77	1.49	1.50	2.3	97.7	2.5	1.0	2.5	1.0	3131	0.00	1.78
27.0	V 20.0	67.8	30.0	4.0	4.0	34.76	1.76	1.48	1.50	2.3	97.7	2.5	1.0	2.5	1.0	3131	0.00	1.78
28.0	0 20.0	66.8	30.0	4.0	4.0	34.93	1.74	1.48	1.49	2.3	97.7	2.5	1.0	2.5	1.0	3131	0.00	1.77
29.0	0 20.0	66.4	30.0	4.0	4.0	35.05	1.74	1.48	1.49	2.8	96.2	2.5	1.0	2.5	1.0	3131	0.00	1.77
30.0	V 20.0	65.7	30.0	4.0	4.0	35.14	1.73	1.47	1.49	2.8	96.2	2.5	1.0	2.5	1.0	3131	0.00	1.77
31.0	0 20.0	65.3	30.0	4.0	4.0	35.23	1.72	1.47	1.48	2.8	96.2	2.5	1.0	2.5	1.0	3131	0.00	1.77
32.0	0 20.0	64.6	30.0	3.9	3.9	35.33	1.71	1.47	1.48	2.8	96.2	2.5	1.0	2.5	1.0	3131	0.00	1.77
33.0	0 20.0	64.2	30.0	3.9	3.9	35.42	1.70	1.47	1.48	2.8	96.2	2.5	1.0	2.5	1.0	3131	0.00	1.77
34.0	V 20.0	63.5	30.0	3.9	3.9	35.51	1.70	1.46	1.48	2.8	96.2	2.5	1.0	2.5	1.0	3131	0.00	1.77
35.0	0 20.0	63.1	30.0	3.9	3.9	35.60	1.69	1.46	1.47	2.8	96.2	2.5	1.0	2.5	1.0	3131	0.00	1.77
36.0	V 20.0	62.5	30.0	3.9	3.9	35.70	1.68	1.46	1.47	2.8	96.2	2.5	1.0	2.5	1.0	3131	0.00	1.77
37.0	0 20.0	62.0	30.0	3.9	3.9	35.79	1.68	1.46	1.47	2.8	96.2	2.5	1.0	2.5	1.0	3131	0.00	1.77
38.0	V 20.0	61.4	30.0	3.8	3.8	35.88	1.67	1.45	1.46	2.8	96.2	2.5	1.0	2.5	1.0	3131	0.00	1.77
39.0	V 20.0	61.0	30.0	3.8	3.8	35.98	1.66	1.45	1.46	2.8	96.2	2.5	1.0	2.5	1.0	3131	0.00	1.77
40.0	0 20.0	60.3	30.0	3.8	3.8	36.07	1.66	1.45	1.46	2.9	96.1	2.5	1.0	2.5	1.0	3131	0.00	1.77
41.0	0 20.0	59.5	30.0	3.8	3.8	36.16	1.65	1.44	1.46	2.9	96.1	2.5	1.0	2.5	1.0	3131	0.00	1.77

42.0	K	20.0	59.2	30.0	3.8	3.8	36.26	1.64	1.44	1.45	3.9	96.1	2.5	1.0	2.5	1.0	3131	0.00	1.77
43.0	K	20.0	58.8	30.0	3.8	3.8	36.35	1.64	1.44	1.45	3.9	96.1	2.5	1.0	2.5	1.0	3131	0.00	1.77
44.0	K	20.0	58.2	30.0	3.7	3.7	36.45	1.63	1.44	1.45	3.9	96.1	2.5	1.0	2.5	1.0	3131	0.00	1.77
45.0	K	20.0	57.7	30.0	3.7	3.7	36.55	1.62	1.43	1.45	3.9	96.1	2.5	1.0	2.5	1.0	3131	0.00	1.77
46.0	K	20.0	57.1	30.0	3.7	3.7	36.64	1.62	1.43	1.44	3.9	96.1	2.5	1.0	2.5	1.0	3131	0.00	1.78
47.0	K	20.0	56.6	30.0	3.7	3.7	36.74	1.61	1.43	1.44	3.9	96.1	2.5	1.0	2.5	1.0	3131	0.00	1.78
48.0	K	20.0	56.0	30.0	3.7	3.7	36.84	1.60	1.42	1.44	3.9	96.1	2.5	1.0	2.5	1.0	3131	0.00	1.78
49.0	K	20.0	55.6	30.0	3.6	3.6	36.93	1.60	1.42	1.43	3.9	96.1	2.5	1.0	2.5	1.0	3131	0.00	1.78
50.0	K	20.0	54.9	30.0	3.6	3.6	37.03	1.59	1.42	1.43	3.9	96.1	2.5	1.0	2.5	1.0	3131	0.00	1.78
51.0	K	20.0	54.5	30.0	3.6	3.6	37.13	1.58	1.42	1.43	3.9	96.1	2.5	1.0	2.5	1.0	3131	0.00	1.78
52.0	K	20.0	53.8	30.0	3.6	3.6	37.23	1.58	1.41	1.42	3.9	96.1	2.5	1.0	2.5	1.0	3131	0.00	1.78
53.0	K	20.0	53.4	30.0	3.6	3.6	37.33	1.57	1.41	1.42	4.0	96.0	2.5	1.0	2.5	1.0	3131	0.00	1.78
54.0	K	20.0	52.8	30.0	3.6	3.6	37.43	1.56	1.41	1.42	4.0	96.0	2.5	1.0	2.5	1.0	3131	0.00	1.78
55.0	K	20.0	52.3	30.0	3.5	3.5	37.53	1.56	1.40	1.41	4.0	96.0	2.5	1.0	2.5	1.0	3131	0.00	1.78
56.0	K	20.0	51.8	30.0	3.5	3.5	37.63	1.55	1.40	1.41	4.0	96.0	2.5	1.0	2.5	1.0	3131	0.00	1.78
57.0	K	20.0	51.6	30.0	3.5	3.5	37.73	1.54	1.40	1.41	4.0	96.0	2.5	1.0	2.5	1.0	3131	0.00	1.78
58.0	K	20.0	51.3	30.0	3.5	3.5	37.81	1.54	1.39	1.41	4.0	96.0	2.5	1.0	2.5	1.0	3131	0.00	1.78
59.0	K	20.0	51.1	30.0	3.5	3.5	37.90	1.53	1.39	1.40	4.0	96.0	2.5	1.0	2.5	1.0	3131	0.00	1.78
60.0	K	20.0	50.8	30.0	3.5	3.5	37.98	1.53	1.39	1.40	4.0	96.0	2.4	1.0	2.4	1.0	3131	0.00	1.78
61.0	K	20.0	50.6	30.0	3.5	3.5	38.06	1.52	1.39	1.40	4.0	96.0	2.4	1.0	2.4	1.0	3131	0.00	1.78
62.0	K	20.0	50.3	30.0	3.5	3.5	38.13	1.52	1.39	1.40	4.0	96.0	2.4	1.0	2.4	1.0	3131	0.00	1.78
63.0	K	20.0	50.1	30.0	3.5	3.5	38.20	1.52	1.38	1.39	4.0	96.0	2.4	1.0	2.4	1.0	3131	0.00	1.78
64.0	K	20.0	49.8	30.0	3.5	3.5	38.27	1.51	1.38	1.39	4.0	96.0	2.4	1.0	2.4	1.0	3131	0.00	1.78
65.0	K	20.0	49.6	30.0	3.5	3.5	38.34	1.51	1.38	1.39	4.0	96.0	2.4	1.0	2.4	1.0	3131	0.00	1.78
66.0	K	20.0	49.3	30.0	3.4	3.4	38.40	1.51	1.38	1.39	4.0	96.0	2.4	1.0	2.4	1.0	3131	0.00	1.78
67.0	K	20.0	49.1	30.0	3.4	3.4	38.46	1.50	1.38	1.39	4.0	96.0	2.4	1.0	2.4	1.0	3131	0.00	1.78
68.0	K	20.0	48.8	30.0	3.4	3.4	38.53	1.50	1.38	1.39	4.0	96.0	2.4	1.0	2.4	1.0	3131	0.00	1.78
69.0	K	20.0	48.6	30.0	3.4	3.4	38.58	1.50	1.37	1.38	4.0	96.0	2.4	1.0	2.4	1.0	3131	0.00	1.78
70.0	K	20.0	48.3	30.0	3.4	3.4	38.64	1.49	1.37	1.38	4.1	95.9	2.4	1.0	2.4	1.0	3131	0.00	1.78
71.0	K	20.0	48.1	30.0	3.4	3.4	38.70	1.49	1.37	1.38	4.1	95.9	2.4	1.0	2.4	1.0	3131	0.00	1.78
72.0	K	20.0	47.9	30.0	3.4	3.4	38.76	1.49	1.37	1.38	4.1	95.9	2.4	1.0	2.4	1.0	3131	0.00	1.78

Appendix B

Experimental Study of Three-Dimensional Withdrawal

The investigation reported in this appendix is concerned with the selective withdrawal features of an intake consisting of a round pipe with a horizontal axis which is positioned on a vertical wall. The fluid system in the adjoining half-space is two-layered with a variable thermocline region. Figure B-1 illustrates the type of intake system. The investigation has been carried out in parallel to the main study and has been reported in a thesis by Katavola (1975). This appendix provides an extraction of the main features and results.

The experimental investigation has been carried out with the following objectives:

1) Determine the critical withdrawal condition below which the intake draws water from one layer only.
2) Determine the behavior of the withdrawal system for the conditions of simultaneous flow from both layers (supercritical condition)
3) Evaluate the dependence of the withdrawal behavior on such factors as size of the intake opening and type of stratification.

The experimental program utilized heated water to generate a thermally stratified fluid system. In this way, stratification was easily established and measurement techniques were less complicated. Care had to be taken, however, to prevent excessive heat losses in the system. This limited the maximum possible density differences that could be employed in an experiment.

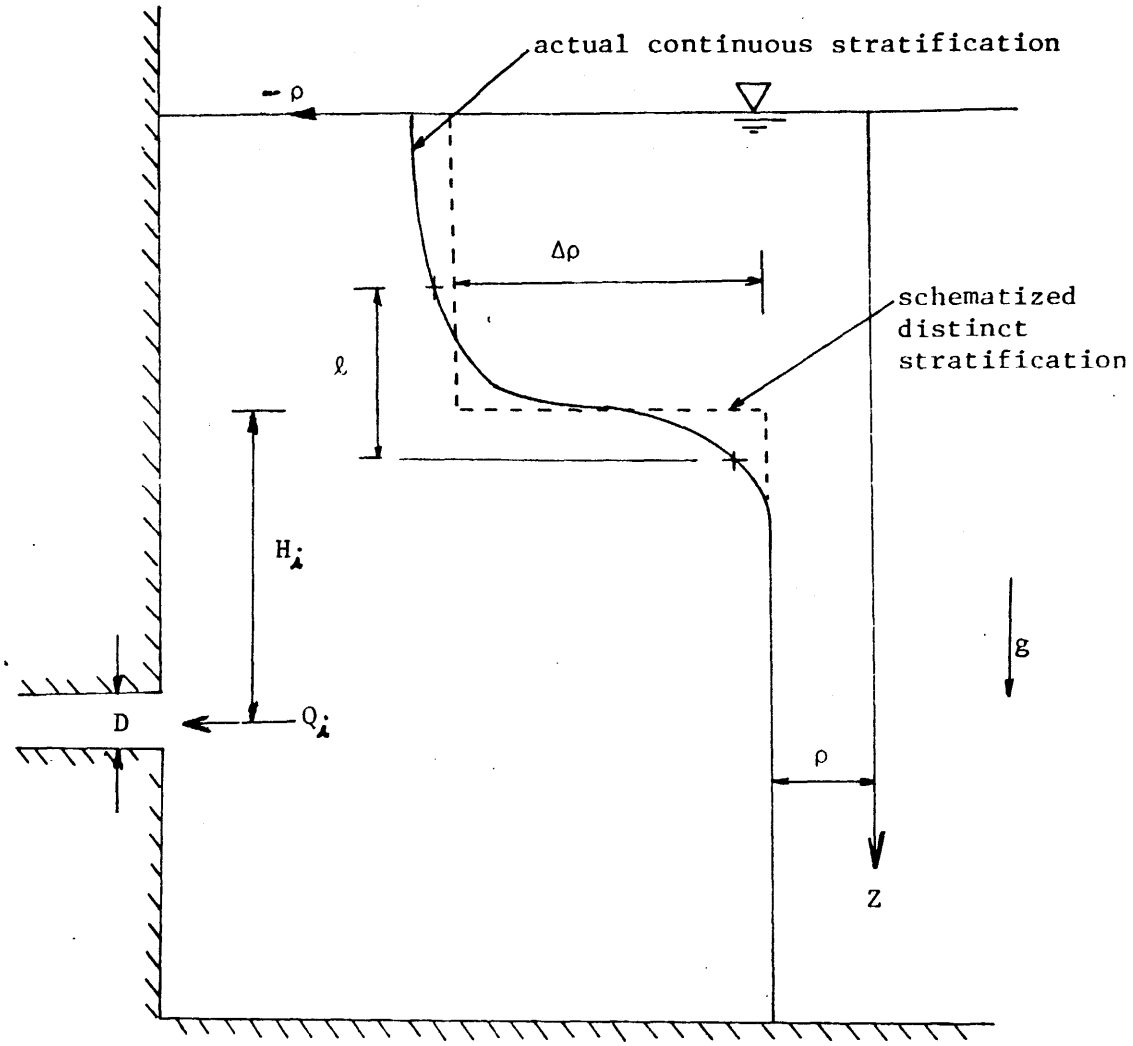

Example of Continuous vs Distinct Stratification

FIGURE B-1

B.1 Experimental Set-up

The entire experimental set-up was comprised of four systems, namely: (i) a test tank, (ii) the intake system, (iii) the discharge system, and (iv) the temperature measurement system. The entire set-up is shown in Figure B-2.

(i) All experiments were conducted in an insulated water tank with dimensions 52 in. x 60 in. and 36 in. deep. Insulation was provided by attaching foam rubber pads to the sides of the steel tank and by placing a clear plastic cover over the top. This proved successful in preventing excessive heat loss during the experiments. Since the diameters of the intakes utilized within the investigation were small relative to the dimensions of the test tank and relatively small intake flowrates were used, drawdown of the interface was limited to a region close to the intakes. The interface elevation a short distance upstream of the intake remained horizontal throughout an experiment which indicated negligible boundary effects.

(ii) A schematic of the intake system is illustrated in Figure B-3. Short lengths of round copper tubings inserted in rubber stoppers were used to model the intakes. Accurate measurements of the inside diameters were made with Vernier calipers. Table B-1 lists the various sizes of inlets investigated within this study. The intake units could be inserted into a horizontal PVC pipe with an inside diameter of 1.465 in. located in the center of a vertical false wall made of plywood. The centerline of the pipe was at an elevation of 12 in. above the tank bottom. A number of bends were placed in the intake pipe line to insure

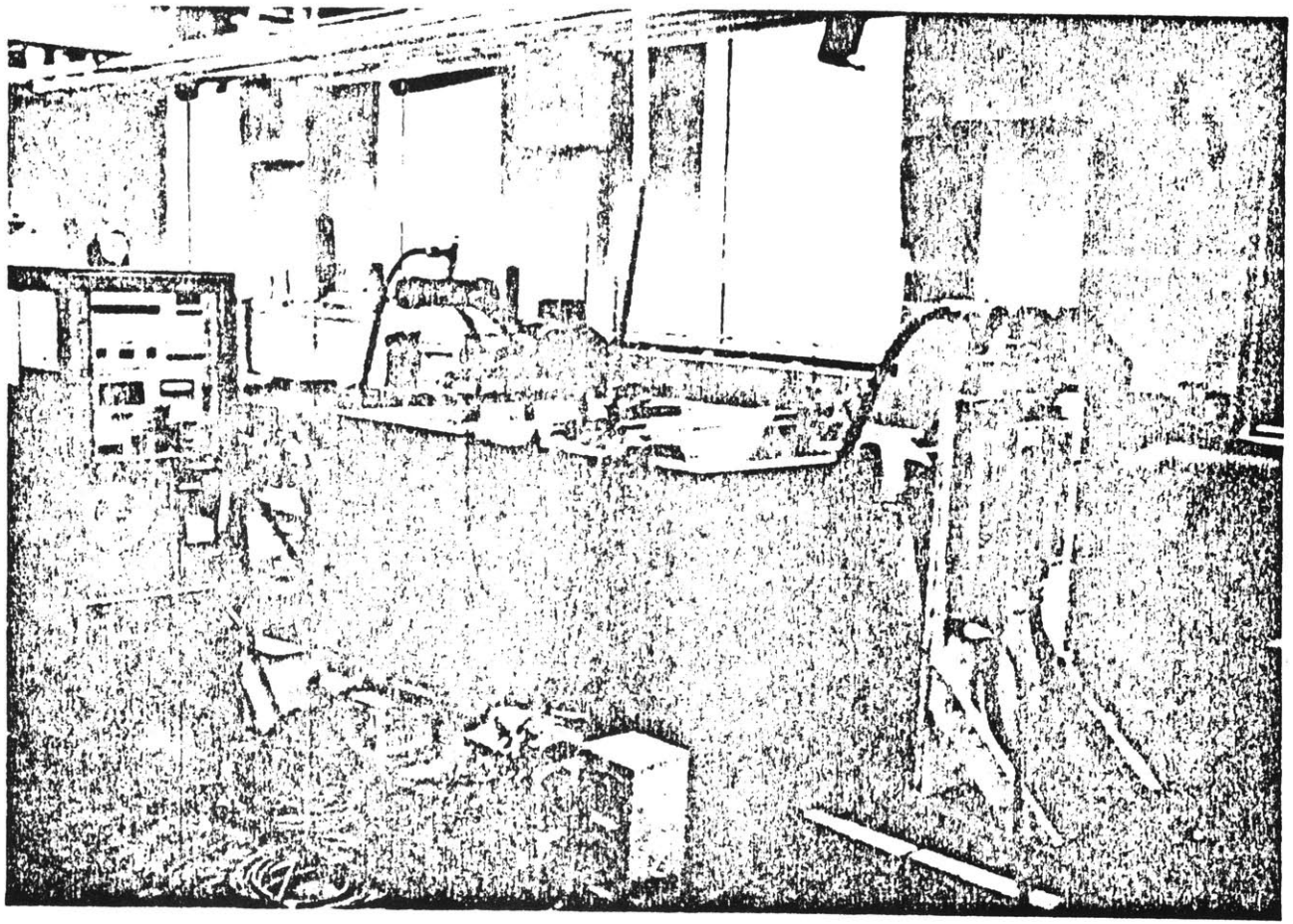

Entire Experimental Set-up

FIGURE B-2

Schematic of Intake System

FIGURE B-3

Table B.1

Size of Intake Openings

Nominal Diameters (in)	Actual Diameters (in)
3/16	0.210
1/4	0.252
1/2	0.550
3/4	0.790
1	1.031
1 1/2	1.465

complete mixing of the intake flows before temperature measurement. A 1/2 hp pump generated the intake flow. The flow was measured by the rotameter flowmeters. One was for flows ranging from 0.5 to 3.0 gpm, the other for flows greater than 3.0 gpm up to 10.0 gpm.

(iii) Figure B-4 illustrates the heated water discharge system. After some preliminary experiments, the primary discharge manifold was designed so that a minimum amount of mixing of hot and cold water took place when discharging and that the hot layer was uniformly distributed in all directions within the test tank. The manifold was made of PVC and had an inside diameter of 3.0 in and extended across the full width of the tank. Ten 0.5 in. holes were drilled into the manifold at 4 in. intervals. This was done to decrease the exit velocities of the discharge flow. The manifold rested on a plywood board with its

discharge holes facing the rear wall of the test tank at an angle of approximately 45°. Horsehair was placed in front of the manifold to further insure uniform inflow distribution. The height of the board and manifold could be adjusted to the various cold water elevations of each experiment. The discharge flow was measured with a calibrated rotameter flowmeter. Hot water was obtained directly from the laboratory steam heat exchanger.

Measurements of the total intake elevation in the tank were obtained by means of a point gage.

(iv) Sixty-six (66) Yellow Springs Instruments No. 701 thermistor probes were used to take temperature measurements at four points A, B, C, D in the test tank and within the intake and discharge flow lines (see Figure B-5). The probes in the tank were arranged in vertical 'clusters' as shown in Figure B-5(b). All the probes have an accuracy of $\pm 0.25°F$ and a time constant of 7 seconds which filters out turbulent fluctuations. Each probe was individually calibrated in a water bath at three temperatures which were within a range expected to occur in any experiment. The calibration constant for a probe was taken to be the average of the three values obtained at these water temperatures. All the physical parameters pertinent to this investigation were based upon the temperature profiles recorded at A, which is sufficiently far from the drawdown zone around the intake, and the temperatures measured within the intake line. Less than 25 seconds was required to complete a scan of the total 34 probes located at these two locations. Data concerning the uniformity of the hot layer distribution was obtained from profiles at A, B, and C. Profiles measured at A and D were com-

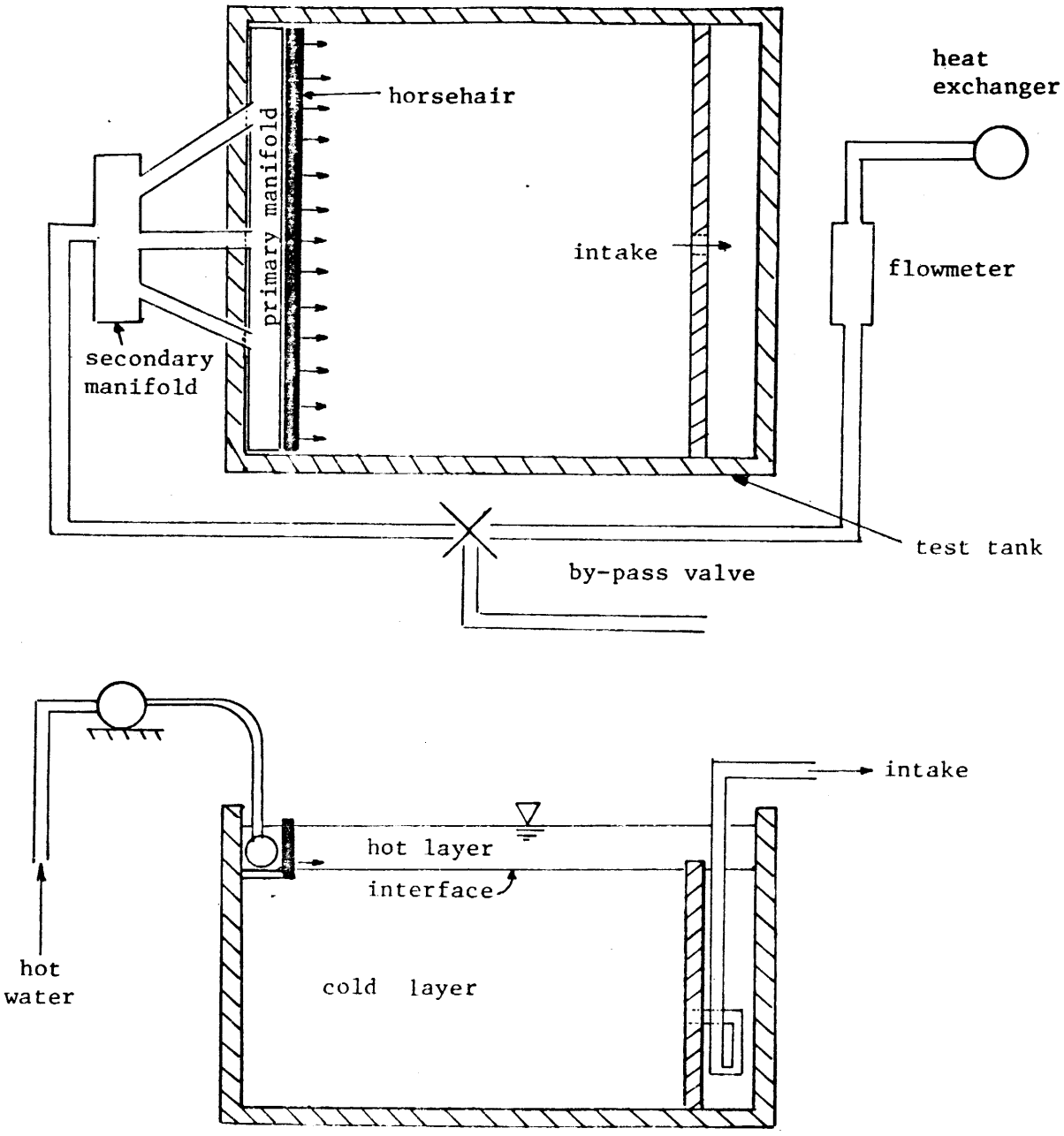

Schematic of Discharge System

FIGURE B-4

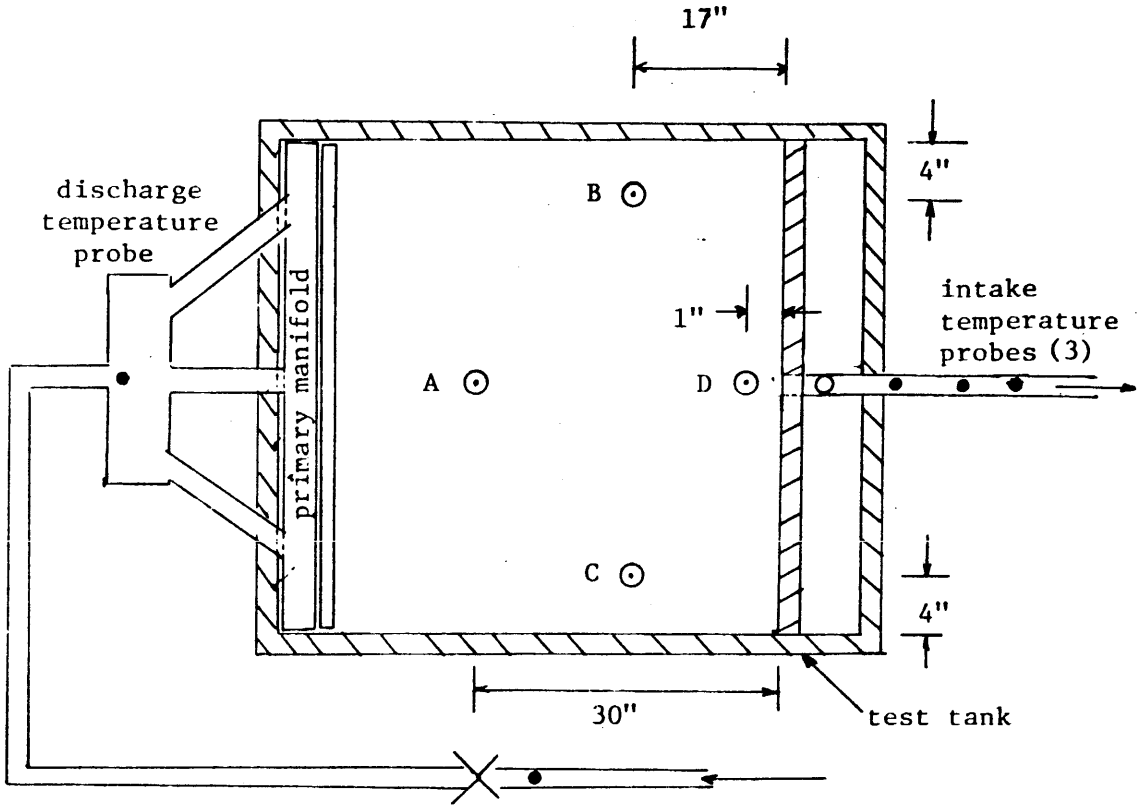

(a) temperature probe locations

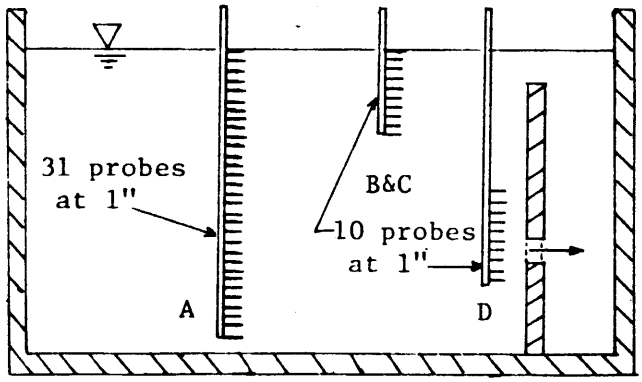

(b) temperature probe arrangements

Temperature Probe Locations and Arrangements

FIGURE B-5

bined to illustrate interface curvature.

The probes were connected to a scanner, reader and printer unit manufactured by Data Entry Systems. Temperature readings at each probe were printed on paper as well as on punched paper tape. The data on the punch tape was converted to computer cards by means of passing the tape through a tape-to-card reader.

B.2 Experimental Procedure

(a) Priming Phase:

Before the start of each run, the temperature of the cold tap water was measured. The temperature of the hot water from the heat exchanger was adjusted according to this reading to obtain the required temperature differential. Within the majority of runs, temperature differences between the hot and cold water ranged from 30°F to 40°F. By means of a by-pass in the discharge line, the temperature of the hot water was allowed to reach a constant value without discharging into the test tank. Once this condition was met, cold water was discharged into the tank to an elevation dependent upon the intake flowrate to be used in the experiment. For flowrates less than 3 gpm, the cold water elevation was raised to 9 in. above the centerline of the intake, for flowrates greater than or equal to 3 gpm, it was put at 15 in. All runs were conducted with the initial interface higher than the inlet elevation. A point gage was used to obtain accurate water surface measurements. Also, blue dye was injected into the layer so that it could be distinguished from the hot upper layer. The base of the board supporting the primary discharge manifold was then positioned just below the

surface of the cold water. By letting the water stand for approximately 10 minutes, any disturbances within the cold water body were dampened out. After placing the clear plastic cover over the top of the tank, to minimize heat losses, the by-pass was closed and hot water flowed into the primary manifold. The hot water was discharged over the surface of the cold water at a flowrate of 4 gpm. An initial upper layer thickness of at least 4 in. was developed in all experiments.

(b) Withdrawal Phase:

When the required total water elevation in the tank was reached, the intake pump was turned on and withdrawal was initiated at the required flowrate. The discharge flowrate was adjusted to equal that of the intake flowrate. Since no makeup of water was supplied to the cold lower layer, there was a gradual dropping of the interface during the experiment. This meant an increase in the upper layer thickness with a corresponding decrease in that of the lower layer. The drop rate of the interface was about .07 in./min/gpm of discharge flow. These small vertical velocities had negligible effects on the dynamics of the selective withdrawal. Two minutes were allowed to pass before taking the first temperature scan. This was an adequate amount of time to assure water from the cold lower layer filled the entire intake line. Temperature scans were taken at various time intervals depending upon the intake flowrate. A scan rate of 2 minutes was used for runs with high flowrates and of 5 minutes for the low flowrates. In addition, as the interface location neared the intake elevation, shorter time intervals were used. The flowrates utilized within the investigation ranged from

0.5 gpm to 8 gpm. A high flowrate experiment took about 50 minutes to run and a low flowrate about 120 minutes. In the majority of the experiments, the interface was allowed to drop below the elevation of the intake and thus, the condition of withdrawal greater than 50% was simulated. At such a condition, the interface is being drawn up into the intake. Dye particles were frequently dropped into the stratified water to study the vertical velocity profiles.

B.3 Governing Parameters

Considering the physical situation illustrated in Figure B-1, the following major physical variables are expected to govern the selective withdrawal characteristics:

$\Delta\rho$ = density difference between the upper and lower layers of an assumed two-layered fluid system

ρ = density of the lower layer

Q_i = total intake flowrate

D = diameter of intake pipe

H_i = interface elevation relative to centerline of intake pipe

ℓ = thermocline width (measure of the nature of stratification of a fluid body)

g = gravitational acceleration

This fluid system is well stratified with a clear distinction between an upper and a lower layer of different densities. However, the two layers are separated by a fluid zone of variable density which provides a grad-

ual transition between the upper and lower layers. The width of this fluid zone which in this study is referred to as the thermocline width, ℓ, always exists in practical applications. Selective withdrawal is expected to be influenced by this variable.

Applying the Buckingham Π-theorem, the seven physical quantities listed above can be grouped into four independent non-dimensional parameters. These parameters are:

Relative density difference = $\Delta\rho/\rho$

Froude number $F^* = Q_i / \sqrt{g\ H^5}$

Relative height of interface = H_i/D

Relative thermocline width = ℓ/D

The majority of real-world stratified fluid bodies, which have temperature or salinity as their stratifying agents, are characterized by small density differences, $\frac{\Delta\rho}{\rho} \to 0$, and small Froude numbers, $F^* \to 0$. However, if density differences are considered, a reduced gravitational acceleration or buoyant acceleration can be defined and is given as:

$$g' = \Delta\rho/\rho \ g$$

The parameters $\Delta\rho/\rho$ and F^* can be combined to form a densimetric Froude number defined as:

$$F = \frac{Q_i}{\sqrt{\Delta\rho/\rho\ g\ H_i^5}} \qquad \text{(B-1)}$$

Thus, for stratified systems involving small density differences it is possible to reduce the number of governing non-dimensional parameters

from four to three. The resultant three parameters being F, H_i'/D, and ℓ/D. This useful simplification is referred to as the Boussinesq approximation and is frequently used in oceanography and environmental fluid dynamics. Also, with such an approximation, one can assume that identical selective withdrawal characteristics exist for interface elevations above and below the intake elevation.

An alternative group of governing parameters can be formed by rearranging the newly formulated parameters into three densimetric Froude numbers based on the different characteristic lengths H_i', D, and ℓ. They are as follows:

$$F = Q_i / \sqrt{\Delta\rho/\rho\ g\ H_i^5} \qquad \text{(B-2)}$$

$$F_D = Q_i \sqrt{\pi/4} \sqrt{\Delta\rho/\rho g\ D^5} \qquad \text{(B-3)}$$

$$F_\ell = Q_i / \sqrt{\Delta\rho/\rho g\ \ell^5} \qquad \text{(B-4)}$$

Experiments of this study were conducted with a time-varying interface elevation, H_i', while the remaining physical variables Q_i, $\Delta\rho/\rho$, D, and ℓ, were assumed constant. It was therefore most convenient to employ these three densimetric Froude numbers in analyzing the results, since F will be the only parameter that will vary within an experimental run. The following is a discussion of the significance of the three Froude numbers F, F_D, and F_ℓ.

F is the primary parameter of the stratified fluid system. It characterizes the buoyant stability of the system, which is expressed

as $\sqrt{\Delta\rho/\rho\ g\ H_i^3}$, in comparison with the inertial forces, which arise through the application of a withdrawal flow Q_i. Changes in F should describe the overall response of the system in terms of selective withdrawal.

F_D and F_ℓ are secondary parameters which can be thought of as disturbances of the primary response. F_D expresses the geometric effects of the discharge openings. Small values of F_D (i.e. large diameters) are expected to lead to stronger entrainment from the upper layer, as opposed to larger values. This is demonstrated, for example, if one considers the case of an intake whose radius, D/2, approaches the interface elevation H_i. Also, small values of F_ℓ (i.e. a large thermocline width) should lead to stronger entrainment, due to the less distinct character of the interface.

Theoretical investigations, such as Craya (1949), consider the ideal case of $F_D \to \infty$ (a point sink intake) and $F_\ell \to 0$ (a discrete stratification) and deal with the primary parameter F only.

The degree of selectivity is defined as

$$\lambda = Q_1 / Q_i \qquad (B-5)$$

where Q_1 is the amount of flow drawdown from the upper layer, and Q_i is the total intake flow. Using a heat conservation equation, an alternate definition is

$$\lambda = \frac{T_i - T_2}{T_1 - T_2} \qquad (B-6)$$

where T_1 and T_2 are the respective temperature of the upper and

lower layers, and T_i is the mixed temperature of the intake flow. For purposes of this study, Eq. (B-6) is preferable from measurement considerations.

In summary, the degree of selectivity or the percent withdrawal will be a function of the three non-dimensional Froude numbers

$$\lambda = f(F, F_D, F_\ell).^* \qquad (B-7)$$

Interfacial friction due to the locally confined withdrawal region is considered negligible within this formulation. Also, surface tension, which is important for the withdrawal of immiscible fluids, such as oil on the surface of water, does not play a role in thermally stratified fluid systems.

B.4 Experimental Program

A continuous change in F during an experimental run was insured by varying the interface elevation. The experimental program was further designed to cover a wide range of values of F_D and F_ℓ as permitted by the existing experimental setup. The capacity of the pump limited the range of flowrates that could be investigated for a given intake diameter. Flowrates ranged from 0.5 to 8.0 gpm and intake diameters from 0.252 to 1.465 in. which resulted in F_D values of 1.4 to 437.

---

*λ values of more than 50% will result for interface elevations below the intake level. In the definition of the densimetric Froude number, Eq. (B-2), it is understood that the length H_ℓ is taken in absolute terms throughout.

The study covered F_ℓ values between 0.05 and 0.33. The values of F_D and F_ℓ were constant for each experiment and, in fact, characterized each experiment. Density differences between .006 and .012, which represent ΔT's of 30°F and 40°F, were used in the majority of the runs. The interface was allowed to drop below the centerline of the intake which resulted in percent withdrawals greater than 50%.

Table B-2 is a summary of the physical variables and non-dimensional parameters for the experiments conducted within the study. The physical variables T_{cold}, T_{hot}, ΔT, and ℓ are all average values determined from the several temperature measurements taken during an experimental run.

B.5 Data Reduction

The techniques employed to reduce the experimental data were based upon the following assumptions:

(1) a quasi-steady condition of withdrawal during each temperature measurement

(2) the cluster of probes located at A was taken to be characteristic of the interface outside the influence of the withdrawal region.

A variety of data reduction techniques can be employed to schematize the continuous density stratification of the experimental data in order to define the characterizing parameters F, F_D, F_ℓ and λ. There is a certain degree of arbitrariness in any kind of schematization. However, the obtained results are useful as long as a consistent data re-

Table B-2

Summary of Run Parameters of the Experiments

	Physical Variables						Non-Dimensional Variables		
Run No.	D (in.)	Q_i (gpm)	T_{cold} (°F)	T_{hot} (°F)	ΔT (°F)	ℓ (in.)	F_D	F_ℓ	$\Delta\rho/\rho$
1	.252	3.0	54.0	94.1	40.1	5.5	310	.10	.0049
2	.252	3.9	58.1	91.0	32.9	6.3	437	.11	.0044
3	.550	6.0	50.1	92.1	42.0	5.6	114	.21	.0051
4	.550	2.0	57.3	94.3	37.0	6.4	38	.05	.0051
5	.550	2.8	57.8	91.6	33.8	5.8	44	.10	.0045
6	.550	5.0	58.4	92.3	33.9	5.8	77	.16	.0048
7	.790	1.5	56.1	90.6	34.5	4.9	9.6	.08	.0045
8	.790	6.5	57.9	90.9	33.0	5.7	41	.23	.0044
9	.790	2.0	61.9	102.4	40.5	6.0	11	.06	.0063
10	1.031	2.5	55.8	96.7	30.9	5.2	7.2	.10	.0055
11	1.031	2.5	63.0	88.7	25.7	3.4	9	.24	.0032
12	1.465	6.0	49.8	90.7	40.9	5.4	7.4	.22	.0049
13	1.465	1.0	53.1	84.9	31.4	3.4	1.4	.14	.0037
14	1.465	6.0	54.8	92.2	37.4	5.3	7.4	.24	.0045
15	1.465	1.5	59.3	93.3	34.0	4.4	2.1	.11	.0047
16	1.465	7.5	63.6	92.5	28.9	5.6	10	.33	.0043

duction procedure is employed. The details of the density (temperature profile) schematization are shown in the following.

In all cases, the parameters $\Delta\rho/\rho$, H_i, and ℓ at each time interval within a run were determined solely from the temperature profiles measured by the cluster of probes at location A. The experimental data recorded on paper tape was converted to computer cards and, along with the water elevation measurement, were input into the data reduction program. The calibration constants and depths of each probe were stored in the program and the program automatically performed the reduction steps.

Figure B-6 illustrates a typical temperature distribution recorded at location A for one temperature scan of experiment No. 11. As can be seen, the system is well stratified with a clear distinction between the upper and lower layer of different densities. The vertical distribution of hot water is uniform to a depth of approximately 3 in. Then there is a zone of variable density which provides a gradual transition between the upper hot layer and the cold lower layer. The temperature of the cold layer is also uniformly distributed. This particular profile was recorded at the start of the run. Similar profiles were obtained throughout the experiment with the thickness of the upper layer increasing with time. A profile such as shown in Fig. B-6 was schematized to a two-layered discretely stratified flow regime in a manner outlined in the figure. This involved the following steps:

a) The temperature of the lower layer, T_2, (i.e. ambient temperature) is the initial cold tap water temperature. T_2 remained constant throughout all experiments.

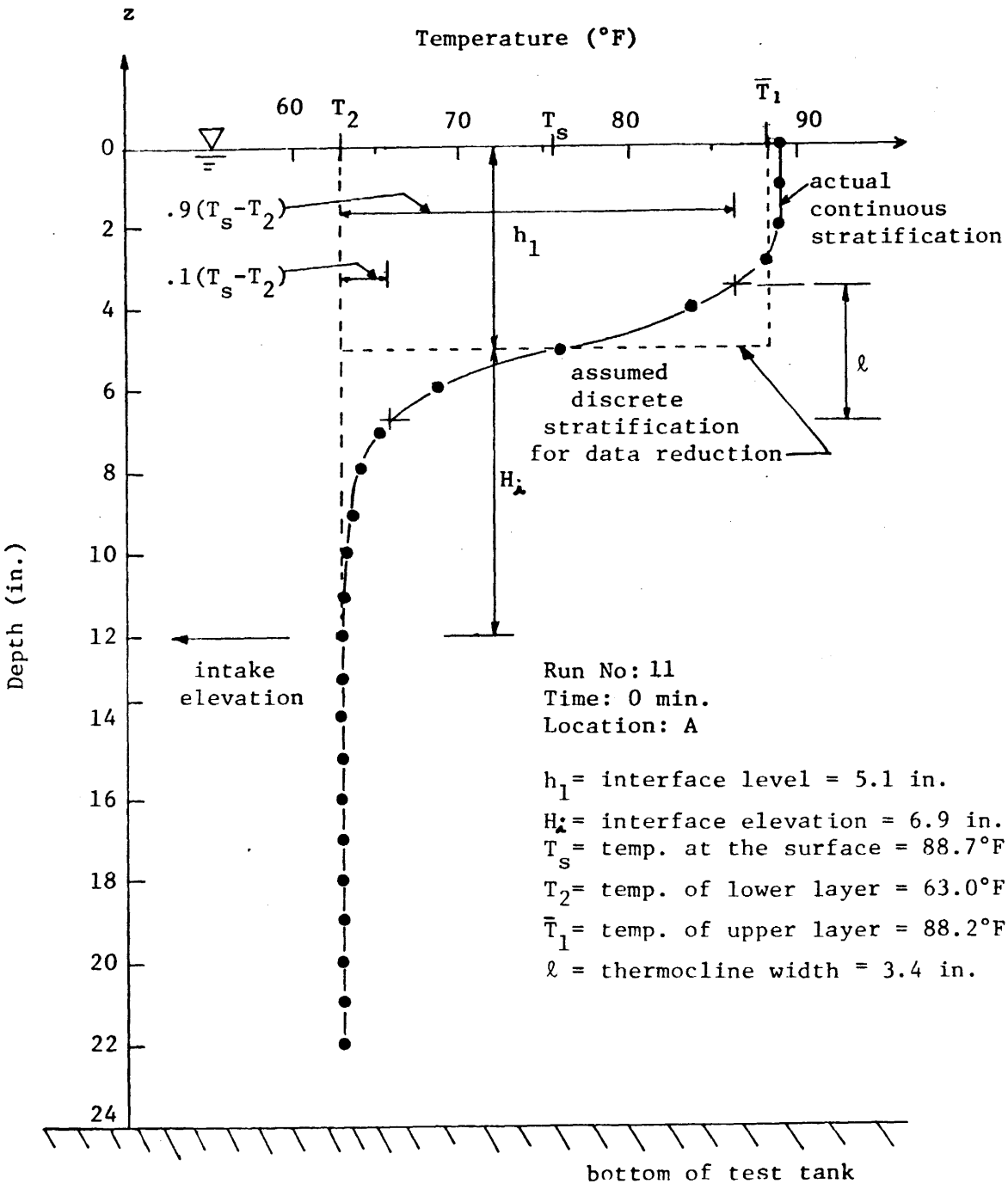

Typical Vertical Temperature Profile of an Experiment

FIGURE B-6

b) The interface position, H_i, is defined to be the elevation at which the temperature rise above the lower layer ambient temperature equals one half of the surface temperature rise above ambient. This definition of the interface position has been uniformly found to agree well with the position of the maximum density gradient, which is a frequently employed characterization of an interface in stratified flow. The difference between the intake position and the level of the interface provided the interface elevation H_i.

c) The next step involved a characterization of a uniform upper layer temperature, $\bar{T}_1$. This was obtained through an integration

$$\bar{T}_1 = \frac{1}{h_1} \int_{z=-\infty}^{z=0} (T(z) - T_2)\, dz \qquad \text{(B-8)}$$

where h_1 = thickness of the upper layer

$T(z)$ = local temperature at position z

This approach assumes that the total buoyancy of the actually diffuse stratification is concentrated in the defined upper layer and seems reasonable as it conserves the heat discharged during an experiment. Practically, this definition of $\bar{T}_1$ was usually within a few degrees F of the actual surface temperature T_s (see Figure B-6).

d) The thermocline width, ℓ, is defined as the difference in the depths associated with 10% and 90% of the value of the difference between the temperature readings at the surface and of the lower layer as illustrated in Figure B-6. The parameter varied somewhat throughout an experiment and an average value of several temperature scans was used to characterize the nature of stratification of the fluid system

throughout the entire run. Therefore, similar to F_D, F_ℓ is approximated as being constant for each experiment.

e) Density of the upper and lower layers of the discretely stratified fluid is obtained from the National Bureau of Standards (1937) tables as

$$\rho_w = 999.973 \left(1 - \frac{(T-3.9863)^2}{508929.2} + \frac{T+288.9414}{T+68.12963}\right) \qquad \text{(B-9)}$$

where ρ_w is the water density in kg/m^3 and T is the water temperature in °C.

f) The three densimetric Froude numbers F, F_D and F_ℓ are determined from Eqs. (B-2), (B-3), and (B-4), respectively.

The percent withdrawal from the upper layer at time j

$$\lambda_j = \frac{T_{i,j} - T_{2,j}}{\bar{T}_{1,j} - T_{2,j}} \times 100\% \qquad \text{(B-10)}$$

where

$T_{i,j}$ = average of the temperature readings of the three intake probes at time j.

B.7 Error Analysis

The main sources of error in the experimental results can be attributed to intake flowrate fluctuations and inaccuracies in temperature measurement. Slight oscillations in intake flowrates occurred throughout an experiment. Attempts were made to minimize this error by

continuously checking flowmeter readings and making any necessary adjustments. It was found that the calibration constants of the temperature probes were a function of water temperature. However, within this investigation, each probe was assigned only one calibration constant for the expected temperature range of the water. This constant was the average of three values obtained at three different water temperatures. The maximum difference in any one calibration constant was 0.6 °F for a difference in water temperatures of 40 °F.

The relative inaccuracies in the temperature measurement are highest at low temperature rises such as those experienced at the intake. This has an effect upon the calculation of λ as given in Eq. (B-10). By taking the average of the readings for the three probes inserted into the intake line, this error source in the value of λ was minimized.

A further error source is due to the inaccuracies in determining the interface elevation H_{λ}. This is of pronounced importance when the interface elevation approaches the intake level so that small changes in H are reflected in large changes of F (Eq. (B-2)). Much of the scatter that is found between the results of various experiments, particularly in the high F range, is probably caused by this problem.

B.8 Basic Characteristics of Selective Withdrawal.

Figure B-7 illustrates the withdrawal behavior for run No. 6 The shape of the curve is typical for the entire experimental program. Considering Figure B-7, the following general comments can be made.

The withdrawal curve can be divided into a subcritical and a su-

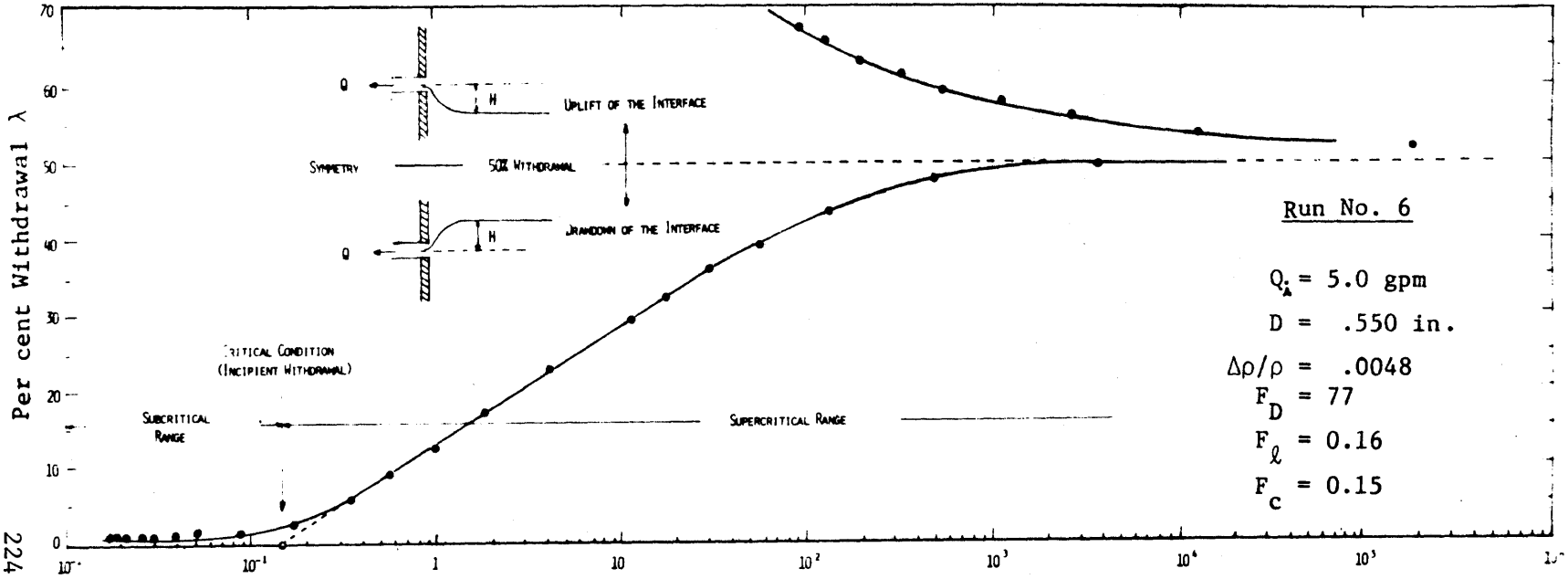

$$F = Q_A \sqrt{\frac{\Delta\rho}{\rho} g H_A^5}$$

Example of Withdrawal Curve of Per cent Withdrawal vs F

FIGURE B-7

percritical range, separated by a condition of incipient withdrawal. The subcritical range is characterized by low values of the withdrawal Froude number F, that is a combination of low flow rates, high density difference, or high interface elevation. Theoretically, the subcritical range should exhibit zero withdrawal effects ($\lambda=0$). However, in all experiments it has been found that a small degree of withdrawal ($\lambda<3\%$) consistently occurs even at values of F well below the incipient condition. This anomaly is probably due to two effects: i) the diffuse ambient interface outside the withdrawal zone (characterized by the thermocline width ℓ and Froude number F) does not provide a distinct differentiation between the two layers. ii) Viscous effects at the interface, which should act as the dividing streamline between the moving lower layer and the stagnant upper layer, cause local interfacial mixing within the withdrawal zone. The condition of small withdrawal rates in the subcritical range is common to other selective withdrawal investigations, for example as reported by Harleman and Elder (1965) and by Slotta and Charbeneau (1974).

The supercritical range exhibits a strong initial response, that is, λ increases significantly as a function of F, and a gradual leveling of the curve to the value of $\lambda = 50\%$ as F approaches infinity. Due to the small withdrawal effects in the subcritical range, the transition between the sub- and supercritical ranges is never abrupt but gradual. However, if the linear increase of λ in the semi-logarithmic plot is extrapolated downward to the line $\lambda=0$, it is possible to define

in a consistent manner a critical Froude number F_c as shown in Figure B-7. F_c signifies the condition of incipient withdrawal. A value of $F_c = 0.15$ can be deduced from the figure, which is considerably lower than Craya's theoretical value of $F_c = 2.54$. The values of F_c were generally found to be functions of the secondary parameters F_D and F_ℓ, but were always at least an order of magnitude lower than Craya's result.

Figure B-7 also indicated λ values of greater than 50% which occur when the interface is located below the level of the intake centerline. The withdrawal curve is approximately symmetric with respect to the λ=50 % line, which indicates that the selective withdrawal characteristics are generally the same for interfaces above and below the intake elevation.

B.9 Complete Results and Sensitivity Studies

The general experimental results are of the form

$$\lambda = f(F, F_D, F_\ell) \qquad \text{(B-11)}$$

and therefore constitute a four parameter problem. The general sensi-

tivity of λ in terms of the major parameter F has been discussed in the example of the previous section and is typical for the entire experimental program. This section discusses the sensitivity of the results due to the geometric effects represented by F_D and F_ℓ. The simultaneous consideration of both parameters is difficult so that the following discussions consider the parametric sensitivity due to one parameter at a time.

Sensitivity due to F_D:

The experiments are separated into groups of approximately equal values of F and are plotted in Figures B-8 (F_ℓ = 0.05 to 0.1), B-9 (F_ℓ = 0.1 to 0.16) and B-10 (F = 0.2 to 0.24). The major observation which can be made is that all withdrawal curves are, within the limits of experimental accuracy, of similar shape in both the sub- and supercritical ranges. Within each graph it is possible to discern a general trend of F_D. Experiments with large values of F_D (i.e. small intake openings) are located to the right in the graph while experiments with small F_D are located to the left. Large intake openings thus indicate a higher tendency for recirculation for a given withdrawal flow rate (value of F). However, this sensitivity is limited. For example, a four-fold increase in F_D (i.e. decreasing the intake diameter by a factor of 2) decreases the selective withdrawal by only about 4%, as can be seen from Figure B-8 (considering a value of $F = 1$ and the difference between $F_D = 9.6$ and $F_D = 44$). Comparison of Figures B-8 to B.10 also demonstrates the relative influence of F_ℓ as is further discussed in the following.

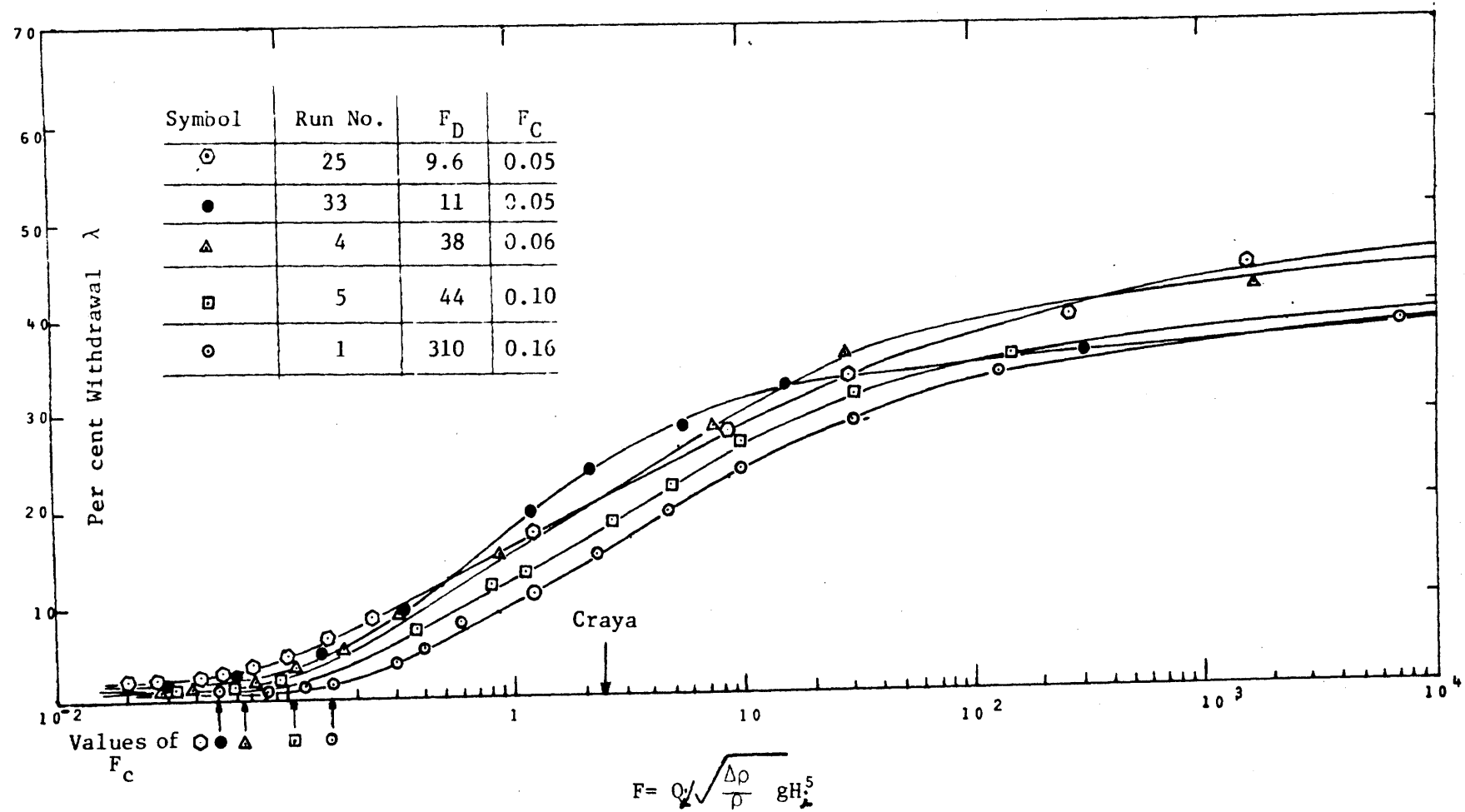

Per cent Withdrawal as a Function of F and F_D
for the Range F_ℓ = 0.05 - 0.10

FIGURE B-8

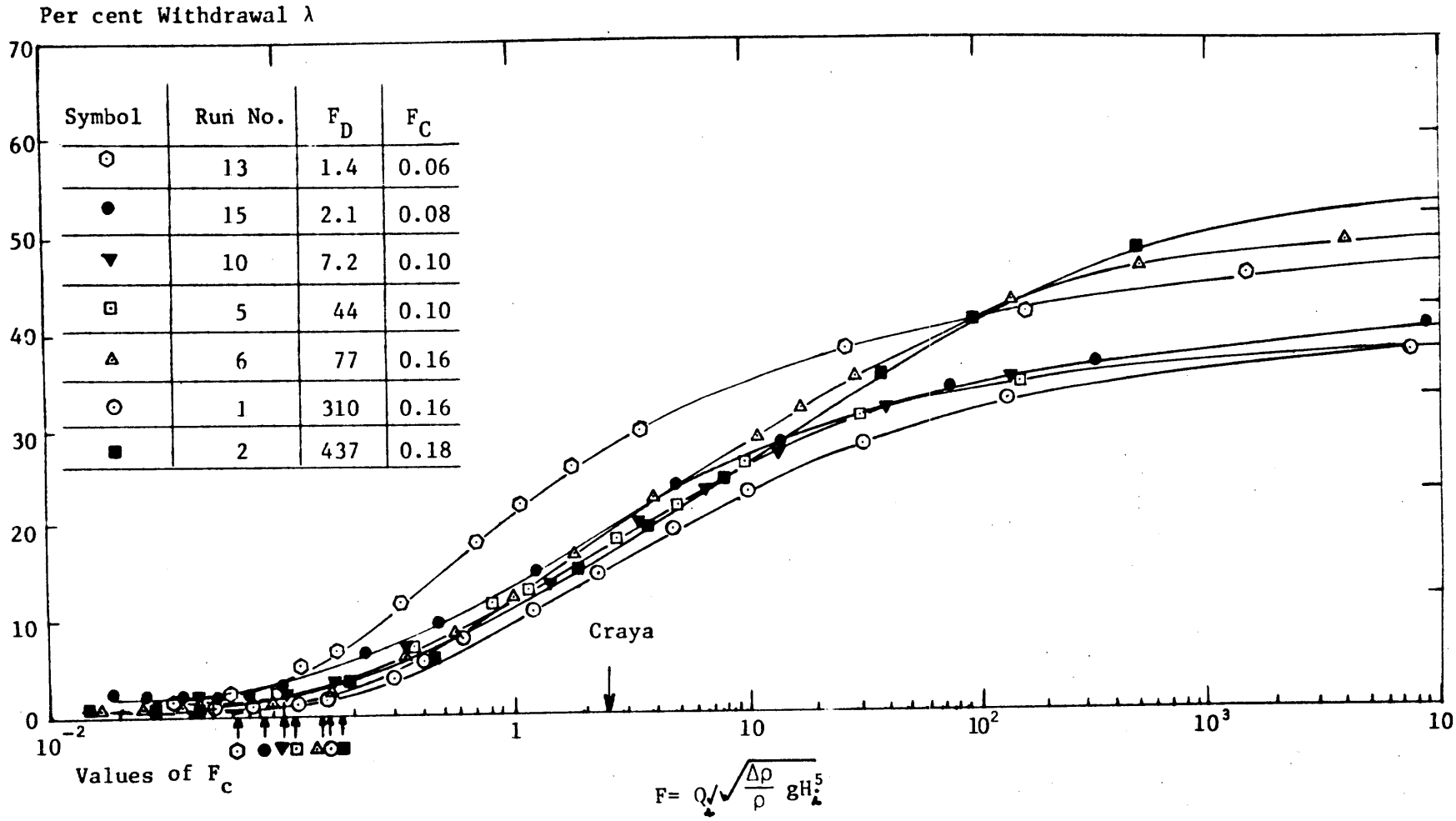

Per cent Withdrawal as a Function of F and F_D
for the Range F_ℓ = 0.10 - 0.16

FIGURE B-9

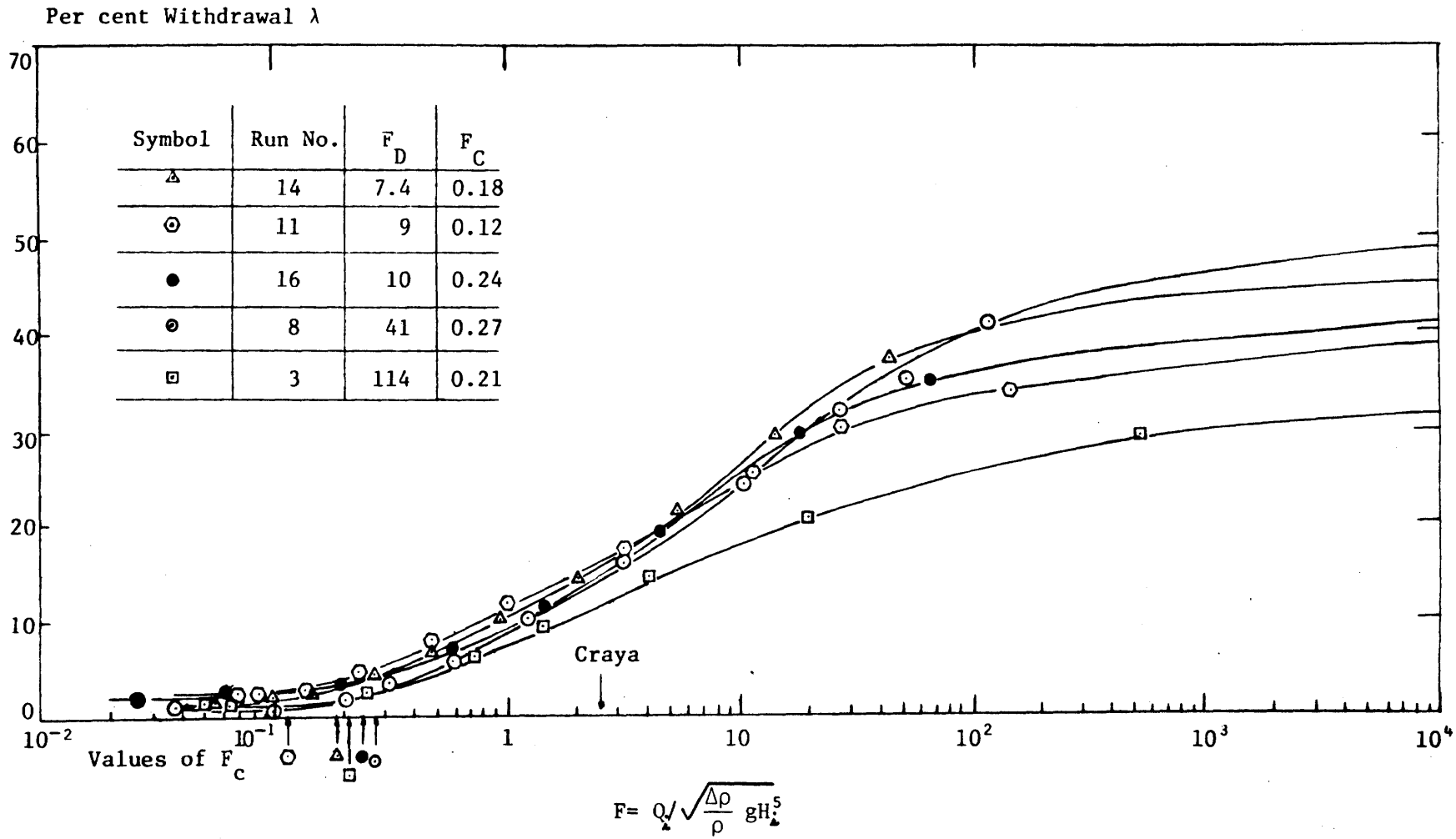

Per cent Withdrawal as a Function of F and F_D
for the Range F_ℓ = 0.20 - 0.24

FIGURE B-10

Sensitivity Due to F_ℓ:

The sensitivity of F_ℓ is demonstrated by plotting experimental results with similar F_D values, as is shown in Figures B-11 ($F_D \approx 10$) and B-12 ($F_D \approx 40$). The geometric effect of the thermocline width is similar in trend to that of the intake diameter D. Figure B-13 illustrates the tendency for higher withdrawal for less discretely stratified systems (small F_ℓ) as opposed to well stratified systems (large F_ℓ). A four-fold increase in F_ℓ results in a decrease in the percent withdrawal of approximately 8% as shown in Figure B-11 at F=1 between $F_\ell = 0.06$ and 0.24.

It is impossible to extrapolate beyond the experimental range to estimate the limiting value of a point sink ($F_D \to \infty$) as has been considered by Craya (1949) (Craya also assumed $F_\ell \to \infty$). The available data which covers two orders of magnitude of F_D is located within a very narrow band. The maximum critical Froude number obtained for Run No. 8 ($F_D = 41$ and $F_\ell = 0.23$) was 0.27 which is considerably lower than Craya's value of 2.54 . A possible cause for such a discrepancy can be attributed to the large values of ℓ / H_c (≈ 1), where H_c is the critical interface elevation, found in the experiments. The magnitude of ℓ/H_c in Gariel's (1949) experiments was in the order of 0.1.

B.10 Regression Analysis

A regression analysis to obtain a best-fit analytical expression $\lambda = f(F, F_D, F)$ for the experimental data has been performed. The

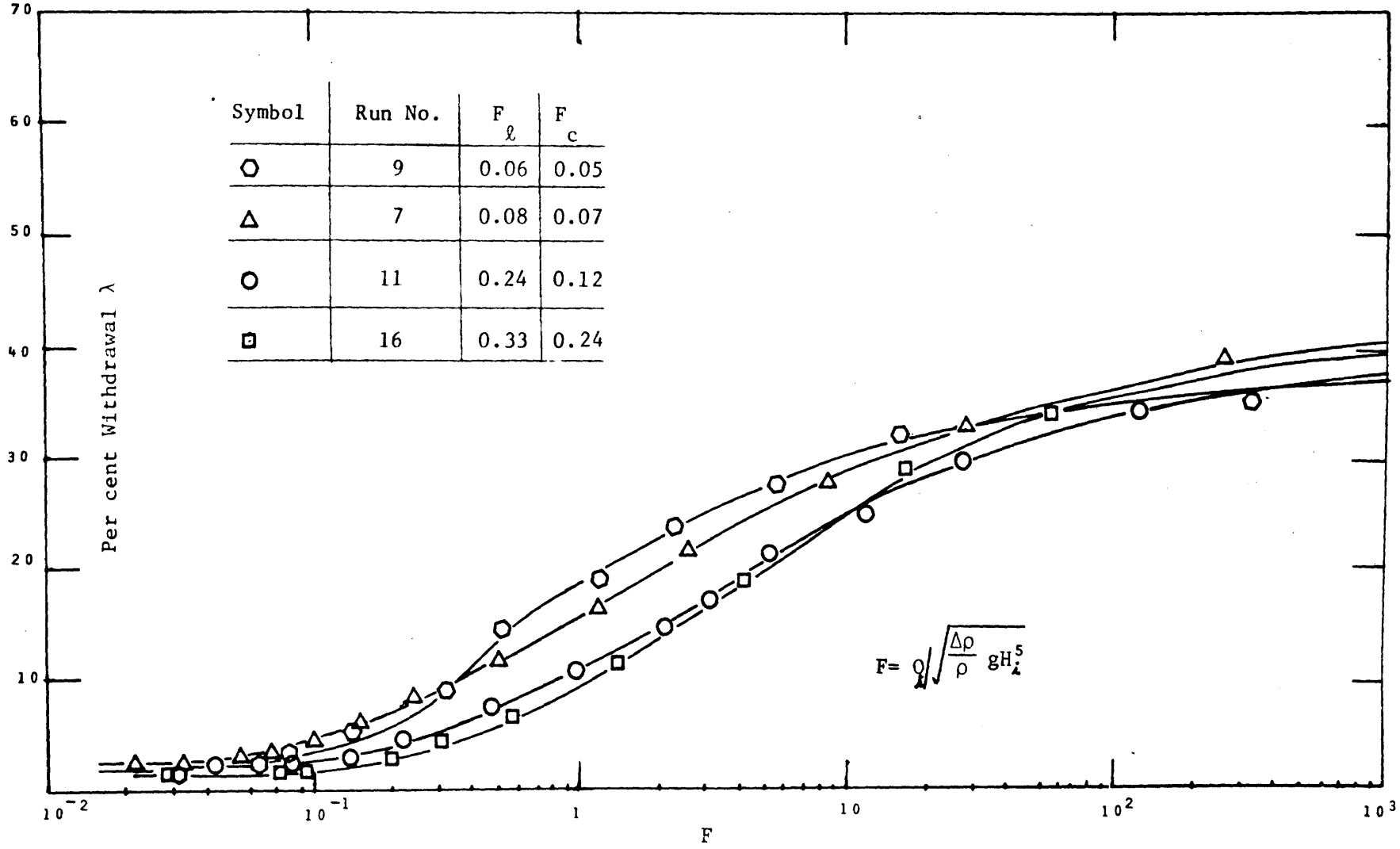

Per cent Withdrawal as a Function of F and F_ℓ for $F_D \simeq 10$

FIGURE B-11

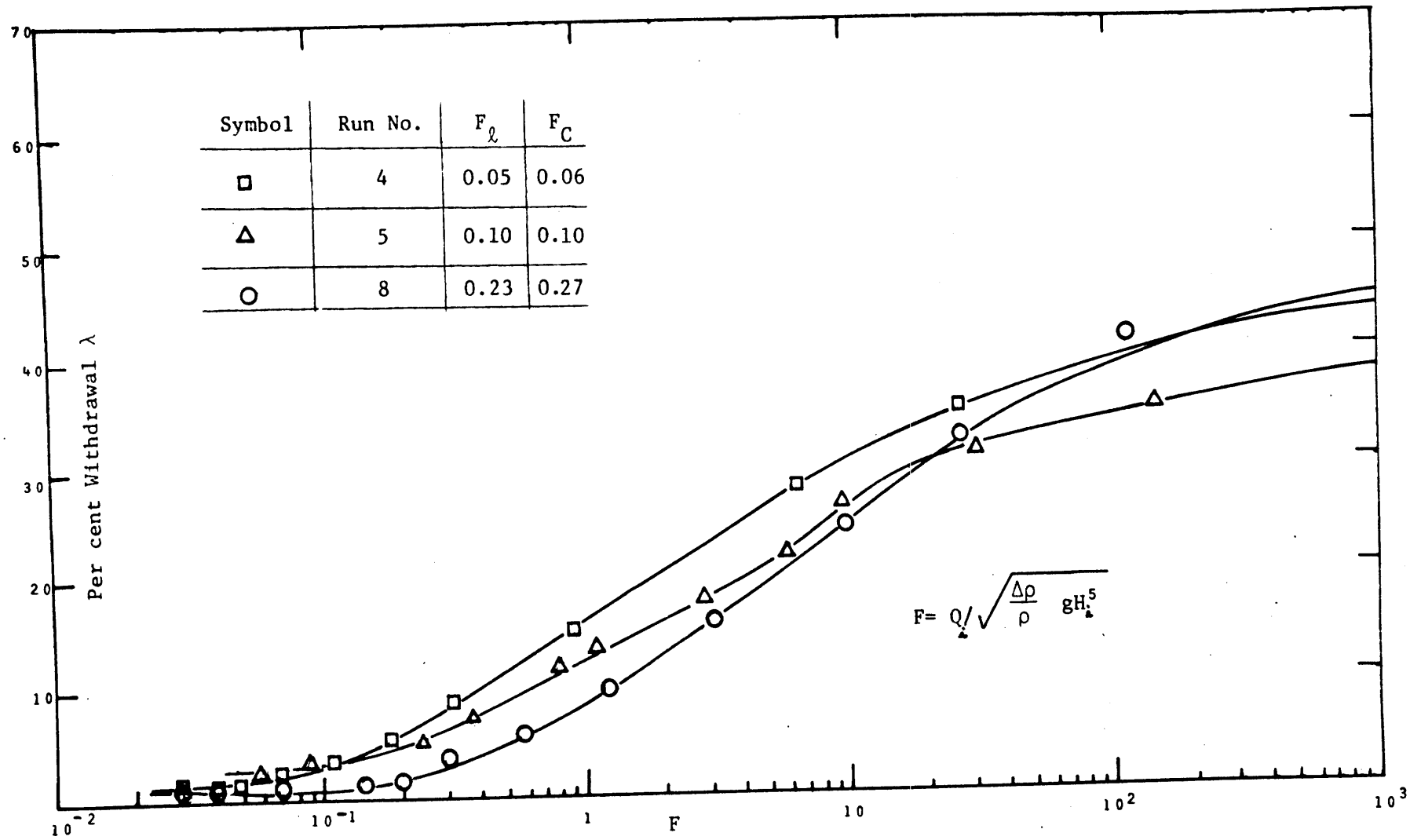

Per cent Withdrawal as a Function of F and F_ℓ for $F_D \simeq 40$

FIGURE B-12

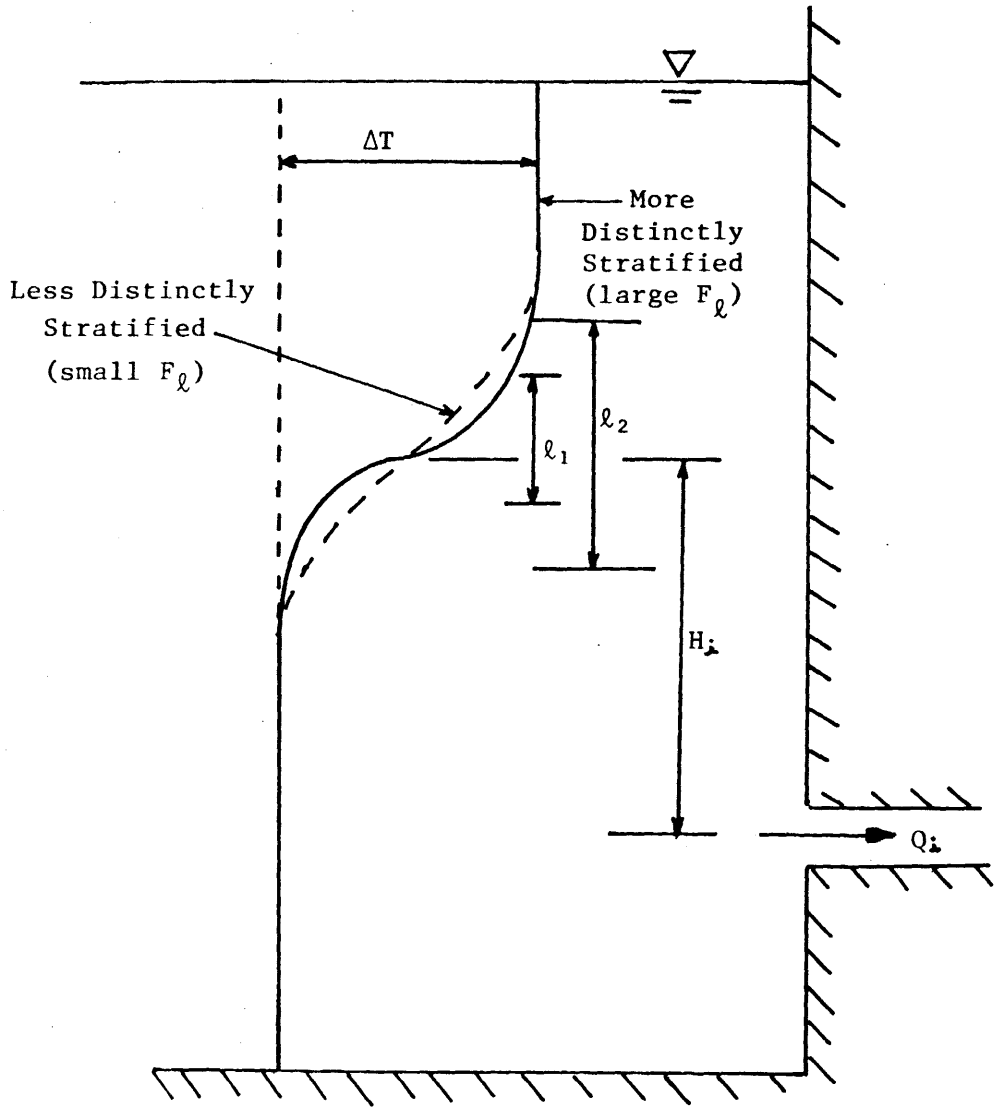

Illustration of Effect of Magnitude of 'ℓ'
on Per cent Withdrawal

FIGURE B-13

basic hypothesis utilized in the analysis is the following:

a) The secondary parameters F_D and F_ℓ do not influence the shape of the withdrawal curve, but only its relative position in a semilogarithmic plot of λ versus F. The position of the curve is then indicated by the incipient withdrawal condition* ($\lambda=0$) and is defined through a critical Froude number

$$F_c = g\,(F_D, F_\ell) \tag{B-12}$$

b) The primary parameter F normalized by its critical value F_c expresses the major withdrawal characteristics

$$\lambda = \left(\frac{F}{F_c} \right) \tag{B-13}$$

This is tantamount to assume that all withdrawal curves (such as shown in Figures B-8 to B-10) are self-similar to each other.

The validity of this basic assumption will be discussed further.

First, Eq. (B-13) is obtained by plotting the critical values of F_c, found from Figures B-8 to B-10, as a function of F_D and F_ℓ. This is shown in Figure B-14. The experimental points are well approximated by a functional relationship

$$F_c = 0.06 \log F_D + 0.64\, F_\ell \tag{B-14}$$

---

* This formulation neglects the small withdrawal rates ($\lambda < 3\%$) in the subcritical range as has been discussed earlier.

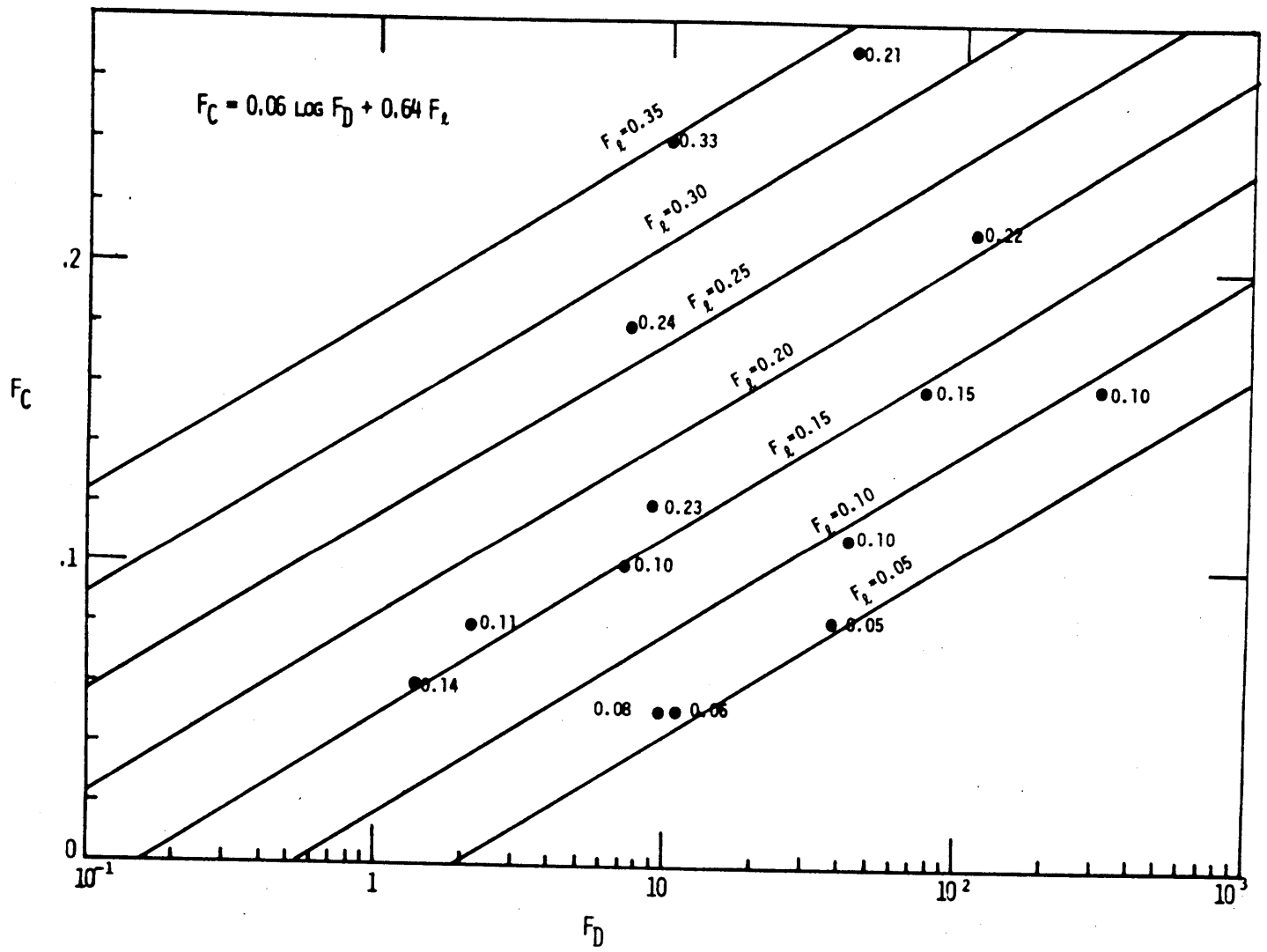

PLOT OF F_D VS F_C TO OBTAIN LINES OF CONSTANT F_ℓ

FIGURE B-14

The second step involves the normalization of the experimental curves of Figures B-8 to B-10 by dividing the abscissa value of F by the theoretical value F_c as expressed in Eq.(B-14). This results in the collapse of all experimental data onto a single graph, Figure B-15. Although the normalized curves show some degree of scatter, there is no apparent trend in terms of the F_ℓ and F_D values, so that the scatter seems to be experimental error only. These possible error sources have been discussed in Section B.6. The following expression represents the mean data trend in an optimal manner

$$\lambda\ (\%) = \begin{cases} 14.2 \log\ (F/F_c) & \text{for } 1 \leq F/F_c \leq 300 \\ 50\ [1 - (F/F_c)^{-.22}] & \text{for } F/F_c > 300 \end{cases} \qquad \text{(B-15)}$$

where F_c is taken from Eq. B-14). The first portion of the curve represents the linear response on the semi-logarithmic plot, the second part the leveling off to the $\lambda = 50\%$ value as $F/F_c \to \infty$.

The experimental range from which Eqs. (B-14) and (B-15) have been developed is

$$1 < F_D < 437$$
$$0.05 < F < 0.33 \qquad \text{(B-16)}$$

The above regression equations are well suited for engineering calculations of selective withdrawal rates with horizontal pipe intakes located on a vertical wall. The results are obtained from round pipe experiments, but can reasonably be applied to openings with other cross-sectional shapes, through the transformation

$$\text{Equivalent Pipe Diameter } D = \sqrt{4A/\pi}$$

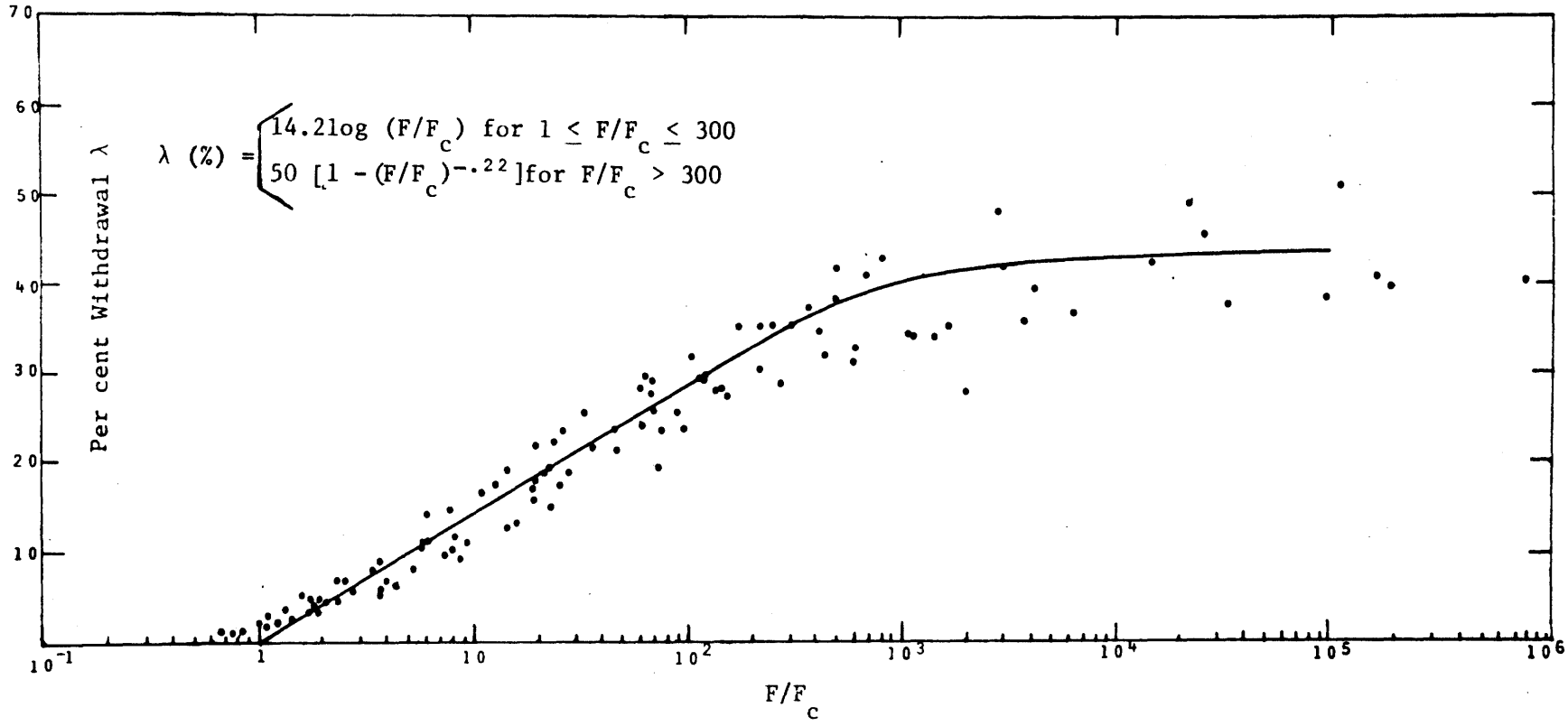

Best-fit Curve for the Experimental Data

FIGURE B-15

where A = cross-sectional area of intake opening. This seems applicable only if the height/width ratio of the actual openings does not strongly deviate from that for a round pipe.

REFERENCES:

Craya, A., "Recherches Théoriques sur L'Écoulement de Couches Superposées de Fluides de Densités Differentes," *La Houille Blanche*, Jan.-Feb., 1949, pp. 44-55.

Gariel, P., "Recherches Experimentales sur L'Écoulement de Couches Superposées de Fluides de Densités Differentes," *La Houille Blanche*, Jan.-Feb., 1949, pp. 56-64.

Harleman, D.R.F., Elder, R.A., "Withdrawal from Two-Layer Stratified Flows," *Journal of the Hydraulics Division*, ASCE, HY4, July 1965, pp. 43-58.

Katavola, D.S., "An Experimental Study of Three-Dimensional Selective Withdrawal from a Thermally Stratified Fluid System," M.S. Thesis, Department of Ocean Engineering, MIT, September 1975.

Slotta, L.S., Charbeneau, R.J., "Ambient Current Effects on Vertical Selective Withdrawal in a Two Layer System, Final Project Report, OWRR Project No. A-025-ORE, Water Resources Research Institute, Oregon State University, Corvallis, Oregon, January 1975.